Development of an Independent Monte Carlo Dose Calculation Tool for Validation of the Monaco Electron Treatment Planning System

Robert J Crane

Thesis Submitted for the degree of

Master of Philosophy

School of Physical Sciences

The University of Adelaide

Supervisors:

Dr Judith Pollard

Dr Scott Penfold

Timothy Crabtree

July 2019

I. Abstract

Monte Carlo (MC) is rapidly becoming the preferred algorithm for radiotherapy treatment planning systems (TPS) to obtain the most accurate dose predictions. Commercial MC TPSs rely on a number of simplifications to allow doses to be calculated in a clinically relevant timeframe. These simplifications are often out of the user's control and may have implications on dose calculation accuracy in certain scenarios. The purpose of this work was to develop an in-house electron MC toolkit that would allow for independent validation of a commercial electron MC TPS and an understanding of the limitations of the commercial TPS.

The accuracy of any MC model depends on the ability to accurately model what is present in real life. One crucial and unknown component of the model that was given priority in this work is the electron spectrum striking the exit window of the linear accelerator. A mono-energetic incident particle beam is not a true representation of the real scenario and cannot achieve sufficient accuracy for MC to be considered a reference for validating a commercial TPS. An optimized incident electron spectrum striking the exit window of the accelerator was determined by weighting mono-energetic electron energies in the form of a continuous distribution. The optimum spectrum for a given therapy beam energy was determined by minimising the difference between simulated and measured percent depth dose (PDD) data from Elekta Synergy and Agility therapy accelerators for multiple fields and source to surface distances (SSD). Spectra were initially determined without applicators present and thereby removed a significant variable in modelling. The accelerator head components that are shared between beam energies were kept constant to ensure accurate representation.

Results using optimized energy spectra matched measured PDDs to within 1%/1 mm except for the first 5 mm. Measured and calculated profiles and output factors were within 2% for all fields and five energies. Spectra were then applied with electron applicators present with resulting PDDs maintaining the same accuracy. Profiles were within 1%/1 mm agreement in the clinical field for SSDs 100 and 110 cm and applicator factors to less than 3%. MC simulation profile results showed improvement over Elekta Monaco 5 TPS electron models particularly in large fields and the build-up region. Improvements were also observed when simulating dose on CT datasets due to the user's greater ability to control voxel sizes and particle repetitions.

This effect was particularly pronounced in geometric surface variations and distinct inhomogeneity boundaries.

Discrepancies and limitations with the current MC modelling ability were discovered by implementing identical shared components when developing models. A design flaw was discovered with the BEAMnrc MLCE module where particle collimation does not appropriately collimate the beam throughout the module. A solution was implemented and reduced BEAMnrc model output errors from 5% to 2% without the use of any correction factors. The APPLICAT module was determined to not sufficiently model applicators to the required standard. The inclusion of applicators into the beam models resulted in underestimation of dose delivered up to 3% and was proportional to applicator size. The applicator misrepresentation used in Monaco 5 and BEAMnrc models results in dose prediction errors for the 6 cm × 6 cm and 10 cm × 10 cm applicators, increasing in magnitude with increasing distance from 100 cm SSD. The 6 cm × 6 cm applicator was found to be most susceptible resulting in output error predictions of -2% to 4% over SSDs 97 to 105 cm respectively.

To achieve the level of accuracy required to be considered a gold standard, MC models require accurate representation of the linear accelerator, appropriate incident spectrum and refinements in modelling. The independent beam model development process has proven vital in determining limitations in current electron beam modelling that would otherwise remain undetected. Currently, Elekta electron MC models do not meet the gold standard as correction factors are required to correct for absolute dosimetry predictions. If sufficient effort and refinements are made, in-house MC models can produce superior relative dosimetry results compared to commercial TPSs due the greater control over the end-to-end dose prediction process with the disadvantage of increased calculation time. An in-house, independent electron MC dose calculation toolkit has proven a valuable tool in validating the performance and understanding the limitations of Elekta's electron MC TPS, Monaco 5.

II.Declaration

I certify that this work contains no material which has been accepted for the award of any other degree or diploma in my name, in any university or other tertiary institution and, to the best of my knowledge and belief, contains no material previously published or written by another person, except where due reference has been made in the text. In addition, I certify that no part of this work will, in the future, be used in a submission in my name, for any other degree or diploma in any university or other tertiary institution without the prior approval of the University of Adelaide and where applicable, any partner institution responsible for the joint-award of this degree.

I give permission for the digital version of my thesis to be made available on the web, via the University's digital research repository, the Library Search and also through web search engines, unless permission has been granted by the University to restrict access for a period of time.

I acknowledge the support I have received for my research through the provision of an Australian Government Research Training Program Scholarship.

Signature: ……

Date: 3/3/2019

III. Acknowledgments

I would like to thank the University of Adelaide for giving me the opportunity to conduct the research undertaken. Special thanks to Judith Pollard who has been invaluable with her support and understanding without which this would have not been possible. I would like to thank Scott Penfold and Timothy Crabtree for their assistance and conversations with project difficulties along the way.

I would like to thank the Townsville Hospital and Health Service for the use of the Cancer Centre and medical devices required to perform the research undertaken. I would like to thank our Director of Physics Louis Fourie for his support and encouragement. I would like to thank my colleagues for their support which certainly made a positive difference to my work environment. I would like to acknowledge David Scott for his much appreciated assistance setting up the BEAMnrc server and general support throughout. I thank Elekta limited global support M.Kalaiselvi for his assistance with beam model enquiries. I would like to thank our local Elekta service engineer Thomas Brostrom for his hours of assistance performing non-routine measurements.

Lastly, I would like to thank my friends and family for their support through the long years. Special thanks to my partner and children through this tough and testing time for supporting me and it will be remembered as a significant milestone.

Sincerely,
Robert Crane

Table of Contents

List of Abbreviations

3D	three-dimensional
AF	applicator factor
BLD	beam limiting device
CT	computed tomography
ECUT	electron transport cut off energy
EGS	electron gamma shower
FWHM	full width at half maximum
GUI	graphical user interface
HU	Hounsfield unit
MC	Monte Carlo
MLC	multileaf collimator
MU	monitor unit
NRCC	National Research Council of Canada
OF	output factor
PBA	pencil beam algorithm
PCUT	photon transport cut off energy
PDD	percent depth dose
PDI	percent depth ionisation
RED	relative electron density
RMS	root mean square
RMSE	root mean square error
SSD	source to surface distance
SSS	spectrum scanning script
STP	standard temperature and pressure
TPS	treatment planning system

Figures

Tables

1. Introduction

1.1. History of Radiation

Since the discovery of X-rays in 1895 by Wilhelm Conrad von Röntgen, the application of radiation to the medical industry was set into motion. In 1903, only eight years after the discovery by Röntgen, external beam radiation therapy was used for the treatment of cancer by Dr Charles L. Leonard.

Ionizing radiation has since been established in the management of cancer in the field known as radiation therapy. The aim of radiation therapy is to deliver doses of radiation to a defined tumour volume while minimising unwanted dose to surrounding healthy tissue. This achieves the optimum chance of treatment success while minimising future complications.

Today, advances in technology and knowledge in radiation therapy have allowed for different treatment methods and regimes to optimise success in the treatment of specific cancers. Various ionizing radiation types and apparatus have been developed each with their own unique physical properties, such as photon, electron and heavy ion particle therapies.

Radiation therapy requires the ability to accurately predict and reliably deliver the required treatment to be successful. Treatment planning systems (TPS) are utilised for designing individualized patient plans by predicting the dose distributions and determining the amount of radiation required. This requires significant knowledge of the physical properties of the ionizing particle and its interaction processes with matter creating multiple unique treatment methodologies.

1.2. Motivation for Study

The motivation for this study is provided by the Townsville Cancer Centre upgrading from the electron pencil beam algorithm (PBA) that was implemented in 2009 with no absolute dose prediction capability to the state of the art commercial Electron Monte Carlo (MC) TPS offered by Elekta, Monaco 5. With the new abilities of the commercial TPS compared to the predecessor, the hospital requires a new method to verify treatment plan accuracy and absolute dose prediction. This provided the opportunity to revise and improve in-house BEAMnrc MC models that used mono-energetic incident particles with minimal model refinement.

This in turn can be used to help commission Monaco 5 under conditions where measurements are difficult or time consuming. With the improvement in in-house MC models and the development of an independent TPS providing the ability to simulate on computer tomography (CT) datasets, monitor unit (MU) verification should be possible under near identical geometries to ensure the best possible dose verification. This allows independent dose distribution comparison if required and provides new capabilities to the hospital.

1.3. Thesis Overview

This thesis describes the development of electron MC models for Elekta's Synergy and Agility radiation therapy linear accelerators for their clinical energies and applicators using the BEAMnrc package. Models were built using specifications of the linear accelerator head supplied by Elekta under a nondisclosure agreement. BEAMnrc simulation results reproduced the relative and absolute dosimetry properties from measured data, meeting the 2% dose or 1 mm distance to agreement criteria. Further effort determined the mechanisms responsible for the dose differences and improved the model dose distributions to a tighter tolerance of 1% or 1 mm.

The history, progression and limitations of algorithms implemented through the years of electron radiation therapy are discussed in Chapter 2. It details the development of the MC BEAMnrc package used by medical physicists to model linear accelerators.

Chapter 3 specifies data collection methods and datasets acquired from linear accelerator measurements during commissioning where linac measurements were used to build the electron beam models. A basic description of the electron beam model using BEAMnrc is given. Data extraction and manipulations are specified from completed BEAMnrc and Monaco 5 models. The extracted data is to be used to determine model accuracy.

A key critical variable in creating an accurate model representation of the accelerator is the ability to determine the electron spectrum exiting the waveguide and striking the exit window of the linear accelerator. The spectrum determined needs to be a solution to all applicator fields for the specific nominal beam energy. Spectra determination requires a complex numerical approach as there is very little information that has been measured and reported. Chapter 4 describes the development and process

of a script to numerically determine the incident electron energy spectrum striking the exit window for the BEAMnrc models. Initial BEAMnrc model results using the determined spectrum are summarised.

The accelerator system to be modelled using MC methods can be considered a linked variable system, as each component can individually be varied in multiple ways in order to achieve the same result. By using an appropriate spectrum any resultant BEAMnrc simulation discrepancies are due to component specifications or incident particle specific parameters. Components that are shared between energies (i.e. exit window and scattering filters) must remain identical in order to create models that are as realistic as possible. This allows a more complex ability to interrogate and improve the models as it reduces the variability among components which should achieve a more accurate and robust model.

It is hypothesised that BEAMnrc models and spectra that are developed from measured data without applicators present can be directly applied to the fields with applicators and maintain their accuracy. This ensures accurate jaw and field size during modelling while also removing a major component (applicators) that may have a significant influence on modelling. Chapter 5 discusses the BEAMnrc model refinement process and reports discrepancies observed and solutions implemented where possible. The Gamma method used to determine model accuracy is described and data processing techniques performed before analysis is explained. The effects of introducing applicators into models are discussed and an example of relative and absolute results achieved with standard applicator inserts is shown.

Chapter 6 shows an example of relative and absolute results from Monaco 5 for standard applicator inserts. Chapter 7 compares the overall accuracy of BEAMnrc models against Monaco 5 models with standard applicators. All beam models were then investigated under conditions outside of the scope of data they were developed with by introducing shaped insert cutouts, geometric variations and heterogeneous mediums. Determined spectra from Monaco 5 and BEAMnrc are compared to observed variations in distributions used to obtain the reported model results.

Developed beam models were simulated utilising patient CT datasets to determine their agreement with Monaco 5 and report inherent limitations on the commercial and in-house treatment planning systems. Chapter 8 describes the development of an independent treatment planning system utilising BEAMnrc and

DOSXYZnrc. This enables the direct comparison against Monaco 5 using patient CT datasets. This chapter also discusses the advantages and disadvantages of both planning systems and various effects affecting the ability to accurately predict dose.

Chapter 9 discusses the overall trends and errors observed during BEAMnrc modelling and the limitation imposed on developed electron beam models. Particular attention was dedicated to investigating output result discrepancies for the Agility accelerator by BEAMnrc and Monaco 5 beam models.

Final conclusions and plausible theories for the discrepancies and limitations on current Elekta Monte Carlo beam models are reported and plausible solutions to be further investigated are summarised in Chapter 9.

2. Background and Literature Review

2.1. Evolution of Electron Dose Prediction Methods

Electron radiation therapy offers a unique dose distribution that cannot be achieved by other therapy methods. In contrast to photons, electrons have a finite range in matter due to the negative coulomb charge of the particle, allowing optimal treatment of proximal tumours to depths of 6 cm. This permits treatment of proximal target areas while leaving critical organs or structures distal relatively unaffected. A comparison between photon and electron percent depth dose (PDD) curves is shown in Figure 2-1.

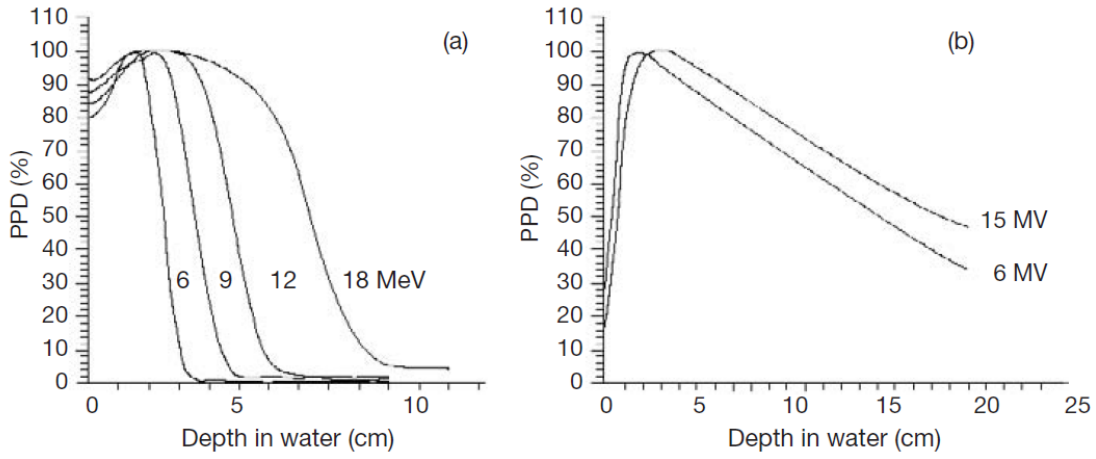

Figure 2-1 Comparison between (a) Electron and (b) Photon Percent Depth Dose Curves for Varying Energies (Podgorsak 2005)

The electron PDD curve has several dosimetry properties that describe the beam as shown in Figure 2-2 and summarised as follows:

D_m is the maximum dose, which occurs at depth R_{100}. The maximum dose is normalised to 100% in PDDs

D_s is the surface dose, measured at a depth of 5 mm

R_{85} is the therapeutic range given by the 85% dose

R_{50} is the depth of 50% dose

R_p is the practical range, the intercept of dose drop off with the bremsstrahlung dose

D_x is the dose due to bremsstrahlung radiation

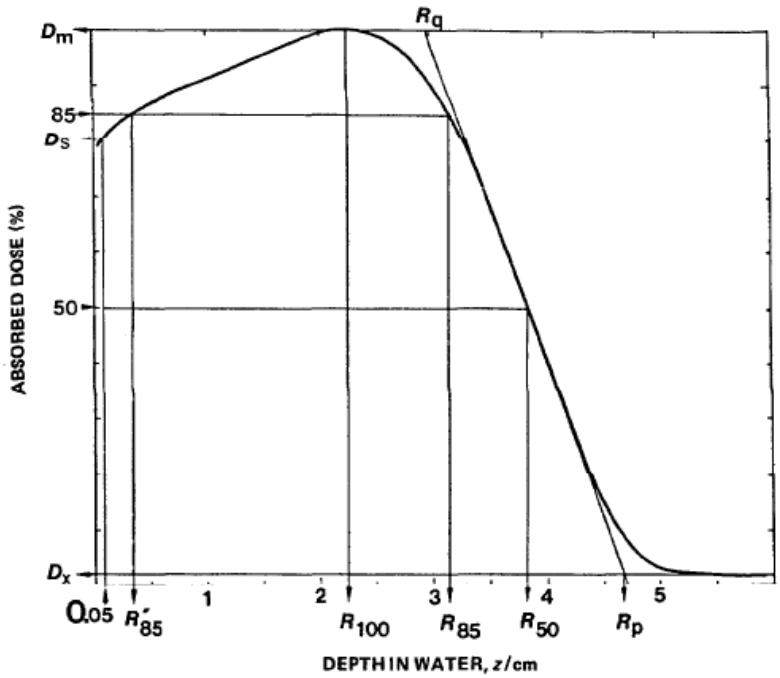

Figure 2-2 Depth vs. absorbed dose distribution (ICRU 1984)

Electron beam therapies became possible around the 1940s with the invention of Van der Graaff generators and betatrons. Van de Graaff generators were used for the first megavoltage electron treatments, however due to their limited maximum energy betatrons became preferred as they reached maximum energy between 5 and 30 MeV. Initial electron physical properties including the designs of scattering foils and dosimetry measurements, procedures and clinical studies were performed on betatrons. Linear accelerators became dominant from the mid-1970s (Hogstrom & Almond 2006).

As the application of electron therapy developed, so did the need for treatment planning systems and their ability to accurately predicted dose. Multiple dose prediction methods were developed across institutions and were based on 1D water geometry. In the 1970s as electron beam therapies were becoming prevalent, the need for regulation and method of dose prediction was recognised. Reviews of electron dose calculation methods were undertaken in the late 1970s (AAPM 1978; Nüsslin 1979) concluding that a pencil beam calculation algorithm was recommended.

Lillicrap, Wilson & Boag (1975) demonstrated that broad beam distributions could be accurately determined by the summation of measured, smaller pencil beam dose distributions. Perry & Holt (1980) developed an algorithm demonstrating how the mean path length of the electron pencil beam could be approximated by the central pencil beam axis. A separate algorithm known as the Hogstrom pencil beam algorithm

(Hogstrom, Mills & Almond 1981) was developed utilising the Fermi-Eyges theory (Eyges 1948). These algorithms improved dose distribution predictions beneath irregular surfaces.

The utilization of CT images on a pixel by pixel basis allowed the ability to model air gaps and curved geometries redefining the individual pencil beams on the patient's surface. Dose in the patient was predicted by summing individual pencil beam doses, which are calculated as if the inhomogeneity structures underlying the beam are infinite in their lateral extent (Hogstrom et al. 1981). In time this was referred to as the two-dimensional PBA as limitations in computational power prevented three-dimensional (3D) calculations. Several groups have evaluated the PBA assessing the accuracy and limitations of the algorithm (Brahme 1985; Mah, Antolaki, Scrimgert & Battistas 1989; Mellenberg 1984). They arrive at similar conclusions that the PBA was accurate for determining dose distributions in the presence of inhomogeneities, except where the anatomy changes rapidly along the longitudinal axis of the patient. The exclusion of longitudinal knowledge in the algorithm led to poor distribution accuracy. This is especially the case for high density heterogeneities and accounting for air-tissue interfaces that are long and parallel to the beam (Mah et al. 1989).

Further development and computing technology advancements allowed the 2D PBA to be extended into the three dimensions (Mah et al. 1989; Starkschall et al. 1991). These were evaluated by multiple groups (Cheng, Harms, Gerber, Wong & Purdy 1996; McShan, Fraass & Ten Haken 1994). While the accuracy of the PBA continued improving, it still had shortcomings. Due to the inability of the Fermi-Eyges theory to predict large scattering angles, it resulted in narrower pencil beam widths and penumbras increasing the dose distribution error in regions of varying density. Electrons were also assumed to reach the practical range even after undergoing large angle scattering, offsetting the effects from large scattering angles predicting dose deeper than what occurs.

Pencil beam algorithms continued to improve on limitations in lateral discontinuities and depth by redefining the PBA properties (mean energy, planar fluence and mean angle) continually with depth (Jette 1996; Shiu & Hogstrom 1991). This was known as the pencil beam redefined algorithm (PBRA), however it was still unable to account for large angle scattering (Shiu & Hogstrom 1991). The PBRA ability to predict dose distributions was investigated and was found to improve dose

distribution agreement over the preceding algorithm. It was not able to achieve dose accuracy within 4% or distance to agreement of 2 mm over all data points, however these were under conditions that were unlikely to be seen clinically (Boyd, Hogstrom & Starkschall 2001). Further improvements in dose distribution prediction would be possible if the PBA used a poly-energetic spectrum instead of the current mono-energetic source (Boyd, Hogstrom & Rosen 1998).

Pencil beam algorithms have earned their place in today's world however focus has trended towards the use of MC methods. MC can be described as computationally mimicking natural environments by its governing laws of physics to come to a statistical convergence. In this sense, the macroscopic solution of a system can be determined by its microscopic interactions.

A MC algorithm was first proposed by Mackie & Battista (1984) who proposed pre-calculated kernels to reduce computation time. Neuenschwander and Born developed a macro MC using pre-calculated kernels (Neuenschwander, Mackie & Reckwerdt, 1995; Neuenschwander & Born 1992) while Keall and Hoban developed the super MC algorithm using pre-calculated kernels (Keall & Hoban 1996). Kawrakow, Fippel & Friedrich (1996) developed the voxel MC (VMC) that did not use pre-calculated data but made assumptions about electron interactions to reduce calculation times by up to a factor of 35. Since their implementation in treatment planning, MC methods have become the "gold standard" for solving radiation transport in three dimensional scenarios.

2.2. Monte Carlo Methods and BEAMnrc

The development of the MC particle transport code came about from the research of high energy electrons and photons at the Stanford Linear Accelerator Center (SLAC). The most commonly used code today, 'EGSnrc', used the electron gamma shower (EGS) developed by the National Research Council of Canada (NRCC) and originally created to optimize and validate calorimeters used with ionizing radiation (Ford & Nelson 1978). In 1985 the fourth and current version, 'EGS4', was released as an open source to the public. The EGS code was extended to lower energies allowing the code to be utilised by medical physicists (Nelson, Hideo & Rogers 1985).

To apply this code to medical linear accelerators, the NRCC in conjunction with the Ottawa Madison Electron Gamma Algorithm (OMEGA) project developed the code

'BEAM' which was released in 1995 (Roger, Faddegon & Ding 1995). The BEAM package was upgraded to BEAMnrc currently used today with the inclusion of the updated EGSnrc user package, allowing significant improvements in radiation transport by improved low energy interaction cross sections, new multiple scattering theory and improvements in the calculation of energy loss (Kawrakow & Rogers 2011).

BEAMnrc allows the simulation on a virtual linear accelerator built from the individual components with their respective physical parameters and material properties that make up the accelerator's head. The source particles are simulated from an origin with specific initial parameters (Rogers, Walters & Kawrakow 2011). The MC method repeats the particle simulation process storing the information at an end plane known as the phase-space. The phase-space file stores the information of each individual particle that reached the end plane and can be further projected onto another structure. The DOSXYZnrc program as part of BEAMnrc package allows the simulation of the phase-space files onto a user designed phantom or supplied CT dataset that enables the calculation and extraction of dose (Walters, Kawrakow & Rogers 2016).

For MC algorithms to be accepted as the 'gold standard', specific knowledge of the linear accelerator is required. The head of the accelerator contains all the components that are responsible for the production, scattering and collimation of ionizing radiation. These specifications are often very hard to obtain because manufacturer companies regard them as sensitive information. As well as the physical properties, little information is known about the theoretical characteristics that greatly influence the simulation. These include the properties of the electron spectrum exiting the waveguide and the effects of the beam transport system on electron beam emittance to focus the electrons on the accelerator head. Without adequate knowledge of the head and beam properties, modelling an accelerator is nearly impossible.

With accurate accelerator head specifications, discrepancies in the build-up region were observed and were a topic of debate for several years. It has been shown for some linear accelerators that using a mono-energetic electron source has been insufficient in accurately matching data from measurements (Bjork, Knoos & Nilsson 2002; Kok & Welleweerd 1999). Incident electron spectrum properties have been investigated to determine their effect on dose distributions, however none account for the under predicted dose in the build-up region (Bjork et al. 2002). Chetty et al. (2007) claimed that to obtain a solution to the PDD dose build-up discrepancy, a detailed

knowledge of the detector response to electron beams was required. In conjunction with small alterations to head components, simulation results could agree within measurement and simulation uncertainties. Efforts to obtain improved agreement gave rise to the multiple source method which analyses phase space files produced by linear accelerator head simulations (Ma et al. 1999). Direct and indirect particles are tracked from their origins to the phase-space plane storing information on their trajectory, energy and fluence. Virtual sources can be created to mimic individual accelerator model components producing similar particle fluences and properties. A beam model can then be created using contributions from each virtual source to fit supplied data.

If MC is to be accepted as the 'gold standard', beam models should surpass the requirements of 2%/1 mm to agreement to measured data suggested by Antolak, Bieda & Hogstrom (2002).

3. Data Collection and Processing

3.1. Linear Accelerator Measurements

Electron beam data was collected during commissioning for a newly installed Elekta Agility linear accelerator and was re-collected for an existing Synergy linear accelerator as the department had access to newer detectors since its original commissioning. Both accelerators have clinical nominal beam energies of 6, 8 10, 12 and 15 MeV with applicators 6 cm × 6 cm, 10 cm × 10 cm, 14 cm × 14 cm, 20 cm × 20 cm and 25 cm × 25 cm, apart from the Agility 25 cm × 25 cm as it was considered to not be required clinically. Beam data was collected as per the Elekta Monaco electron beam data requirements. Data was acquired using a PTW 3D water tank scanner with multiple detectors. Profiles were acquired using an electron diode (PTW Type 60017) to ensure the best spatial resolution while PDDs were collected with an Advanced Markus (PTW Type 34045), Roos parallel plate ionization chamber (IBA PPC40) and an electron diode. Multiple detectors were used for PDDs to ensure there was no spatial resolution limitation or energy dependence in the data required for model development and to assist discrepancy investigations discussed later. Outputs were acquired using the Roos, Advance Markus ionization chamber and electron diode depending on the field size to ensure minimal volume averaging.

Collected data consisted of open field (without applicators present) measurements for 4 fields with beam limiting devices (BLD) ranging from 8 cm to maximum 40 cm. Profiles and output factors were taken in air using an electron diode over the range of 70 to 90 cm SSD. With applicators present, eight inplane and crossplane beam profiles and PDDs were taken for each clinical energy and applicator at SSDs of 100 and 110 cm. Profiles were acquired at depths ranging from 5 mm under the water's surface to 1 cm past the practical range. Output factors (OF) for applicators with standard inserts, known as applicator factors (AF), were measured for each energy/applicator for SSDs of 100 and 110 cm and were normalised to the 10 cm × 10 cm applicator at 100 cm SSD.

The movement speed of the mechanical arm of the 3D scanner tank was reduced to 5 mm per second to minimise waves generated by the resonant frequency of the bar pushing the water in the A-B, left/right direction. This was particularly important for low dose profiles due to the high dose gradient with depth in the PDD. This

significantly reduced variation in the profile data with depth. Profile measurement points were spaced at 4 mm inside and outside the field size and 2 mm over the penumbra for open fields. With applicators included, the step size was reduced to 1 mm in the penumbra region and 3 mm for regions of high dose and low gradient.

Data was processed through PTW software Mephysto: profiles were centred by their 50% dose levels, symmetrised and smoothed once using a least-squares algorithm. Any additional smoothing in the Mephysto software was avoided, as it reduced the sharp dose gradients, broadening the penumbras. The penumbra broadening removed the spatial resolution advantage of using a diode. Percent depth ionisation (PDI) measurements were converted from ionisation to dose using the stopping power ratio of air to water as a function of depth and smoothed once. Data was then interpolated to 1 mm spacing. Collected data was then submitted to Elekta to build the Monaco TPS beam models. The data also served to verify both the Elekta TPS and in-house BEAMnrc MC models.

Additional open field beam energy and applicator specific data was collected for the in-house MC models as initial profile and absolute dosimetry simulation results were not agreeing with measured data. Extra measurements for each energy and applicator field size consisted of open field PDDs, profiles and outputs where applicators were not present. Measurements were taken at 80 cm SSD and depths of dose maximum and 50% dose levels as well as PDDs and outputs at 80, 90 and 100 cm SSD. Open field measurements were required to ensure accurate jaw positions and their absolute outputs without the influence of the applicator. 80 cm SSD profiles were chosen so that they could be fully obtained whereas at 100 cm they would be outside the range of the scanning tank. For MC purposes, the shorter SSD reduced the simulation times because relative field size dimensions are scaled down. This also saves simulation times as fewer particles are required for the same uncertainty as that for 100 cm SSD.

3.2. Linear Accelerator Beam Models

3.2.1. Representation in BEAMnrc Package

MC simulations require an accurate representation of the environment in order to produce simulation results comparable with reality. If the fundamental interactions of the particles are well understood and the environment is precisely modelled, the

results will converge on the true solution. If the represented system in MC does not adequately match the true environment, the accuracy of the result diverges from the true solution by the influence and significance of the misrepresented sections. To minimise the uncertainty in MC results, the linear accelerator head should be modelled as accurately as possible. Figure 3-1 shows an overview of the first stage linear accelerator head modelled in BEAMnrc to the MLC where components and modules do not vary with applicator selection for a given beam energy.

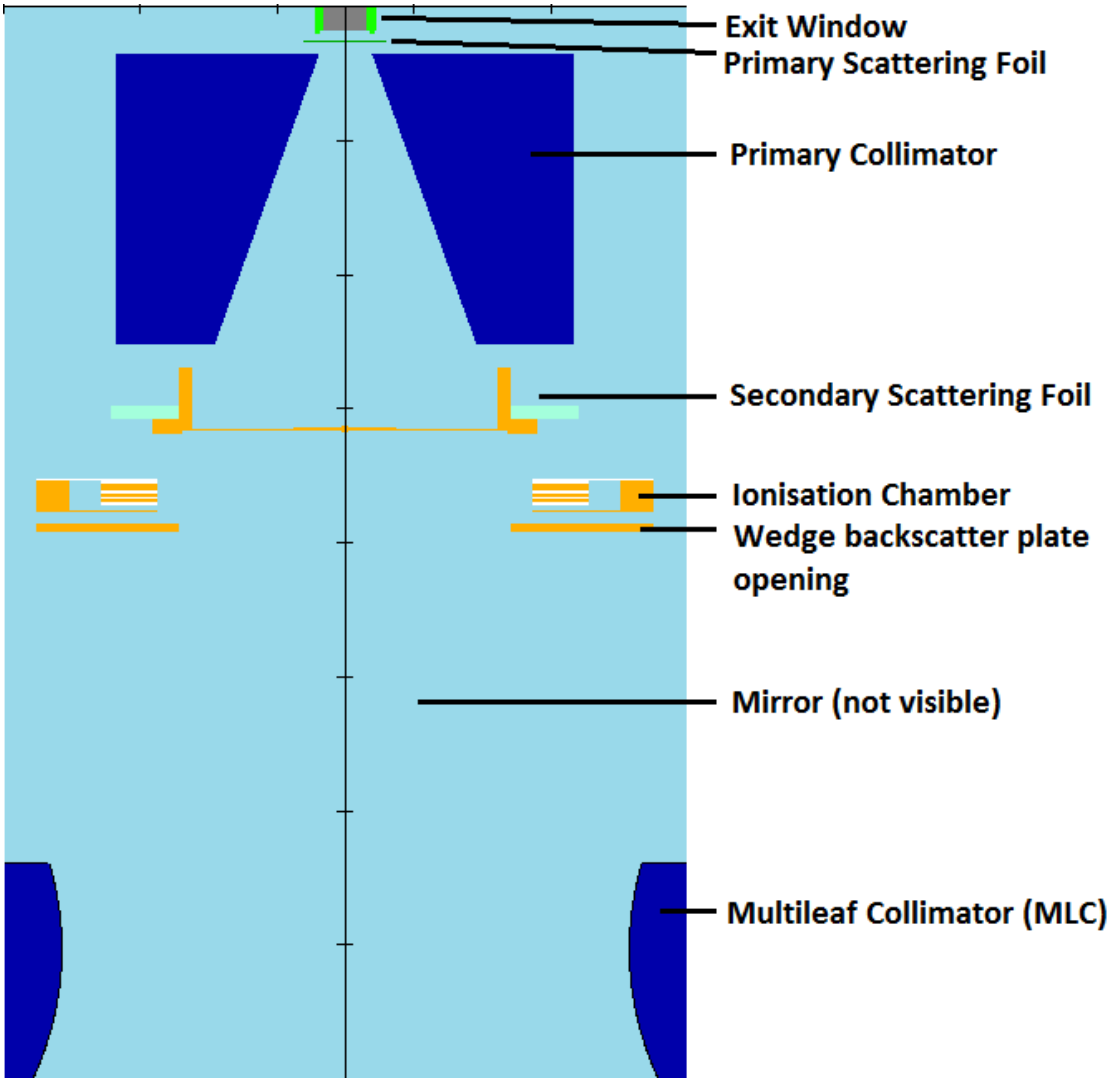

Figure 3-1 Diagram of BEAMnrc modelled linear accelerator head from the exit window to the level of the MLC.

MC simulation transport parameters were kept consistent across all energies, applicators and accelerator models. Specific parameters used in this thesis are shown in Figure 3-2. The electron and photon simulation is terminated below the global electron

(ECUT) and photon (PCUT) cut off energies. These were set to low values of 0.521 and 0.01MeV respectively to accurately account for their low energy contributions to the dose distribution. These settings were kept consistent in the BLDs such as the primary collimator, multi-leaf collimator (MLC) and jaws to ensure accurate low energy scattering conditions. As a result, simulations times were increased but this was required to ensure any simulation dose distribution discrepancies were not due to a lack of low energy particles. The remaining parameters were assessed for their effect on PDD prediction. After having been found to have no impact, were left at the default values.

```
:Start MC Transport Parameter:

 Global ECUT= 0.521
 Global PCUT= 0.01
 Global SMAX= 1e10
 ESTEPE= 0.25
 XIMAX= 0.5
 Boundary crossing algorithm= EXACT
 Skin depth for BCA= 0
 Electron-step algorithm= PRESTA-II
 Spin effects= On
 Brems angular sampling= Simple
 Brems cross sections= BH
 Bound Compton scattering= On
 Compton cross sections= default
 Pair angular sampling= Simple
 Pair cross sections= BH
 Photoelectron angular sampling= Off
 Rayleigh scattering= Off
 Atomic relaxations= On
 Electron impact ionization= On
 Photon cross sections= xcom
 Photon cross-sections output= Off
```

Figure 3-2 BEAMnrc simulation transport parameter settings

To allow comparison of dose variation between applicators and over a range of SSDs, the same number of BEAMnrc incident particles was used for each applicator. This was achieved by placing the phase-space below the MLC where components remain unchanged irrespective of applicators selected. This phase-space file was then projected onto the second stage of the model containing the jaws and applicators. This allows dose comparisons between simulations as the dose results determined by DOSXYZnrc are normalised to the number of particles simulated in the initial BEAMnrc simulation and not the number of simulated particles defined in DOSXYZnrc. For example, doubling the number of particles in the initial BEAMnrc stage would result in double the absolute dose from DOSXYZnrc. However, doubling the number of particles simulated in the DOSXYZnrc stage would only reduce the dose uncertainty and not increase the absolute dose.

BEAMnrc modules were designed to represent reality to the best of their ability. To reflect this, selected components were modified from their standard application in BEAMnrc. The secondary scattering foil was adjusted from the standard specifications to include surrounding material that was supplemented with physical measurements of the carousel as shown in Figure 3-3 a) standard module and b) modified module respectively. As the diaphragm/jaw module does not allow for curvature, it was modified to mimic curved surfaces. The jaw was reconstructed from four individual jaw modules with varying angles as shown by Figure 3-3 c). Particle boundary cut off limits for each module were extended to the maximum field size irrespective of jaw positions in case transmission and internal component scattering influenced simulation results.

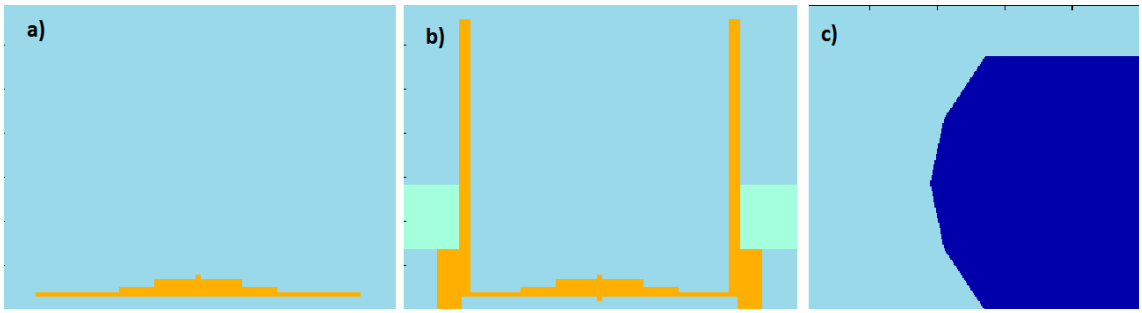

Figure 3-3 Beam model variations from standard specification to better represent the real environment. a) Elekta specifications provided for the secondary scattering foil. b) Scattering foil including surrounding carousel. c) Curved jaws generated from 4 individual jaw modules.

DOSXYZnrc was used to project the phase-space files from BEAMnrc simulations onto desired phantoms to obtain resultant dose distributions. Basic homogenous water block phantoms were used when comparing against scanned data acquired in a water tank. DOSXYZnrc tracks each particle and energy deposited through its interactions resulting in the dose deposition throughout the phantom.

As dose is deposited per particle interaction, the statistical uncertainty depends on the number of interactions in the volume to be analysed. Larger voxel volumes reach lower uncertainties with fewer relative particle iterations however become prone to volume averaging. Volume averaging produces dose estimation errors when sharp dose gradients are encompassed in a single voxel. This averages a small volume of high/low dose throughout the full voxel volume of a different dose amount. Phantoms can be designed in such ways that benefit the individual purpose of the simulation reducing simulation time requirements, this creates three distinct phantom types.

PDD phantoms were designed with a high resolution of 1 mm with z plane (depth) but may span wider in the x/y plane as dose profiles do not vary significantly near the central axis. Since we are only interested in the central region, particles that cannot reach the central column volume are discarded saving simulation time. PDD simulations range between 2 to 6 hours depending on energy and field size.

Profile phantoms were only concerned with dose at a few depths and have a larger resolution (2 mm) in the z plane and higher resolution in the x/y plane. Simulation times for profiles range from 14 to 24 hours as particles were only rejected once they have reached a depth where they no longer influence the deepest profile.

The third set of phantoms used for final applicator simulation results was designed to have high resolution in all dimensions and requires significantly more particles and memory allocation. Simulations times for applicator results range between 18 and 32 hours.

The uncertainty generated by BEAMnrc for each situation was investigated and results were used to determine the best comprise between time and accuracy. Variation of PDD simulation uncertainties with number of incident particles are shown in Figure 3-4. The need for higher PDD accuracy due to the requirement for accurate interpolation meant longer simulations times were required. While PDD simulation times were the shortest of the three options, the number of PDD simulations required for

the developed method was an order of magnitude larger than profile simulations due to all applicator field sizes requiring each discrete energy simulated.

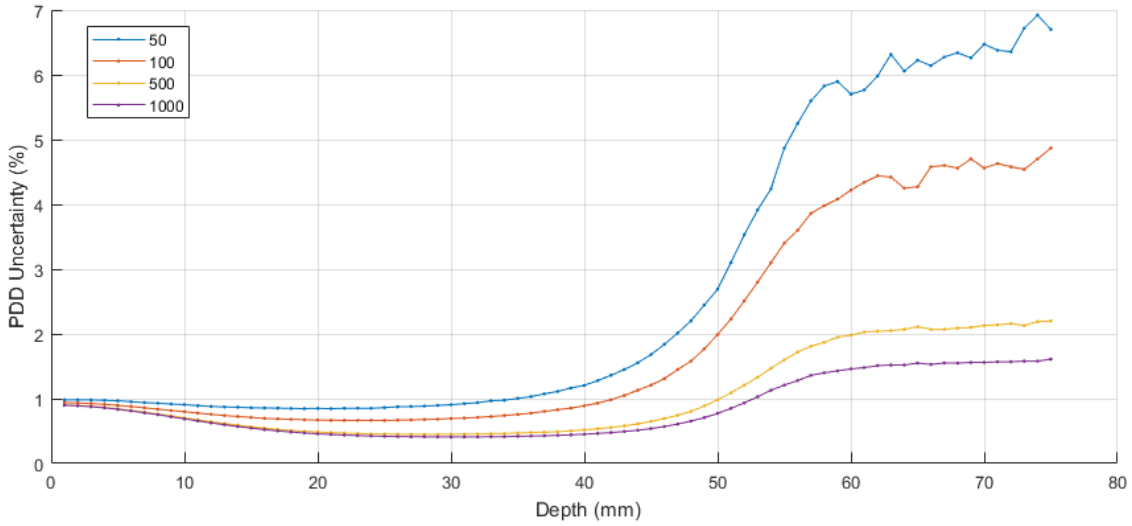

Figure 3-4 Simulated PDD percentage uncertainty with depth for a 10 MeV model for various number of incident particles ($\times 10^6$)

Open field profile simulation uncertainty was also determined and shown in Figure 3-5 at a depth of maximum dose. High profile accuracy was not required as simulation results were representative over a large area and were symmetrised and smoothed when building the models to reduce noise levels. Incident particle numbers for profile simulations were not modified with each field size; this results in higher uncertainties in larger fields compared to smaller fields.

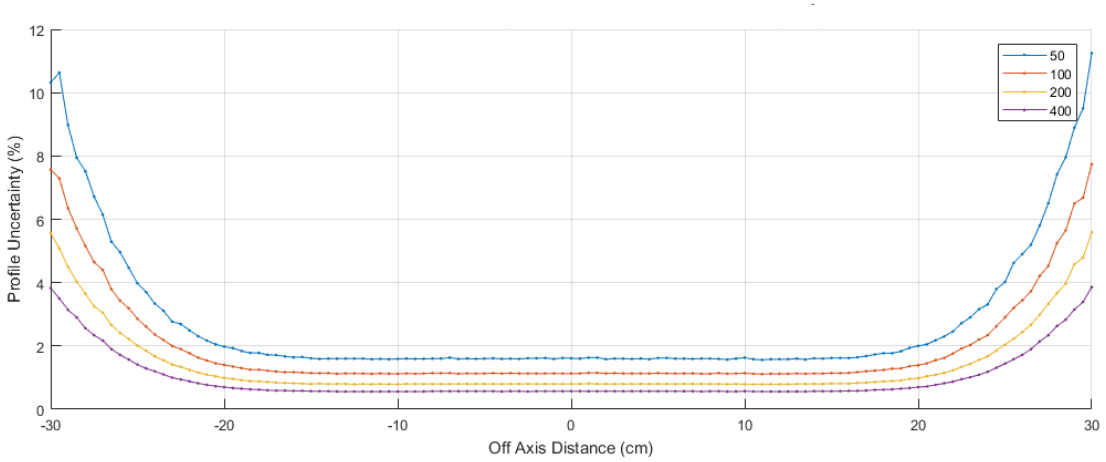

Figure 3-5 Simulated D_m profile percentage uncertainty for a 10 MeV model for various numbers of incident particles ($\times 10^6$)

Final simulations used voxel sizes of 4 × 4 × 1 mm and 0.32 × 0.32 × 1 mm for open field PDDs and profiles respectively. To maintain similar statistical uncertainty the number of incident particles was chosen to be 500 million for PDDs and 800 million for profiles. Final simulations with applicators present had voxel dimensions of 2 × 2 × 1 mm and were simulated with one billion particles. The larger number of incident particles was chosen such that large fields would still have reasonable uncertainty as there are fewer interactions per volume compared to smaller fields. Care was taken to ensure particle recycling from the phase-space file was kept less than 10 times. Simulation transport parameters used for all DOSXYZnrc simulations are listed in Figure 3-6.

```
#########################
 :Start MC Transport Parameter:

 Global ECUT= 0.521
 Global PCUT= 0.01
 Global SMAX= 1e10
 ESTEPE= 0.25
 XIMAX= 0.5
 Boundary crossing algorithm= EXACT
 Skin depth for BCA= 0
 Electron-step algorithm= PRESTA-II
 Spin effects= On
 Brems angular sampling= Simple
 Brems cross sections= BH
 Bound Compton scattering= Off
 Compton cross sections= default
 Pair angular sampling= Simple
 Pair cross sections= BH
 Photoelectron angular sampling= Off
 Rayleigh scattering= Off
 Atomic relaxations= Off
 Electron impact ionization= Off
 Photon cross sections= xcom
 Photon cross-sections output= Off

 :Stop MC Transport Parameter:
 ########################
```

Figure 3-6 DOSXYZnrc simulation transport parameter settings

3.2.2. Beam Model Dose Distribution Data Extraction

BEAMnrc MC simulation models were projected onto a water block phantom in DOSXYZnrc and dose distribution results were extracted using Matlab incorporating a 3D linear interpolation to enable profile extraction at any depth. PDDs, profiles and outputs were taken from each simulation result for each applicator and energy combination. Simulation data did not have any smoothing algorithms applied to allow the assessment of statistical uncertainties and raw result accuracy.

When Elekta's models were developed and returned, the relevant PDD, profile dose distribution and output data were extracted. A block phantom was generated in the planning system and simulations were completed for each model, energy, applicator and SSD combination. Interest points were placed in the phantom at depths coinciding with measurement depths and relevant dose plans were extracted. A Matlab script was developed to cycle through the dose plane files extracting the profiles, PDDs and outputs. In total, approximately 4000 dose plane files were extracted from the TPS. Extracted data was left unmodified to represent the highest level of accuracy achievable by the TPS.

The planning system was investigated to determine what calculation parameters should be chosen to optimise the efficiency for clinical implementation. Final parameters were chosen to be 2 mm grid size with maximum number of histories possible ($1 \times 10^6/cm^2$). This was chosen to achieve a balance between accuracy, noise and calculation time and is discussed in further detail in Section 6.3 and 8.5.

4. Numerical Spectrum Determination

4.1. Background

A significant variable can be removed from the MC modelling environment by determining the electron energy spectrum striking the exit window of the waveguide that represents the true scenario. As relative and absolute dosimetry results are dependent on the energy of the incident beam, the MC system is sensitive to any changes in the energy. With a reliable spectrum and energy fit, any further discrepancies in the model would be due not to the spectrum but to another factor.

An unknown variable possibly constraining the spectra distribution is its energy window. The energy window, if present, is due to the effect of the bending system positioned after the wave guide that removes electrons energies above or below a limit (for a slitless slalom this would be the top and bottom walls of the system). With an energy window variable included in the model, the minimum and maximum energy of the distribution can cut abruptly. If applicable, it would result in shifting the spectrum to compensate for the new mean energy. This adds additional complexity to the task of finding an appropriate spectrum.

To find the appropriate spectrum a systematic numerical method was required. A numerical method of determining a spectrum is based on the ability to determine a solution by combining multiple weighted mono-energetic beams. This requires a coefficient matrix of simulated discrete energy PDDs to be solved against a measured PDD.

The first attempt at determining a spectrum was to find the solution to a system of linear equations. Solutions were not physically possible for an accelerating waveguide as spectra determined consisted of few discrete energies with significant spacing between them with no obvious distribution reasoning.

The succeeding numerical method multiplied the coefficient matrix by varying weighted continuous distributions. The resultant predicted PDD was then compared against the measured PDD, an overall error was determined by subtracting the two and summing the absolute error for each depth along the PDD. Each Gaussian distribution was varied by its defining parameters (mean energy, FWHM, energy window) to find an appropriate spectrum solution. PDDs from the 25 cm × 25 cm applicator were used to

determine a suitable spectrum as it is less prone to PDD variation due to the influence from the jaw and applicator along the central axis of the dose distribution.

4.2. Spectrum Scanning Script

Matlab was used to create the Spectrum Scanning Script (SSS) to cycle through varying Gaussian parameters keeping a history of overall PDD error for the parameter combination. The result produced an error map where the lowest value represents the best fit, shown in Figure 4-1 with maximum error capped at 50.

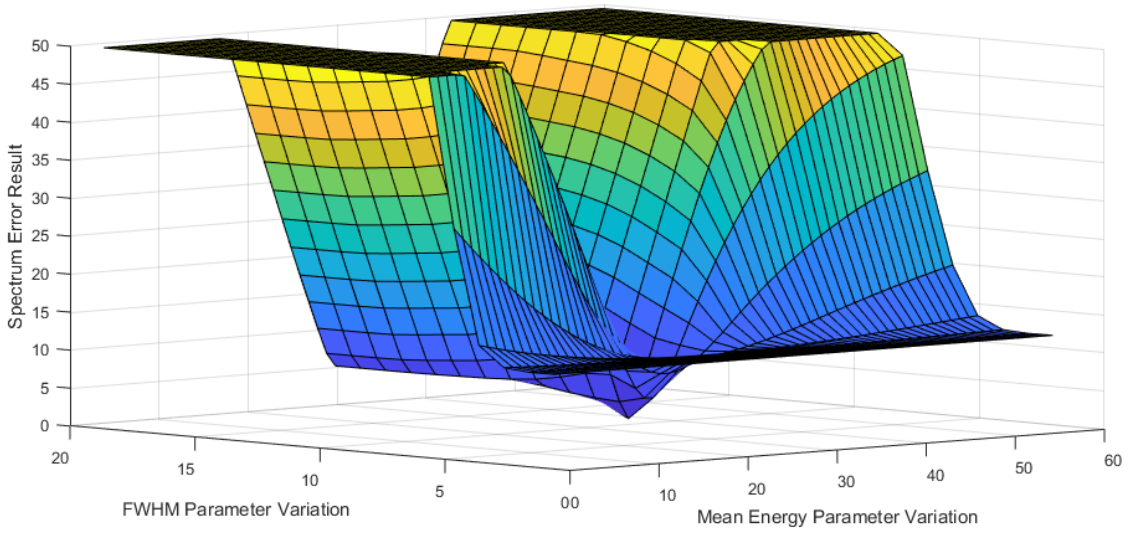

Figure 4-1 Simulated PDD agreement error map with measured data produced by SSS with varying spectral parameters for a set energy window

The SSS could determine spectra that resulted in improved PDD agreement to measurement. While it provided a good fit for the 25 cm × 25 cm field, deviations and loss of accuracy were still observed with the remaining applicators for the same energy shown by Figure 4-2.

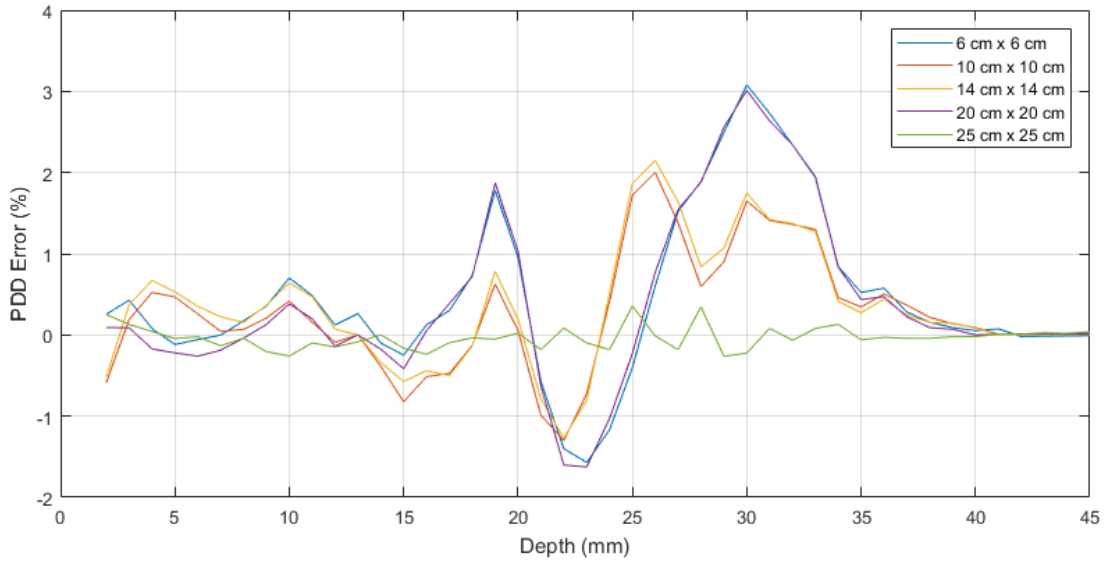

Figure 4-2 6 MeV PDD error using spectrum generated from 25 cm × 25 cm applicator applied to remaining applicator fields

The average error between simulated and measured PDDs produced by this simulation was 0.23% as shown in Table 4-1 which lists the percentage error at each depth for each applicator PDD. The error may be due to choosing one of the vast number of suitable spectra determined by the SSS when only fitting to the 25 cm × 25 cm applicator PDD. A unique solution would look like a gravitational singularity point in Figure 4-1. However, the error map shows a path of minimum error indicating multiple possible solutions with the same effective result.

Table 4-1 Error determination of the simulation

Applicator (cm)	6 × 6	10 × 10	14 × 14	20 × 20	25 × 25	Average
PDD Error	0.31%	0.23%	0.25%	0.30%	0.04%	0.23%

To remove the errors observed across all applicators, a dataset was created for all applicators and a field size 40 cm × 40 cm with no applicator. All coefficient sets were combined in a single large coefficient dataset. This would find a best fit spectrum for the energy across all input PDDs. Combining multiple PDDs reduces the effect of an error in a single PDD as any error would be averaged over the full applicator dataset. To constrain the SSS further, PDDs for multiple SSDs were incorporated in the coefficient dataset. This would allow it to take into account any change of PDD shape

with SSD. This increased the number of PDD simulations required to build the coefficient dataset from five (25 cm × 25 cm applicator with five discrete energy PDDs) to ninety (six field sizes, five discrete energy PDDs for three SSDs).

4.2.1. Coefficient Matrix Interpolation

The coarse input of the coefficient matrix energy resolution may also be a factor hindering the SSS. Limited discrete input energies produce a jagged stepped distribution and may be preventing a satisfactory fit. Increasing the input resolution allowed the SSS to generate a smoother and greater variation in distributions permitting higher spectrum refinement.

The resolution of the coefficient matrix could be increased by two methods: increasing the discrete energy PDDs simulated or interpolating the existing PDDs. Reducing the discrete coefficient matrix energy resolution from 0.5 MeV to 0.25 MeV resulted in a noticeable improvement in the error across the PDDs. This increased the simulation time required to build the coefficient matrix by a factor of two. The need to re-simulate and rebuild the coefficient matrix during the fine-tuning phase of the model would mean the same time would be required to rebuild a new spectrum. A finer resolution would require an unacceptably large time. Time management became a significant priority as the SSS process had to be repeated many times before a final solution was determined.

To reduce the simulation time for the project to become manageable, the number of discrete energies simulated would need to be reduced. This in turn decreases the accuracy in the discrete PDD energy interpolation method. Due to the non-linear relation of discrete PDD energies, a simple spline interpolation method was not able to accurately produce interpolated PDDs. With fewer PDDs to use for interpolation, each PDD required higher accuracy to ensure effective interpolation.

To interpolate between energies to accuracy within 0.25% as shown in Figure 4-4 b), the following process was implemented in Matlab. The input discrete simulated energy PDDs were smoothed using the Savitzky-Golay filter (Savitzky & Golay, 1964). PDDs were normalised to their respective maximum dose, then normalised to their respective depth of 50% dose shown in Figure 4-3 b). The depth R_{50} was chosen over depth of maximum dose as it could be accurately determined to sub-millimetre precision.

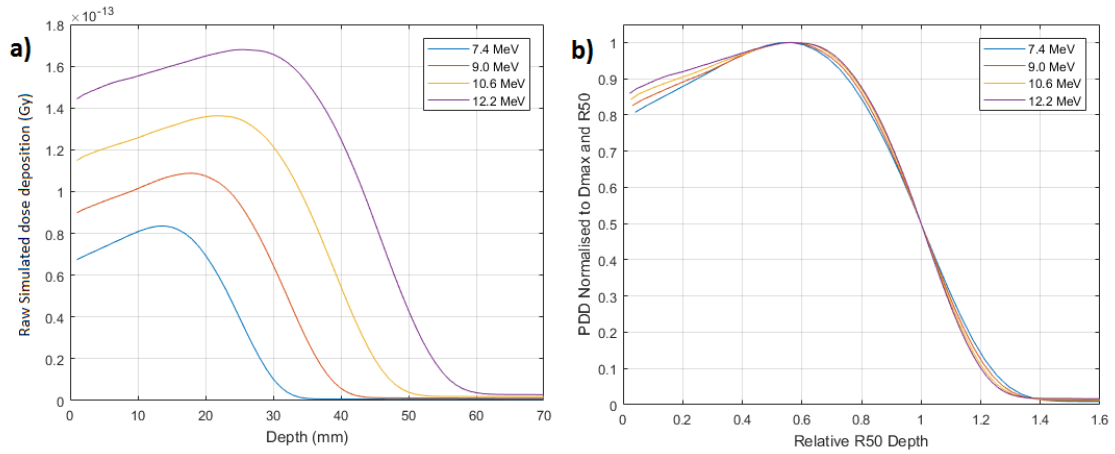

Figure 4-3 a) Four simulated discrete Energy PDDs. b) PDDs normalised to D_m and R_{50} for interpolation

PDDs were interpolated using the spline method for their relative depth. Interpolated PDDs were multiplied by their respective interpolated maximum dose and 50% dose depth, shown in Figure 4-4 a). Initially four discrete input energies were used however interpolated PPDs were prone to errors from noise with few input PDDs. To reduce this effect, the number of input PDDs was increased to five and simulation accuracy was also increased by increasing the number of particles simulated to reduce noise variations.

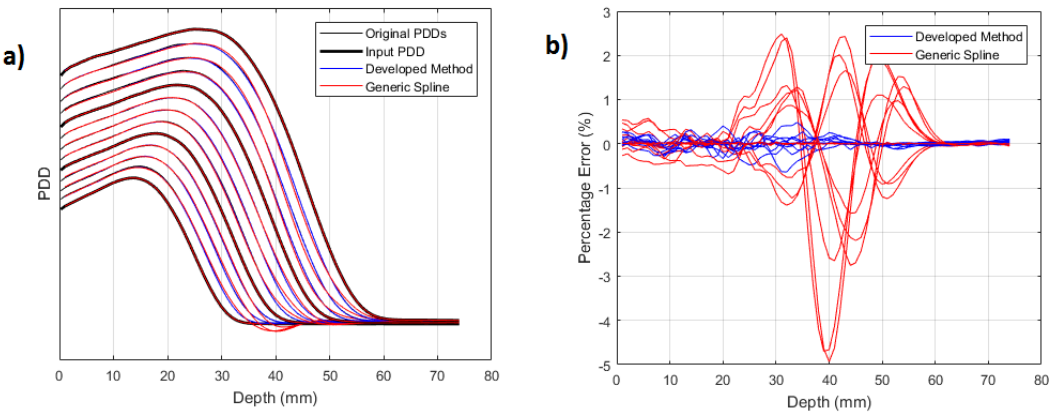

Figure 4-4 Interpolation method comparison. a) PDD interpolation for 13 PDDs with four discrete PDDs in input matrix coefficient matrix b) Interpolation method PDD error from simulated PDDs

With a reliable interpolation method, the simulation PDD input coefficient matrix energy resolution can be reduced as desired. The interpolation method implemented significantly reduced the simulation time requirement without sacrificing PDD accuracy. A high-resolution coefficient matrix allowed an effectively continuous spectrum and removed any uncertainty arising from the prior resolution limited distribution. The variation in resultant spectra determined with different energy resolutions is shown in Figure 4-5.

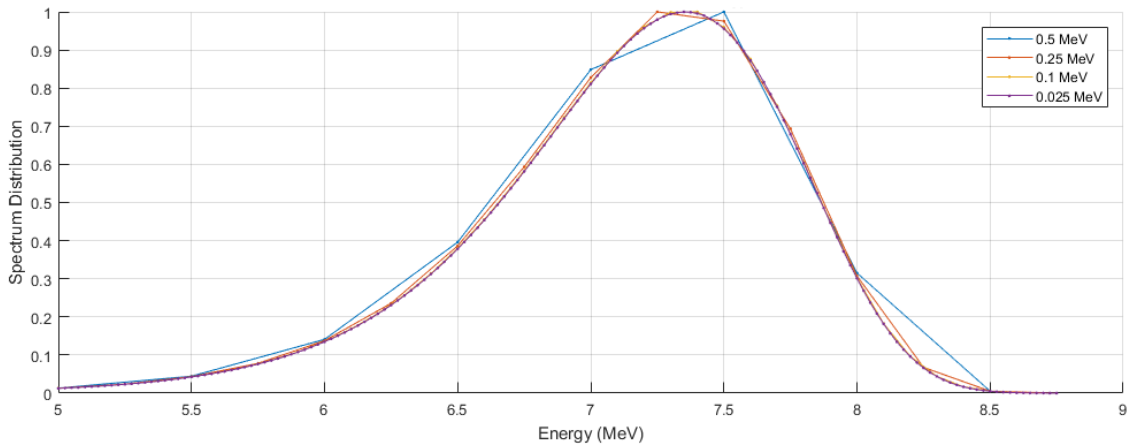

Figure 4-5 Determined Landau distribution spectra for various coefficient matrix discrete energy bin resolutions

4.2.2. Landau Distribution

Using a continuous spectrum, the SSS did not provide satisfactory agreement of simulation PDD with measurement. PDD data still showed a discrepancy in the build-up region and absolute dose accuracy was not within an acceptable range. This was theorized to be due to the limitation of the symmetry of Gaussian distributions. To remove the limitation from the Gaussian distribution a Landau distribution was adopted.

The Landau distribution was inverted on the x-axis to mimic theorised particle distributions exiting the accelerating waveguide to enable a low energy (tail) distribution larger than in a Gaussian distribution. The distribution was further modified with the addition of an exponential variable to enable greater variability in the head and tail contributions. The spectrum variations available now covered most possible single peak distributions, thus incorporating all possible Gaussian distribution variations over all FWHMs, mean and peak energy as well as applying an energy window.

4.2.3. Spectrum Refinement

Since the interpolation method can maintain accuracy during interpolation, the final energy resolution was chosen to be 0.025MeV. This was decided as it produced the finest practical resolution that BEAMnrc would accept. The variation in determined spectrum for a 6 MeV electron beam incident on the exit window is shown in Figure 4-5 for resolutions 0.5, 0.25, 0.1 and 0.025 MeV. The SSS refines the spectrum by cycling through the following variables in the order of energy window, tail drop off rate, FWHM and mean energy. By storing the error from each iteration for each variable, it produces a 5-dimensional error matrix. Each of these variables is discussed further in this section.

If present, an energy window will affect the minimum, maximum or both energy limits of the distribution. The SSS steps through increasing the minimum and decreasing the maximum energy while storing the overall error for that window. When cycled through all windowing options, it produces a 2D error map shown by Figure 4-6.

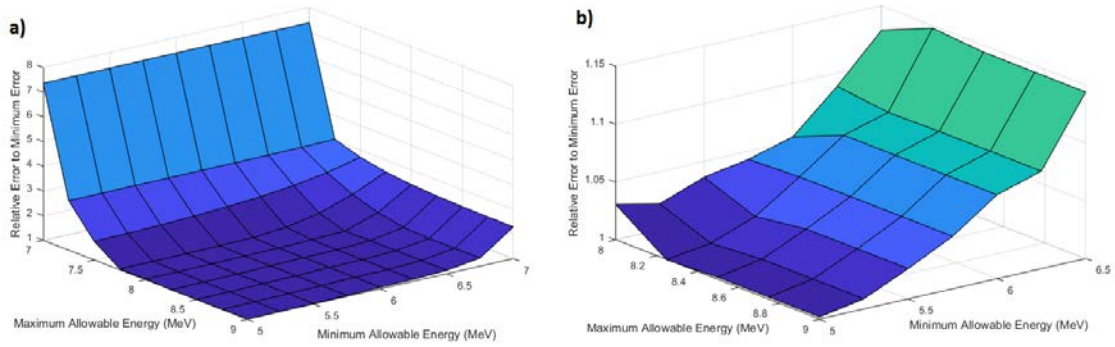

Figure 4-6 PDD error map varying minimum and maximum energy window limits. a) Relative Error Map over full energy Range. b) Zomed in flattened region of a)

The flattened region in Figure 4-6 shows that the SSS can find suitable spectra within a certain energy span range. This indicates a spectrum for a given energy window can be determined to give similar results within a range of set energy windows. Figure 4-6 b) shows the minimum energy window has immediate effect while maximum has a range limit before it impacts on solution accuracy. The spectra determined for selected windowing cases above are shown in Figure 4-7 and Figure 4-8 where the minimum and maximum window respectively was restricted. Figure 4-9 shows determined spectra with varying minimum and maximum energy restrictions.

The spectra shown in Figures 4-7 to 4-9 produce overall solution accuracies to within 5% of the best spectrum overall PDD error of 1.8228.

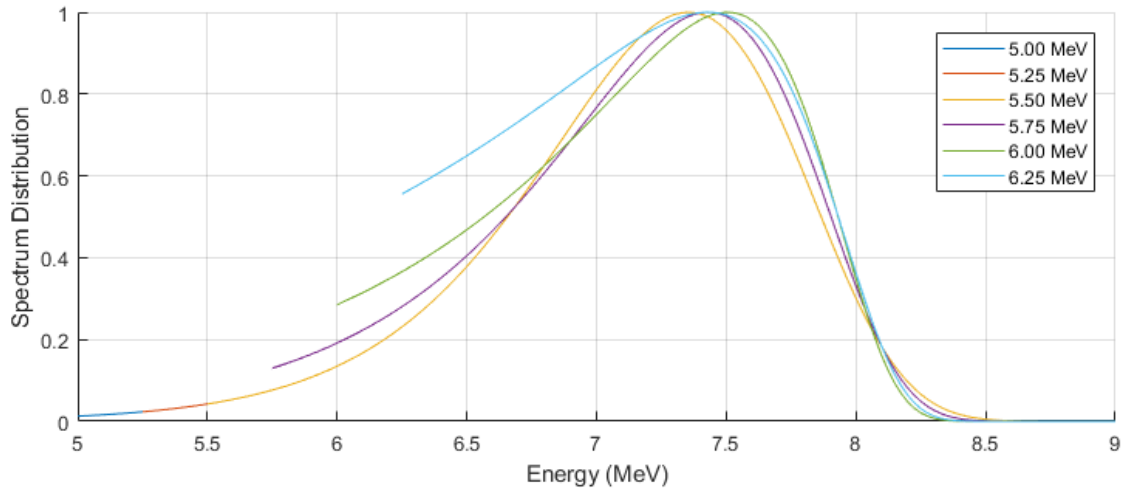

Figure 4-7 SSS determined optimal spectra when increasing the minimum energy limit

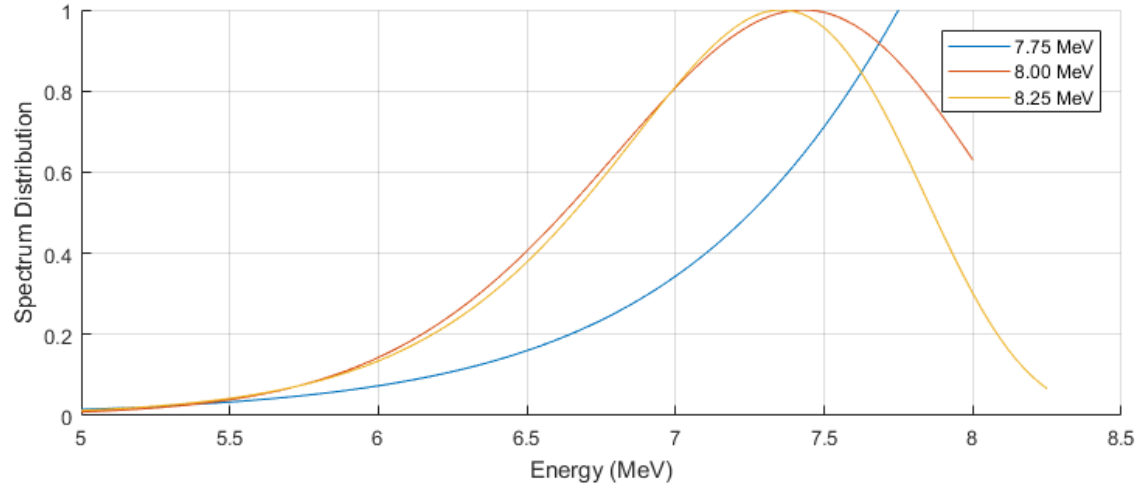

Figure 4-8 SSS determined optimal spectra when decreasing the maximum energy limit

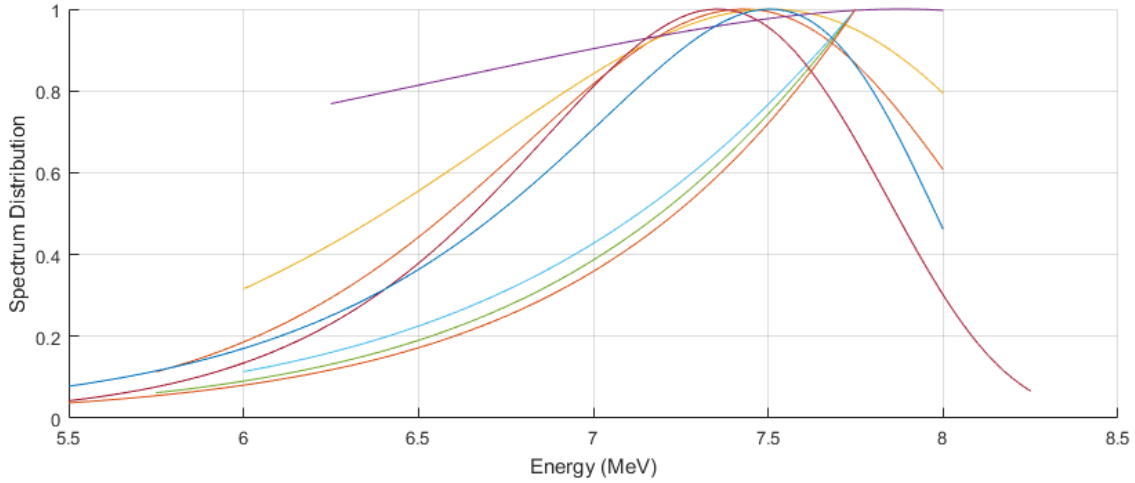

Figure 4-9 SSS determined optimal spectra when varying minimum and maximum energy limit

Within an energy window, the SSS determined the best fit spectrum by modifying the shape and position of the Landau distribution. To modify the rate at which the Landau tail varied, an exponential term was introduced into the equation. This effect is demonstrated by Figure 4-10 (Energy window not yet applied). The FWHM variation for a single low drop off rate is demonstrated by Figure 4-11. This drop off rate variable allowed the Landau distribution to vary and mimic Gaussian distributions. The last variable in the SSS was the modification of the mean/peak energy. The peak energy was initially set to below that of the minimum window energy in case a distribution could have only reducing distribution with energy. For a set drop off rate and set FWHM, the distribution was scanned across the energy window, as shown by Figure 4-12.

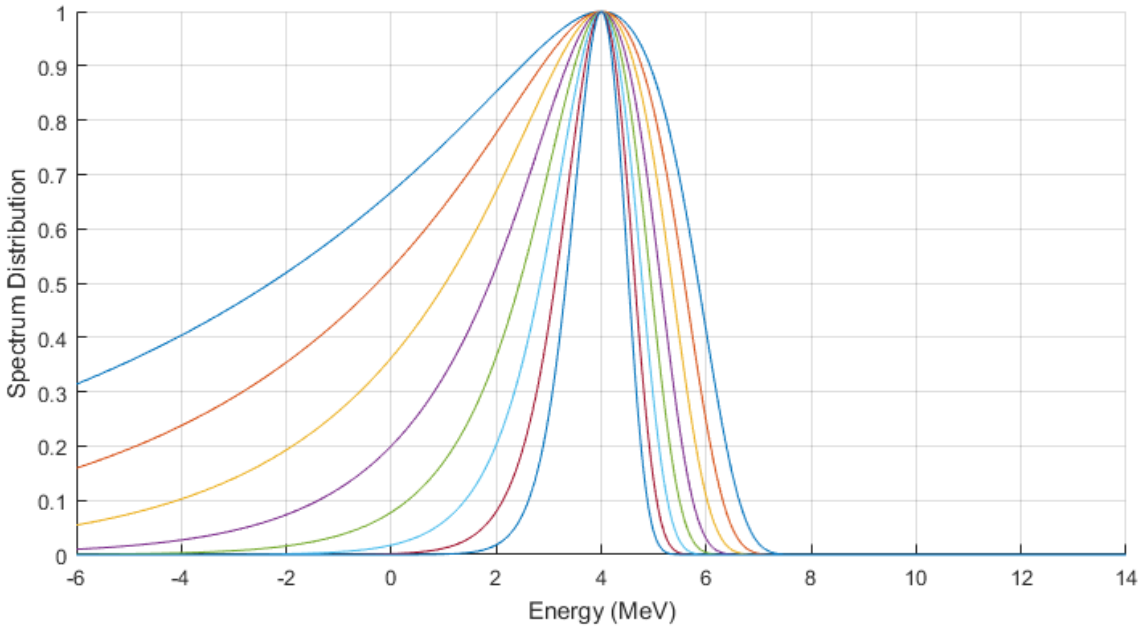

Figure 4-10 Tail drop off rate variable effect on Landau distribution

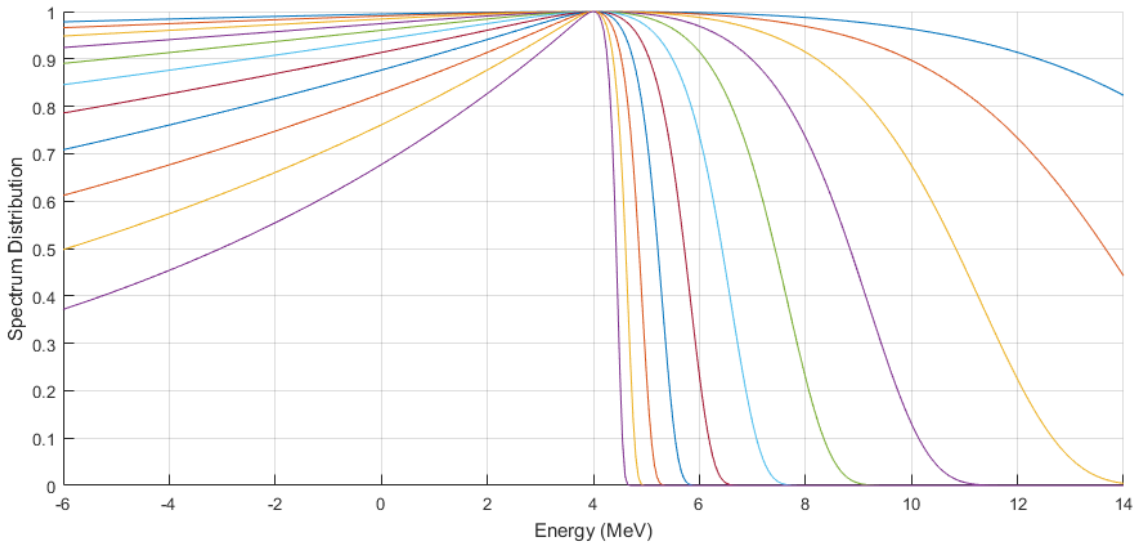

Figure 4-11 FWHM effect on Landau distribution with a low drop off rate

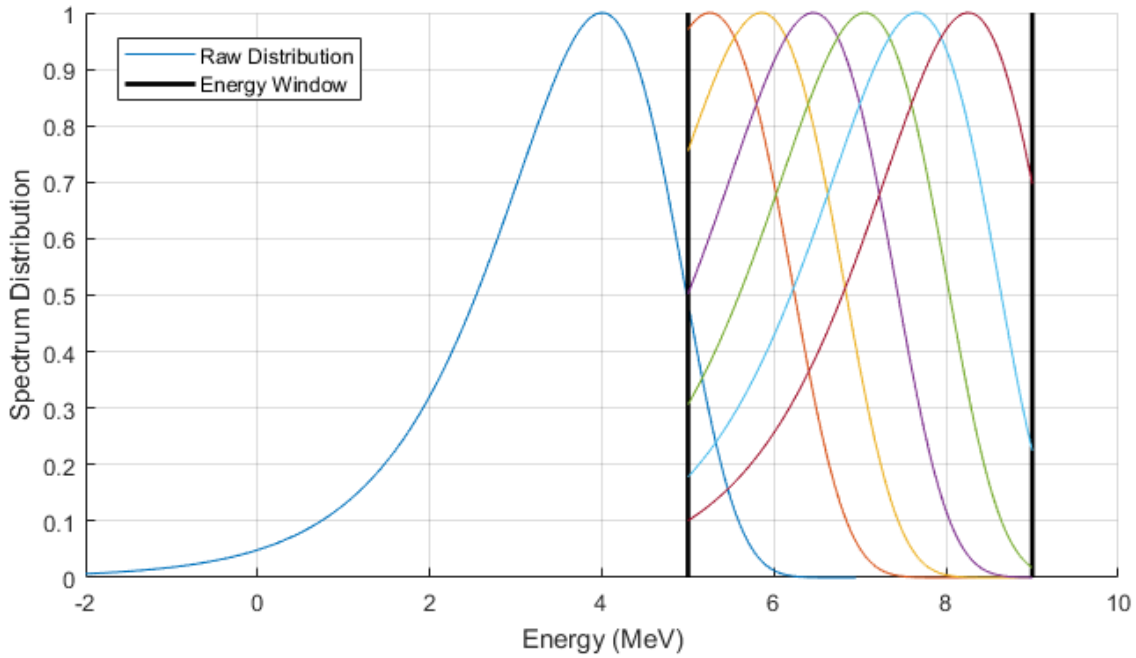

Figure 4-12 Modified Landau distribution scanned across an energy window

Given the number of variables and the freedom of each, the SSS would take a significant time to compute if all variables were analysed at a high resolution. To reduce the script time, the SSS was optimised to run at coarser initial parameter resolutions. Once the best solution was determined for a coarse resolution, the resolutions of the variables in the selected region were reduced and the SSS was rerun. This was implemented in three optimising stages, reducing the resolution each time narrowing down to the lowest error solution. This reduced the SSS run time to five minutes.

4.3. Unrefined Open Field Results

4.3.1. PDD Accuracy

With an optimised SSS, the determined spectrum was able to closely match all measured PDDs to within ±2% as shown by Figure 4-13. It is clear from the errors over all fields that the SSS was not able to find a spectrum that could precisely match all measured applicator PDDs. The final spectrum is a compromise of the input data to find an overall best solution.

One distinct effect is the fitting compromise due to the field size. Smaller field sizes have consistently positive errors while larger field sizes have negative errors. The

SSS was not able to find a spectrum that could increase the dose in the build-up region while maintaining accuracy throughout the entire PDD.

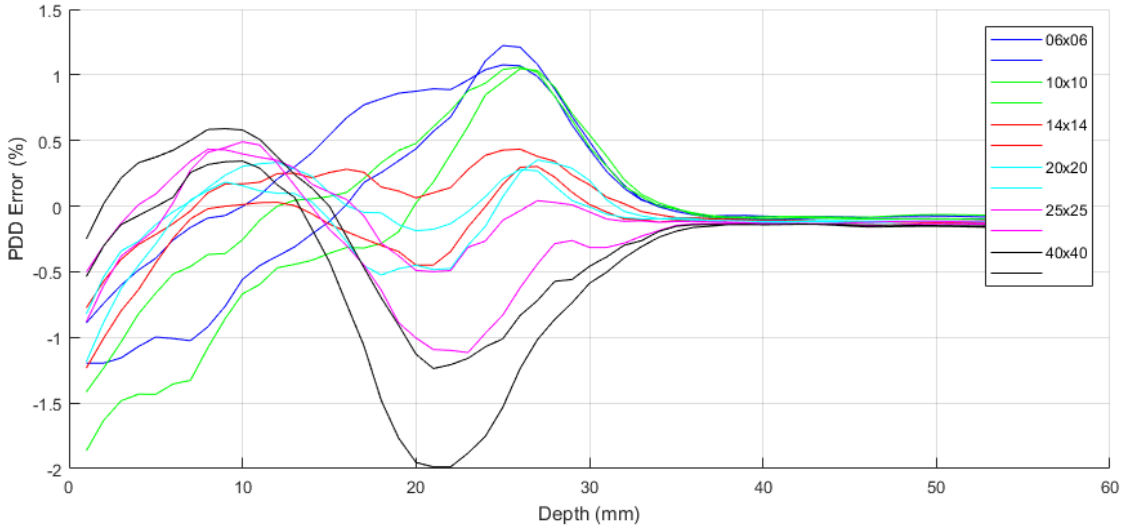

Figure 4-13 PDD error from determined spectrum for 6 MeV for all fields without applicators present at SSDs 80 and 100 cm

4.3.2. Profile Accuracy

As the spectrum matches all PDDs within ±2%, any profile disagreement cannot be due to the spectrum/energy dependence. BEAMnrc simulated profile agreement is shown in Figure 4-14, where open fields represent applicator fields without the applicator present and are normalised to the central axis. Half profiles are shown for visual ease as profiles are near symmetric from central axis in the same plane. Figure 4-15 shows the error by subtracting measured profiles from those simulated in Figure 4-14. Jaw positions were altered to match the 50% dose level in the penumbra. Inplane and crossplane profiles at depths of maximum and 50% PDD dose were also normalised to the central axis before comparison.

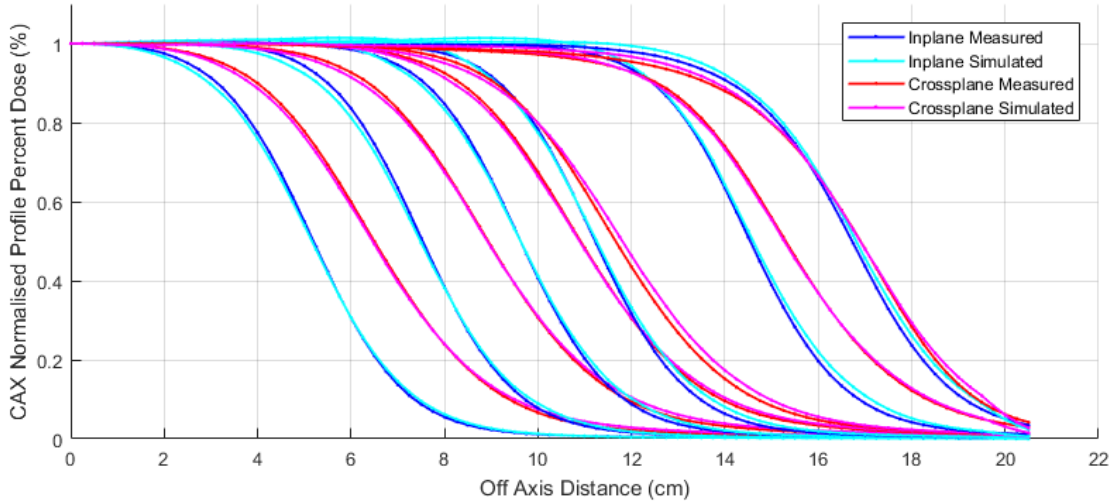

Figure 4-14 Simulated and measured open field inplane and crossplane half profiles at D_m for a 10 MeV beam at 80 cm SSD

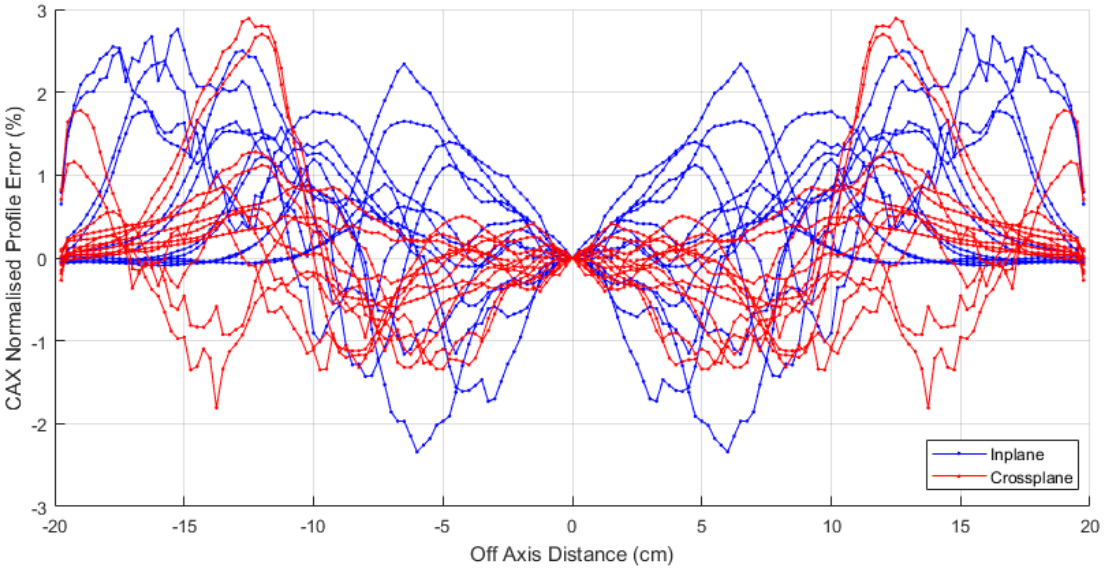

Figure 4-15 80 cm SSD 10 MeV open field inplane and crossplane profile error at D_m and R_{50} for six open applicator field sizes

Errors up to 4% were observed for all energies modelled while most errors were within 2%. These errors can be reduced by modifying component properties within the BEAMnrc accelerator model as discussed in Section 5.

4.3.3. Output Accuracy

While sufficient PDD agreement was achieved, the absolute dose prediction of the respective field sizes for multiple SSDs still did not agree with measured data. Outputs were compared to those measured at 80 cm SSD and normalised to the 10 cm × 10 cm applicator field size. The error was determined by subtracting the measured data from the simulated data; a negative result means the simulation results did not achieve sufficient dose.

Figure 4-16 shows output error with equivalent square field size for applicator fields without applicators attached over the five energies. There is a clear trend of increasing output error with increasing field size. For each energy, the marker points represent the applicator field size 6 cm × 6 cm, 10 cm × 10 cm, 14 cm × 14 cm, 20 cm × 20 cm, 25 cm × 25 cm and open field 40 cm × 40 cm, left to right.

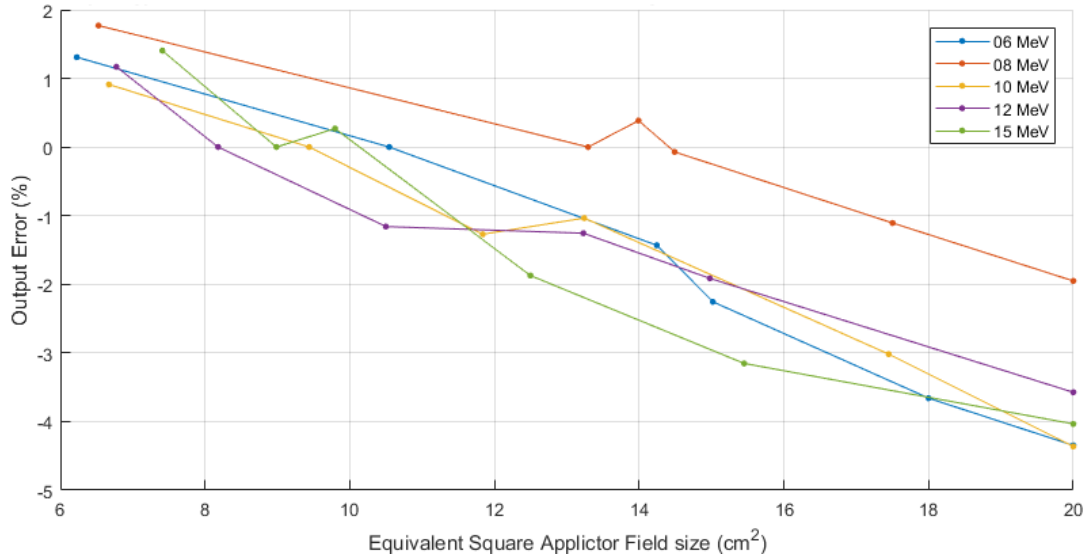

Figure 4-16 80 cm SSD Synergy output error for SSS determined spectra for five energies with open applicator equivalent square field size

As the spectrum was optimised to fit the PDDs, a solution for the absolute component of the PDDs cannot be achieved by modifying the spectrum. It could be possible that a simulation component/parameter could be responsible for not spreading out the dose over the field by being narrowly forward focused (i.e. thin scattering filters or acute incident beam angle divergence). Another possible explanation could be the

inability for MC to accurately represent the accelerator head to sufficient detail in BEAMnrc.

4.4. Spectrum Uncertainty

The developed SSS was successfully able to remove the energy dependence variable from the MC modelling system. This enabled the fine tuning of other BEAMnrc model and module parameters to achieve simulation results in better agreement with measurements. During the process of iterative refinement, various spectra were determined that could differ from the prior iteration with only a minor module change that should not have affected the effective energy (e.g. tweaking jaw settings).

An example of spectrum variation was found by making a slight jaw adjustment of a beam model which produced the spectrum change shown by Figure 4-17. Both spectra were analysed for open field simulations and produced near identical results for PDD, profile and output agreement. The implication of this result was the SSS could determine a significant number of suitable spectra resulting in near identical results thus allowing a range of 'acceptable' spectra. This could potentially lead to conflict between varying spectra determined from multiple parties using individual techniques. Currently there is very little knowledge of spectra exiting medical linear accelerator waveguides and even whether spectra are consistent between accelerators. If the continuous spectrum fits the measured dataset, until proven otherwise is up to the user's discretion as there is currently no practical method of validating any derived spectrum.

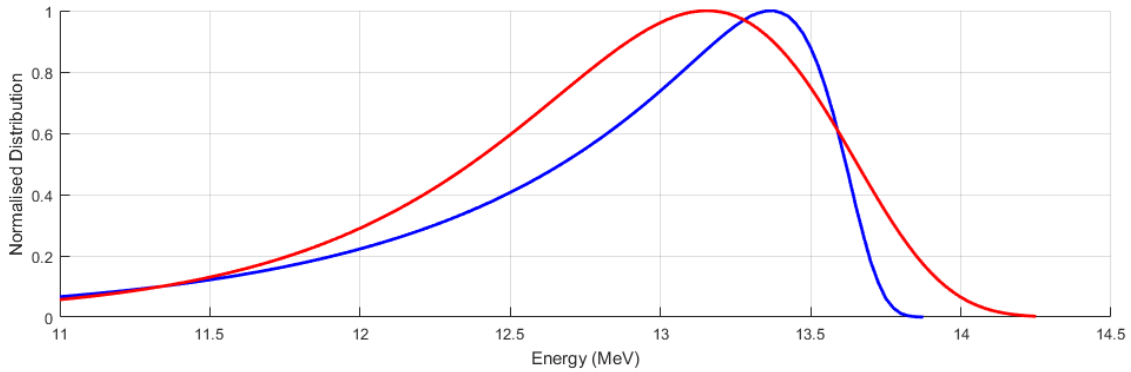

Figure 4-17 Spectrum variation for a 12MeV beam model producing identical results

During the applicator introducing stage described in Section 5.4, it was found that the energies needed to be adjusted due the difference in beam energy at the different dataset and times of data collection. When open field and applicator output factor ratios (Section 5.6) were compared it was noticed that there were initially significant differences for some energies. These corresponded to the datasets where a large energy (R_{50}) shift exceeding 0.5 mm was observed. The output measured from all applicators varied but when normalised to the reference 10 cm × 10 cm applicator, the respective applicator factors varied. This presented new absolute dosimetry problems as outputs no longer matched previous data, suggesting applicator factors are energy dependent. This adds additional data uncertainty when creating beam models. It is unlikely that all the required data can be gathered on the one occasion and requires good linear accelerator beam stability during the period of collection to ensure the beam energy remains consistent.

4.5. Discussion

A core assumption in the ability of the SSS to produce representable spectra was that the input measured PDD data was accurate and reliable. If any error was present in the input data, this error reduced the ability for the SSS to accurately fit to data and any error would be induced in the resulting spectrum. Several circumstances may be currently affecting the PDDs used in the SSS. Reasons for suspecting input PDD data come from the inability to effectively fit to the build-up region and pattern discrepancies observed with field size in simulated PDD results from determined spectra. Evidence for a discrepancy can be seen in Figures A-1 to A-10 where a consistent pattern was observed. Discrepancies between R_{50} values increase from smaller fields to larger fields in the dose drop off region for all energies and both accelerator models. This indicates an increasing inability to accurately match measured PDDs with increasing field size.

The first uncertainty is the varying bremsstrahlung PDD values between different detectors. Although differences of only 1% were observed, this is nearly twice the dose at lower energies. The higher bremsstrahlung readings were observed with the electron diode and Exradin ionisation chamber. This could possibly be due to energy dependence of the diode or wall and stem interference of the Exradin chamber. The advance Markus ionisation data was chosen as it should have minimal energy dependence while maintaining 1 mm depth resolution. To minimise this effect on the

SSS, the region to be fitted was limited up to the practical range of the PDD to avoid potential overfitting to the bremsstrahlung tail.

The second uncertainty comes from the conversion from ionisation to dose through the application of stopping powers. While the portion of dose from bremsstrahlung tail is approximately 1-3%, the contribution to the overall dose near the surface is higher. By applying the electron stopping power ratio to the full ionisation, the conversion of the photon portion is technically incorrect. By applying the stopping power conversion, the shape of the PDD could vary particularly near the surface region. This could be a cause for the build-up region discrepancies. This was investigated and found not to be significant. Any error in the ~1-3% photon contribution would be on the order of the correction of the stopping powers which is determined to vary by 5% over 2 cm. Thus 5% of the 1-3% is not larger enough to be considered the cause. The PDD agreement between various detectors (including diodes that measure dose directly) only show variations within 0.5% in the build-up region.

A separate possible cause of the discrepancy is the inability of BEAMnrc to accurately represent reality. Where modules and gaps between modules are placed in the BEAMnrc model, their surrounding environment is ignored. The best example is the mirror module in the accelerator model. The mirror module enables the thin layer of mirror material but has no option to include surrounding walls or shielding. This in turn could alter the shielding and scattering conditions. This would affect the PDD coefficient matrix being used to fit to measured data. An accurate solution may not be possible as the two datasets are not equivalent representations.

The third and least likely explanation is that the incident spectrum has the possibility of a second peak or hump. As electrons travel through a waveguide, the majority become ‘bunched’ by the radiofrequency field during acceleration. It is possible that electrons that do not form the bunch could fall behind a cavity in the waveguide and undergo unusual forces. These would still have to travel through the slalom bending system and stay within an energy range but could alter the spectrum with a hump changing the electron distribution from the assumed single peak. This is unlikely as measurements have been performed that do not indicate a hump (Hu & Wang 2014; Kok & Welleweerd 1999).

4.6. Summary

The numerical method using the developed spectrum scanning script (SSS) successfully determined suitable spectra to accurately match measured PDD data within ±2% using a coefficient dataset of simulated discrete energy PDDs. Sufficient spectrum distribution refinements were made to ensure any limitations in fitting to the measured PDD data was not due the limitation of the script or incident spectrum. From this we can conclude that any discrepancies still present in the simulation model results are not due to the incident spectrum on the exit window or effective energy of the electron beam. Initial BEAMnrc model results were able to match PDDs to within 2% and profiles within 4% without any module refinement. Absolute dose results spanned an error of 6% over field sizes for all model energies and the discrepancies could not be resolved by the SSS.

5. BEAMnrc Beam Models

5.1. Background

The process of finding an improved agreement between measurement and an MC simulation by modifying an accelerator head module in BEAMnrc is simple in principal. The difficulty arises because of the very large number of possible modifications. If simulated beam profiles (as shown in the above Figure 4-14) are predicting greater doses than those measured, the following modifications could all be made to reach a similar solution:

- Increasing incident electron energy
- Modifying exit window thickness
- Modifying primary foil thickness
- Modifying primary foil position
- Modifying secondary foil thickness
- Modifying secondary foil position
- Modifying incident beam divergence

As the SSS was responsible for determining the incident energy spectrum, the profile dependence on incident particle energy is removed from being a possible cause. However, the energy spectrum is dependent on the remaining parameters mentioned.

If a component is common between beam energies, any changes made for one energy must be made to the other required energies sharing the component. The component configuration with beam energy will allow a greater ability to distinguish which component may be responsible for discrepancies. Shared component configurations are listed in Table 5-1. There are variables that can be different for each beam energy such as incident beam divergence and focal spot size while variables such as exit window thickness are identical in all energies. Due to the difficulty in discriminating between energy unique variables, they are to be assessed last if better agreement cannot be obtained with shared components.

Table 5-1 Linear accelerator carousel configuration with electron energy

Energy (MeV)	Primary Foil ID	Secondary Foil ID
6	3	6/8
8	4	6/8
10	3	10/12/15
12	4	10/12/15
15	6	10/12/15

The process of beam model refinement was complex and extremely time consuming due to the simulation requirements of the SSS. The concept is described in Figure 5-1. All beam jaw settings were optimised to match open field measured data while using standard component specifications supplied by Elekta. PDD, profile and output agreement were assessed for individual energies and then compared against other energies to find similar discrepancies. A component or parameter could then be selected and modified to achieve improved agreement.

For example, if simulated profiles produced consistently larger relative dose off-axis for all field sizes for the 6 and 8 MeV models only, this would suggest the secondary scattering filter may require modification. However, if the profiles for 15 MeV were not in agreement but 10 and 12 MeV were, only the primary scattering foil or an incident beam parameter would require modifying to find an acceptable solution.

Within a single component three main options are possible; modifying thickness, position, or a combination of the two. An iterative process was established resulting in improvements with every iteration. If primary foil 3 is to be modified, energies 6 and 10 MeV will require new coefficient matrices for the SSS to determine new spectra. Due to the number of iterations, the number of SSDs used in the SSS was reduced to two, saving one third of the simulation time. Changes in particle scattering components may require the adjustment of jaw settings as beam divergence may be affected, this in turn affects outputs and the distribution's profile shape.

The process of refinement was continued until acceptable agreement was achieved or no solution could be determined. In cases where no immediate solution was determined, further investigations into the potential causes were established.

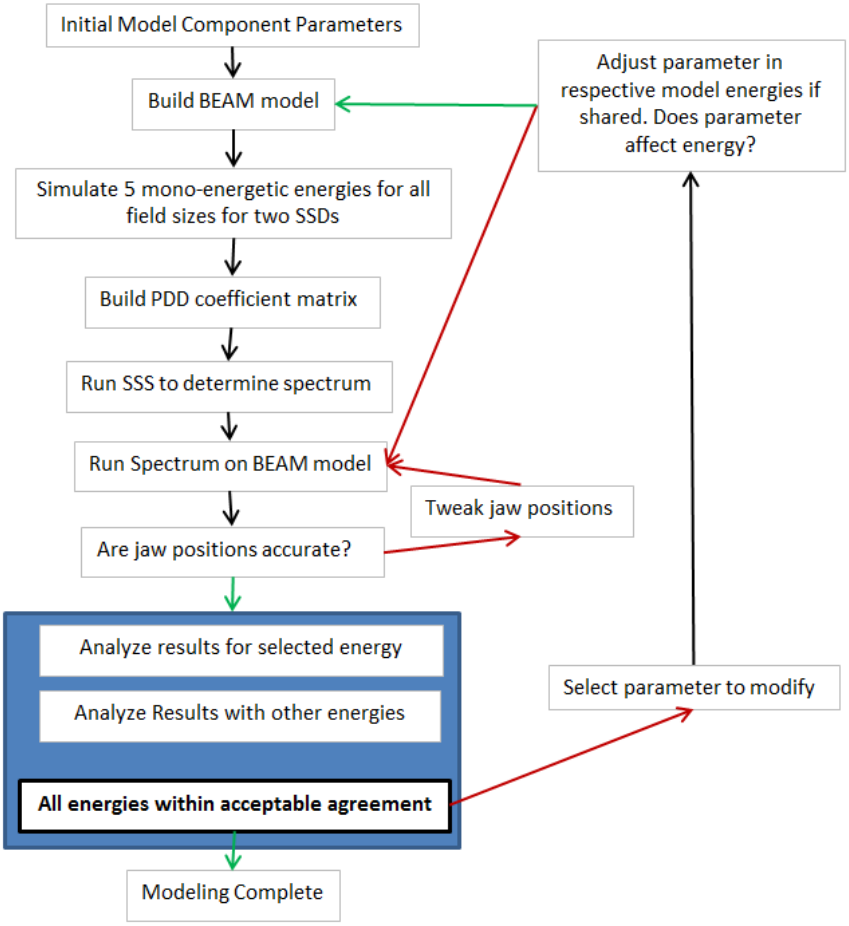

Figure 5-1 Modelling refinement workflow. Green arrows indicated a "yes", red arrows indicate a "no".

After several iterations of refinement, multiple disagreements still existed in all beam model energies. All component variables were adjusted, however a beam model solution could not be found to match all measured data. While reasonable PDD and profile agreement could be determined no adjustments were able to match measured OFs.

Significant effort was dedicated to investigating whether a component could be varied within an acceptable range to bring the outputs to an acceptable agreement. Each component was varied within 10% of its specified value. The outputs were simulated and compared to measurements over three SSDs, for all field sizes normalised to 100 cm SSD 10 cm × 10 cm fields. Figure 5-2 shows the output error with field size for a 6 MeV beam with original specified component parameters. Sixteen component variations were investigated by modifying component positions, thicknesses and beam parameters including beam divergence and spot size, shown by Figure 5-3. While

individual components are not labelled, the overall conclusion was that none were able to remove the slope of the variation of output error with field size. This indicated that none of the tested components could be responsible for the discrepancy.

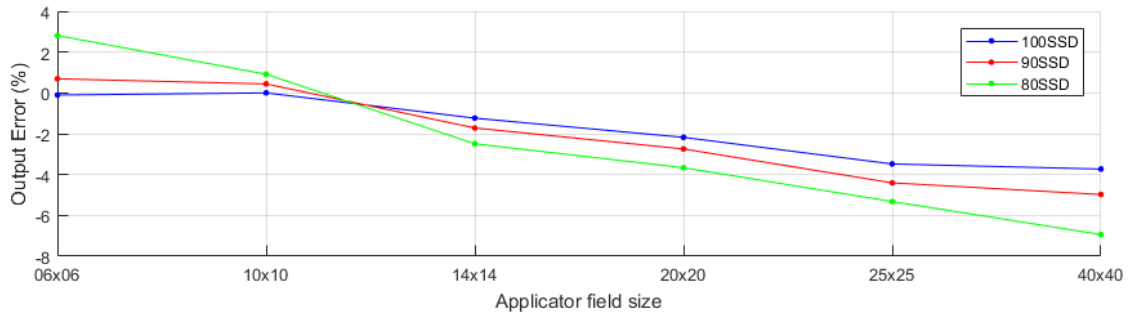

Figure 5-2 Simulated output error using Elekta specified accelerator component parameters for Synergy 6 MeV beam with open field size for three SSDs normalised to 100 cm SSD 10 cm × 10 cm field size

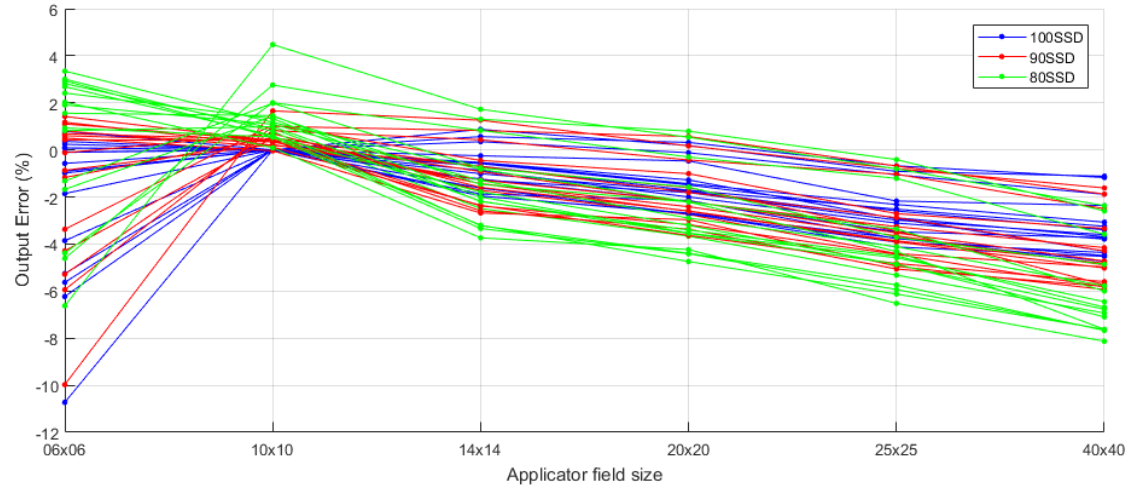

Figure 5-3 Effect of individually varying multiple component specifications on outputs over three SSDs normalised to 100 cm SSD 10 cm × 10 cm field size

Correction factors needed to remove the discrepancies in the output factors were calculated. Figure 5-4 shows the remaining error if each applicator had correction factors of 0.990, 1.000, 1.020, 1.024, 1.039 and 1.048 for each field size respectively. The correction factors were found to be linear with equivalent square field of the field size as shown by the purple plot in Figure 5-4. When applied, outputs over the three SSDs agreed to within 0.5% with the exception of the 6 cm × 6 cm applicator. This is

due to its sensitivity with component variation given the small field size. These correction factors were not accepted as a solution as this negated the purpose of keeping simulations as realistic as possible.

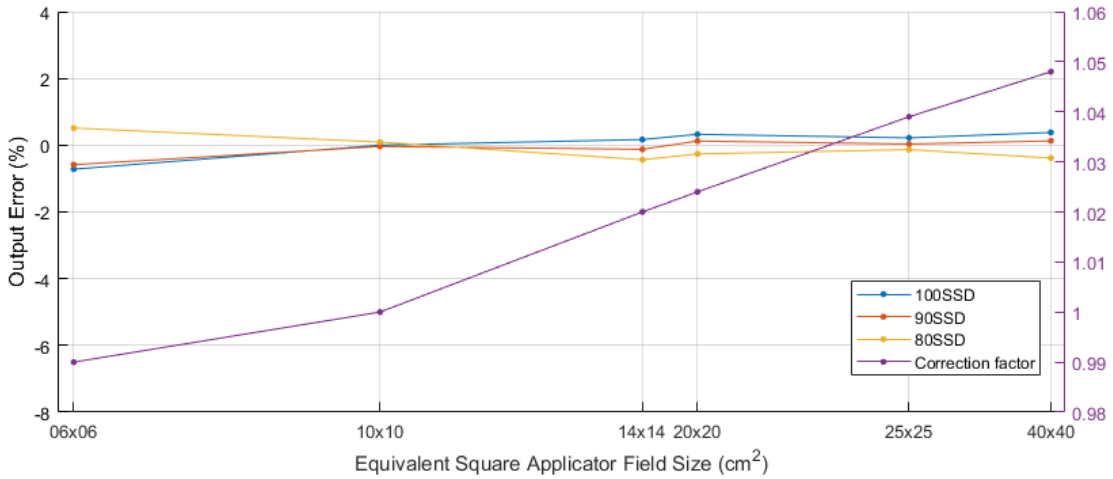

Figure 5-4 6 MeV output error with a correction factor applied for each field size

5.2. MLC Module Error and Solution

To resolve the output discrepancy each module and parameter was heavily scrutinised. Discrepancies were found when investigating the MLC module, MLCE (specific for Elekta accelerators in BEAMnrc), that resulted in significant errors being introduced into the models produced. This error and solution are discussed below in detail.

The MLCE module sits roughly 30 cm below the exit window. Due to beam divergence this equates to an opening of approximately 6 cm square at its top surface. By simulating the 40 cm × 40 cm square field it was noticed that the inplane and crossplane profiles were different. This was thought to be due to the variation of the inplane and crossplane incident angle of the beam on the exit window that is not accounted for in MC modelling. This is possible as the linear accelerators bending magnet would affect the beam angle of divergence in the plane of the bending system (inplane) and not in the crossplane.

A phase space plane was generated before and after the MLCE module. While there was no data to compare against, the purpose of the test was to determine the effect the MLCE module had on beam isotropy. Pre MLCE phase space results showed an

isotropic inplane and crossplane profile as expected. This showed the isotropy was maintained while entering the MLCE module but post MLCE profiles indicated that the module introduced anisotropy as shown in Figure 5-5. This led to the conclusion that the anisotropy was introduced due to the MLCs.

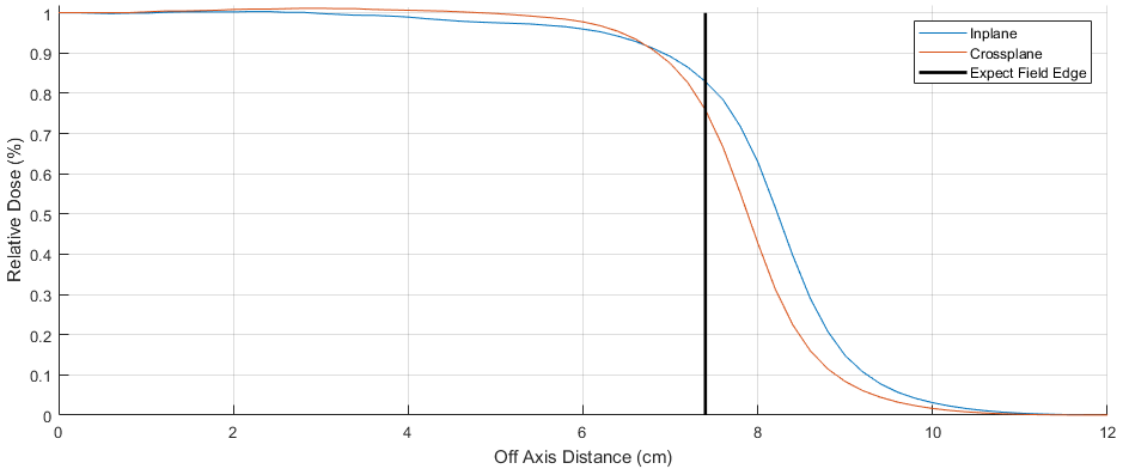

Figure 5-5 Simulated inplane and crossplane profiles directly below MLCE module

More importantly, it was noticed there was a significant difference in field size between inplane and crossplane profiles. This is important since the MLCE module should produce a maximum field size of 40 cm in both dimensions. Due to the curvature of leaf ends in the crossplane and flat edge in the inplane one could expect small differences. However, it would be expected that the leaf ends should provide more shielding than observed. This indicated an error introduced when the beam passes through the MLCE module.

Further investigation revealed that the MLC curvature (crossplane) produced the appropriate field size and it was the flat edge (inplane) that was incorrect. Figure 5-5 shows expected field size marked by the black line. This line represents the air/shielding boundary in the MLC module. A scatter plot of electrons with energies above 8 MeV indicated they reached this point without significant interaction. One should expect a few particles to exist in the curve leaf direction due to the curvature and intra-leaf leakage. The scatter plot in Figure 5-6 shows particles exist (in blue) in the flat edge (inplane) to a greater extent than in the MLC plane (crossplane). Given the number and positions outside their theoretical range, it would suggest that the flat edge boundary did not exist in the simulation environment.

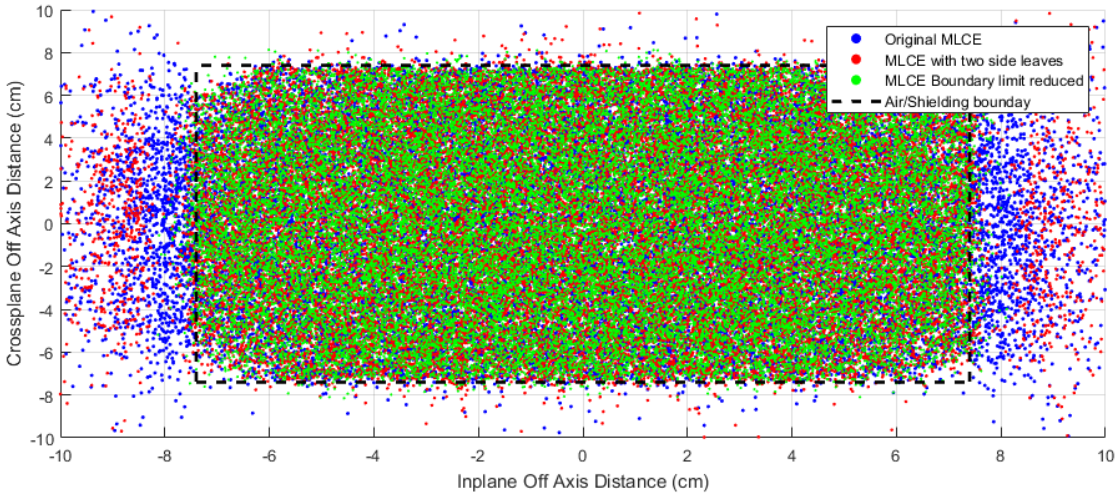

Figure 5-6 Scatter plot of simulated electron particle positions with additional MLCE limitations

The theory is depicted in Figure 5-7 where leaf positions are shown and electron tracks are depicted in yellow. As some shielding was present it was proposed the module only limited the beam in the inplane at the surface of the module and not throughout (right scenario). Where in reality, the full area is shielding material and would prevent particles travelling throughout the depth of the MLC (left scenario).

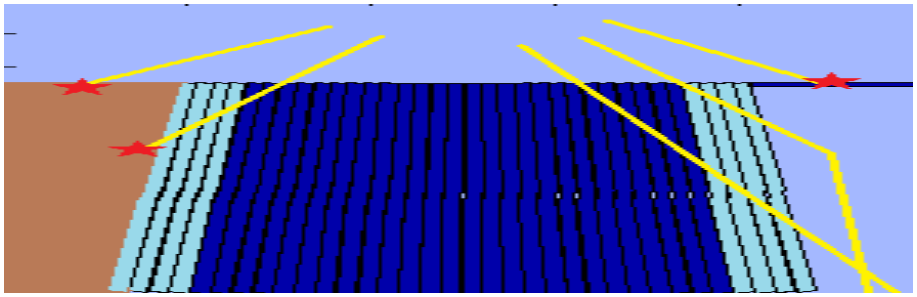

Figure 5-7 Theory explaining particles existing outside shielding interface

To artificially simulate a wall, extra leaves were introduced into the MLCE module and were positioned across the entire field as shown in Figure 5-8.

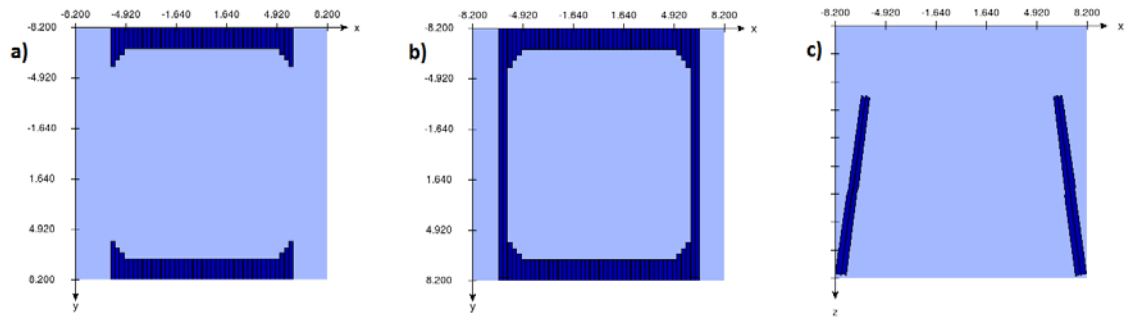

Figure 5-8 Alterations made to MLCE module. a) Original module in xy plane. b) Two additional leaves acting as a wall boundary in xy plane. c) Module boundary set to edge of leaf in xz plane

Initially one leaf was added and the above tests re-examined. This showed that one leaf did not provide sufficient shielding and the number of leaves were increased to two. This removed particles where the leaves were present but some still existed beyond the leaves. The boundary limit for the module was then reduced up to the extra leaf end limit. The effects of each limitation stage are shown by the scatter plot in Figure 5-6.

The profile simulations previously shown in Figure 5-5 were repeated and results shown in Figure 5-9. The inplane and crossplane field size produced with the modified MLCE module are in good agreement between each other and expectations.

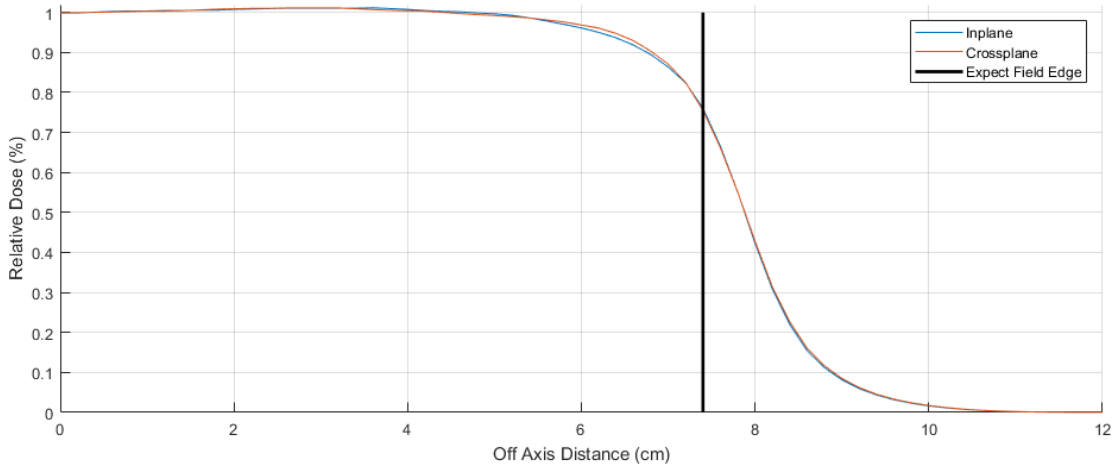

Figure 5-9 Inplane and crossplane profiles under the MLCE module modified to simulate an artificial wall

This effect was only significant in Elekta's Synergy models as MLCs are fully retracted for all electron field exposing the side wall of the MLC housing and the inplane and crossplane jaws alone are used for field size collimation. Agility models only have an inplane jaw and utilise the MLCs for crossplane beam collimation therefore only exposing the MLC sidewall for a 40 cm inplane field.

The removal of particles due to the artificial walls affects both the scattering conditions and radiation passing through the accelerator head influencing the maximum simulated dose. With a revised and significant change in the MLCE module, all models were now redundant and required re-simulation. The same fine-tuning workflow was used to obtain the solution to the outputs.

This modification to the MLCE fits the observed output error stated previously in chapter 4.3.3; as field size increased the simulated output deviation from measurement increased. The initial error in the output discrepancy was due to the normalisation value of the 10 cm × 10 cm field. The modified MLCE reduced the outputs by a greater amount for smaller fields shown by Figure 5-10. Normalising to the original 10 cm × 10 cm output made the 40 cm × 40 cm appear low but in fact the 10 cm × 10 cm output was high making the 40 cm × 40 cm low comparatively. Normalising to the modified 10 cm × 10 cm output increased the relative difference for the larger field and reduced the relative difference for smaller fields as shown by Figure 5-11.

Outputs now achieved accuracy to within 1% for open field sizes 10 cm × 10 cm and larger over the three SSDs. The exception was small 6 cm × 6 cm field sizes where outputs were sensitive to fine tuning due to the limited field size.

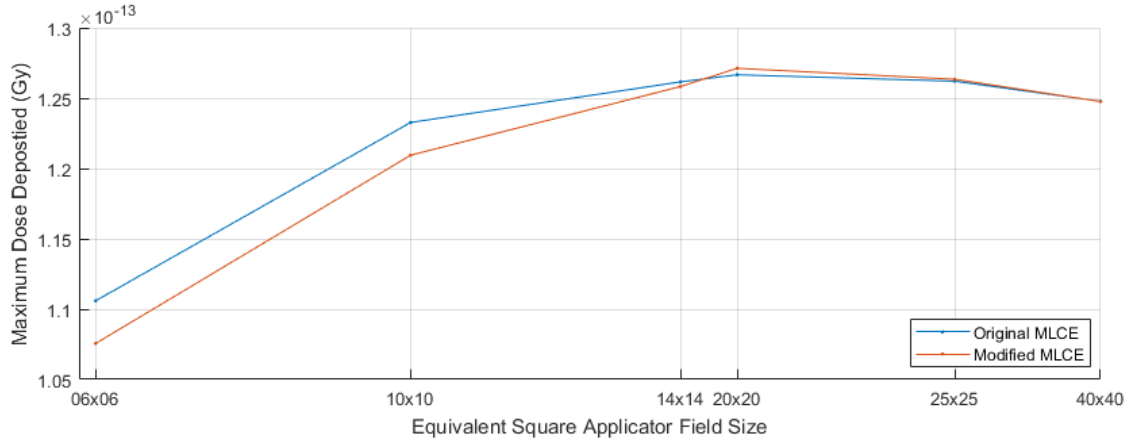

Figure 5-10 Simulated maximum dose variation due to the addition of an artificial wall in the MLCE module

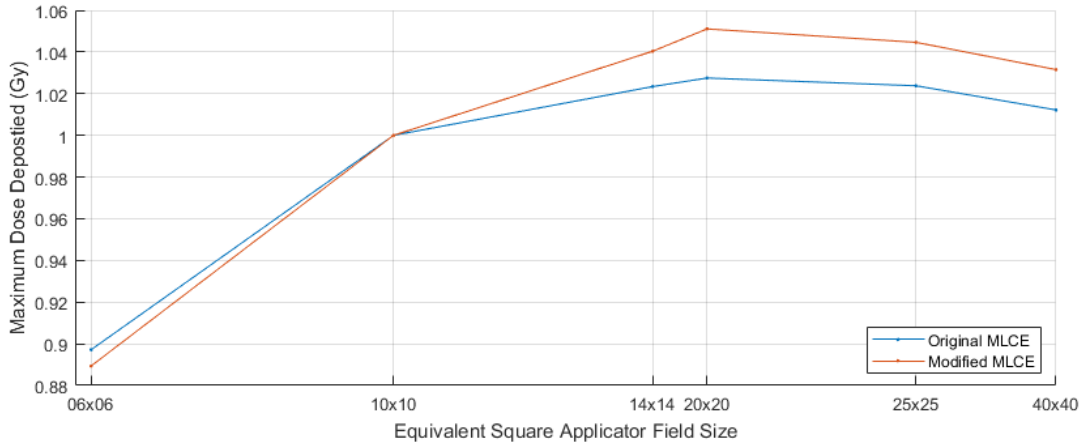

Figure 5-11 Relative output factor difference between 10 cm × 10 cm normalisation Pre and Post MCLE modification

5.3. Refined Open Field Model Results

Of the ten BEAMnrc electron beam models developed, only one component required significant variation from provided specifications. The 15 MeV primary filter for both Synergy and Agility models required an increase in thickness by 13% to achieve agreement. This modification was required as when compared to 10 and 12 MeV models which achieve excellent profile and output agreement, the primary filter was the only component not shared. The same thickness was required for both Synergy and Agility accelerator models further confirming the validity in accepting the modification.

PDD results achieved acceptable agreement all within 2% shown by Figure 5-12. Error results for all Elekta Synergy and Agility model PDDs and their respective five energies are show in Appendix A.

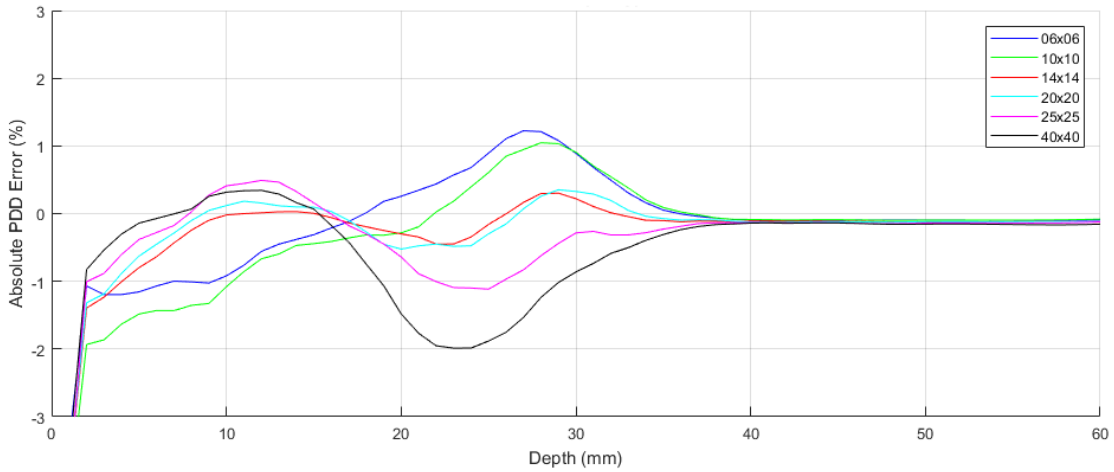

Figure 5-12 Post MLCE modification Synergy 100 cm SSD 6 MeV simulated PDD error with SSS spectrum from measured data for fields without applicators

The same simulation and error as described in section 4.3.2 in the unrefined model results (Figure 4-15) is shown by the improved refined open field results (Figure 5-13) after the MLCE modification. Profile errors were improved from a range of 4% to the majority within 1% over all field sizes for each nominal electron energy. Results for Elekta Synergy and Agility model profiles and their respective five energies are show in Appendix A.

Significant time was invested building the models to this stage as any errors in the open fields are carried through when applicators are reintroduced. With confidence in the models without applicators present, discrepancies which occur with applicators are likely due to this additional component.

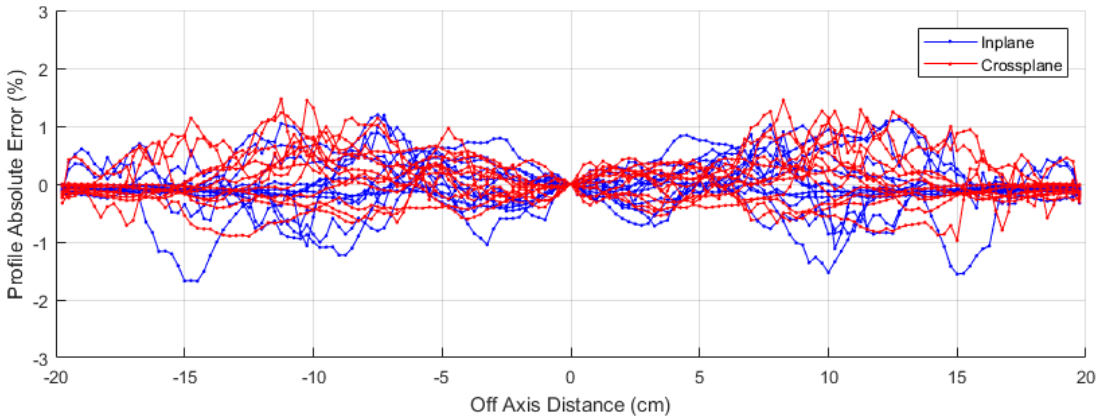

Figure 5-13 Post MLCE modification Synergy 80 cm SSD 10 MeV open field D_m and R_{50} profile percentage errors for all applicators

Outputs over three SSDs (80, 90 and 100 cm) from each field size were compared against measurement to ensure accurate dose reduction with distance from source. Tabulated values are presented in Tables A-1 to A-10 in Appendix A and shown in Figure 5-14 and Figure 5-15. With the exception of 6 MeV 6 cm × 6 cm, outputs for both models were within 1% over the 20 cm SSD and 6 cm × 6 cm were within 2%. The dose reduction with distance accuracy indicates an appropriate effective source distance was modelled in the simulation. While results in Figure 5-14 appear random, Figure 5-15 indicates a consistent pattern where applicator outputs deviate from measured data with field size for an individual beam energy with the exception of the 40 cm × 40 cm field. The exception of the Agility output error 40 cm × 40 cm field size may be due adverse effects of the MLCE modification to open fields. The possible cause of output deviation with field size was not investigated due to time constraints but may be due to the linear accelerator MU variation with field size that is not accounted for in the simulation environment. The MLCs are used to define the field for Agility unlike the Synergy, potentially increasing the scatter contribution to the linear accelerators ionisation chamber altering the charge reading with field size. This indicates it may be possible to increase the accuracy of the Agility outputs further by up to 1% if it can be accounted for.

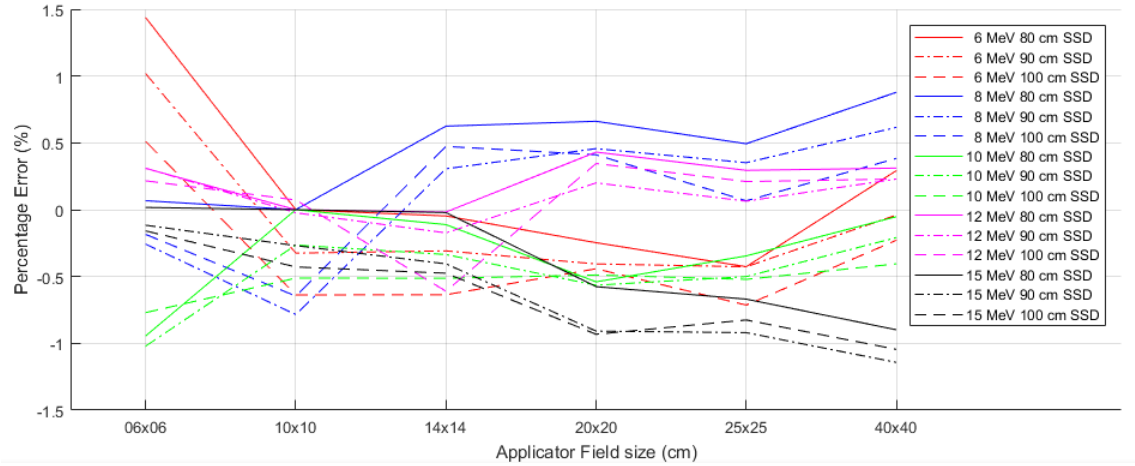

Figure 5-14 Post MLCE modification Synergy output errors for open fields for SSDs 80, 90 and 100 cm normalised to 10 cm × 10 cm 100 cm SSD

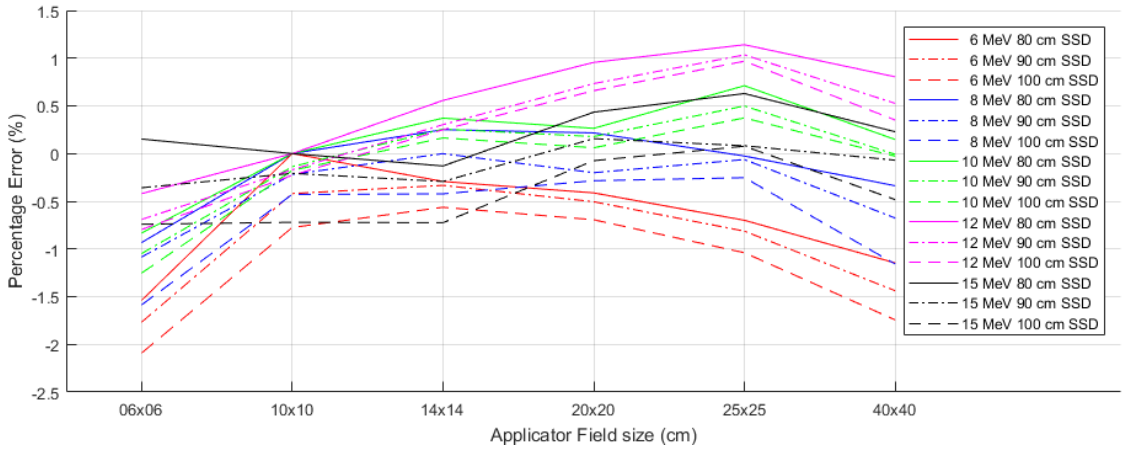

Figure 5-15 Agility output errors for open fields for SSDs 80, 90 and 100 cm normalised to 10 cm × 10 cm 100 cm SSD

5.4. Reintroducing Applicators into Models

If the hypothesis of maintaining model accuracy when applying open field models to applicators holds true, by simply adding the applicators back into the model there should be no loss of accuracy unless the inaccuracies are introduced by the applicator. The attachment of each applicator to the linear accelerator is independent from accelerator beam control parameters. The spectrum determined for open fields should still be applicable and results should maintain their accuracy.

PDD results from simulations with applicators gave various levels of R_{50} agreement from measurement. Of the 10 models developed only three PDDs

maintained sufficient accuracy. The remaining seven PDDs had R_{50} range discrepancies from 0.2 mm up to 0.8 mm and were consistent for all applicators for each given model energy. This implied a systematic error is present that is independent between energies but not applicators. Simulated R_{50} variation from open field PDDs to applicator field PDDs varied less than 0.2 mm particularly for larger fields. As this variation is less than the observed difference up to 0.8 mm, it would suggest the difference was not due to the applicators.

The cause for energy disagreements was determined to be related to the different measured datasets used as reference. Data was initially collected for fields with applicators present; only when modelling efforts failed to obtain sufficient agreements was data collected for fields without applicators present. Between the two collection times, the R_{50} of the beams drifted by the discrepancies observed. The spectra determined previously for open fields were no longer applicable (unless no energy drift was present) when the applicators are present as they represent different datasets. The only 'true' solution would be to retune the beam on the accelerator to match the applicator R_{50} and re-collect the open field data. This was not practical considering the time involved.

The practical solution modified the open field PDDs by the difference of the energy drift. The SSS would then determine the spectrum suitable for applicator fields. This was achieved by adjusting the open field R_{50} proportionally to the applicator field R_{50}. While this would result in a small error in the build-up region, the benefit is accepted by matching the energy and profiles than collecting an entire new dataset. The shifts required are shown by Table 5-2.

Adjusting the spectra to the energy of the measured applicator dataset is required allowing a direct comparison against the commercial TPS that was built with the R_{50} from the applicator dataset and not the open field dataset. The new spectra are applied to all subsequent models with applicators present.

Table 5-2 Required open field PDD shifts (mm) to match original measured applicator data

Energy (MeV)	Synergy	Agility
6	0	-0.8
8	0.2	0
10	0.3	0
12	-0.55	-0.2
15	0.2	-0.4

When applying the spectrum of the new R_{50}, it was observed that the open field outputs no longer maintained the accuracy previously reported. This agrees with the dependence of outputs on energy. While the dose deposited by the 10 cm × 10 cm field also varied, it is negated due to the fact that the value is used for normalisation.

The significant benefit of producing an in-house Monte Carlo model is the ability to make a direct comparison against commercial TPSs using the same input data. This comparison is only viable if the in-house model is able to meet strict accuracy constraints. Any differences observed between the models produced would be due to the methods utilised in building the models and sacrifices the commercial TPS makes to produce results quickly.

5.5. Applicator Model Results

The gamma method (Low & Dempsey 2003; Low, Harms, Mutic & Purdy 1998) was used to determine the beam model accuracy from the reference data measured. The gamma method compares the simulated value at each point against the reference measured dataset. A gamma value is determined by Eq. 5.1 listed below and the concept depicted in Figure 5-16. A gamma value of one or less indicates the simulated value is within either of the criteria set and is considered to have successfully passed. In this case the criteria are agreement to dose (D) or distance required to obtain a dose agreement (d). A continuous gamma method was used where reference values are linearly interpolated to determine the lowest gamma value. A criterion of 1%/1 mm was used to ensure a strict assessment of beam models so they may be considered a gold standard.

$$\Gamma(r_r, r_e) = \sqrt{\frac{|r_e - r_r|^2}{\Delta d^2} + \frac{[D_e(r_e) - D_r(r_r)]^2}{\Delta D^2}} \tag{5.1}$$

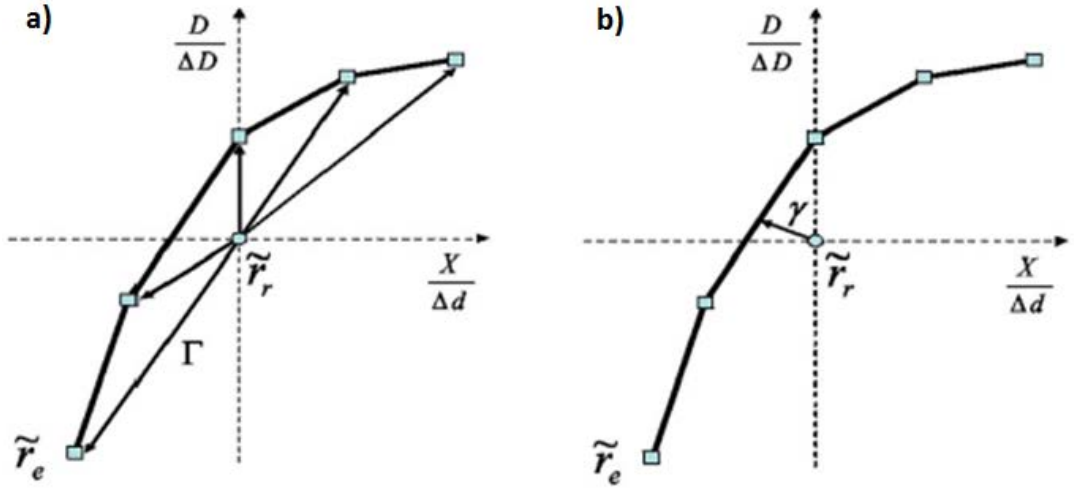

Figure 5-16 Gamma method technique for a) discrete points and b) linear interpolation between points (Ju, Simpson, Deasy & Low 2008)

To make a direct gamma comparison every dataset assessed separated the relative and absolute properties. PDDs were normalised to the maximum dose while profiles were normalised to the central axis. Due to the uncertainty of MC results, PDDs and profiles were normalised using a Savitzky-Golay smoothed value with a span of 5 units for PDDs and 10 units for profiles. This minimised any uncertainty in the normalisation region and was used over a region average due to volume averaging and single point outliers in small fields.

The analysis method was automated in Matlab and implemented for both in-house and commercial models. PDDs were analysed from a depth of 3 mm onwards as measurements near the surface are unreliable due to detector limitations. Profiles extended more than 5 cm outside the field size to ensure adequate shielding representation. The dose percentage criterion was not scaled with each profile dose level and results in higher fail rates due to the effective tighter criteria with lower dose profiles. For example, 1% of the 100% profile equates to 1% however for the 20% profile after normalisation it equates to 0.2%.

5.5.1. Standard Applicator Insert PDDs and Profiles

A gamma index table was produced for each accelerator model, SSD, energy and applicator combination for the in-house MC models. The root mean square (RMS) error was calculated for each profile and PDD and stored in a gamma index table. An

example of the gamma index table is shown in Table 5-3 for the Synergy 100 cm SSD 6 MeV 20 cm × 20 cm BEAMnrc model. Figures 7-3 to 7-11 are selected profile plots (highlighted in yellow in the table). The RMS error row (in bold) for each combination was extracted and collated into separate tables in Appendix B.

Table 5-3 Gamma index result table for In-house MC Synergy Electrons 100 cm SSD, 6MeV 20 cm × 20 cm gamma (1%, 1 mm)

	PDD	Inplane							Crossplane						
		P1	P2	P3	P4	P5	P6	P7	P1	P2	P3	P4	P5	P6	P7
Total # points	45	181	181	181	181	181	181	181	181	181	181	181	181	181	181
$\gamma > 1$ (fail)	9%	47%	25%	20%	10%	17%	7%	19%	24%	8%	7%	1%	6%	12%	25%
$\gamma < 1$ (pass)	91%	53%	75%	80%	90%	83%	93%	81%	76%	92%	93%	99%	94%	88%	75%
RMS γ	0.32	1.32	0.99	0.86	0.59	0.69	0.57	0.88	0.86	0.57	0.53	0.41	0.50	0.62	0.94
Maximum γ	1.31	3.26	2.72	2.19	1.47	1.42	1.82	4.61	3.00	1.36	1.61	1.16	1.47	1.81	3.25
R_{50}	2.50														
γ pass < d_{max}	69.2%														
γ pass > d_{max}	100.0%														
γ pass < 50%		43%	53%	64%	78%	81%	99%	100%	80%	91%	97%	100%	100%	100%	74%
γ pass > 50%		60%	90%	91%	98%	85%	89%	67%	73%	93%	91%	98%	90%	79%	75%

% Dose	100	90	80	50	20
Δ Dose (cm)	0.00	-0.01	-0.02	-0.01	0.00

Profile	P1	P2	P3	P4	P5	P6	P7
Depth (cm)	0.50	1.00	1.30	1.86	2.06	2.50	2.93

5.5.2. Outputs with Standard Applicator Inserts

Calculated output factor deviations from measured values for standard applicator inserts were determined for the BEAMnrc models. As simulated open field output factors were found to be within 1%, errors greater than this can be attributed to the presence of the applicators. Figure 5-17 and Figure 5-18 show results from BEAMnrc simulations for applicator factors over 100 and 110 cm SSDs for both accelerator models and all energies. Applicator factors were normalised to 100 cm SSD 10 cm × 10 cm similar to clinical practice. Simulation applicator output errors of 1% and above are observed for larger fields (14 cm × 14 cm and larger) and remain consistent over the two SSDs. The 6 cm × 6 cm and 10 cm × 10 cm applicators were observed to have dose reduction amount error with increased SSD. This is shown by the 'gap' between the solid and dashed line for each energy in Figure 5-17 and Figure 5-18 that reduces with larger applicators. Dose reduction agreement varied to measurement by 2% over 10 cm SSD increase that was not present without applicators (~0.6%). These discrepancies are discussed further in section 5.6.

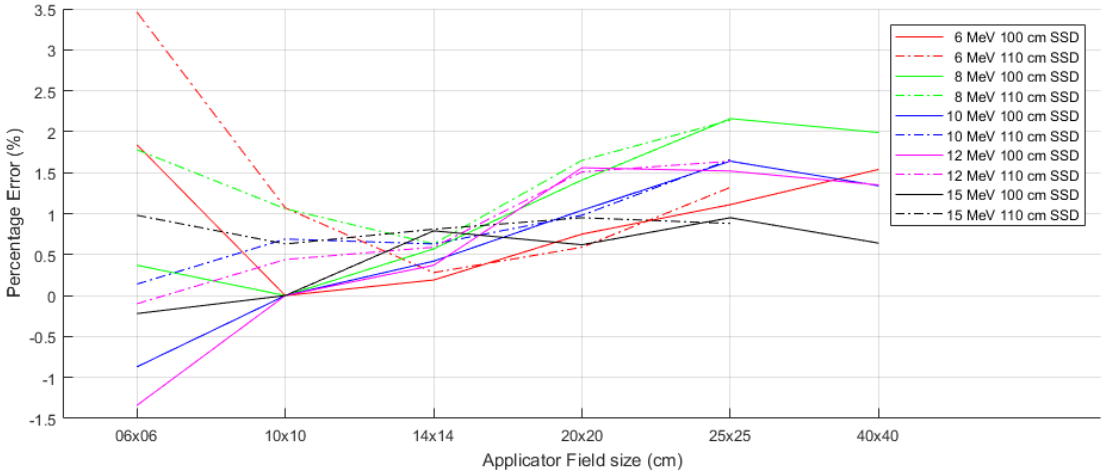

Figure 5-17 Synergy in-house MC applicator output errors for five energies and applicators for 100 and 110 cm SSD

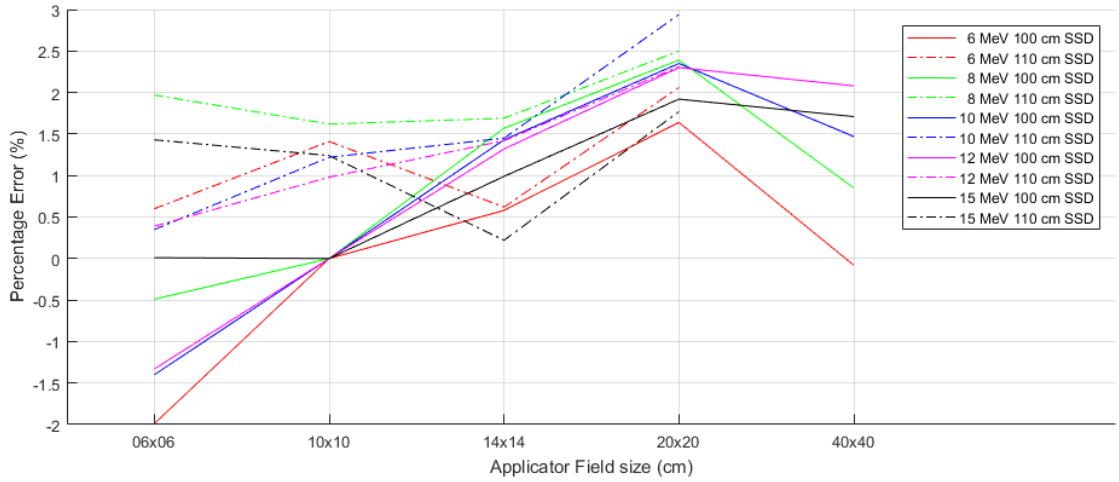

Figure 5-18 Agility in-house MC applicator output errors for five energies and applicators for 100 and 110 cm SSD

5.5.3. Unresolved Model Discrepancies

Further improvement in model accuracy to measured applicator data is also possible for both in-house and commercial MC modelling methods outside the field penumbras. The inplane profile in Figure 7-5 at ±15 cm off-axis shows that both modelling methods do not appropriately account for applicator leakage outside of the main field. While the Monaco 5 algorithm does not account for this at all and removes the dose from the profile, the in-house BEAMnrc does not account for it enough since it predicts higher dose than measured. The in-house model uses the measured dimensions in both planes from the real applicator where the inplane shielding material is not as wide as the crossplane dimensions. The lack of shielding must then be due to another cause. This is supported by Figure 7-4 crossplane profiles that, at the same off-axis distance, achieve better agreement. This suggests there is an anisotropy and discrepancy present.

After the MLCE module was modified, output agreement from measured data for both models were within 1% for open fields when normalised to the 10 cm × 10 cm field size and absolute dose reduction over 20 cm SSD variation are within 0.6% of its respective output. Once the applicators were included in the models, this agreement was not preserved. This indicated the applicators themselves introduced a discrepancy. The discrepancy affected both the output factors relative to the 10 cm × 10 cm field size and the absolute dose reduction with SSD for each field size. Output factor errors of

2% and dose reduction errors of more than 2% from their respective outputs are observed.

The change in measured to simulated output error for Synergy and Agility is represented in Table 5-4 where the difference in outputs was found by subtracting the open field from the applicator field results. A pattern was observed and is by averaging the results for each energy for the same applicator where the error increases with field size as show in Figure 5-19.

Table 5-4 100 cm SSD Synergy and Agility percent difference from measurement for open field and applicator outputs normalised to 10 cm × 10 cm

Synergy							
		Simulated Open Field Output Factor Error (%)					
		100 cm SSD					
		6x6	10x10	14x14	20x20	25x25	40x40
Energy (MeV)	6	1.44	0.00	-0.05	-0.25	-0.43	0.29
	8	0.07	0.00	0.63	0.66	0.49	0.88
	10	-0.95	0.00	-0.11	-0.54	-0.35	-0.05
	12	0.31	0.00	-0.02	0.43	0.29	0.31
	15	0.02	0.00	-0.02	-0.58	-0.67	-0.90

Agility							
		Simulated Open Field Output Factor Error (%)					
		100 cm SSD					
		6x6	10x10	14x14	20x20	25x25	40x40
Energy (MeV)	6	-1.54	0.00	-0.29	-0.41	-0.70	-1.15
	8	-0.93	0.00	0.25	0.22	-0.03	-0.34
	10	-0.83	0.00	0.37	0.26	0.71	0.15
	12	-0.42	0.00	0.56	0.96	1.14	0.80
	15	0.15	0.00	-0.13	0.43	0.63	0.23

		Simulated Applicators Output Factor Error (%)					
		100 cm SSD					
		6x6	10x10	14x14	20x20	25x25	40x40
Energy (MeV)	6	1.84	0.00	0.19	0.75	1.11	1.54
	8	0.37	0.00	0.57	1.41	2.16	1.99
	10	-0.87	0.00	0.42	1.04	1.64	1.34
	12	-1.34	0.00	0.37	1.56	1.52	1.35
	15	-0.22	0.00	0.79	0.62	0.95	0.64

		Simulated Applicators Output Factor Error (%)					
		100 cm SSD					
		6x6	10x10	14x14	20x20	25x25	40x40
Energy (MeV)	6	-1.99	0.00	0.58	1.64		-0.08
	8	-0.49	0.00	1.57	2.39		0.85
	10	-1.40	0.00	1.43	2.35		1.47
	12	-1.33	0.00	1.32	2.30		2.08
	15	0.01	0.00	0.99	1.92		1.71

		Output Factor Error Difference (%)					
		100 cm SSD					
		6x6	10x10	14x14	20x20	25x25	40x40
Energy (MeV)	6	0.40	0.00	0.24	0.99	1.54	1.25
	8	0.30	0.00	-0.05	0.75	1.67	1.11
	10	0.07	0.00	0.53	1.58	1.99	1.40
	12	-1.65	0.00	0.38	1.13	1.22	1.03
	15	-0.23	0.00	0.81	1.20	1.62	1.54
	mean	-0.22	0.00	0.38	1.13	1.61	1.27

		Output Factor Error Difference (%)					
		100 cm SSD					
		6x6	10x10	14x14	20x20	25x25	40x40
Energy (MeV)	6	-0.45	0.00	0.88	2.05		1.07
	8	0.45	0.00	1.32	2.18		1.18
	10	-0.57	0.00	1.06	2.09		1.32
	12	-0.91	0.00	0.77	1.35		1.28
	15	-0.14	0.00	1.12	1.49		1.48
	mean	-0.33	0.00	1.03	1.83		1.27

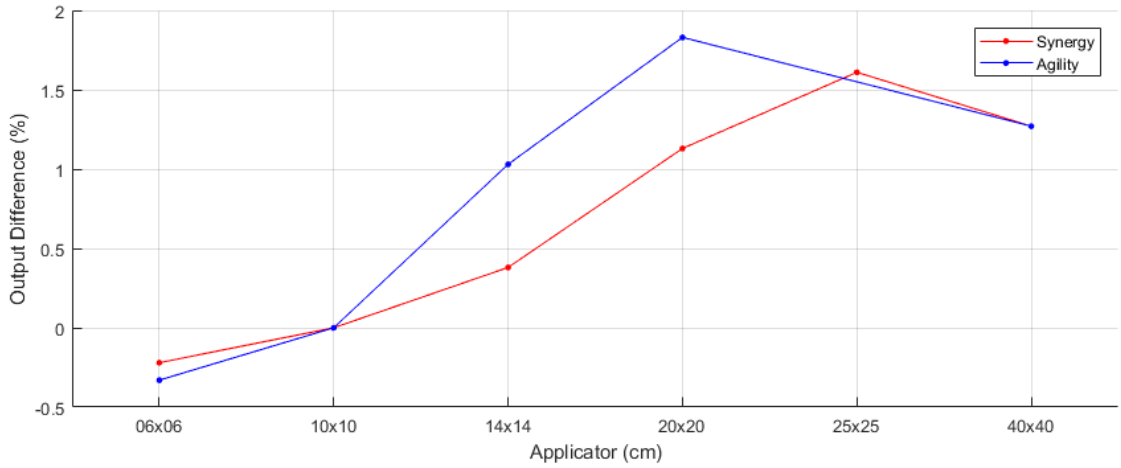

Figure 5-19 100 cm SSD 10 cm × 10 cm normalised Synergy and Agility simulated output error difference by introducing applicators

The pattern observed was particularly unusual as the effect cannot be due to the linear accelerator ionisation chamber MU discrepancy with field size as it was not present in the open field output results. As the applicators are suspected to be introducing an error, the normalisation to the 10 cm × 10 cm applicator could be further complicating the analysis. To remove any additional difficulties arising from normalising to a field with an applicator, the fields were normalised to the 40 cm × 40 cm field.

Output measurements were taken with and without the applicators to determine the effect on dose by the applicator's presence. This uses the 40 cm × 40 cm field as a reference point between open and applicator fields; the same circumstances were simulated in BEAMnrc. Ratios were determined for simulations and measurements where open field simulation output values were divided by their values with applicators present and are shown in Table 5-5. A ratio of less than one indicates that the output is higher with the applicator present. This suggests that the presence of applicator material contributes additional dose to the point of measurement.

Table 5-5 Ratios of measured and simulated outputs without applicators divided by outputs with applicators present for the respective applicator and energy field size

Synergy simulated with and without applicator output ratios					
	Applicator (cm)				
Energy (MeV)	6x6	10x10	14x14	20x20	25x25
6	0.967	0.961	0.958	0.974	0.972
8	0.969	0.943	0.960	0.976	0.970
10	0.972	0.964	0.967	0.983	0.972
12	0.974	0.971	0.975	0.983	0.990
15	0.965	0.962	0.973	0.985	0.988

Synergy measured with and without applicator output ratios					
	Applicator (cm)				
Energy (MeV)	6x6	10x10	14x14	20x20	25x25
6	0.953	0.947	0.943	0.968	0.971
8	0.956	0.932	0.951	0.977	0.975
10	0.962	0.955	0.964	0.986	0.980
12	0.959	0.962	0.971	0.984	0.992
15	0.946	0.951	0.970	0.985	0.990

Agility simulated with and without applicator output ratios					
	Applicator (cm)				
Energy (MeV)	6x6	10x10	14x14	20x20	25x25
6	0.956	0.961	0.964	0.970	
8	0.959	0.959	0.965	0.973	
10	0.967	0.961	0.973	0.983	
12	0.969	0.964	0.974	0.987	
15	0.962	0.962	0.974	0.985	

Agility measured with and without applicator output ratios					
	Applicator (cm)				
Energy (MeV)	6x6	10x10	14x14	20x20	25x25
6	0.933	0.950	0.959	0.975	
8	0.934	0.948	0.960	0.975	
10	0.941	0.948	0.969	0.985	
12	0.941	0.953	0.972	0.984	
15	0.938	0.952	0.972	0.985	

A further set of ratios were determined comparing the difference of measured from the simulated with and without applicator ratios and are shown in Figure 5-20 where Agility results are shown in blue and Synergy results in red.

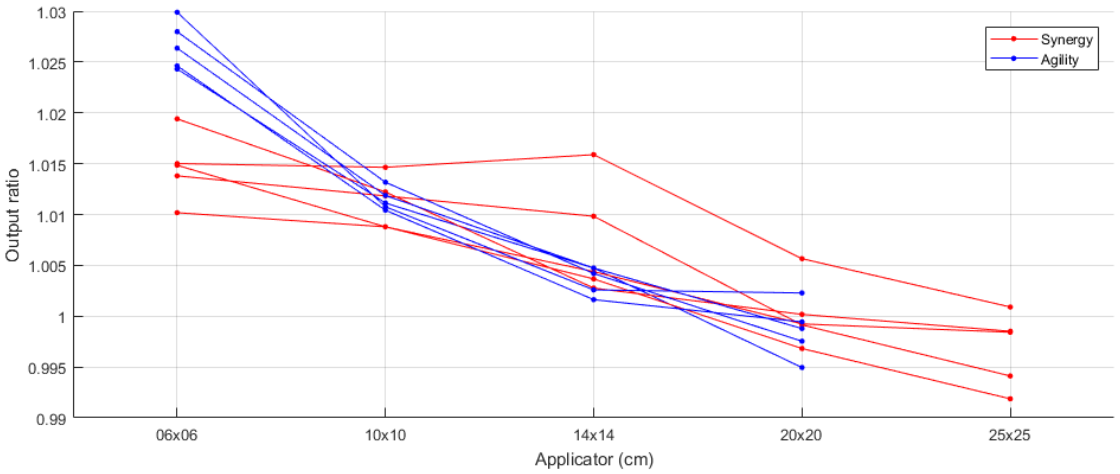

Figure 5-20 100 cm SSD 40 cm × 40 cm normalised Synergy and Agility ratio of measured and simulated outputs for with and without applicators for five energies

A result of one in Figure 5-20 indicates the ratio of measured output with applicators to without applicators is equal to the simulated ratio. This enabled a comparison of how the dose varies between the simulation and measurements by the

addition of the applicator. Measured ratios were lower than simulated ratios suggesting that the models in MC are not contributing enough additional dose with the applicators present. The loss of additional dose was dependent on field size and approaches measurement for applicators 20 cm × 20 cm and larger. This can be understood where the smaller applicators are closer to the centre of the field creating new scatter sources closer to the measurement point.

Figure 5-20 Agility results produce closer agreement between energies than Synergy results. This could be due to the large variations from default field sizes for the Synergy to match results from previous accelerators in the department. This test could be more tightly controlled by using a set field size for all energies with and without applicators. However current results are sufficient to reveal the cause of the applicator output discrepancy. This explains the offset errors in Figure 7-19 that are dependent on the applicator and confirms that simulated cutouts are not supplying enough dose. By accepting the 10 cm × 10 cm applicator value as the reference value (equivalent to 100 MU per Gray), the wrong normalisation value was used which introduces error in other applicators.

The remaining discrepancy was the increased error in dose drop off rate with SSD. Figure 5-21 and Figure 5-22 show the error from each applicator with standard cutout obtained by subtracting the 110 cm SSD results from the 100 cm SSD in Figure 5-17 and Figure 5-18 for the BEAMnrc and Monaco TPS respectively.

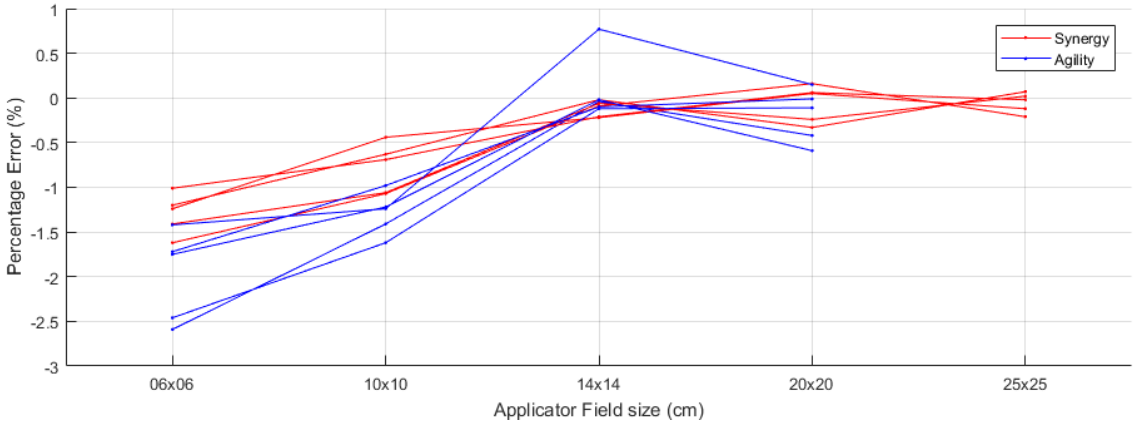

Figure 5-21 Synergy and Agility in-house MC applicator dose drop off output error from 100 to 110 cm SSD

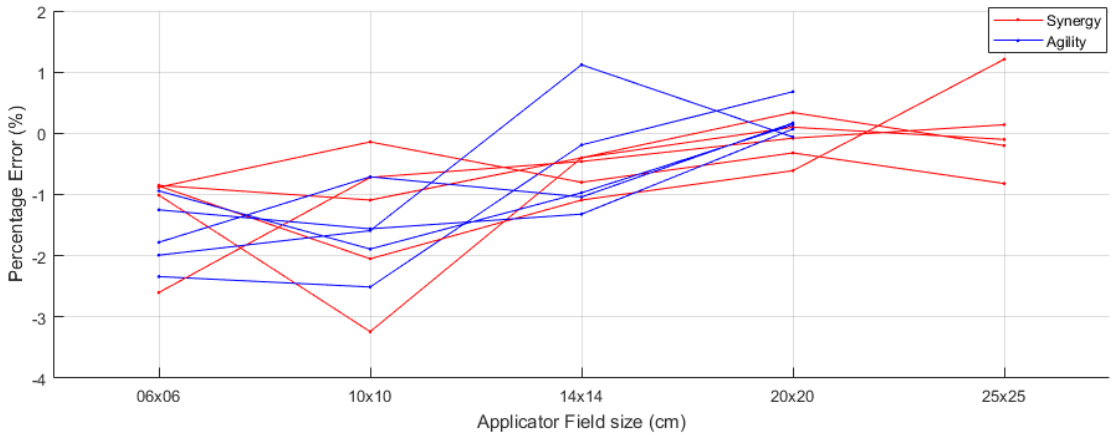

Figure 5-22 Synergy and Agility Elekta TPS applicator dose drop off output error from 100 to 110 cm SSD

Open field results gave agreement within 0.6% for all energies without applicators present over a 20 cm SSD span. With applicators present, the error has increased to 2.5% over a 10 cm SSD span as can be seen in Figure 5-21. The magnitude of the error diminishes with increasing applicator size and stabilises at the 14 cm × 14 cm applicator. The trend is apparent in Elekta's TPS however not to the same accuracy as in-house simulations because the precision of simulation results is limited by Elekta's maximum simulated particle number. This finding agrees with data shown in Figure 7-19 where the error gradient with SSD decreases with larger applicators and stabilises at the 14 cm × 14 cm applicator. The negative error indicates the simulated dose at 100 cm SSD is lower than measured relative to 110 cm SSD.

This suggests a new effective source is missing or underestimated in the region of the applicator. This is supported by Figure 7-19 where smaller applicators increasingly underestimate dose when approaching the applicator end. An overestimation of dose when moving away from the applicator suggests the new underestimated source is close the end of the applicator.

5.6. Discussion

Further time and refinement of the open field profiles would enable improved model agreement. Due to time constraints, errors in model profile agreement to measured data in the penumbras after the MLCE was modified were accepted. Through further investigations the cause of the errors could be determined and agreement improved. To compensate for the penumbra disagreement, field sizes were matched to

90% dose levels in the penumbras as this region was within the clinical applicator fields. This is shown by the errors in Appendix A where errors greater than 1% are outside the clinical field size. The flow on effect to the model should be minimal as the clinical field size profiles were already within 1%.

The discrepancies observed in 5.5.3 indicate that missing applicator material must be responsible. The overly simplistic representation of the applicator module in the BEAMnrc excludes all sections of material that do not form the collimating structure. Material that is present in the light field (illuminated green) is in the direct path of the beam. Figure 5-23 (a) shows material that is not represented in the BEAMnrc model highlighted in red (symmetrical in the inplane dimension) compared to what is used in the BEAMnrc (b).

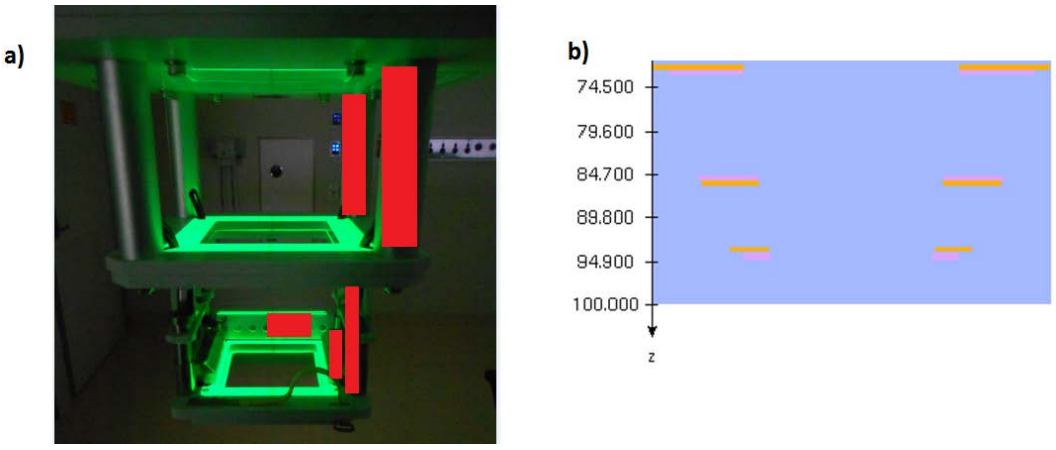

Figure 5-23 Highlighting discrepancies between applicators (a) and their representation in BEAMnrc (b)

This indicates a significant portion of excluded material is near the end of the applicator. This suggests that the missing material is the cause of both discrepancies. Further indications to missing material arise from the inplane profiles lack of shielding just outside the field edges as observed in Figures 7-4 to 7-10. In reality, extra material is present due to the cutout securing mechanism; this would further shield for inplane profiles only. A detailed effort was undertaken to try and include all material near the end of the applicator and poles between shielding layers. The precise applicator model is shown in Figure 5-24 (note additional material such as poles and springs are not observed as they are not present in the central inplane plane).

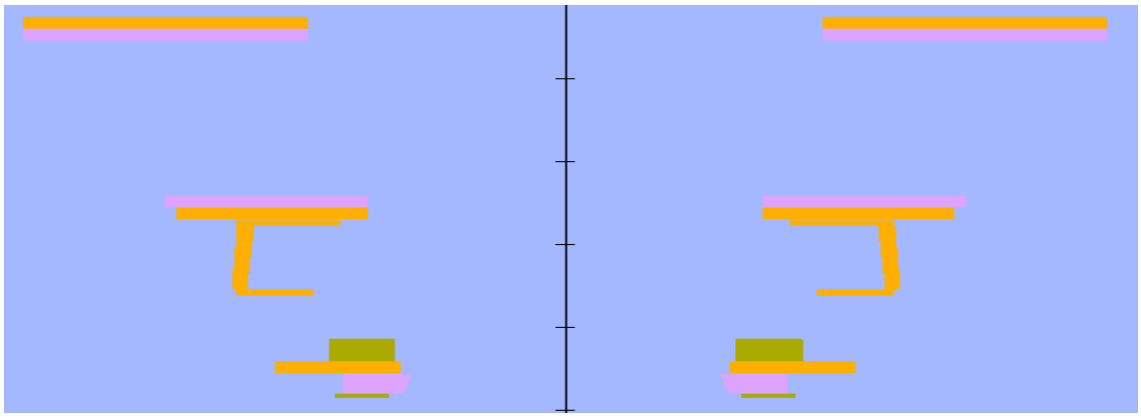

Figure 5-24 6 cm × 6 cm applicator modelled precisely in BEAMnrc

Unfortunately, the simulation with these modifications would not complete and simulation could not be resolved. The cause for the simulation error was not found and components were reduced until a simulation would complete. To investigate the missing material theory, only the cutout securing material (green material in Figure 5-24) was included and simulated. The results for the difference in a PDD are shown below in Figure 5-25. Simply adding the small amount of material (although in the direct beams path) could raise the PDDs output by 1.35%. This confirms the notion that extra material can increase the dose delivered to D_m and by doing so modify the position of the effective source. Therefore, it is not possible to obtain accurate output and dose drop off results without the inclusion of the missing material.

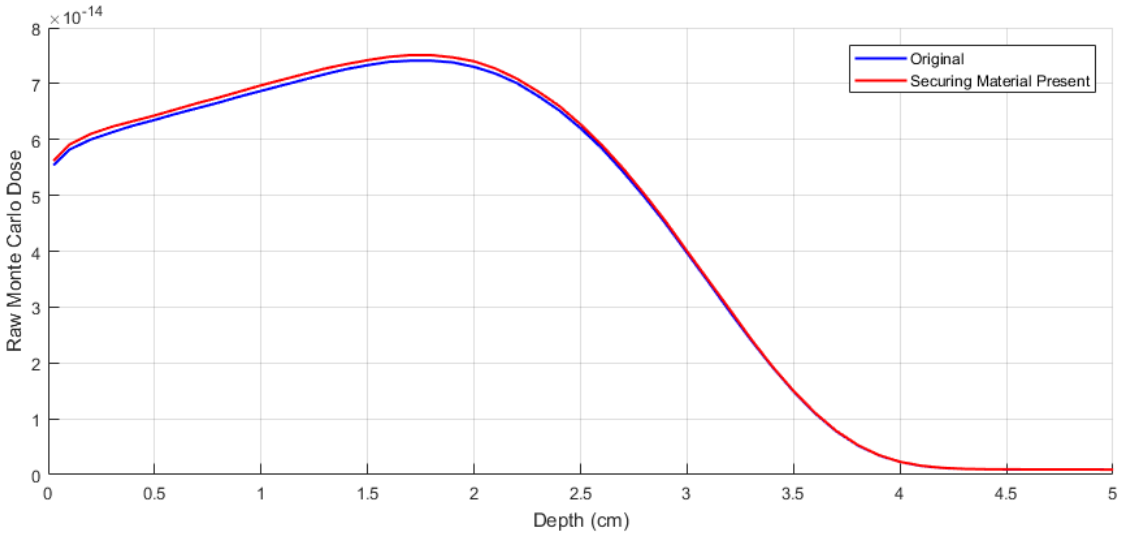

Figure 5-25 Depth dose results for the 6 cm × 6 cm applicator with the inclusion of the cutout securing material in the BEAMnrc simulation

5.7. Summary

By implementing a shared module component modelling refinement process, an error was found within the NRC BEAMnrc MLCE module used. By creating artificial walls in the MLCE module the initial BEAMnrc model output discrepancies were resolved. Rebuilt models achieved open field accuracy to within 2% for PDDs and the majority of profiles within 1% agreement to measured data. With the exception of 6 MeV 6 cm × 6 cm; outputs for both models were within 1% over the 20 cm SSD and 6 cm × 6 cm were within 2%. Dose reduction with SSD was within 0.6% relative to the respective OF for all energies without applicators present over a 20 cm SSD span.

After introducing applicators into the BEAMnrc models, new discrepancies were observed. Results using the determined open field spectra were not suitable when compared against the applicator measurement dataset. This was due to the difference in the beam energy at the different dataset collection times. Open field PDDs were adjusted to the R_{50} depths of the applicator dataset and resimulated. Variation in incident spectrum energy adjustment are shown in Appendix D.

The accuracy of PDDs and profiles for each combination of depth, energy applicator SSD and accelerator model were determined against measurements using the gamma method and the RMS gamma results are collated in tables in Appendix B. Relative results from applicators with standard inserts indicate successful model development as the RMS gamma value of less than one indicates the profile is in better agreement than 1%/1 mm. Surface and depth of 20% dose profile gamma results exceed the passing value due to the high uncertainty in the BEAMnrc simulation in the surface region and the stricter relative criteria at the 20% value respectively.

Applicator output errors with standard inserts of 1% and greater were observed for larger fields (14 cm × 14 cm and larger) and remain consistent over the 100 and 110 cm SSD. 6 cm × 6 cm and 10 cm × 10 cm applicators were observed to have disagreements with dose reduction with SSD varying by 2% over 10 cm that were not present without applicators (~0.6% over 20 cm SSD).

By utilising the 40 cm × 40 cm field as a reference and comparing simulation open field absolute dose relative to applicator field dose to measured values it was found the BEAMnrc APPLICAT module was not contributing enough additional dose with the applicators included. The absence of dose was dependent on field size and approached agreement to measured data for applicators 20 cm × 20 cm and larger. By

accepting 10 cm × 10 cm applicator dose value as the reference, an incorrect normalisation value was used which introduced an error in other applicators.

The discovered discrepancies are a fault of the overly simplistic representation of the applicator using the APPLICAT module because it excludes all sections of material that do not form the shielding layers. There is strong evidence in both the relative and absolute dosimetry that suggests this is due to the missing material in the applicators in the simulation environment. This flaw was unable to be resolved in the time available and the effects remain present in developed BEAMnrc models.

6. Monaco 5 Electron Beam Models

6.1. Background

Elekta's treatment planning system, Monaco, utilises the coupled multi-source method for electron treatment phase space generation while patient dose calculations are performed with the VMC++ algorithm that is based on the VMC method. Several variance reduction techniques are used and depending on energy, beam quality, voxel resolution, cut-off energies and materials VMC is 50-150 times faster than the EGS4 code. Further detailed specifics can be found in the Monaco External Beam Dose Calculation Algorithms Technical Reference guide (Elekta, 2014).

Monaco beam models are generated by Elekta from a supplied prescribed list of measurements and the custom models are returned to the clinic. Beam models are then incorporated into the TPS ready for validation and implementation. PDDs, Profiles and OFs were collated from extracted dose planes and underwent processing identical to that used for extracted BEAMnrc simulation profiles as described in Section 5.5. The same Gamma analysis method as described in Section 5.5 was used to ensure identical and fair evaluation to allow direct comparison between modelling methods.

6.2. Results

6.2.1. Standard Applicator Insert PDDs and Profiles

A gamma index table was produced for each accelerator model, SSD, energy and applicator combination for the Elekta Monaco models. An example of the gamma index table is shown in Table 6-1 for the Synergy 100 cm SSD 6 MeV 20 cm × 20 cm Monaco 5 beam model. The RMS error was calculated for each profile and PDD and stored in the gamma index table. Figures 7-3 to 7-11 are selected profile plots (highlighted in yellow in the table). The RMS error row (in bold) for each combination was extracted and collated into separate tables in Appendix B.

Table 6-1 Gamma index result table for Elekta TPS Synergy Electrons 100 cm SSD 6MeV, 20 cm × 20 cm gamma (1%, 1 mm)

	PDD	Inplane							Crossplane						
		P1	P2	P3	P4	P5	P6	P7	P1	P2	P3	P4	P5	P6	P7
Total # points	45	361	361	361	361	361	361	361	361	361	361	361	361	361	361
$\gamma > 1$ (fail)	4%	20%	14%	8%	7%	10%	42%	32%	48%	14%	7%	3%	14%	11%	49%
$\gamma < 1$ (pass)	96%	80%	86%	92%	93%	90%	58%	68%	52%	86%	93%	97%	86%	89%	51%
RMS γ	0.71	1.04	0.76	0.53	0.51	0.56	1.09	1.21	1.50	0.84	0.55	0.43	0.65	0.60	1.83
Maximum γ	1.23	3.91	2.92	2.10	1.62	1.87	2.93	3.54	4.43	2.80	2.06	1.32	1.78	2.31	5.25
R_{50}	2.50														
γ pass < d_{max}	84.6%														
γ pass > d_{max}	100.0%														
γ pass < 50%		95%	100%	100%	100%	100%	100%	100%	47%	100%	100%	100%	100%	100%	99%
γ pass > 50%		70%	76%	87%	88%	83%	28%	45%	56%	76%	89%	95%	77%	81%	18%

% Dose	100	90	80	50	20
Δ Dose (cm)	-0.10	-0.09	-0.09	-0.09	-0.09

Profile	P1	P2	P3	P4	P5	P6	P7
Depth (cm)	0.50	1.00	1.30	1.86	2.06	2.50	2.93

6.2.2. Outputs with Standard Applicators Inserts

Differences between output factors and measured data for standard applicator cutouts were determined for the Monaco 5 models. Figure 6-1 and Figure 6-2 show results from Monaco 5 for applicator factors over SSDs 100 and 110 cm for both accelerator models and all energies. Errors up to 2% are observed for the 6 cm × 6 cm and 10 cm × 10 cm applicator between 100 to 110 cm SSD. In general, 100 cm SSD outputs are within 1% but discrepancies are larger for 110 cm SSD.

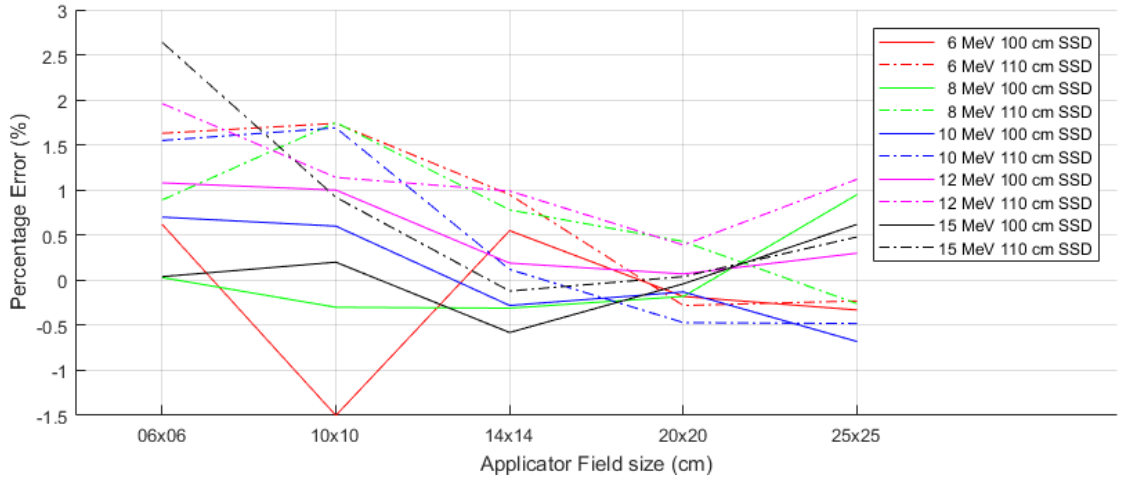

Figure 6-1 Synergy Elekta TPS applicator output errors for 100 and 110 cm SSD

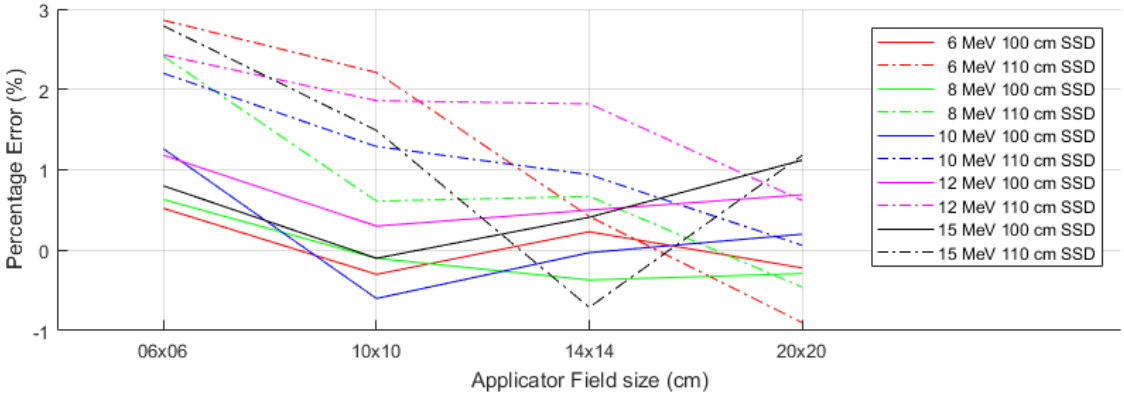

Figure 6-2 Agility Elekta TPS applicator output errors for 100 and 110 cm SSD

6.3. Summary

Monaco model profile and PPD prediction were found to successfully meet the clinical gamma criteria of 2%/2 mm for both Synergy and Agility models for the five

energies and applicators combinations over SSDs 100 and 110 cm. Monaco models were also assessed with the stricter gamma criteria of 1%/1 mm to be compared against in-house BEAMnrc models. Standard applicator field gamma RMS error results are summarised by Figure 6-3 where a calculation grid size of 2 mm was used. Outputs were found to be within 1% for both accelerator models at 100 cm SSD and within 3% at 110 cm SSD and are discussed further in section 7.5. Output results are prone to variation due to the statistical uncertainty of the simulation results on a pixel by pixel basis.

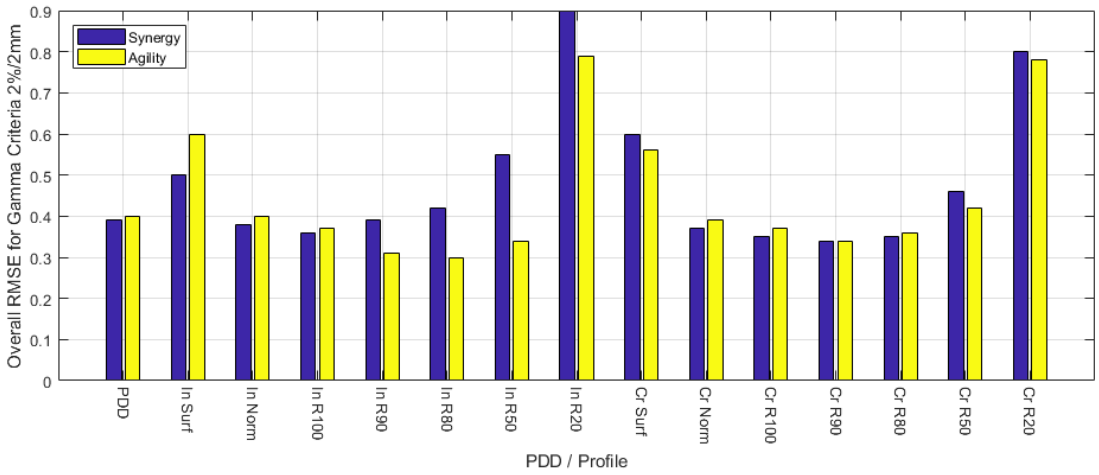

Figure 6-3 Monaco Beam model profiles RMS error with clinical gamma criteria of 2%/2 mm

By varying the grid size, the surface boundaries are merged with surrounding air, expanding the volume with a reduced CT HU value for the external voxels. A larger calculation grid size has an impact on the PDD's R_{50} as shown by Figure 8-9 but significantly lowers the statistical noise in the simulation. This is shown in Figure 6-4 where the overall PDD RMS error is similar between a 1 mm and 2 mm grid size and worse for 3 mm, however a significant profile improvement is obtained with the 2 mm grid. As the 1 mm grid requires roughly twice the simulation time of the 2 mm, a calculation grid size of 2 mm was chosen as a compromise between calculation time, model agreement and clinical requirement.

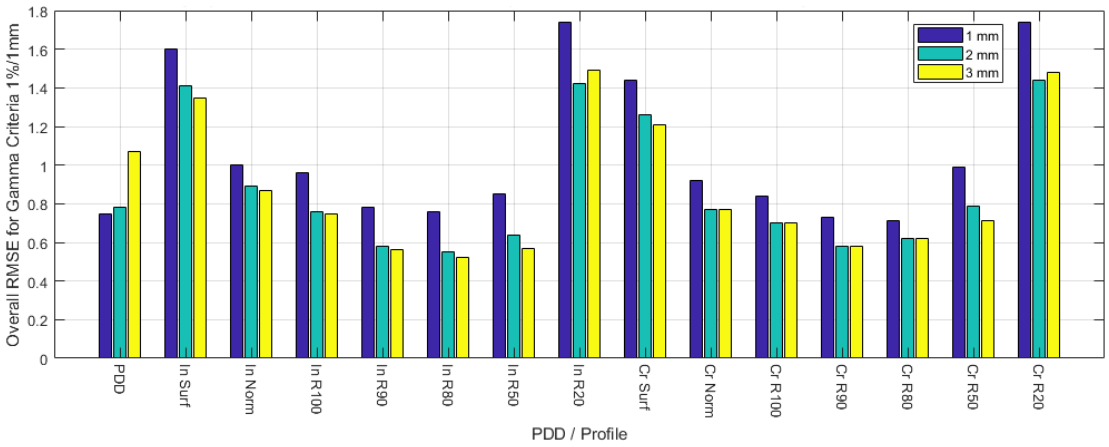

Figure 6-4 100 SSD Agility model RMS profile summary error variation with Monaco 5 calculation grid size

7. Comparison between BEAMnrc and Monaco 5 Models

7.1. Background

With all electron beam models completed, extracted data was evaluated for standard applicator cutouts. Results described below in section 7.3 concluded all models developed were successfully able to meet the strict gamma analysis passing criteria of 1%/1 mm. Electron dose distributions could then be simulated under conditions outside of the scope of data used to develop each model. Supplemented with measurements, models were tested and evaluated to determine whether simulation agreement was maintained reflecting the robustness of the models.

Model applications under various conditions were tested with increasing complexity by introduction of shaped cutout fields, surface geometric variations from flat slab geometry and with the inclusion of inhomogeneities using tissue equivalent slabs. Details of each condition are described further in each section below with the corresponding results. Each condition was reproduced in both Monaco 5 and BEAMnrc and respective data was extracted and evaluated using the same gamma techniques as for standard applicator fields.

Spectra determined by Monaco and BEAMnrc for each electron beam model are compared in Section 7.2 to observe general distribution variations and their respective results.

7.2. Spectra Comparison

Both commercial and in-house developed modelling methods produced successful beam models. A comparison between the spectra would indicate if the independent methods resulted in similar spectral distributions for each energy.

Information about the spectra striking the exit window is not readily available from Elekta but they do provide spectral distributions at the end of the applicator. Elekta's spectrum distribution is represented by a modified Woods-Saxon distribution where coefficients are stored in the beam model files.

Spectral distributions (electrons only) were determined from BEAMnrc from the phase space files for a 20 cm × 20 cm applicator in a region two thirds of the field size

to avoid any applicator edge interactions. This should produce a similar scenario and allow for comparisons between the two modelling methods.

Figure 7-1 and Figure 7-2 below show the distributions for BEAMnrc striking the exit window and the resulting distribution at the patient's surface with Elekta's distributions at the patient's surface for 6 MeV Synergy and Agility beams. Appendix D shows spectral distributions for the remaining energies for both accelerator models.

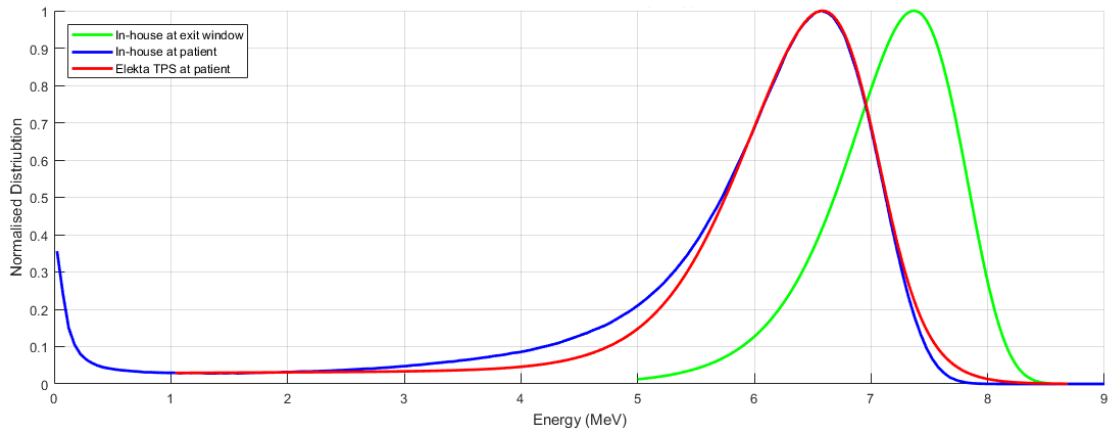

Figure 7-1 Synergy 6 MeV beam model spectrum determined by Elekta and in-house modelling methods

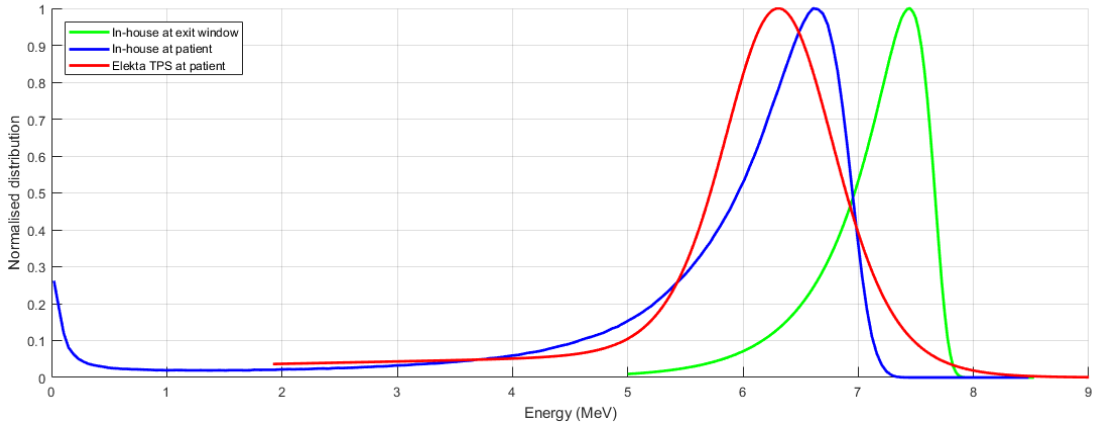

Figure 7-2 Agility 6 MeV beam model spectrum determined by Elekta and in-house modelling methods

7.2.1. Discussion

The majority of the spectra determined by Elekta using a modified Woods-Saxon distribution and the modified Landau method used in this thesis produce

comparable results. The spectra distributions show a Landau or right biased Gaussian distribution with the exception of Elekta's 6 MeV Agility shown in Figure 7-2 where the distribution is skewed to the left. Noticeable similarities are seen in the Synergy 6, 10 and 12 MeV and Agility 8 and 12 MeV models while the Synergy 8 MeV (Figure D-6) and Agility 15 MeV (Figure D-13) have little resemblance. In-house determined spectra are not modified while Elekta has implemented an electron cut off between 1 to 2 MeV varying between models developed. An electron of energy 2 MeV is still capable of deposition dose to a depth of 1 cm, but given the number of particles relative to the entire distribution the exclusion of these particles may not be relevant. The exclusion of low energy particles could help optimise the distribution for Elekta and may also serve as a technique to reduce simulation time.

7.3. PDDs and Profiles with Standard Applicators Inserted

PDDs and profiles from Monaco 5 and BEAMnrc were compared against measurement as mentioned in section 5.5.1 and 6.2.1. These comparisons are shown below in Figures 7-3 to 7-11.

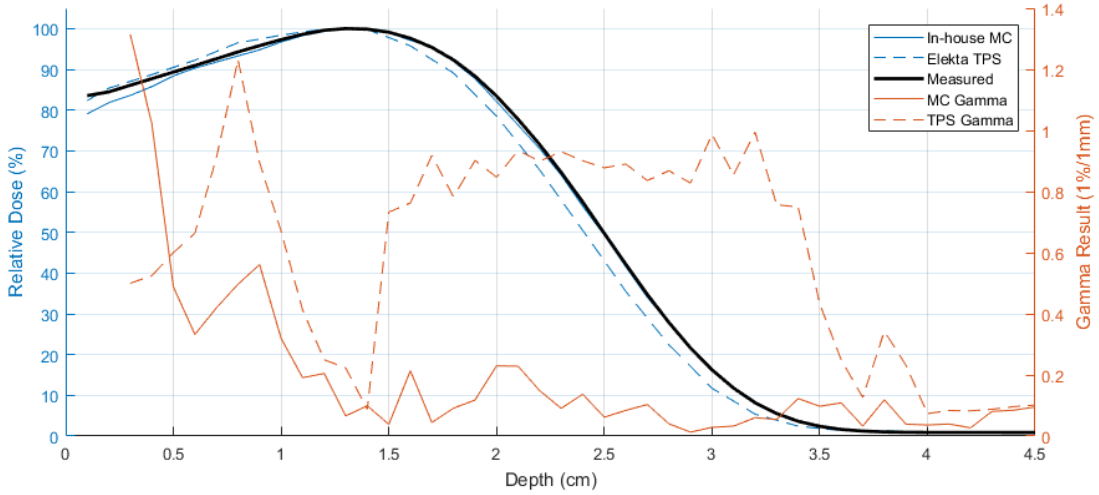

Figure 7-3 In-house MC and Elekta TPS PDD agreement from measured 100 cm SSD 6 MeV 20 cm × 20 cm standard cutout

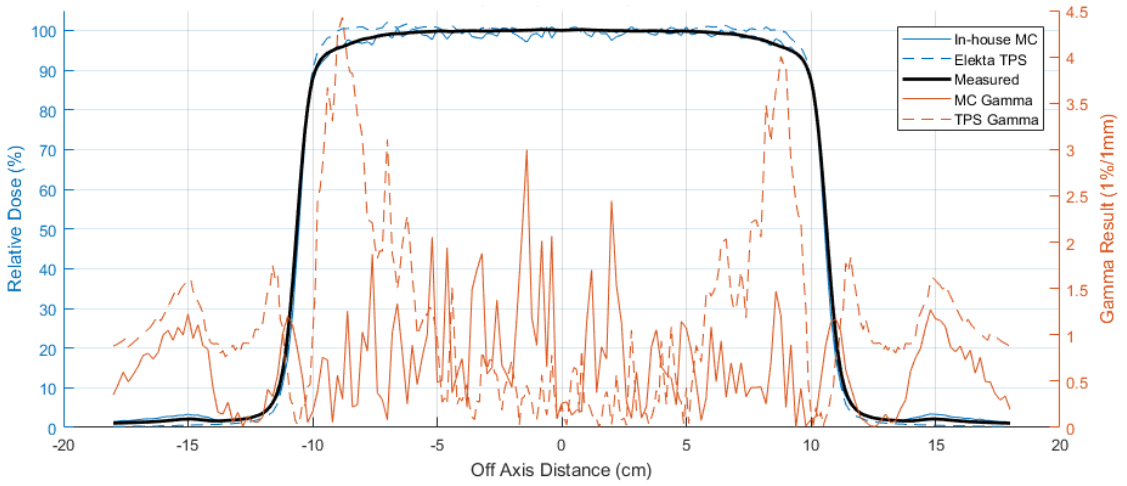

Figure 7-4 100 cm SSD 6 MeV 20 cm × 20 cm standard cutout in-house MC, Elekta TPS and measured surface dose crossplane profile (0.50 cm) with respective gamma results

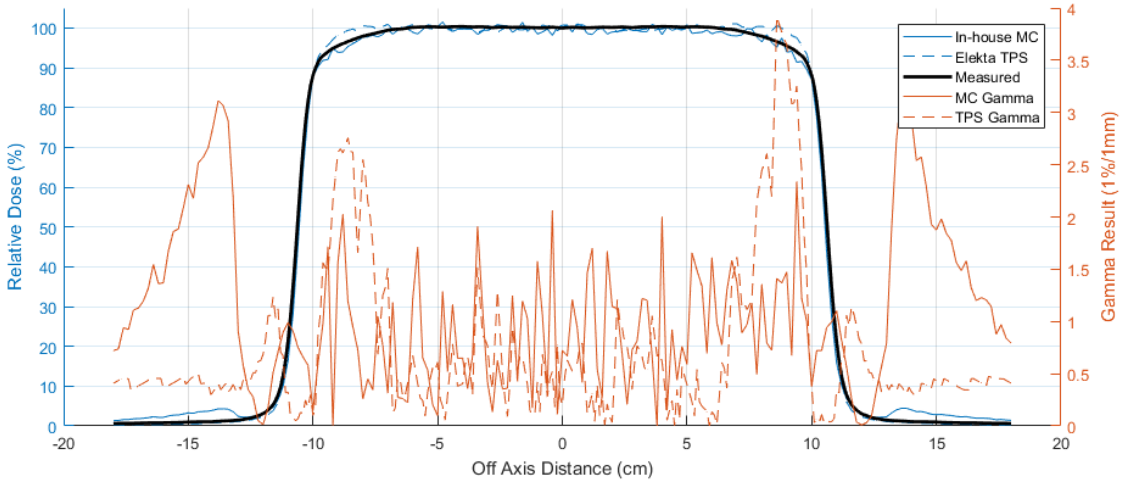

Figure 7-5 100 cm SSD 6 MeV 20 cm × 20 cm standard cutout in-house MC, Elekta TPS and measured surface dose inplane profile (0.50 cm) with respective gamma results

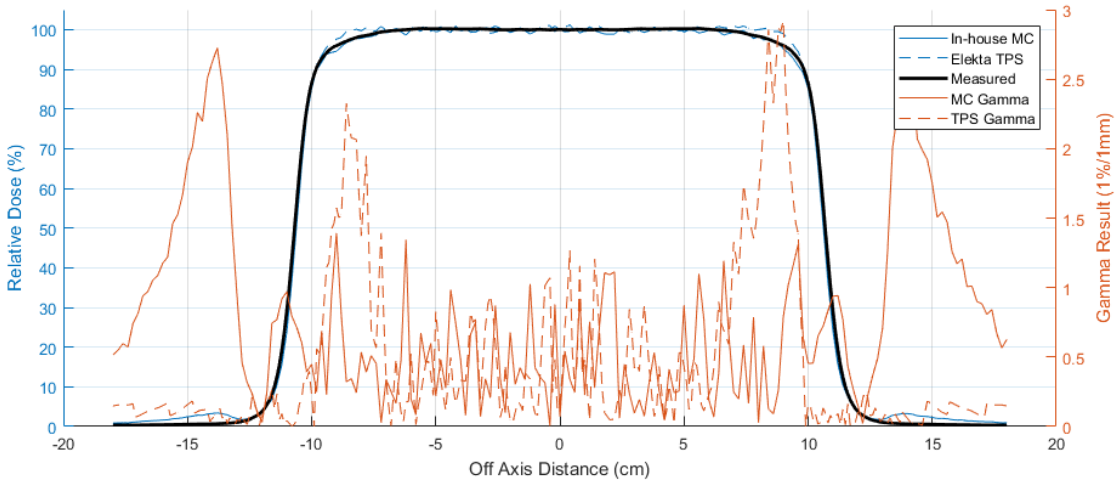

Figure 7-6 100 cm SSD 6 MeV 20 cm × 20 cm standard cutout in-house MC, Elekta TPS and measured inplane profile (1.00 cm) with respective gamma results

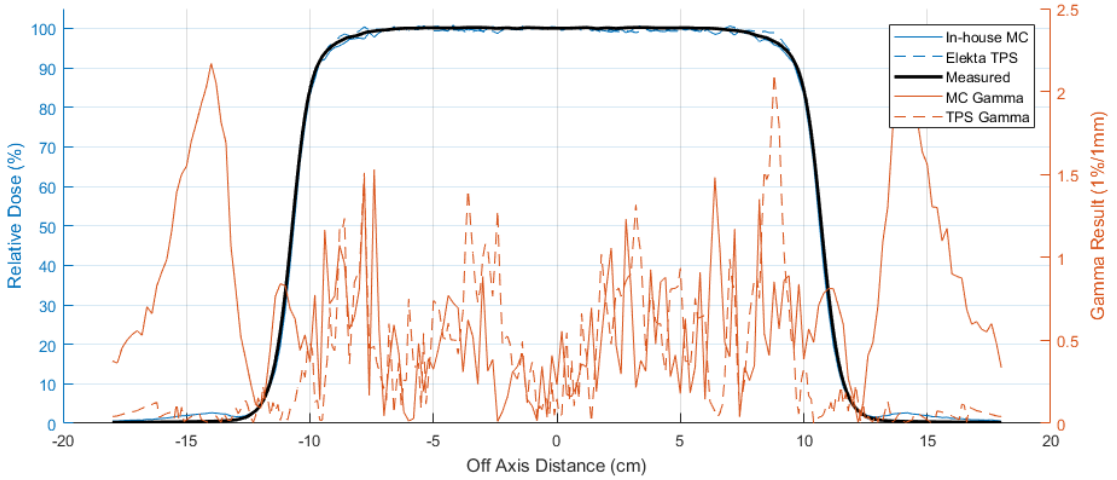

Figure 7-7 100 cm SSD 6 MeV 20 cm × 20 cm standard cutout in-house MC, Elekta TPS and measured D_m inplane profile (1.30 cm) with respective gamma results

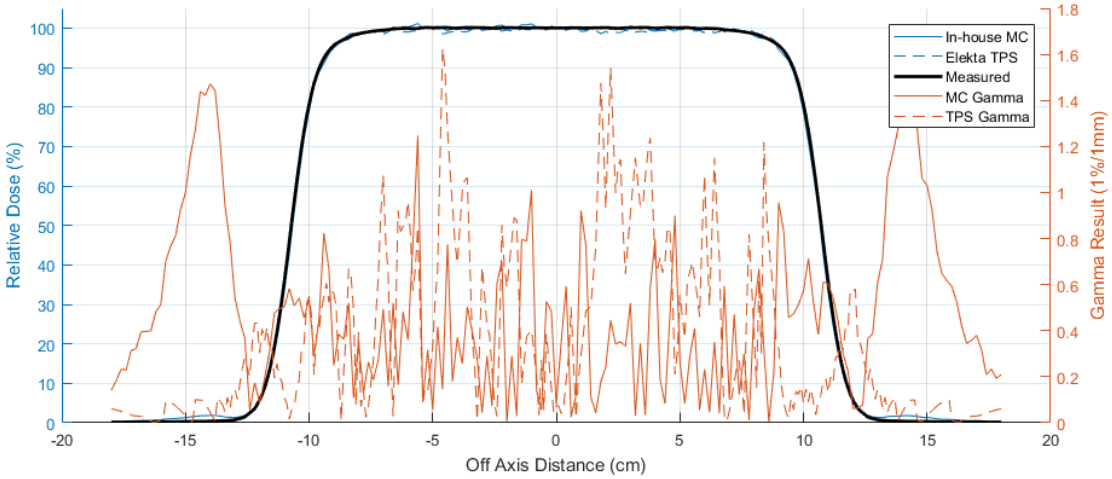

Figure 7-8 100 cm SSD 6 MeV 20 cm × 20 cm standard cutout in-house MC, Elekta TPS and measured R_{90} inplane profile (1.86 cm) with respective gamma results

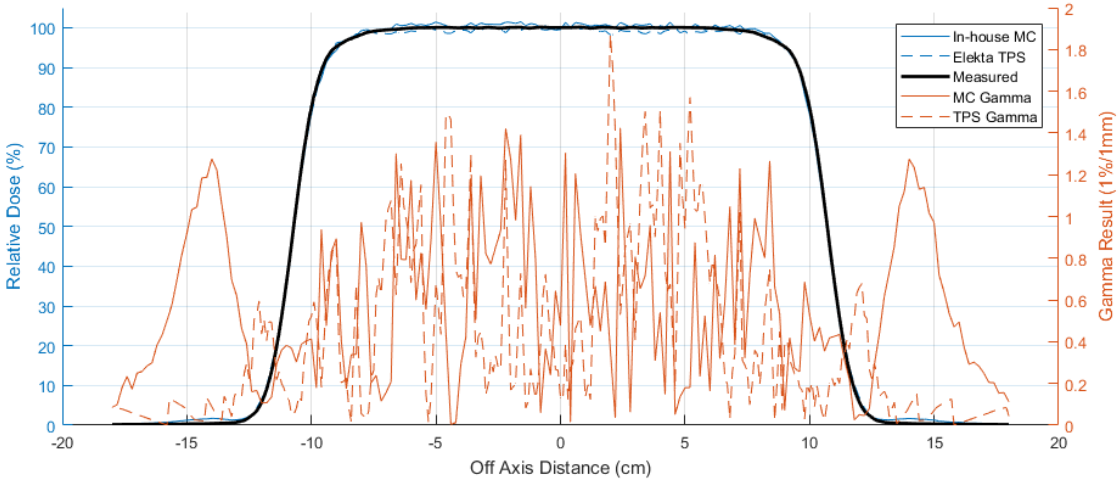

Figure 7-9 100 cm SSD 6 MeV 20 cm × 20 cm standard cutout in-house MC, Elekta TPS and measured R_{80} inplane profile (2.06 cm) with respective gamma results

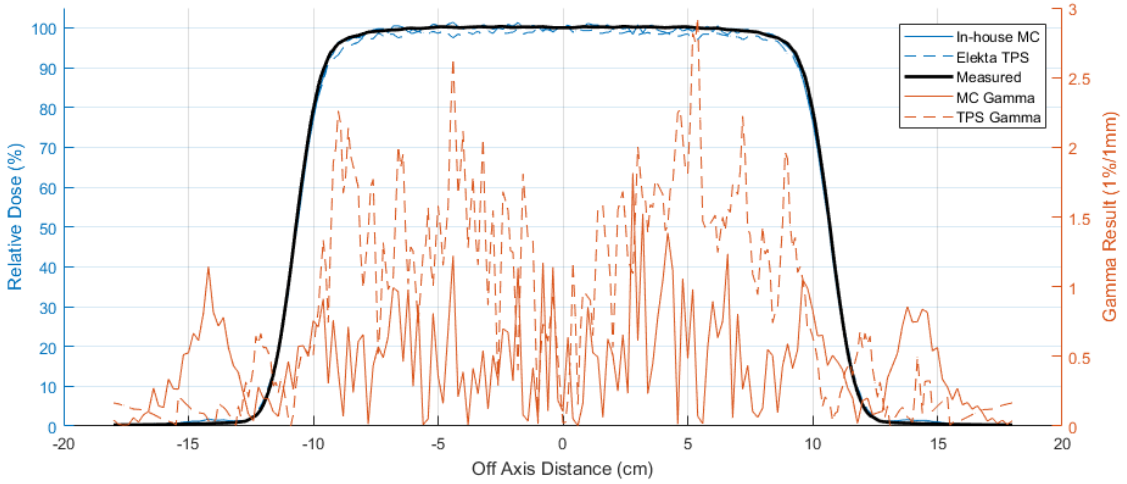

Figure 7-10 100 cm SSD 6 MeV 20 cm × 20 cm standard cutout in-house MC, Elekta TPS and measured R_{50} inplane profile (2.50 cm) with respective gamma results

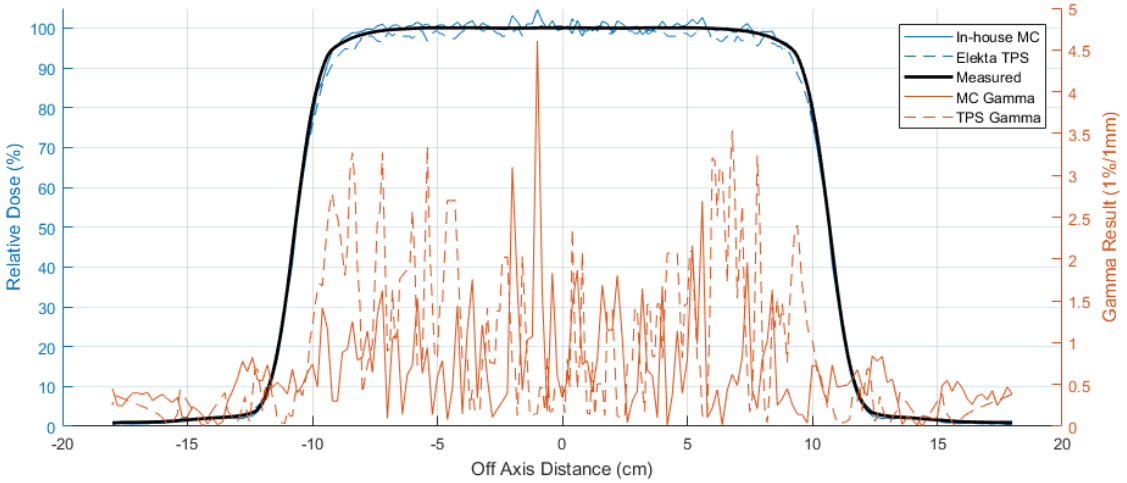

Figure 7-11 100 cm SSD 6 MeV 20 cm × 20 cm standard cutout in-house MC, Elekta TPS and measured R_{20} inplane profile (2.93 cm) with respective gamma results

7.3.1. Results

The RMS error for each PDD and profile determined in section 6.2.1 that are shown in RMS error index Tables B-1 to B-4 were further condensed to make a comparison between the developed and commercial model. An RMS value was calculated from the RMS error index tables utilising values from the applicator and SSD for each energy. The overall model RMS error values for each model and energy are shown in Figure 7-12 and Figure 7-13. While no longer representing a true RMS error, it enables a comparison of the overall model accuracy for the selected energy.

An additional data set, Sm3, shows the result if the in-house models were smoothed with a noise filter spanning three units. A RMS error reduction in Sm3 overall gamma value indicates the BEAMnrc model data is susceptible to noise. The smoothed result is what would be expected by increasing the number of simulated particles in both the BEAMnrc and DOSXYZnrc simulation phase. Monaco results cannot be improved any further as the maximum allowed number of particles is already used for all results.

Figure B-1 and Figure B-2 in Appendix B shows overall RMS error values in the summary column of Tables B-1 to B-5 for individual profiles across SSDs and energies.

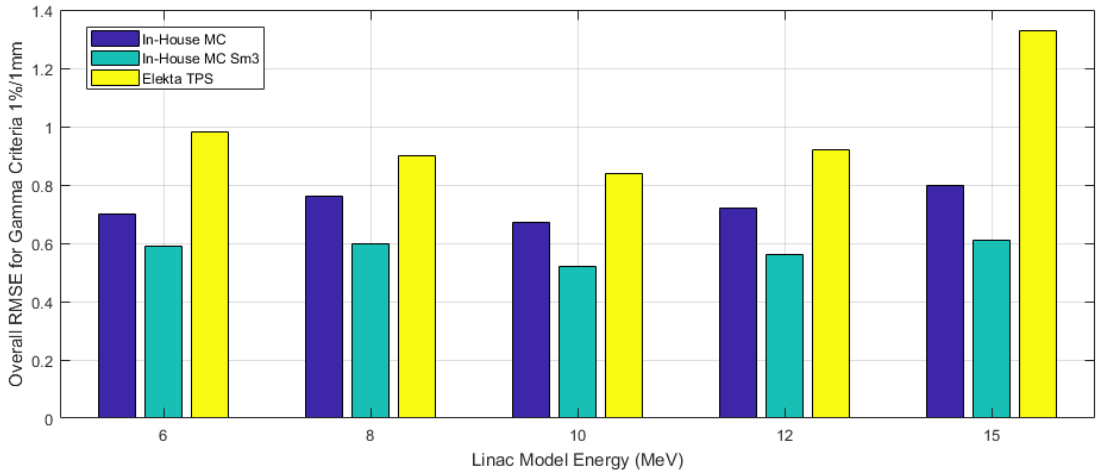

Figure 7-12 Comparison of Elekta Synergy beam models with standard applicator cutout for overall RMS error result

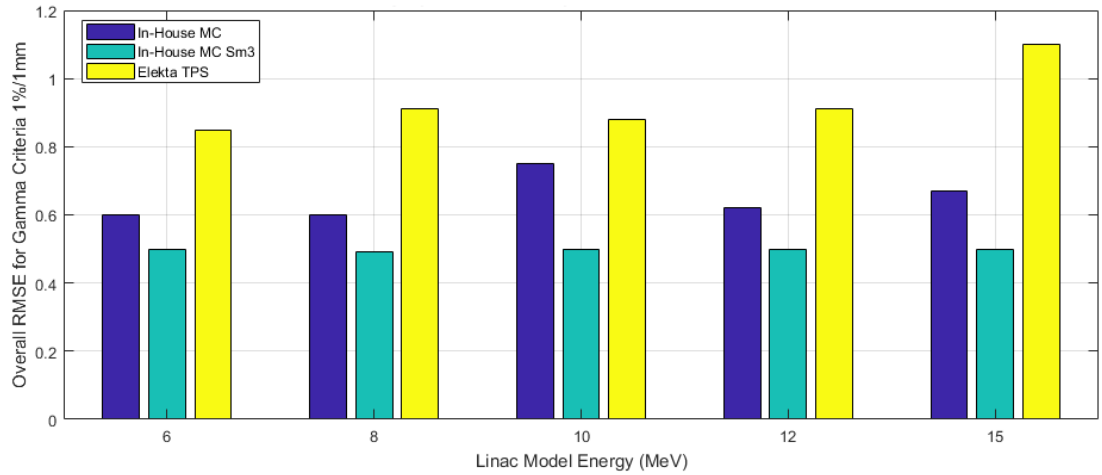

Figure 7-13 Comparison of Elekta Agility beam models with standard applicator cutout for overall RMS error result

7.3.2. Discussion

In-house developed models were able to achieve superior gamma passing rates compared to those by Elekta. This could be due to the considerable effort and time in refinement in the in-house models that a global company cannot offer to each individual customer. While in-house models achieved superior results, the effect of smoothing the data represent by Sm3 indicates that better performance could be achieved. Noise variations can be reduced by increasing the number of particles in all stages of the simulations. Any benefit achieved by increasing the number of particles simulated needs to be balanced against the increased simulation time.

The majority of Elekta beam models was found to have excellent profile agreement for small fields that was not maintained with larger fields. This suggests that the fine tuning of the scattering foils and incident electron spectrum were not specifically customised or may be a limitation of the virtual source construction. For the majority of large field beam models, the off-axis profile prediction is higher than measured in the build-up region and lower than measured near the practical range as shown by Figure 7-14 and Figure 7-15 respectively. While the prediction errors are of little clinical consequence, it remains a refinement opportunity for Elekta to achieve improved beam model agreement.

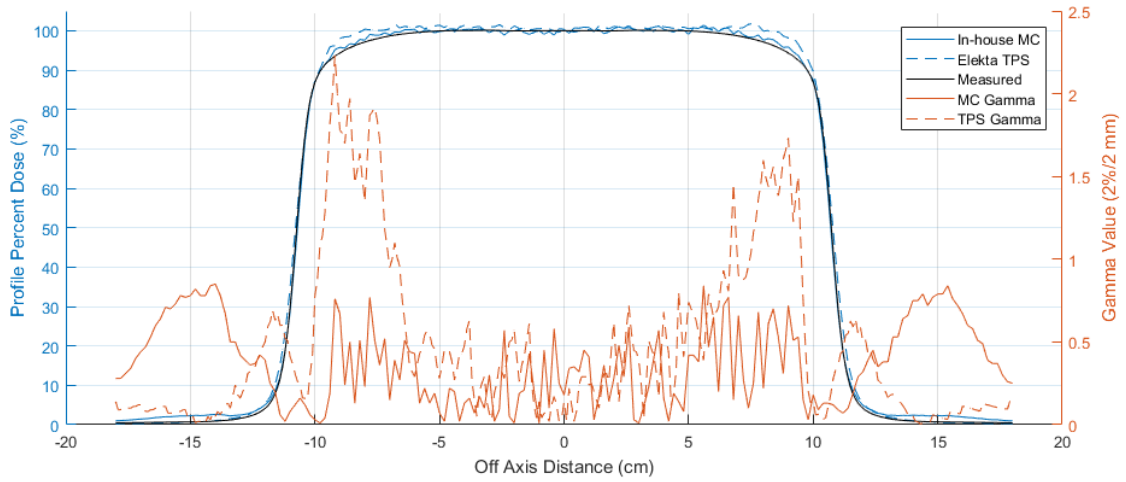

Figure 7-14 Profile displaying Monaco 5 dose overestimation off-axis for a large field in the build-up region. 100 cm SSD Agility 12 MeV 20 cm × 20 cm standard cutout in-house MC, Elekta TPS and measured inplane profile (2.00 cm) with respective gamma results

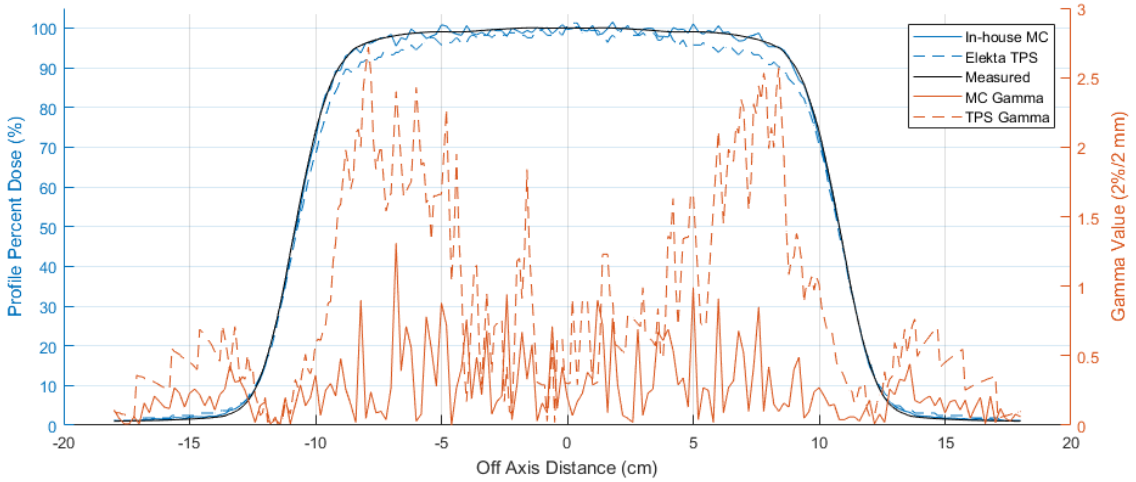

Figure 7-15 Profile displaying dose underestimation off-axis for a large field near the practical range region. 100 cm SSD Agility 12 MeV 20 cm × 20 cm standard cutout in-house MC, Elekta TPS and measured inplane profile (5.47 cm) with respective gamma results

7.4. Shaped Fields

While standard applicator cutout results represent the models' ability to match supplied modelling data, an effective robust model must maintain the same accuracy when applied to any field. A shaped cutout was chosen for each of three applicators. Relative outputs, PDDs and inplane and crossplane profiles at depth D_m for three SSDs (97, 100 and 105 cm) were measured for each energy for both Synergy and Agility models. The cutouts are described in Table 7-1. The same process was followed comparing PDD and profile data as in section 7.3 against measurements.

7.4.1. Results

The resulting gamma index for PDDs and profiles is shown in Table B-6 and overall RMS error summary shown by Figure 7-16. Outputs were measured for the five energies and were normalised to the 10 cm × 10 cm applicator at 100 cm SSD. Output error results are shown in Figure 7-17 and Figure 7-18 for Synergy and Agility respectively. Figure 7-17 and Figure 7-18 group outputs by colour for all energies for each cutout to allow easier comparison.

Table 7-1 Shaped cutout details

Applicator (cm)	Shape	Inplane Field Size (cm)	Crossplane Field Size (cm)
6 × 6	Rectangle	4	5
10 × 10	Oval	5	8
14 × 14	Oval	12	8

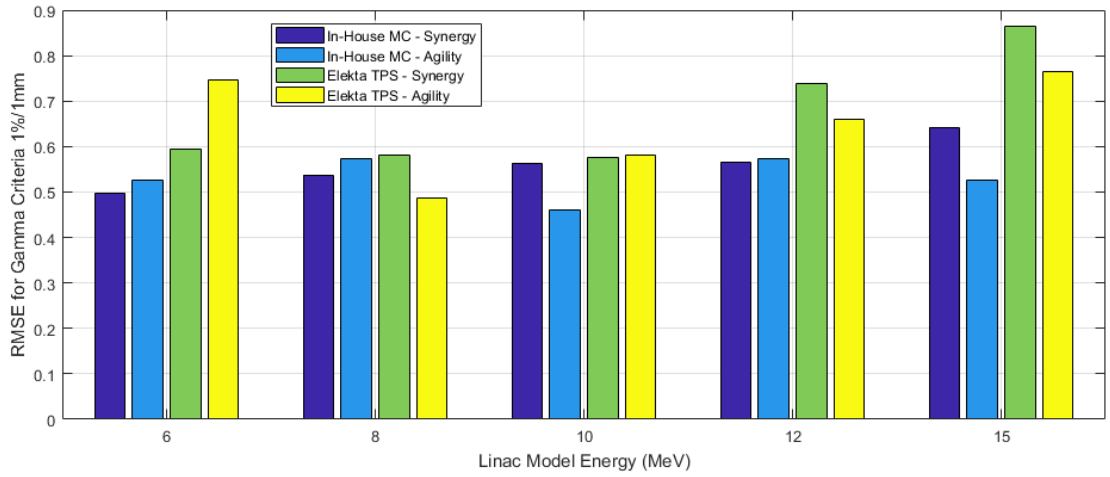

Figure 7-16 Overall RMS error summary for all shaped cutout fields from three applicators for 97, 100 and 105 cm SSD for each energy

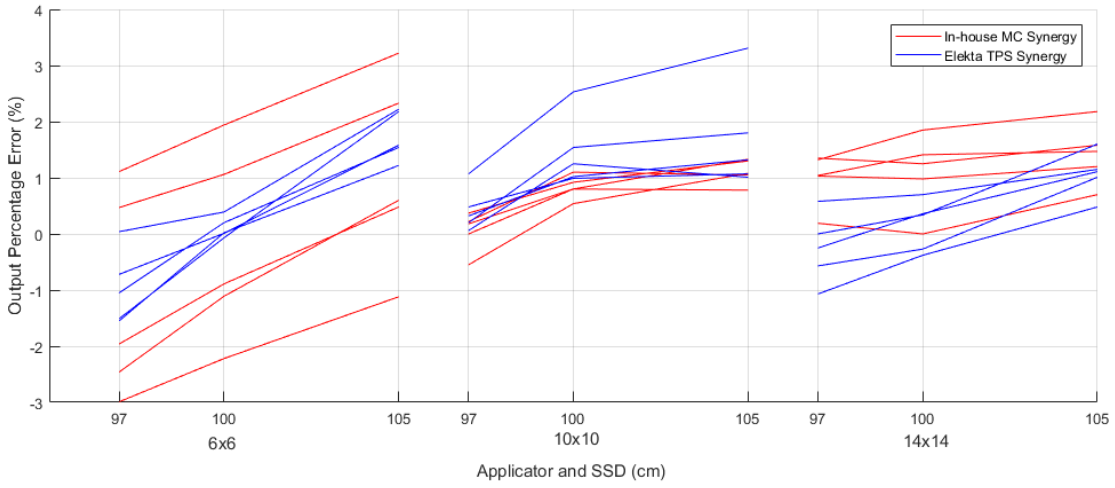

Figure 7-17 Synergy output error from measured for five energies over 97, 100 and 105 cm SSD for three applicators with shaped fields

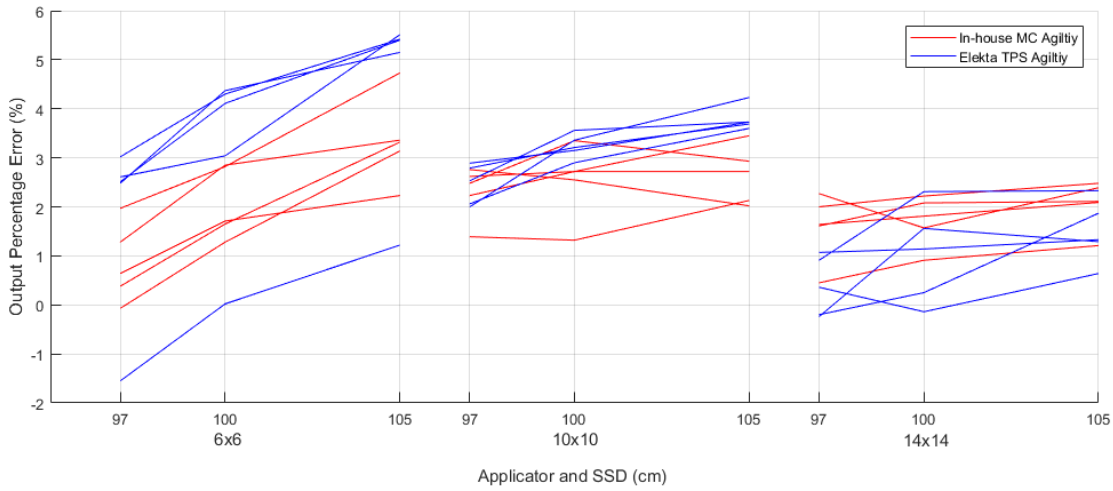

Figure 7-18 Agility output error from measured for five energies for 97, 100 and 105 cm SSD for three applicators with shaped fields

7.4.2. Discussion

Initial profile results for shaped fields were excellent with all models passing the 1%/1 mm gamma criteria. The gamma results are considerably better for the Elekta models compared to the Elekta open field results. The improvement in Elekta gamma results is likely due to the restricted field sizes where the off-axis profiles' errors are outside the cutout field sizes. In addition, profiles were acquired at D_m only due to data and time constraints. Profile agreement was found to be best in the region of maximum dose and errors were observed in the build-up and practical range region. Larger field size measurements were not acquired because the majority of clinical treatments is within the dataset measured.

Output agreement for shaped fields was found to be within 0±3% for the Synergy models and 2±3% for the Agility models. Agility shaped outputs for the 6 cm × 6 cm and 10 cm × 10 cm applicators were found to be up to 5% different from measurement and warranted further investigation.

7.5. Output Factors for Various Electron Insert Shapes

To record extra information on outputs with each energy and model, additional output factors were measured and tabulated. By measuring multiple field sizes over several SSDs, further knowledge would be gained about possible cause of disagreements. Sixteen symmetrical cutouts listed below (C-circle, Sq-Square) were

measured spread among applicators over six SSDs ranging from 97 to 105 cm for each energy.

Applicator and cutouts:

- 6 cm × 6 cm – 4C, 5C, 6C
- 10 cm × 10 cm – 6C, 7C, 8C, 9C
- 14 cm × 14 cm – 10C, 11C, 12C, 13C, 14C
- 20 cm × 20 cm – 14C, 14Sq, 16Sq, 18Sq

A concerted effort was applied to the Agility model as Synergy accelerators are due to be retired in the near future and the time for data collection was not justified for both models. In total, 480 additional outputs were measured on the Agility model; each measurement was also simulated in the in-house BEAMnrc and planned in the TPS to determine their predictive ability.

7.5.1. Results

The measured outputs and percentage errors for the BEAMnrc and Monaco are tabulated in Tables C-1 to C-3 in Appendix C. Errors from both model methods are shown in Figure 7-19 grouped by applicators and energy. Each cutout in Figure 7-19 is indistinguishable but is shown to demonstrate general errors and trends. Satisfactory results were observed by Monaco 5 over all SSDs for applicators 14 cm × 14 cm and 20 cm × 20 cm. Applicators 6 cm × 6 cm and 10 cm × 10 cm were satisfactory near 100 cm SSD however calculated values deviated from measurements with SSD varying from 100 cm. Similar SSD dependent deviations were observed in the smaller applicators of the in-house BEAMnrc simulations with an additional shift in error. The 14 cm × 14 cm and larger BEAMnrc model applicator calculation results remain accurate with varying SSD however all require a shift to be centred on zero.

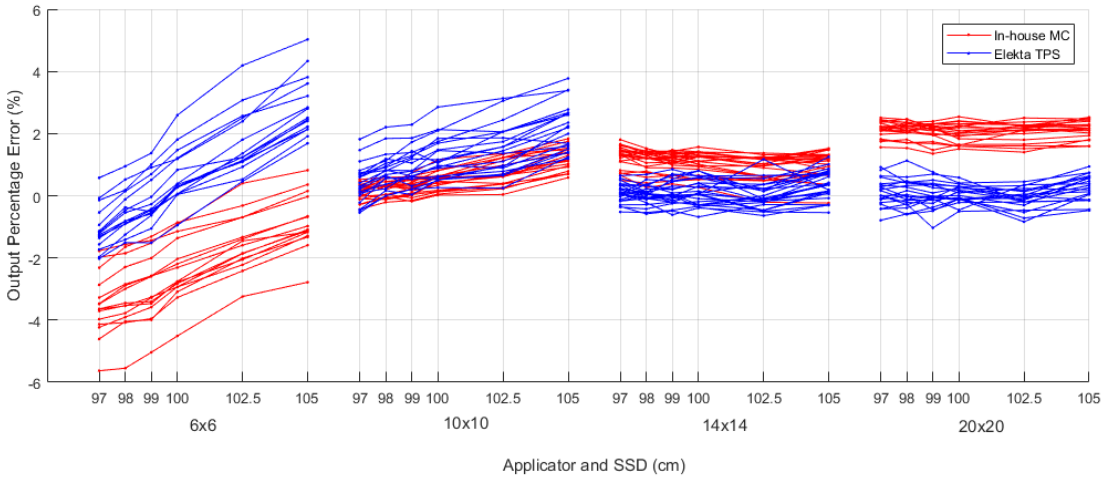

Figure 7-19 Agility output errors for various applicators, cutouts and SSDs for five energies

Further investigation into anisotropic inplane/crossplane shaped cutouts need to be conducted as the isotropic results shown in Figure 7-19 do not match the absolute observed shifts of ~3% for 10 cm × 10 cm and ~1% with 14 cm × 14 cm applicators with the shaped cutouts in Section 7.4.

7.5.2. Discussion

Monaco 5 output results shown in Figure 7-19 achieve accurate outputs at 100 cm SSD for all applicators but become less accurate for SSD differing from 100 cm for the 6 cm × 6 cm and 10 cm × 10 cm applicators. As an applicator module is also used for modelling Monaco beams, this indicates that the raw outputs for individual applicators have been modified by a correction factor. This factor is most likely the applicator output factors supplied by the client during beam model data submission. Due to the missing material as discussed in Section 5.6, the output error still increases with distance from 100 cm SSD for the 6 cm × 6 cm and 10 cm × 10 cm applicator.

Similar output results can be achieved by the in-house BEAMnrc model by applying correction factors for individual applicators. The correction required for each energy was found to be the error of the open field outputs with the applicator discrepancy relative to the 40 cm × 40 cm field after normalising to the 10 cm × 10 cm applicator, as discussed in section 5.5.3 shown by Figure 5-20. Energy averaged correction factors from Figure 5-20 were determined to be 1.023, 0.989 and 0.979 for the 6 cm × 6 cm, 14 cm × 14 cm and 20 cm × 20 cm applicators respectively. Due to

the open field output errors, correction factors are unique to each energy and applicator. Figure 7-20 shows the Agility output accuracy under the same conditions as Figure 7-19 where the MC results have been corrected by the open field applicator error at 100 cm SSD.

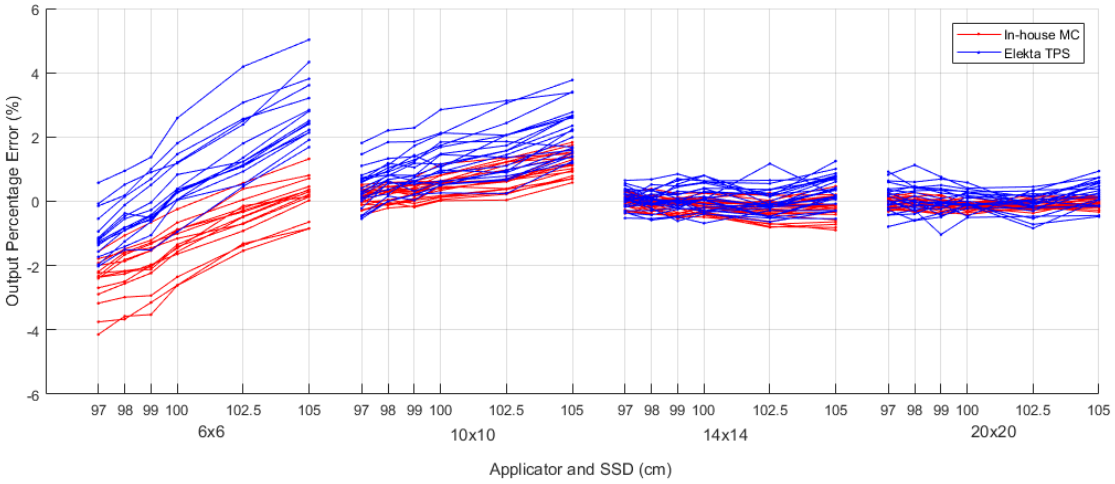

Figure 7-20 Agility output errors with applicator specific correction value for various applicators, cutouts and SSDs for five energies

7.6. Surface Geometry Variations

To further test the effectiveness of model application, beams were measured under non-perpendicular flat geometric conditions. Oblique beam incidence and stepped fields were measured in a water tank and equivalent simulations were performed for both modelling techniques.

Oblique fields were measured with a 20 cm × 20 cm applicator with standard cutout at a gantry angle of 340° at 100 cm SSD for Synergy and Agility accelerators. PDD, profiles and outputs were measured for each energy. Crossplane profile results at depths of 0.50, 2.30 and 4.08 cm (Surf, D_m and R_{50}) are shown below in Figures 7-21 to 7-23 for the Agility 10 MeV model.

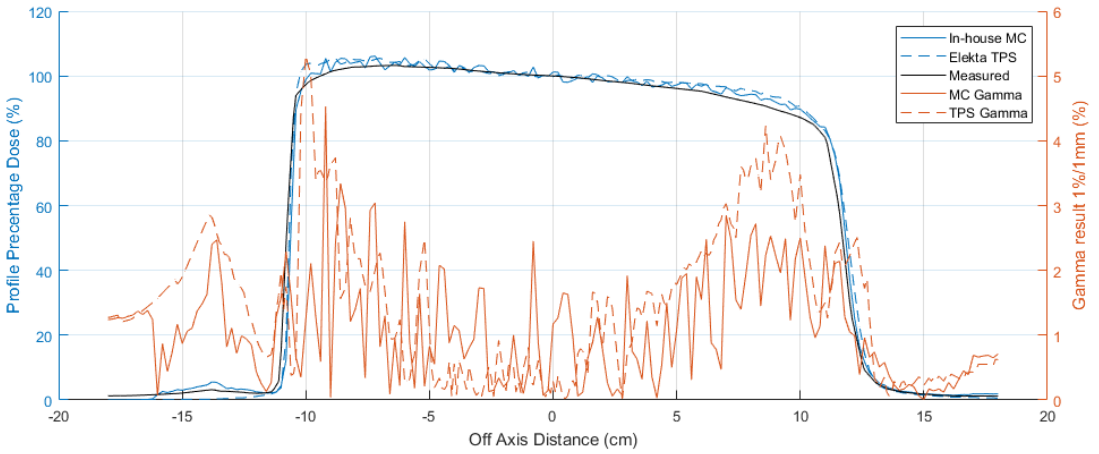

Figure 7-21 100 cm SSD Agility 10 MeV 20 cm × 20 cm 340° oblique beam incidence standard cutout in-house MC, Elekta TPS and measured surface crossplane profile (0.50 cm) with respective gamma results

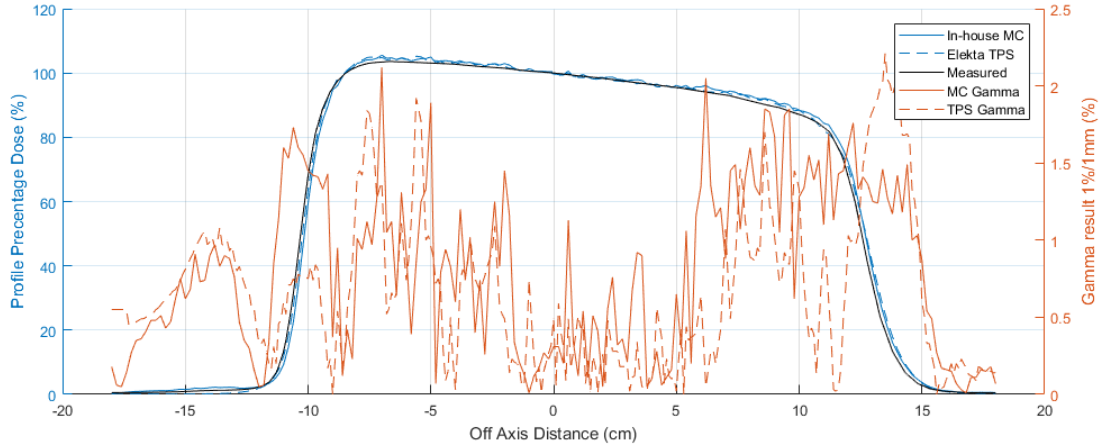

Figure 7-22 100 cm SSD Agility 10 MeV 20 cm × 20 cm 340° oblique beam incidence standard cutout in-house MC, Elekta TPS and measured D_m crossplane profile (2.30 cm) with respective gamma results

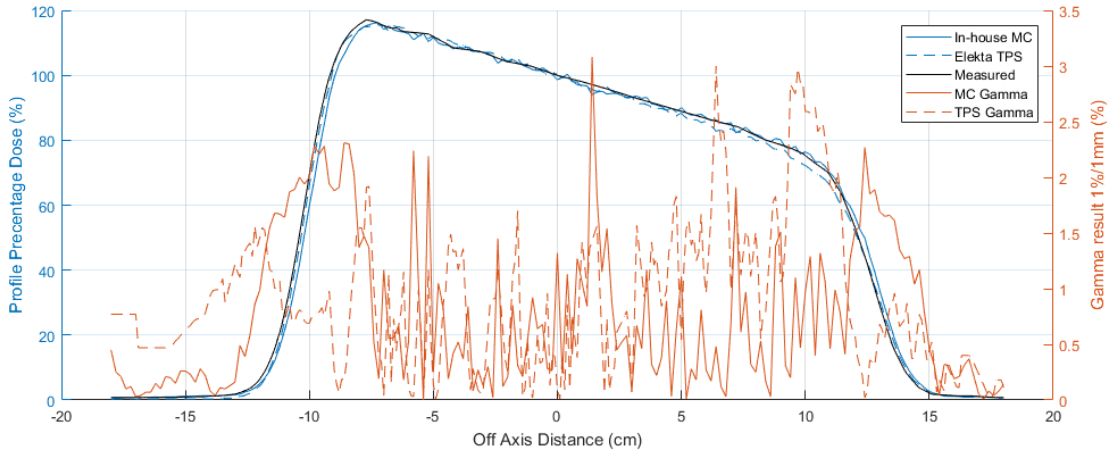

Figure 7-23 100 cm SSD Agility 10 MeV 20 cm × 20 cm 340° oblique beam incidence standard cutout in-house MC, Elekta TPS and measured R_{50} crossplane profile (4.08 cm) with respective gamma results

Stepped surface profiles were measured to verify distinct surface height variations. Profiles were measured by placing water equivalent slabs that were suspended on rails at the surface of the water using the 14 cm × 14 cm applicator with standard cutout at 100 cm SSD to the water. Three stepped thicknesses of 5, 10 and 20 mm were tested to allow for differences in higher beam energies. Profiles were normalised to −4 cm off-axis to the unmodified water surface. Care was taken to ensure the slab was parallel with the water surface and no bubbles were present underneath. Profiles were measured with an electron diode at the same depths for the standard applicator and energy.

Profile depths in Figure 7-24 were taken from open field depths of 0.50, 1.20, 1.80, 2.52, 3.34 and 3.87 cm (representing surface, norm, D_m, R_{90}, R_{80} R_{50} and R_{20} respectively, displayed in order from top to bottom on the right side of Figure 7-24). A variation in R_{50} has a significant effect when comparing profiles in the PDD fall off region due to the high dose gradient. Because of the effect of R_{50} variation due to difference in measurement time from the original model dataset, gamma index tables are not a true representation of result accuracy but are able to compare the differences between the modelling techniques.

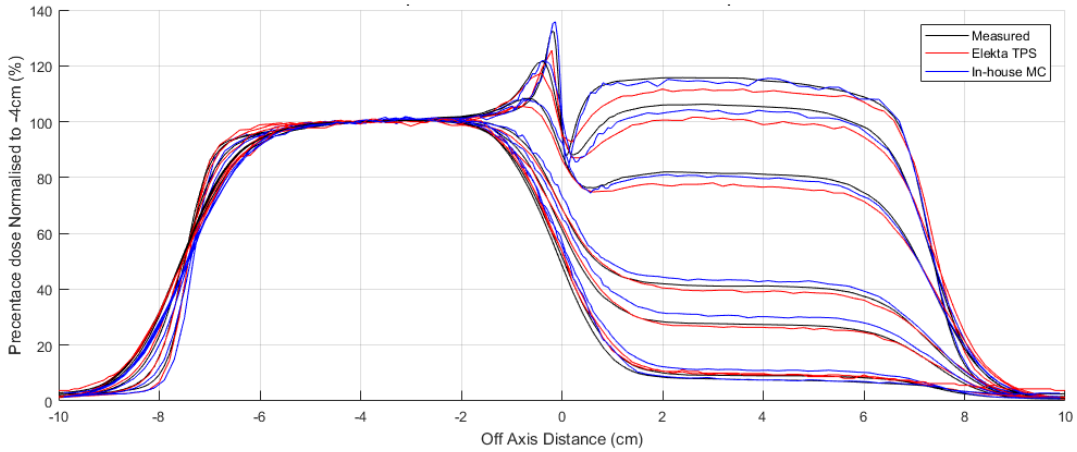

Figure 7-24 8 MeV 14 cm × 14 cm with mid field 10 mm stepped water surface crossplane profiles normalised to -4 cm off axis at depths Surf, Norm, D_m, R_{90}, R_{80}, R_{50} from positive off axis distance top to bottom respectively

7.6.1. Results

Table B-7 shows the oblique profile RMS error values for each energy and model. The overall RMS summary is depicted in Figure 7-25. Results for in-house BEAMnrc simulations are raw simulation values and could be improved with a noise filter applied or by increasing the number of particles simulated. Outputs were measured for each energy and compared against dose predictions, listed in Table 7-2. It should be noted that the parallel ionisation and diode detectors used to measure outputs may be prone to angular incidence dependence. The results should still indicate any gross errors if present.

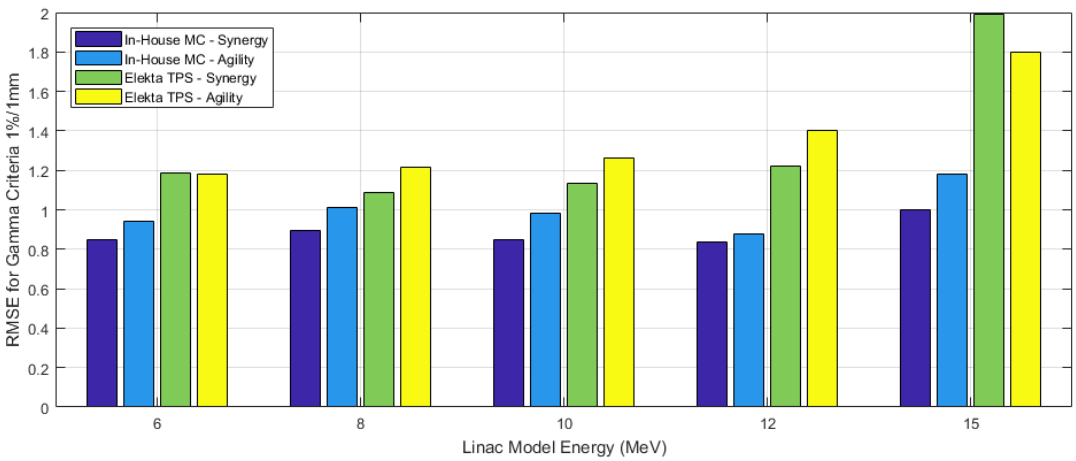

Figure 7-25 Overall RMS error summary for 340° oblique incidence for each model at five energies

Table 7-2 340º Oblique output error for a 20 cm × 20 cm applicator

		Oblique Output Error (%)				
		Energy (MeV)				
		6	8	10	12	15
Synergy	In-house	-0.07	1.56	-0.20	0.68	0.77
	Elekta TPS	0.27	-0.36	-0.83	-0.71	0.30
Agility	In-house	1.85	2.70	2.49	2.69	2.55
	Elekta TPS	0.49	-0.48	0.56	1.17	1.31

Gamma RMS error profile results from measured stepped surface profiles are shown in Table B-8. A gamma criterion of 2%/2 mm was used to allow for the more difficult conditions. Overall RMS errors grouping each model by energy are presented in Table B-8 and are shown in Figure 7-26, Figure 7-27 and Figure 7-28 for surface steps of 5, 10 and 20 mm respectively.

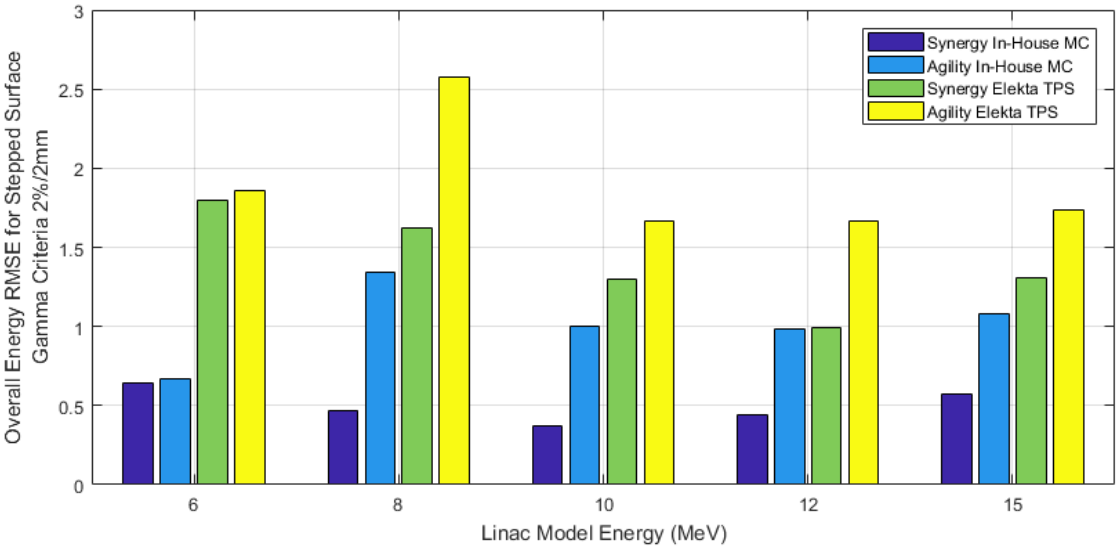

Figure 7-26 Crossplane profile RMS error summary for 5 mm stepped surface for each model at five energies

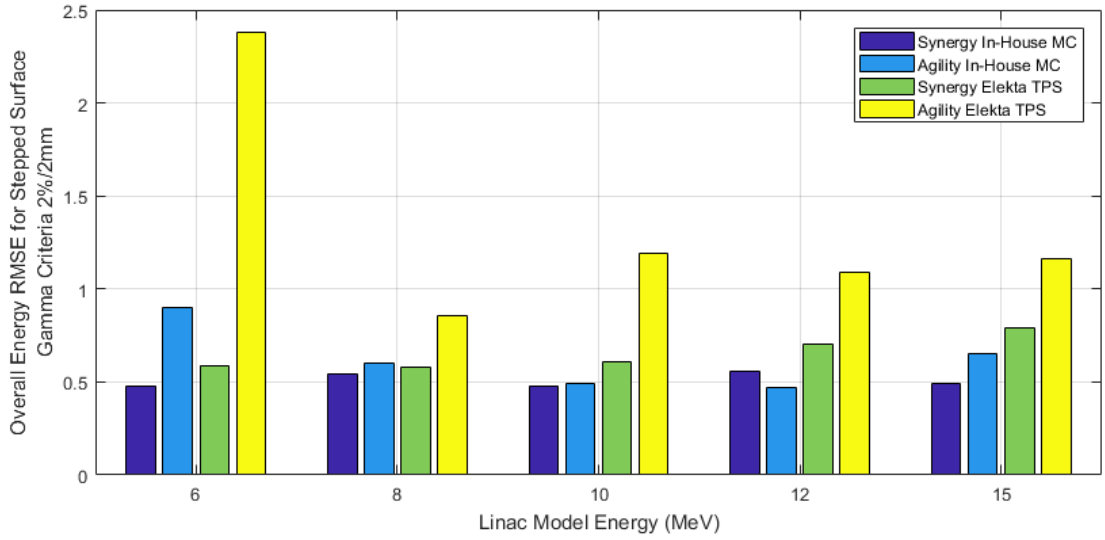

Figure 7-27 Crossplane profile RMS error summary for 10 mm stepped surface for each model at five energies

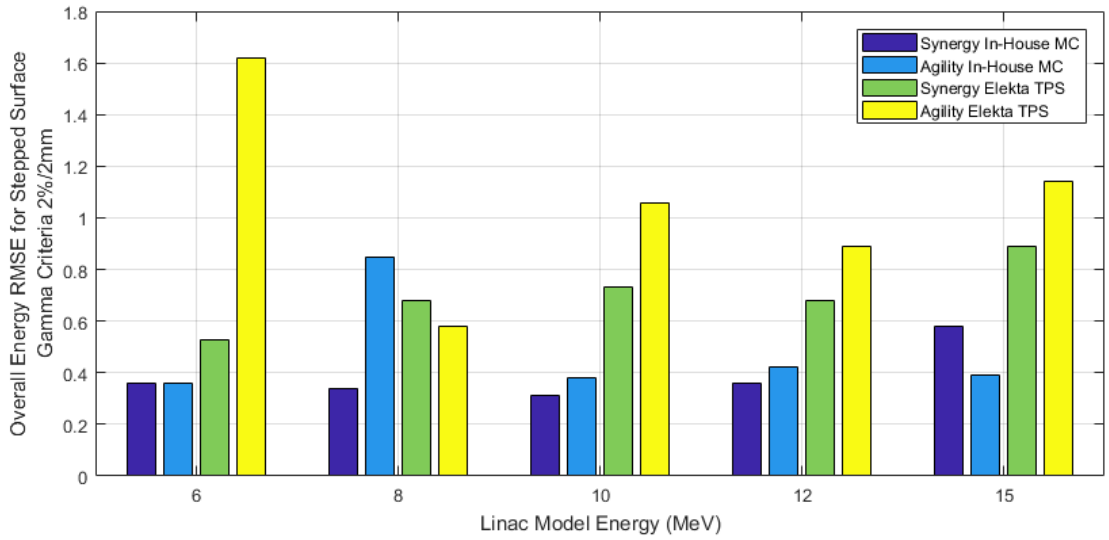

Figure 7-28 Crossplane profile RMS error summary for 20 mm stepped surface for each model at five energies

7.6.2. Discussion

Poorer agreement is obtained with oblique fields than with open fields, as can be seen by comparing the RMS index summaries in Table B-7 and Tables B-1 to B-4. The in-house models were all able to achieve overall gamma RMS values under 1.2 while the majority of Elekta's models gave values less than 1.4 with the exception of 15 MeV.

Elekta's 15 MeV models had noticeable off-axis profile errors in the opens fields that carried through to oblique field results.

Initial in-house MC oblique field output factor results were poor with errors exceeding 2% for four of the five energies. The required applicator output corrections discussed in section 7.5 confirm the output errors observed. For all oblique fields the 20 cm × 20 cm applicator was used, which was found to require a correction of ~2%. When applied this reduced the errors of the oblique outputs to within 1.3% compared to measurement as shown below in Table 7-3 for both in-house Synergy and Agility models.

Table 7-3 Applicator specific adjusted oblique output error

	Oblique Output Error (%)				
	6 MeV	8 MeV	10 MeV	12 MeV	15 MeV
Synergy	-0.82	0.14	-1.23	-0.88	0.15
Agility	0.14	0.25	0.13	0.33	0.58

Overall stepped field RMS data shows that in-house MC models can predict dose better than Elekta's TPS. This can be attributed to the ability to simulate the environment exactly as measured where the TPS loses the ability to maintain distinct edges when calculating dose as discussed in section 8.5. The loss of distinct edges reduces the magnitude of hot and cold spots produced by the stepped surface and therefore fails more data points. This can be seen in Figure 7-24 where the TPS it not able to match the measured hot and cold gradients as well as BEAMnrc does. The blurring of distinct edges by the TPS also affects the effective energy of the incident beam. The change in R_{50} of the TPS makes a direct comparison against BEAMnrc difficult as the simulation environments are no longer identical.

7.7. Inhomogeneities

Two scenarios were able to be measured by placing lung and cortical bone equivalent tissue equivalent slabs in the water tank to perform measurements. PDDs were measured from underneath the slab where the slab covered the full field. Profiles were measured across the full field where the slab was positioned mid-field. The 14 cm × 14 cm applicator with standard cutout was chosen to minimise any field size dependence with energy.

The tissue equivalent slabs are 1 cm thick and placed at a depth such that there was 1 cm of water from the surface to the slab. As noticed earlier, a direct comparison was not possible as any minor changes in R_{50} of the beam on the day from when the model data was acquired would have significant effect on profile comparison in the dose drop off region. Slabs were scanned helically to obtain CT Hounsfield unit (HU) numbers however resultant HUs' were not reliable due to the thin slab thickness and beam hardening of the high density cortical bone. The relative electron density (RED) and material density were taken from their respective datasheets and used in the simulation specifications however could not be verified.

7.7.1. Results

PDD measurements were taken up to 2 mm below the slab in the field and to the surface without the slab present. The PDDs were normalised to a point 2 mm below the slab to incorporate absolute dose variations. PDDs were taken for each energy for both accelerator models with lung and bone equivalent slab. An example is shown in Figure 7-29.

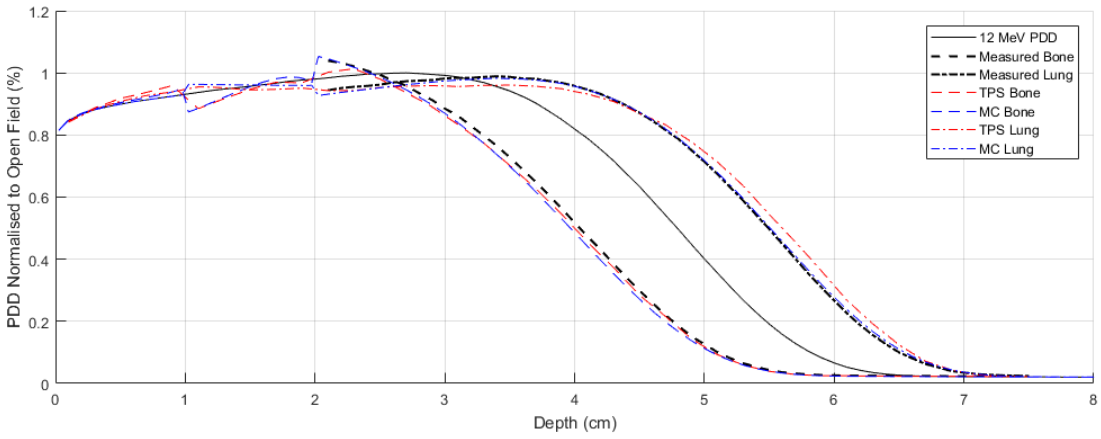

Figure 7-29 Effect of 1 cm lung and bone slab 1 cm deep in water on 12 MeV PDD

Selected crossplane profiles are shown where the tissue equivalent slab is only present in half of the irradiation field. Profiles were normalised to the same position as for stepped fields at −4 cm, representing an unmodified beam. Agility 12 MeV profiles are shown below at depths of D_m (2.60 cm) and R_{50} (4.08 cm) for the lung (Figure 7-30) and cortical bone (Figure 7-31) slab. Gamma criteria of 2%/2 mm were chosen as beam models struggled to pass these criteria. Profile gamma pass rates are stored in the index

Table B-9 and the overall RMS error grouped for each beam model at five energies are shown in Figure 7-32 and Figure 7-33 for the lung and cortical bone slab respectively.

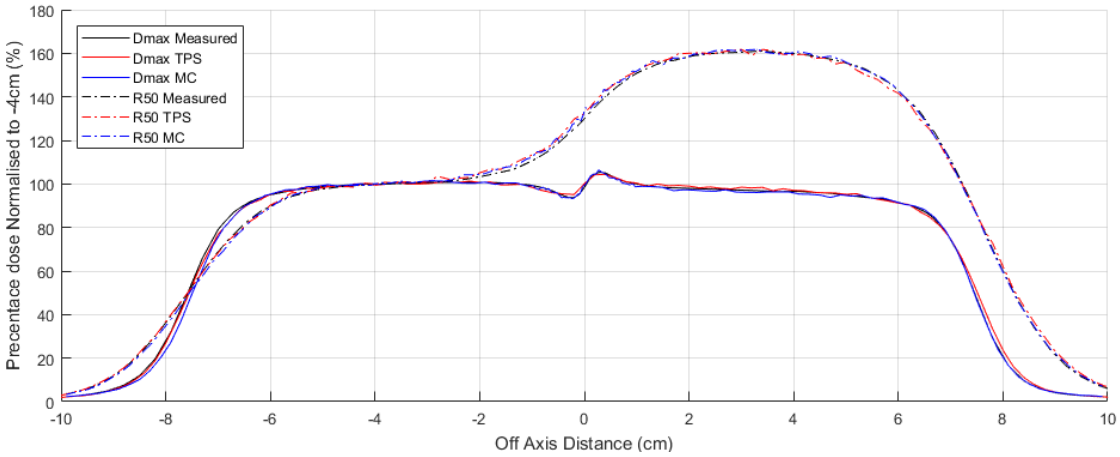

Figure 7-30 100 cm SSD 12 MeV 14 cm × 14 cm profiles at D_m and R_{50} for 1 cm lung slab 1 cm deep in water across half the field normalised to -4 cm off axis

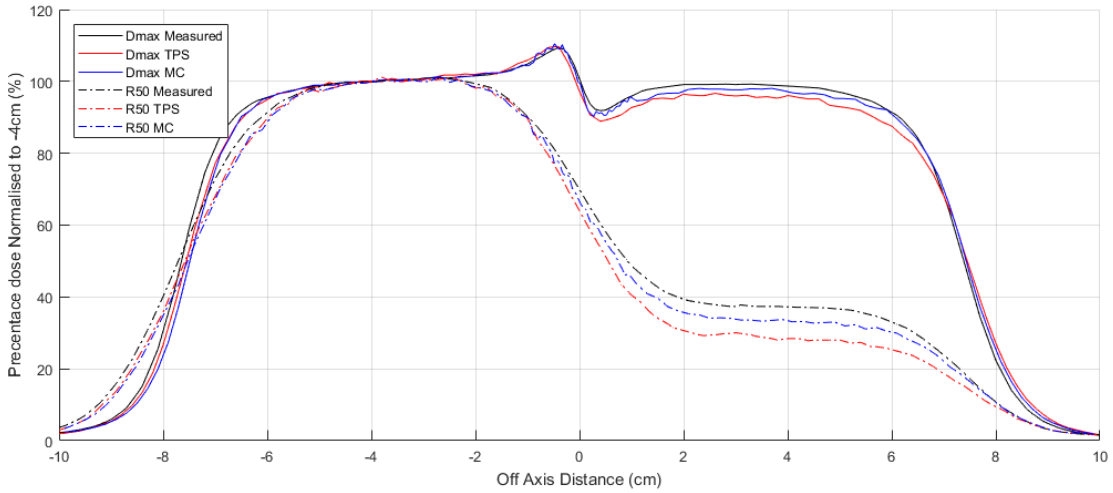

Figure 7-31 100 cm SSD 12 MeV 14 cm × 14 cm profiles at D_m and R_{50} for 1 cm cortical bone slab 1 cm deep in water across half the field normalised to -4 cm off axis

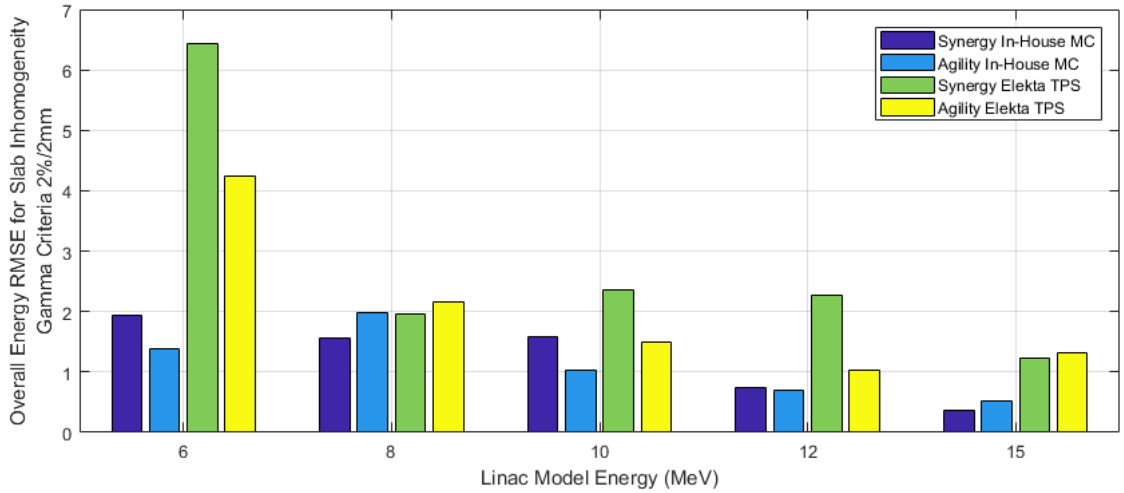

Figure 7-32 Crossplane profile overall RMS error summary for 1 cm Lung inhomogeneity 1 cm deep across half the field

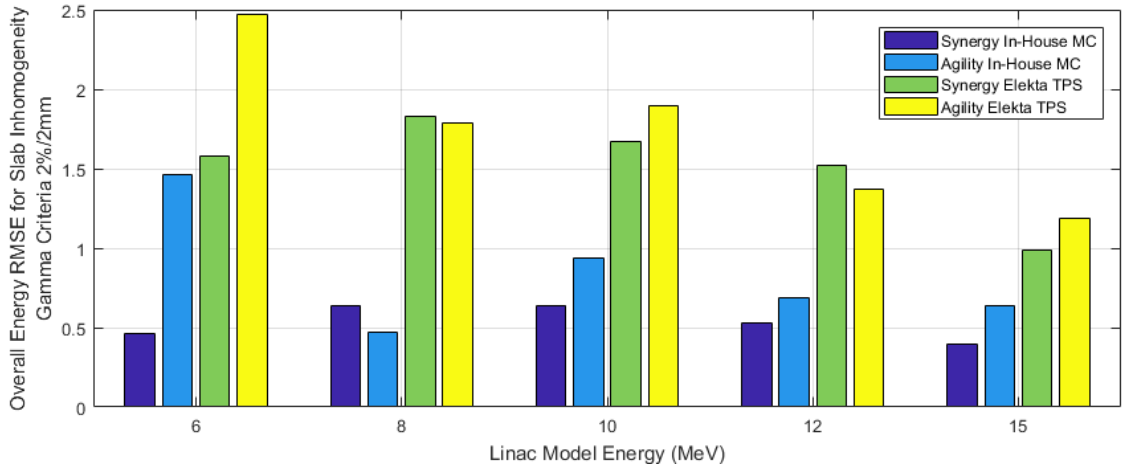

Figure 7-33 Crossplane profile overall RMS error summary for 1 cm Cortical Bone inhomogeneity 1 cm deep across half the field

7.7.1. Discussion

Inhomogeneity PDD results indicate that both methods are able to effectively account for a material slab covering the entire field. While slight differences between methods exist, they were both able to accurately predict dose beyond the inhomogeneity. Accurate measurements and data comparison were made difficult due to multiple factors. The RED for the materials could not be confirmed and were set to the documented value in both calculation methods. Monaco 5 allows the user to set a RED and assigns the properties of the voxel to the nearest tissue equivalent material of that density from a look up table of tissue materials. BEAMnrc has predefined

materials for each voxel where the density of the material can be altered while the composition remains unchanged. Dataset collection effective energy changes from initial measurements were not account for when comparing against measurement, however any comparison error would affect both methods equally. Due to the calculation grid, Monaco 5 is not able to maintain any sharp or distinct boundary interfaces blurring the surface of the water and edges of the slab and the effect with the inhomogeneity present is unknown. With the mentioned uncertainties, PDDs traversing through lung and cortical bone is sufficiently accounted for.

Half field profile results indicate a variety of agreement for both prediction methods. Any errors associated with measurement and comparison uncertainties are significantly increased in the results observed. Profile overall RMS gamma results for lung are poorer than that of the cortical bone. This is because of the normalisation point (−4 cm off-axis) chosen representing the unmodified profile. Profiles are always above or below 100% after D_m due to the reduced/increased beam absorption through the slab and any PDD error is exaggerated due to the profile being measured across a high dose gradient. Thus a 2% gamma criterion is in a profile region where the dose gradient can be 8% per millimetre and is highly susceptible to measurement/simulation error. Higher beam energies have shallower build-up gradients and lower dose gradients in the drop off region and are less susceptible resulting in improved gamma agreement.

Inhomogeneity profile RMS summary results show in-house MC methods are able to predict dose to a greater accuracy in the region and beyond an inhomogeneity compared to that by Monaco 5. The poorer agreement by Monaco 5 with measurement may be due to the loss of distinct boundaries when calculating dose resulting in modified effective energy. The sensitivity of gamma pass rates for profiles across two high dose gradients requires accurate representation in the simulation environment. The clinical relevance is not a concern as profiles may only require a sub-millimetre adjustment to find agreement. With a calculation grid of 2 mm, the required distance to agreement is within the same voxel and is highly sensitive to the grid placement itself.

7.8. Summary

While Monaco 5 models successfully passed the clinical gamma criteria of 2% and 2 mm, the model prediction ability struggled to pass the stricter criteria of 1%/1 mm for all tested scenarios. In-house developed MC beam models proved superior to

Monaco 5 beam models when compared to the gamma RMS results for both Synergy and Agility accelerator models as shown by Figure B-1 and Figure B-2. The variations of electron spectra at the patient's surface are presented demonstrating the variation in spectra possible achieving acceptable results as the majority of Monaco 5 models do pass the strict gamma criteria of 1%/1 mm. This indicates that there is a greater requirement of the spectrum for matching the R_{50} and less specific influence in the entirety of the distribution.

Monaco 5 OF results achieve accurate outputs compared to measurements at 100 cm SSD for all applicators but the error increases with SSD for the 6 cm × 6 cm and 10 cm × 10 cm applicators. As an applicator module is also used for modelling Monaco beams, this indicates that the raw outputs for individual applicators have been modified by a correction factor. Similar output results can be achieved by the in-house BEAMnrc models by applying correction factors for individual applicators based on the applicator with standard insert OF. Due to the missing material as discussed in Section 5.6, the output error still increases with distance from 100 cm SSD for the 6 cm × 6 cm and 10 cm × 10 cm applicator and a solution is yet to be implemented.

Model results under complex geometries maintained dose predictive ability to a high accuracy given the difficulty of measurement and data comparison circumstances. In-house models were found to be superior in oblique, stepped surface and inhomogeneity tests. Monaco 5 was able to account for the various geometric and inhomogeneity situations but could not achieve accurate dose predictions where sharp gradients or distinct boundaries were present. Monaco 5 oblique field results were influenced by the off-axis profile agreement for large fields and could obtain better agreement if further effort in modelling scattering foils was made.

8. Independent TPS using BEAMnrc and DOSXYZnrc

8.1. Background

Having an accurate in-house MC model is a significant benefit that allows the control over all parameters and design, however if it cannot be applied to patient specific treatments its use becomes limited. While accurate comparisons are made using a scanning tank, it is considerably more difficult to gather and compare results in any other geometry. While a flat surface is sufficient for commissioning and basic beam model interrogation, the end goal is the ability to produce accurate and reliable predictions on patient equivalent geometries.

To make a direct, yet independent comparison to the commercial TPS, a separate planning system is required. By developing a TPS using BEAMnrc and DOSXYZnrc, an independent dose calculation validation of the primary TPS for individual patients can be made which would be impossible with measurements.

8.2. CT DICOM to DOSXYZnrc Phantom

A Matlab script was created to convert CT DICOM data to voxelized geometry compatible with DOSXYZnrc. The script offered several advantages compared to the BEAMnrc 'ctcreate' script allowing control over voxel geometric manipulations and exclusions, as well as overrides of material densities.

A graphical user interface (GUI), shown in Figure 8-1, was designed in Matlab to visualise and simplify the process of creating the phantom for DOSXYZnrc. The purpose of the GUI was to manipulate the CT dataset to reduce simulations times by reducing the volume exported.

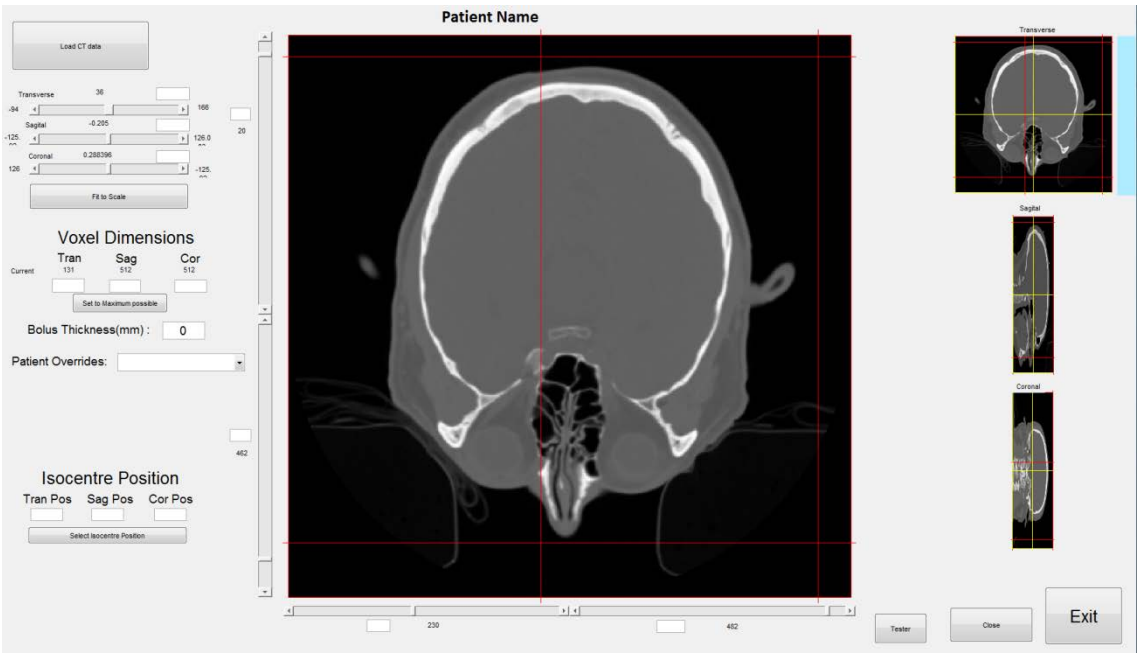

Figure 8-1 Screenshot of the graphical user interface developed in Matlab to convert CT data to a voxelized geometry for dose calculation in DOSXYZnrc

The volume reduction is shown in Figure 8-2 where the user shifts limits representing the boundary for the reduced dataset designated by red lines as show in Figure 8-1. The reduced CT dataset allows the use of the smaller voxel geometric dimensions without the need to merge voxels to be within the voxel number limit set by DOSXYZnrc. At first, the user had the option of merging voxels to fit within voxel limit of 256 × 256 × 128 in the DOSXYZnrc executable. This limit was then increased to 512 × 512 × 256 so that if needed CT data could be directly imported. The drawback of increasing the voxel limits is the significant memory resource a single simulation requires. At this resolution, only four subsequent simulations could be performed at any time with 8GB of RAM. The DOSXYZnrc executable allocates memory to a simulation based on the maximum voxel limits, even if the simulation itself has dimensions less than the maximum. For this reason, two DOSXYZnrc executables were created: one for CT simulations (512 × 512 × 256 voxels allowing 4 simulations) and another for generic PDD and profile simulations (256 × 256 × 128 voxels allowing ~30 simulations).

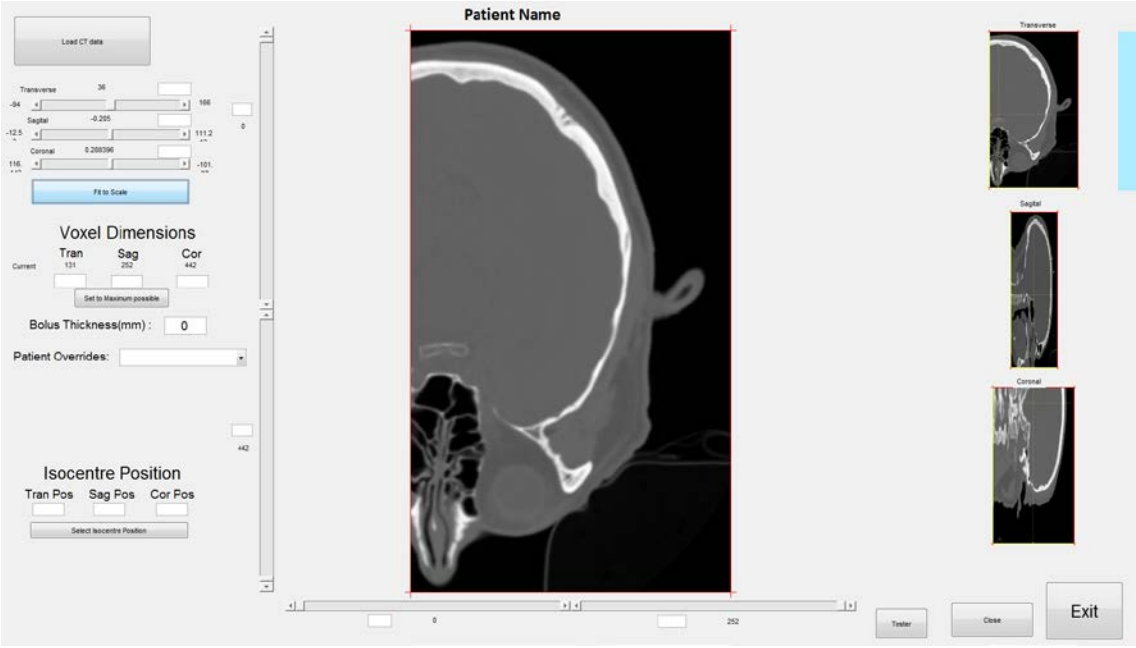

Figure 8-2 CT dataset volume reduced to relevant clinical area

Once the CT dataset volume reduction is finalised, the user has the option of modifying the HU of the CT dataset. Options included allowing the CT voxels to be unmodified (using a specified CT HU to density ramp), overriding to a density of 1 g/cm^3 for water composition or a density of 1 g/cm^3 for tissue equivalent material composition. Other options for any override density and material can be included if working with QA phantoms. This option was introduced to allow a direct comparison with current clinical workflow for electron output factor determination.

The last time saving technique used in the script removes planes containing only air. This script scans the volume in each plane direction and assesses whether any patient data is present. If the plane only contains air, it is removed from the volume. This process is repeated until a patient boundary is detected in each direction. This removes unnecessary simulations in the air that only contribute to longer simulation times. The .egsphant phantom file was then generated for simulation.

The phase space file for patient simulation is generated using the phase space files of the developed electron models up to the point of the cutout insert. The user enters the cutout insert dimensions and completes the simulation generating the phase space to be simulated on the generated CT dataset. A separate GUI ‘Beam Placement’, shown by Figure 8-3, allows the user to choose the appropriate phase space file and to enter beam specific parameters. Required beam parameters include: gantry, collimator,

couch, patient SSD and beam entry point. These parameters are copied from the commercial TPS plan to ensure a direct comparison of the treatment prediction. A visual aid is displayed to help ensure data is entered correctly. When completed, the GUI generates the .egsinp file required for DOSXYZnrc simulation. With the phase space, .egsphant and .egsinp files generated, simulations are possible.

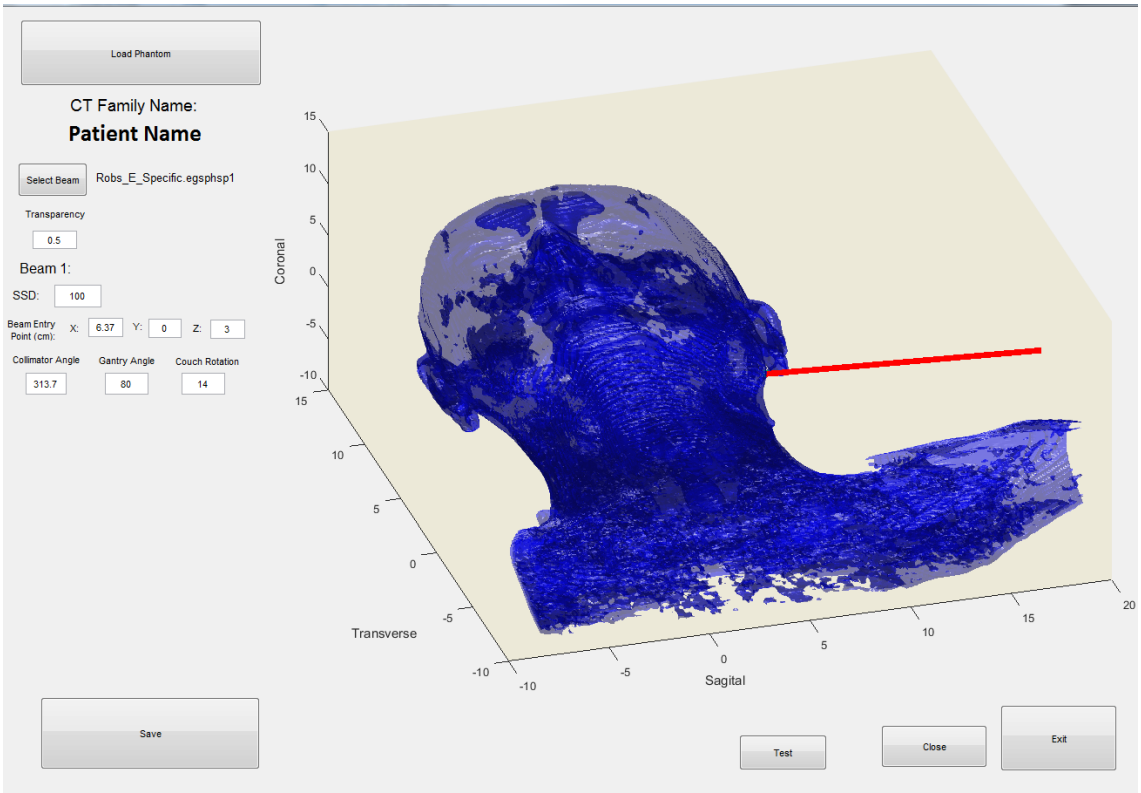

Figure 8-3 GUI to assist and create .egsinp file for DOSXYZnrc

The simulation was then run in DOSXYZnrc generating a .3ddose dose file. The final GUI 'Results' uses the CT dataset to generate the phantom and the .3ddose file produced from the simulation on the phantom and overlays the datasets. An example is show in Figure 8-4. The GUI allows the user to enter a normalisation point that represents the point in the commercial TPS used to prescribe the required dose. By entering the desired dose per fraction, the simulation value at that location is compared against the value from reference dose for the selected energy (10 cm × 10 cm maximum dose value). The required correction factor is determined by the ratio between the patient simulation value at the desired location and the reference dose for the specific energy. The required MU to be delivered by the accelerator to achieve the specified

dose to the reference point is calculated. Future development can allow the extraction of dose planes or entire 3D if the need arises.

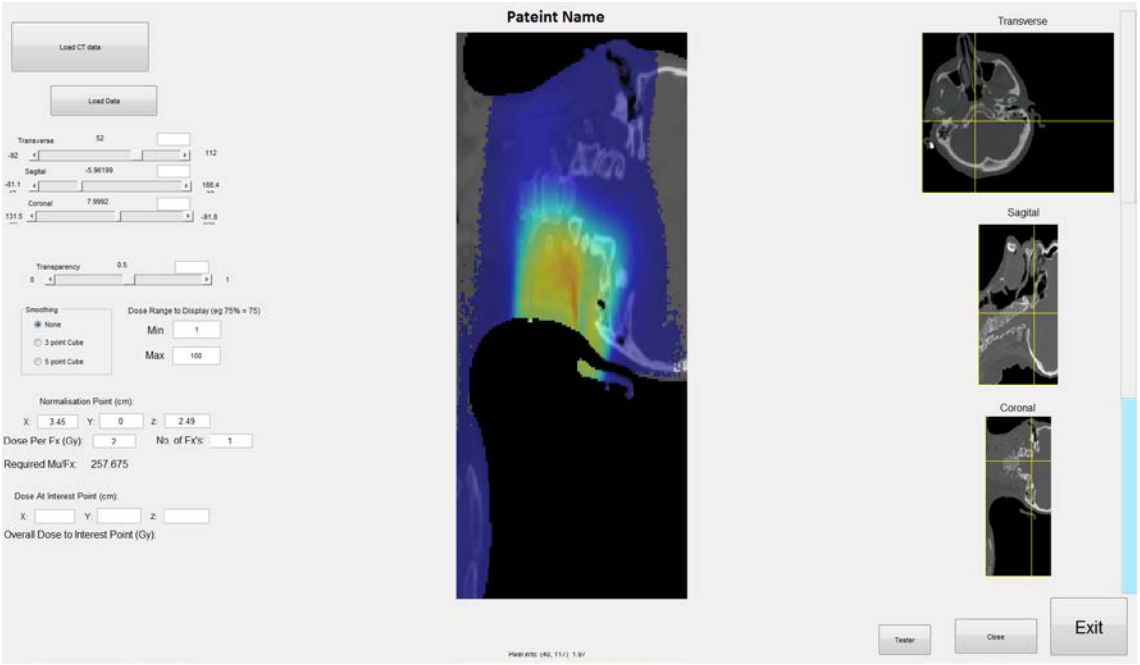

Figure 8-4 Results GUI to analyse DOSXYZ simulation results and obtained required MUs to achieved desired dose to reference point

8.3. DOSXYZnrc: Isource 2 Geometry and Simulation Parameters

Before commencing simulations, coordinate systems between BEAMnrc, DOSXYZnrc and the linear accelerator must be aligned. Isource 2 is the required simulation setting that allows previously generated phase space files to be projected onto CT datasets and simulated in DOSXYZnrc. It is noted in the DOSXYZnrc manual that a 180 degree rotation in the collimator (Phicol) is required to maintain BEAMnrc system coordinates. Making this adjustment no longer allows for the rotation of the gantry in DOSXYZnrc. To allow for rotations in all planes to mimic the operation of the accelerator, the Phi was set to 90 to allow for Theta to represent the gantry. As Phi was 90, Phicol required an offset of 90 instead of 180. Phi and Phicol deviations from 90 represent couch movements and collimator rotations respectively. The setup is depicted in Figure 8-5 and the following accelerator parameters are adjusted by the formulas given:

- Couch Rotation (Phi) – modular (90+couch angle,360);
- Gantry Rotation (Theta) – modular (540-Gantry angle,360);

- Collimator Rotations (Phicol) – modular (Collimator angle+90,360);

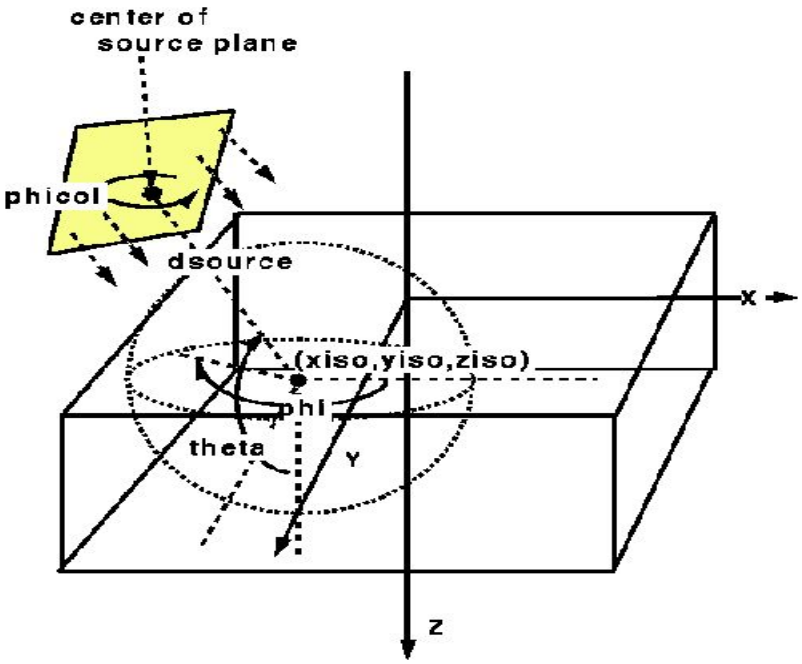

Figure 8-5 ISource 2 Orientation specifications (Walters et al., 2016)

Dsource is the distance from the phase space file to the point of interest in the CT dataset represented in DOSXYZnrc. In this case it represents the distance from the end of the phase space file generated at the bottom of the insert cutout to the patient's surface or beam entry point of the patient (acquired from Monaco). Dsource distance is calculated during the generation of the .egsinp file and is the SSD minus the set distance designated by the position of the cutout phase space file set at the bottom of the insert cutout. The Dsurround parameter is set to a length that covers the direct distance from surface entry point to the position of the phase space, with an additional allowance to ensure adequate coverage at various gantry angles due to the width of the phase space.

The .egsphant generated from CT data contains a minimum of two material properties (air and water). Due to this, the 'howfarless' option must be unticked even though the entire patient was set to water to follow current clinical procedures. This has a significant effect on simulation time (an increase on the order of 13 times) as mentioned in the DOSXYZnrc manual. Simulations can be run in parallel, however due to the restriction of each simulations reserving the maximum RAM, the number of parallel simulations is restricted to the amount of RAM available. While eight cores are

available, only a maximum of four cores could be used when running CT simulations in parallel.

8.4. Independent TPS Limitations

While the basic level of design in the independent TPS allows simulations, the user ability to customise CT data cannot match that of a commercial TPS. This makes it difficult in the cases where patients require specific CT data modifications for treatment. For example, users do not have the ability to draw contours, fill in regions with material or override markers placed on the patient's skin. This prevents a direct clinical comparison between the Monaco 5 and BEAMnrc predictions.

To encompass the majority of clinical requirements, the independent TPS includes the ability to apply a uniform thickness bolus over the patient. The patient's surface is scanned to locate surfaces in three dimensions. The patient's surface is then extended by the desired bolus thickness determined by the geometric spacing of the voxel dimensions. A separated dataset of bolus is created and superimposed on the original dataset. This allows patient overrides to be treated independently of the bolus allowing each to have separate density overrides applied. Figure 8-6 shows a patient dataset with bolus applied.

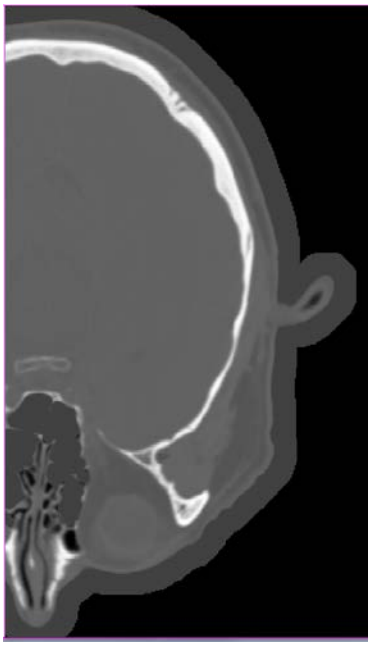

Figure 8-6 Patient Bolus applied to Figure 8-2

A separate script that allows a basic patient position marker removal was also created. The script assessed the surface layer of the patient, scanning for high density materials. If located, the pixels associated with the wires were removed. This process is shown in Figure 8-7, however it does not allow corrections for artefacts produced by the markers that modify internal voxels (streaking through patient).

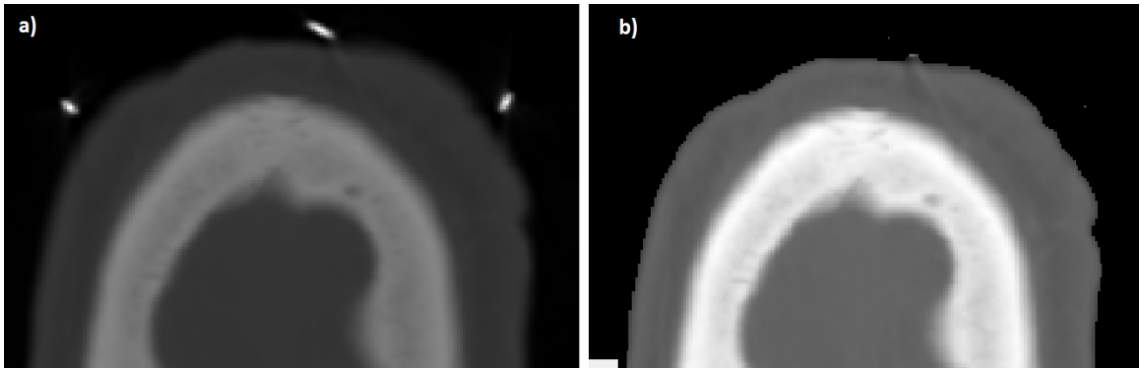

Figure 8-7 Demonstration of marker removal script. a) Pre-script CT dataset. b) Post script effect on CT data

8.5. Commercial TPS Limitations

The in-house developed treatment planning system is a crucial step in enabling accurate patient treatment validation. The most significant advantage is the ability to determine dose in patient geometries where it is impossible to perform measurements. The ability to compare clinically realistic situations enables a genuine comparison between planning systems. The power and freedom of an in-house planning system was understood by understanding the limitations and reasoning set on commercial planning systems.

The greatest limitation set on a commercial TPS is the requirement to set a grid size to an arbitrary whole millimetre value that generates a cubic voxel. Raw voxel dimensions obtained from a CT dataset are set to a relative fraction of the field of view window. Current CT scanners enable reconstructions that result in an array of dimensions 512 × 512 × number of slices. While slice thickness is constructed in units of millimetres the voxel dimensions are equal to the field of view divided by 512. A field of view of 400 mm results in voxel dimension of 0.78125 mm × 0.78125 mm times the slice width. If a treatment planning system uses a set grid size of 2 mm, 2.56 voxels would require merging to produce the new grid dimensions. This merging results in known limitations for the commercial planning system (Elekta, 2014).

Manipulation of the raw CT dataset voxels to create a new simulation grid results in image blurring due to the merging of voxels. This can affect distinct boundaries where scattering conditions would normally change rapidly. Increasing the simulation grid would blur the boundary interchanges and create a gradual difference. An example is shown in Figure 8-8 for a 10 mm stepped surface with a 4 and 1 mm grid size. While the 1 mm edge blurring is negligible, plans are clinically calculated at 2 mm where the blurring is significant enough to reduce edge boundary scattering effects and introduce false hot and cold regions near the patient surface.

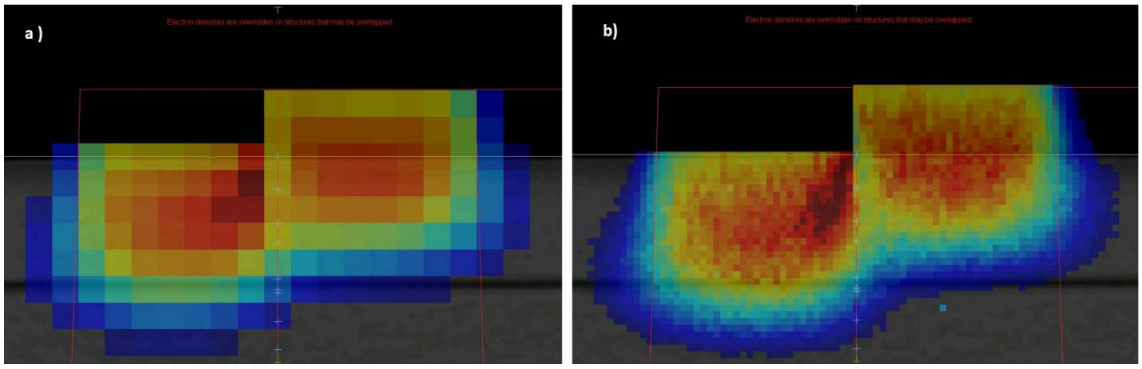

Figure 8-8 Voxel merging effect of a) 4 mm and b) 1 mm simulation grid for a 10 mm stepped surface

The first obvious boundary was the patient-air interface. If a calculation grid voxel partially includes patient material, the entire voxel is to be considered part of the new patient volume with a decreased CT value due to averaging with air. This in turn expands the patient volume in all dimensions relative to the size of the new calculation grid and results in dose outside of the patient compared to the CT scan.

The effect on electron PDDs is shown in Figure 8-9 where the effective energy is shifted deeper with larger voxel size. This effect can skew results when the surface variations coincide with voxel borders. This is shown in Figure 8-8 a) where the 10 mm step is flush with a 4 mm simulation grid and dose is entirely within the volume compared to the regular surface where dose extends 2 mm outside the patient. This results in a 1 mm difference in the PDD R_{50} depths between the two surfaces. Figure 8-8 b) surfaces are both affected by the same averaging and produce comparable PDDs that are approximately 0.25 mm shallower than measured.

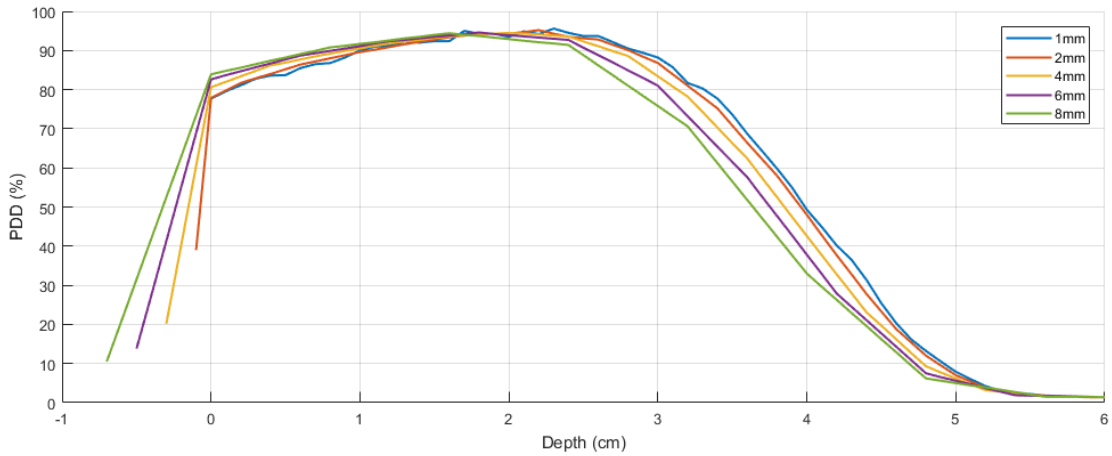

Figure 8-9 Elekta TPS PDD dependence on simulation voxel size for a 10 MeV electron beam

The effect of skewed dose predictions near the boundary interfaces due to the altered simulation environment is seen in Figure 7-24 (stepped surfaces) and Figure 7-29 (distinct inhomogeneity boundary). If a stepped edge boundary does not fall on a voxel edge exactly, the portion in the neighbouring voxel is merged reducing the CT number for the simulation voxel. This effectively changes the stepped edge to a steep gradient. The result is incorrect scattering conditions where profiles are observed to have a less pronounced hot and cold zone underneath the step. PDD boundary interfaces of Monaco 5 are found to be blurred when compared against BEAMnrc simulations where a higher resolution grid size near the boundary was used.

Due to the mentioned limitations associated with the application of a grid, Monaco 5 final calculation parameters were set to a grid size of 2 mm with the maximum number of histories. The chosen grid size was a trade-off between boundary interface merging errors, PDD agreement and statistical uncertainty of the dose. A 2 mm cubic grid size is large enough to introduce false steps over a curved surface creating a misrepresentation of dose resulting in a sawtooth distribution pattern as shown by Figure 8-10.

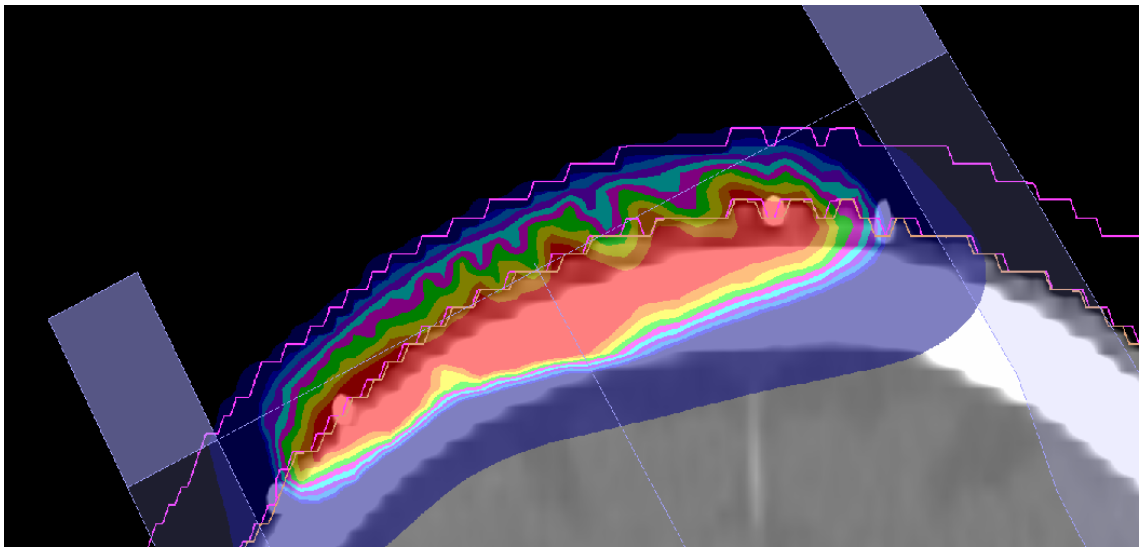

Figure 8-10 Sawtooth dose effect from a 2 mm grid size over a curved surface

By using an independent planning system, the user has the option to simulate on unmodified voxel dimensions. This removes any patient boundary expansion and volume averaging resulting in the most accurate dose distributions possible (CT raw voxel dimensions are less than 1 mm). This increases the statistical uncertainty due to the smaller voxel volumes, but the user has the ability to increase particle number repetitions to achieve the desired accuracy.

8.6. Results

The purpose of developing an accurate beam model was to increase the confidence in the results when it is applied to complex conditions. By successfully surpassing the gamma analysis criteria of 1%/1 mm, the confidence in results when applied to CT datasets was maintained.

The independent MU verification process is yet to be fully implemented clinically as the initial trial period is currently in progress. Currently only a small number of patient simulations (<10) have been completed but results are encouraging. Required MU prediction results were all within 3% between BEAMnrc/DOSXYZnrc and Monaco 5 where patient geometries can be adequately recreated in DOSXYZnrc. Unique modifications such as filling gaps or varying bolus (not present during the CT scan) have an effect depending on their influence on the dose prescription point.

Results for patient MU verification were also analysed for accuracy when the corrections for each applicator were applied as discussed in section 7.5. Results were

improved from 3% to 2%; this was noticeable in the 14 cm × 14 cm applicator as most patients were treated with the 10 cm × 10 cm and 14 cm × 14 cm applicators. 6 cm × 6 cm applicator measurement shaped field sizes were not significantly reduced from full field size and did not vary from 100 cm SSD to record more significant differences from measured output factors with simulated.

Individual circumstances such as patient geometry curvature/step, beam energy and field size of the treatment can produce errors greater than 7% in output factors determined by the assumption of slab geometry. Although the independent MU verification is yet to be clinically implemented, it is able to flag treatment dose accuracy where large disagreements are found between current clinical procedures using an insert cutout OF library assuming flat geometry. This indicates the need for patient dose verification using in-vivo dosimetry methods.

8.7. Summary

The development of an independent TPS allows the user to fully understand the limitations set upon commercial TPSs using calculation approximations to predict dose in superior timeframes compared to full MC methods. The largest compromise in calculation time is the manipulations of raw CT voxels to form a new dose grid of arbitrary millimetre dimensions. The modification of raw CT voxels leads to flaws introduced into the dose calculation. The requirement to merge voxels to a coarser resolution results in boundary blurring expanding the patient boundary and reducing any distinct boundary interfaces within the patient. This leads to calculation errors due to false stepped surfaces that significantly affect scattering conditions and dose predictions, and modifications in beam energy due to boundary expansion.

The commercial modified dose calculation grid voxelising makes it difficult to make exact comparisons between measurements especially under curved geometries or distinct boundaries. The developed independent TPS only utilises raw CT voxel dimensions and the largest dosimetry prediction limitation is determined by the slice width. The independent TPS can allow the use of interpolation methods to reduce slice thickness to minimise the surface step effect in the slice width dimension.

The independent TPS allows treatment verification under circumstances that are impossible to measure and allows a more accurate insight into the predicted dose distribution without significant limitations other than calculation time.

9. Conclusion

9.1. Summary

Through the development of the spectrum scanning script (SSS) combined with the model iterative refinement workflow and modified MLCE module, the resultant in-house BEAMnrc electron beam models successfully achieved the desired overall gamma analysis criteria of 1%/1 mm shown in Figure 7-12 and Figure 7-13 when compared to measurement. The five beam energies with five applicators for both Elekta linear accelerator models passed the gamma criteria for standard applicators, shaped and oblique fields. Initial results indicate models can also accurately replicate dose measurements through inhomogeneities and stepped fields but this accuracy cannot be confirmed with certainty due to small energy variations at the different time of measurement resulting in a significant impact on profile gamma passing rates in the high dose drop off region.

Variations between continuous spectra determined by the SSS indicate that numerous suitable solutions are possible. Different spectral distributions were shown to be able to achieve similar relative and absolute dosimetry results. Without an ability to restrict the spectrum distribution further, any solution deemed to give acceptable results is sufficient and the choice is up to the user's discretion. The complex nature of spectrum exiting the wave guide may never be precisely measured. Even if it were, it would have to be determined if it is consistent across multiple machines and would still only act as a general distribution guide.

The SSS determined a suitable spectrum to match measured PDDs for each electron beam model. Removing the spectrum variable from the simulation parameters allowed the ability to discriminate between the virtual linear accelerator modules for possible causes of disagreements between simulation results and measurements. Combined with identical shared components between model energies, the removal of the spectrum variable enabled the in-depth interrogation of the linear accelerator component modules and beam parameters. The ability to scrutinise models lead to the discovery of multiple flaws that may have otherwise remained undetected.

BEAMnrc models and incident spectra were initially created by matching open field data where applicators were not present in the beam path to ensure accurate jaw positions. Simulation results matched measured profile data to within 1% over the

clinical range but could not match open field output measurements. Through interrogation and confidence in other model modules, the MLCE module was determined to be the cause of the discrepancy. The MLCE module did not correctly account for particle shielding in the plane perpendicular to the leaf direction. This was accounted for by introducing additional leaves that spanned across the entire field acting as the boundary wall. The modification reduced the output discrepancy and produced results within 2% but the majority within 1% of measurement.

Of the accelerator component specifications supplied by Elekta, only one component required adjustment outside the specified tolerance. The 15 MeV primary filter required an increased thickness of 13% to obtain agreement with measured data. This increase was made with confidence due to the interrogation of component sharing between energies and similar requirements for both accelerator models modelled.

By observing and comparing the absolute dosimetry errors between energies, applicators and models it was concluded that there is missing material in the beam modelling of the applicators. The hypothesis of missing material near the end of the applicator is supported by the evidence from the output discrepancies reported. This supports both the missing dose and dose drop off rate with SSD that would predominately affect smaller applicators where material is closer to the measurement point. This hypothesis was tested by adding a small portion of material in the path of the direct beam which was found to increase the output for a 6 cm × 6 cm applicator by 1.35%. Further supporting evidence is observed from the lack of shielding in profile results where additional material is present in real life but not accounted for in the BEAMnrc model. This suggests that for an electron model to be an authentic representation of reality, the applicator misrepresentation in the simulation environment would need to be corrected.

While correction factors can be applied to individual applicators to correct for output discrepancies, the artificial correction digresses from the accepted perception that Monte Carlo methods are the most accurate method for calculating dose. While a correction factor can negate an output offset, it cannot correct for the absolute dose variation with SSD.

Shaped field outputs from Monaco 5 were found to be centred on measured values however were susceptible to SSD variation for smaller fields. In-house BEAMnrc model results achieved similar output precision (Figure 7-19) however were

not able to achieve a similar accuracy. This indicates that the commercial TPS applies an output correction per applicator. The applicator dependent dose output correction factor does not correct the underlying cause as the dose discrepancy with SSD still exists for the 6 cm × 6 cm and 10 cm × 10 cm applicators. BEAMnrc models can achieve the same output accuracy with an applied applicator dependent correction factor (Figure 7-20) indicating equal modelling abilities and flaws.

If MC methods are to be accepted as a true dose prediction algorithm, results should not require any corrections to match measurements. The mentioned discrepancies and causes were only discovered by not accepting the differences as limitations of MC. If MC is based on known fundamental principles, the only reason discrepancies should be present is the inability to accurately model reality or defects in the acquired data.

While both Monaco and in-house modelling methods could create beam models passing the overall gamma criteria of 1%/1 mm, the in-house BEAMnrc models achieved a better overall gamma pass rate. This can be attributed to the greater ability to control the simulation environment and parameters to allow more accurate representation of reality. While in-house models were determined to be superior, they do not serve to replace commercial TPS as the ability of the latter to produce sufficiently accurate results within superior timeframes cannot be replaced. Instead they can be used to determine planning system limitations and allow patient dosimetry verification where it is difficult or impossible to perform.

In-house models cannot be utilised to their full potential without an independent planning system to allow the incorporation of CT datasets. While slab geometry was sufficient for TPS commissioning and validation, it does not allow the application of models onto patient specific geometries and mediums. Several advantages arise from developing an independent planning system. The significant advantage is the control of voxel geometric and medium manipulations for simulations. An independent planning system allows the option to use raw CT dataset geometries to remove the consequences of modifying voxel geometries. This in turn increases the simulation time, however the increased time may be acceptable for verification purposes where the simulation is only required once. Simulation time is dependent on beam energy, field size, patient dataset dimensions and voxel size, simulation uncertainty and the purpose of MU verification or dose plane comparison. A very rough estimate of BEAMnrc simulation time is 100

times longer than Monaco to verify MU and 200 times longer to extract dose planes, divided by the number of cores used for parallel simulations.

Commercial planning systems only allow a simulation grid spacing of millimetre units. A larger spaced calculation grid compromise is influenced by the increased simulation time required to achieve a similar result uncertainty when using a smaller calculation grid. The modification to the calculation grid requires manipulation of raw CT voxel geometries determined by the CT scan to match dimensions that no longer have a physical meaning. This grid modification creates undesired situations such as patient border contours, boundary interfaces and voxel averaging that would not exist if the raw CT voxel geometries were used. These effects are pronounced when used with electron models due to the sensitivity in distinct boundaries and stepped surfaces that are exacerbated by larger grid spacing. These situations may be the next hurdle for computing advancements to overcome to allow for simulations on raw voxel geometries while maintaining reasonable timeframes.

In conclusion, Elekta's current commercial electron treatment planning system, Monaco 5, produces accurate and reliable dose predictions more quickly in comparison to the in-house TPS developed in this work. Although it is unable to sufficiently solve fundamental Monte Carlo modelling problems, correction factors are able to correct dosimetry results to within acceptable limits. Developed in-house BEAMnrc beam models are currently prone to the same fundamental flaws however with further modelling effort can be rectified.

While the SSD dose drop off flaw is yet to be rectified, knowledge of its existence is crucial in ensuring best possible patient care. For example, care should be taken when using the 6 cm × 6 cm applicator at reduced or extended SSDs where output accuracy can fail in excess of 2% when SSD varies by only a few centimetres from 100 cm.

9.2. Future Work

The foremost effort should be to investigate and resolve dose discrepancies observed due to the inclusion of applicators. Simulations should be conducted where applicators are represented more precisely in BEAMnrc to resolve absolute dose discrepancies observed while also possibly revealing new discrepancies.

While the accelerator MU variation with field size was found not to be a significant contributor for the Synergy model, it is possible that the Agility model could be susceptible to MU variation with field size. The Agility model uses the MLC to define the field size and the resultant backscatter could affect scattering conditions to the ion chamber. The observed output variation in open field results indicates there is a link between field size and output error. With an improved film dosimetry methodology, it should be possible to determine MU variations.

The discrepancy between measured and simulated PDDs was unable to be explained. Investigations suggest that it could be due to the inability to precisely represent the accelerator head in BEAMnrc. Possible causes are the inability to mimic shielding walls/components or extra components that are not in the path of the primary beam. This can be investigated to modify BEAMnrc models to determine their effects on resulting PDDs.

Finally, with the known accuracies and limitations of the developed electron models it may be possible to investigate the potential introduction of electron arc therapy. The independent planning system could prove invaluable when validating a commercial TPS plan. This could enable a new method of treatment and validation with confidence.

Appendix A - Open Field Results without applicators

A.1. PDD Error without applicators for determined spectra

A.1.1. Synergy

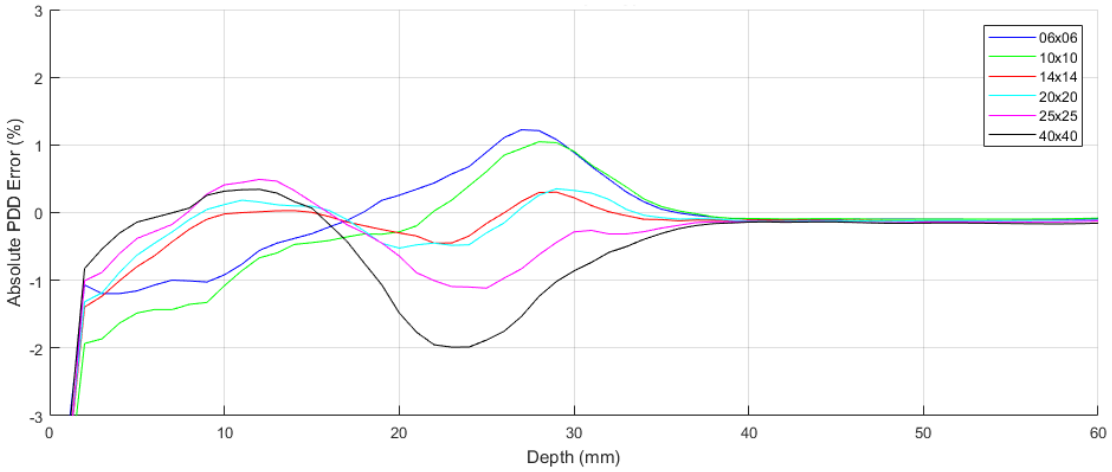

Figure A-1 Post MLCE modification Synergy 100 cm SSD 6 MeV simulated PDD error with SSS spectrum from measured data for fields without applicators

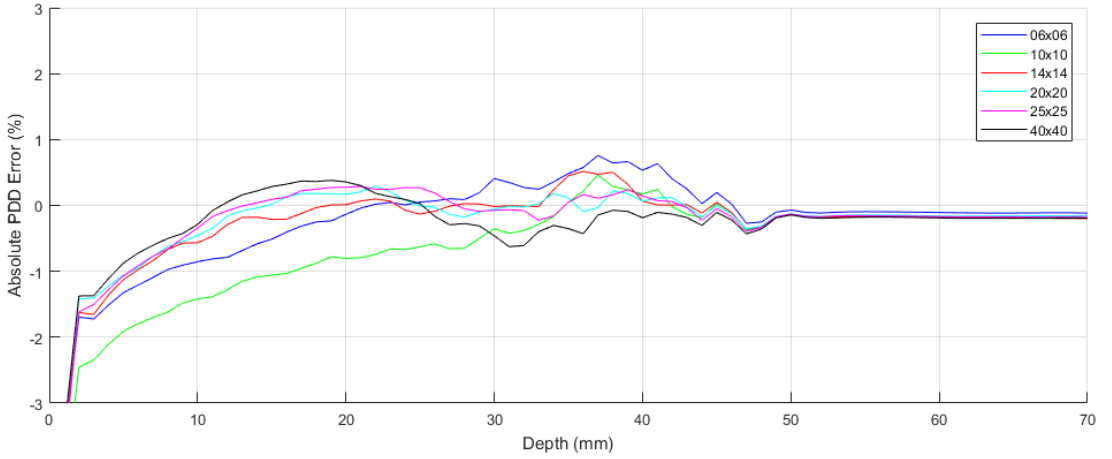

Figure A-2 Post MLCE modification Synergy 100 cm SSD 8 MeV simulated PDD error with SSS spectrum from measured data for fields without applicators

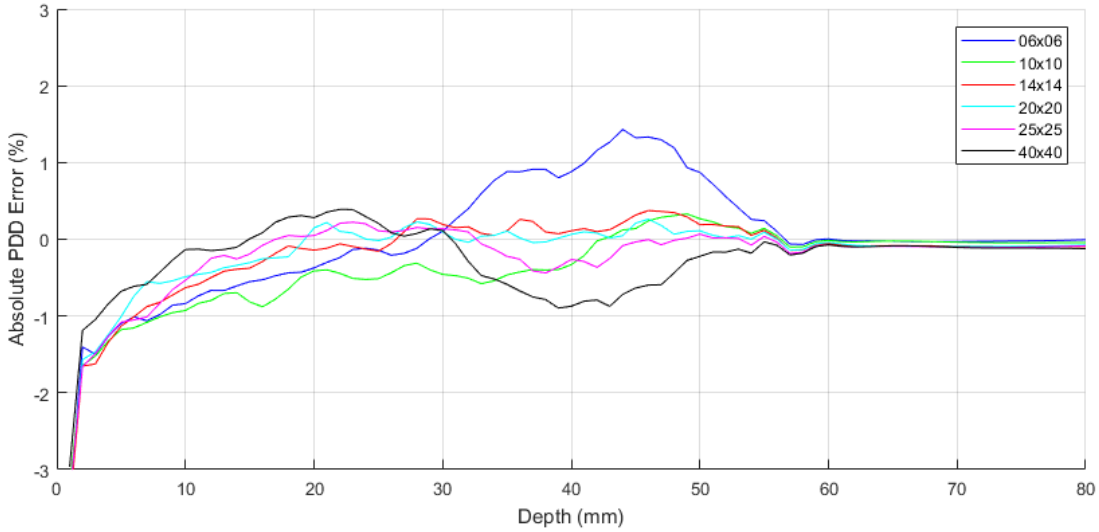

Figure A-3 Post MLCE modification Synergy 100 cm SSD 10 MeV simulated PDD error with SSS spectrum from measured data for fields without applicators

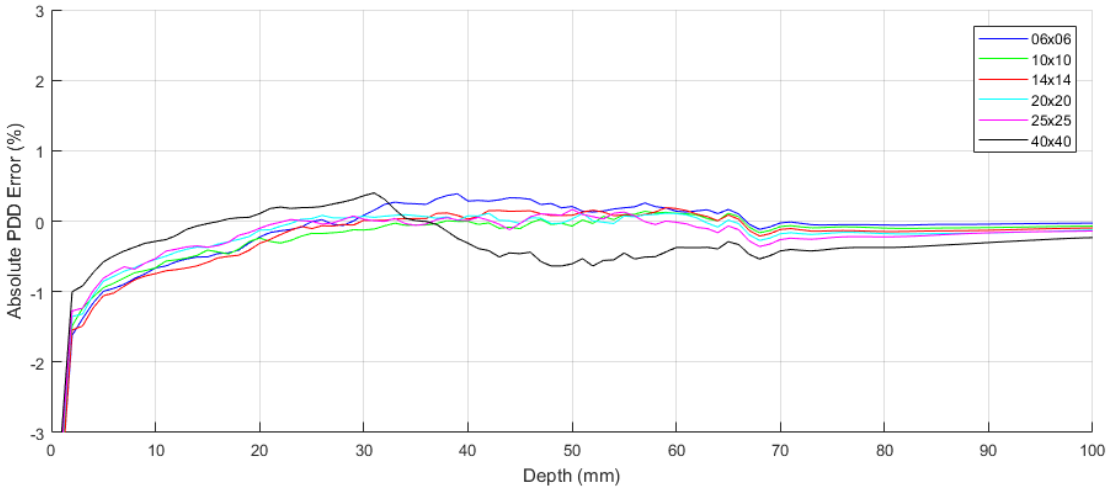

Figure A-4 Post MLCE modification Synergy 100 cm SSD 12 MeV simulated PDD error with SSS spectrum from measured data for fields without applicators

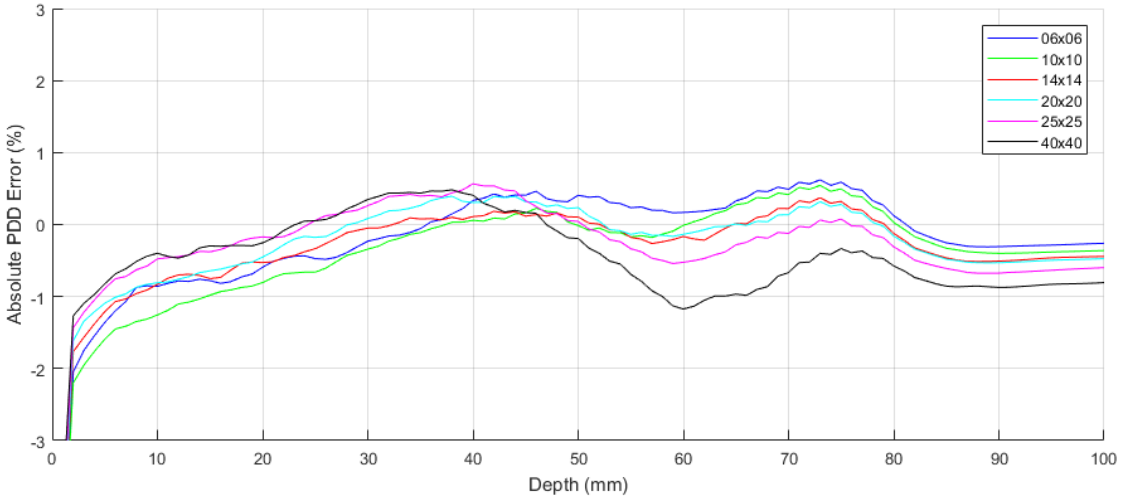

Figure A-5 Post MLCE modification Synergy 100 cm SSD 15 MeV simulated PDD error with SSS spectrum from measured data for fields without applicators

A.1.2. Agility

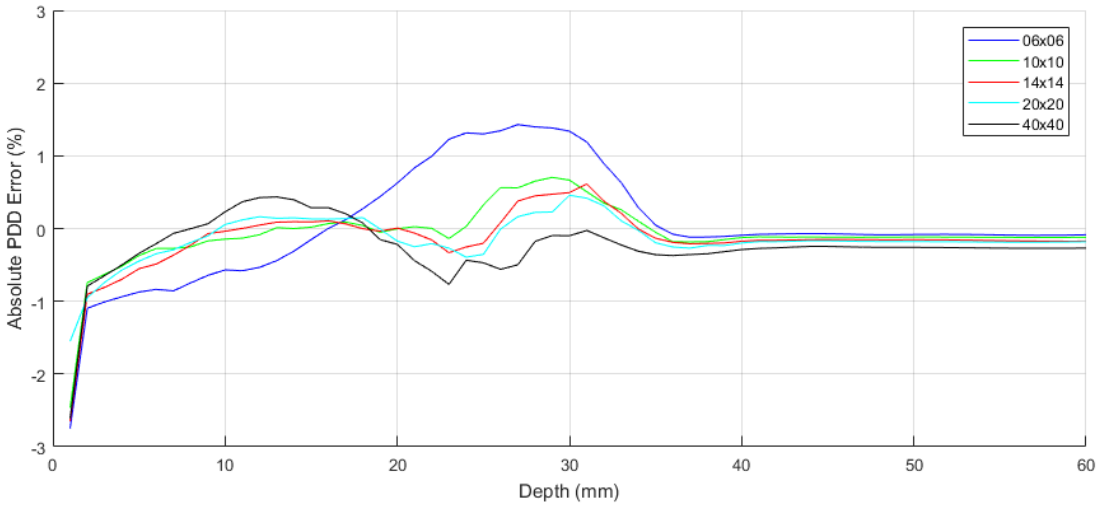

Figure A-6 Agility 100 cm SSD 6 MeV simulated PDD error with SSS spectrum from measured data for fields without applicators

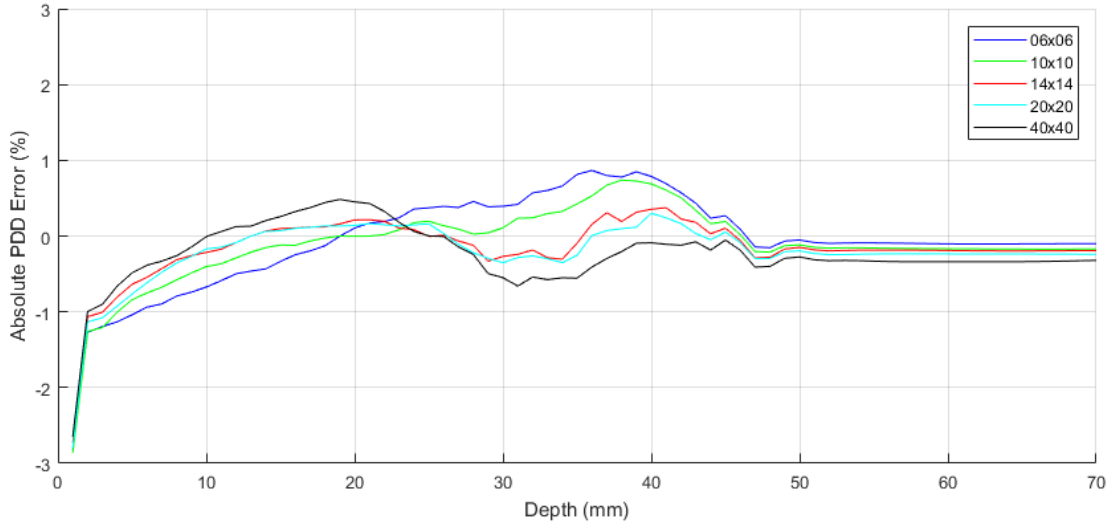

Figure A-7 Agility 100 cm SSD 8 MeV simulated PDD error with SSS spectrum from measured data for fields without applicators

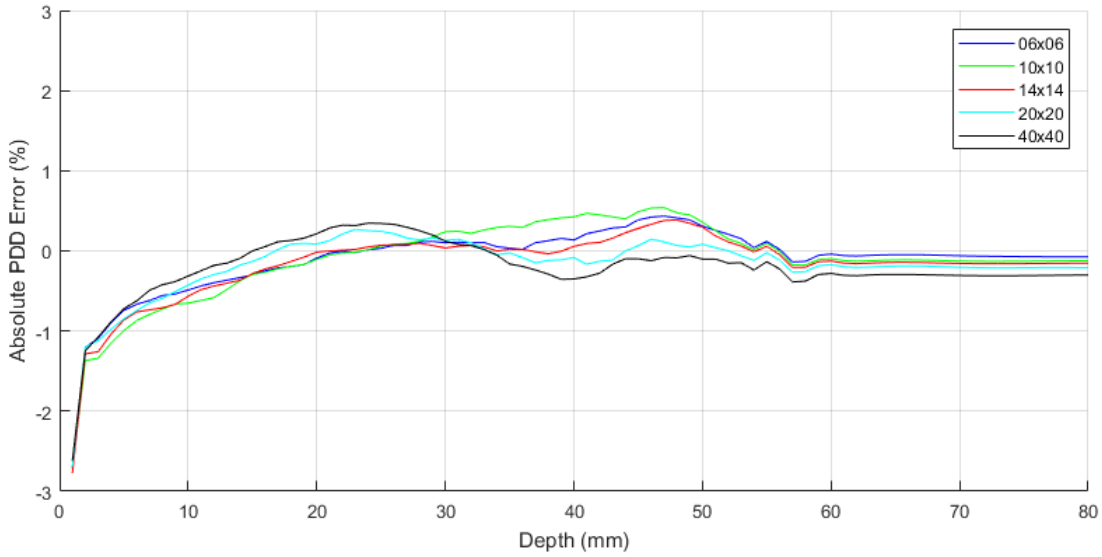

Figure A-8 Agility 100 cm SSD 10 MeV simulated PDD error with SSS spectrum from measured data for fields without applicators

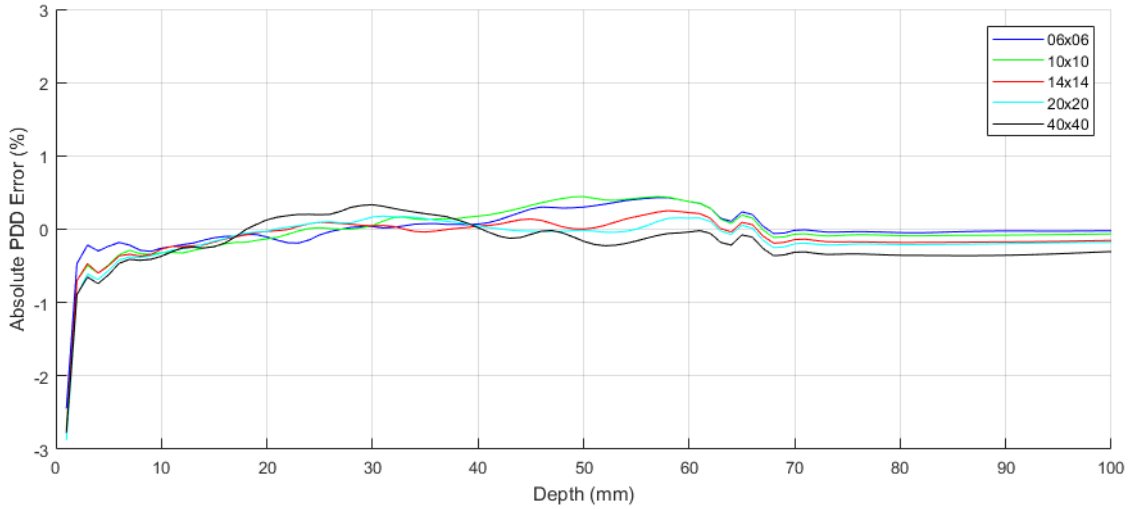

Figure A-9 Agility 100 cm SSD 12 MeV simulated PDD error with SSS spectrum from measured data for fields without applicators

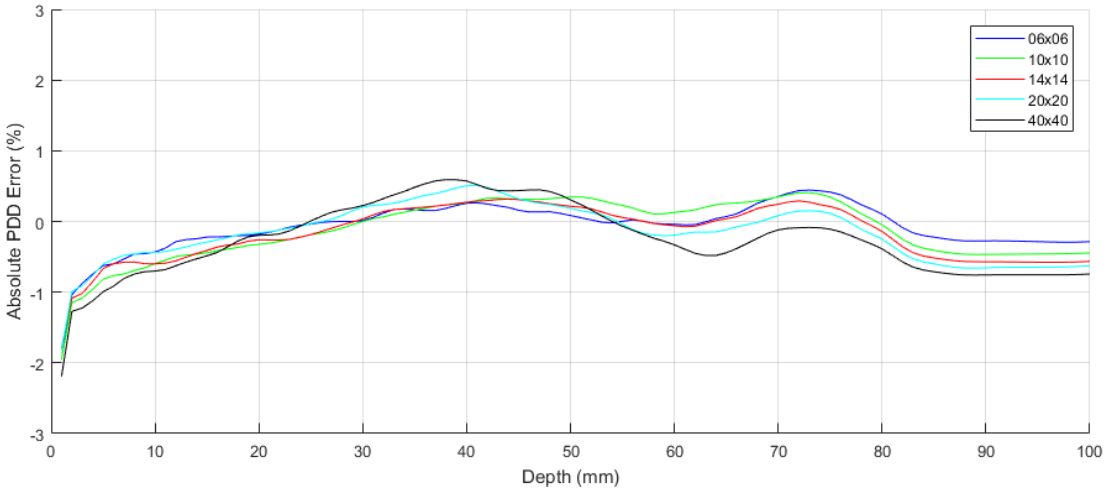

Figure A-10 Agility 100 cm SSD 15 MeV simulated PDD error with SSS spectrum from measured data for fields without applicators

A.2. Profile Error without applicators for determined spectra

A.2.1. Synergy

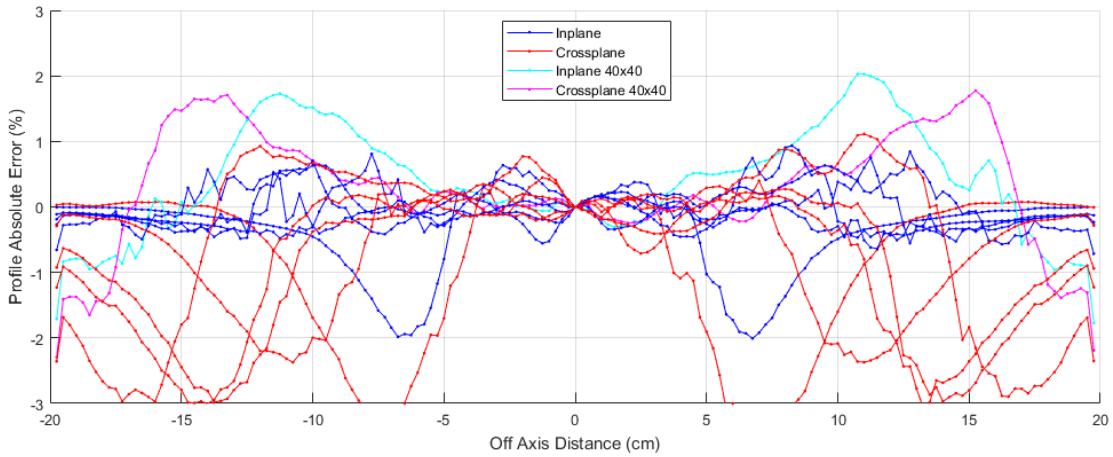

Figure A-11 Post MLCE modification Synergy 80 cm SSD 6 MeV open field D_m profile percentage errors for all applicators

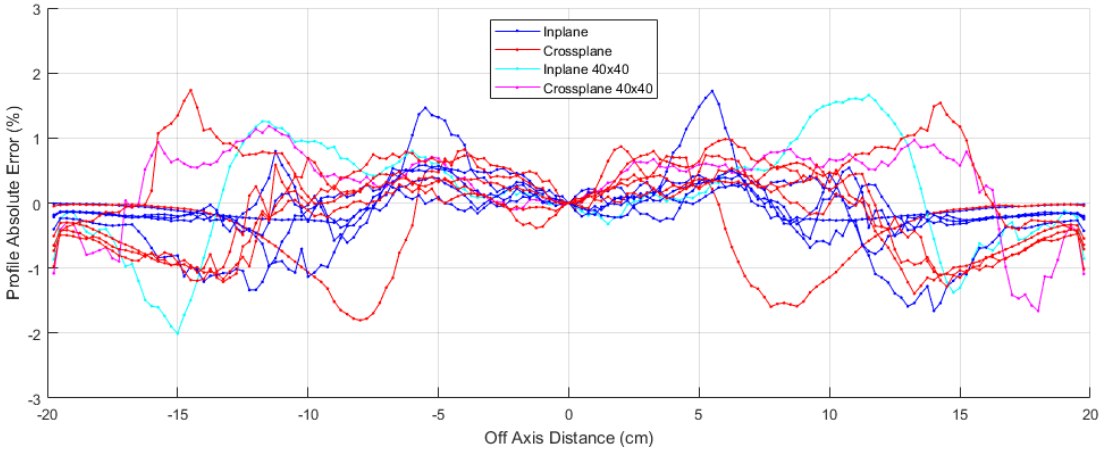

Figure A-12 Post MLCE modification Synergy 80 cm SSD 8 MeV open field D_m profile percentage errors for all applicators

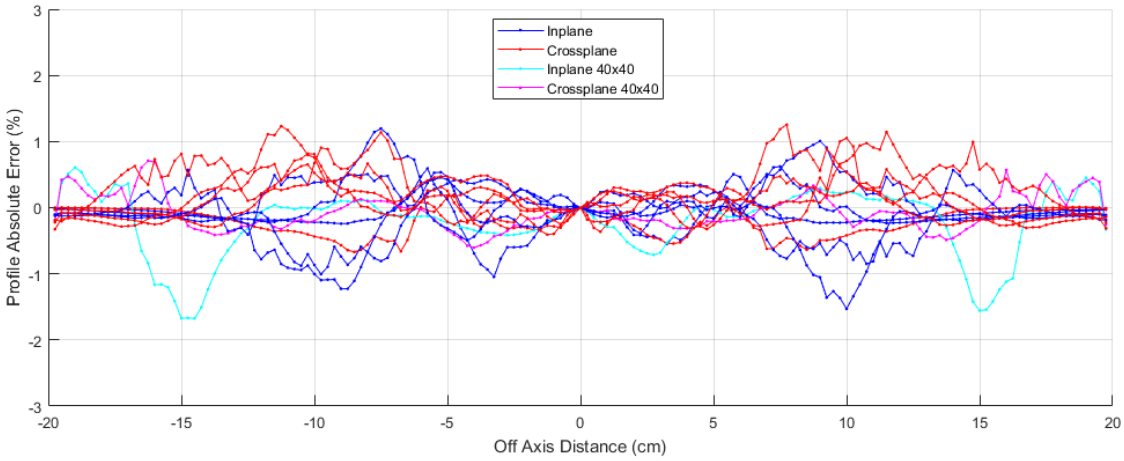

Figure A-13 Post MLCE modification Synergy 80 cm SSD 10 MeV open field D_m profile percentage errors for all applicators

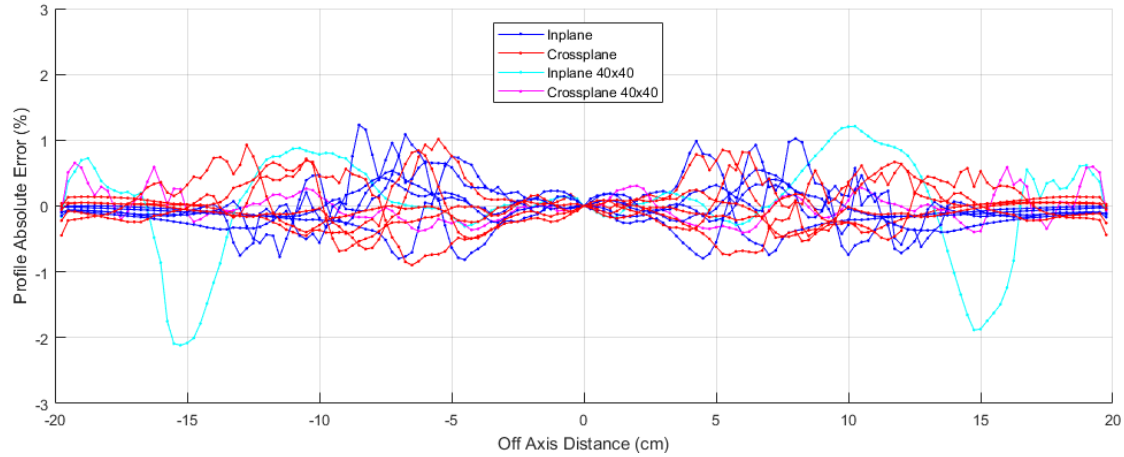

Figure A-14 Post MLCE modification Synergy 80 cm SSD 12 MeV open field D_m profile percentage errors for all applicators

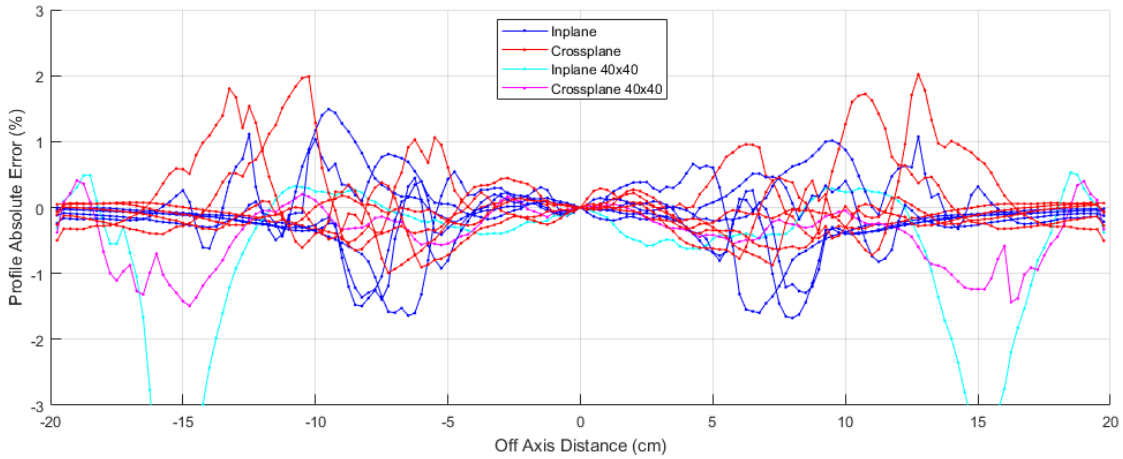

Figure A-15 Post MLCE modification Synergy 80 cm SSD 15 MeV open field D_m profile percentage errors for all applicators

A.2.2. Agility

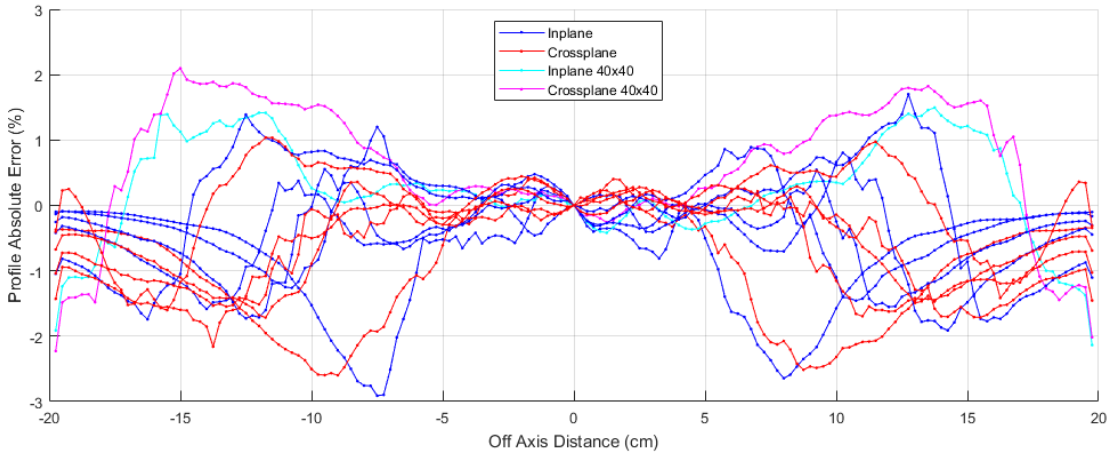

Figure A-16 Agility 80 cm SSD 6 MeV open field D_m profile percentage errors for all applicators

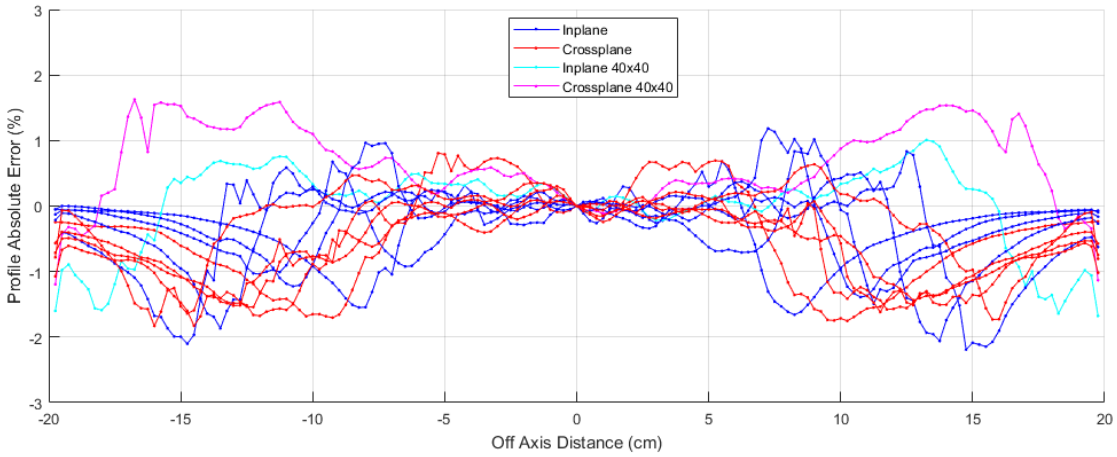

Figure A-17 Agility 80 cm SSD 8 MeV open field D_m profile percentage errors for all applicators

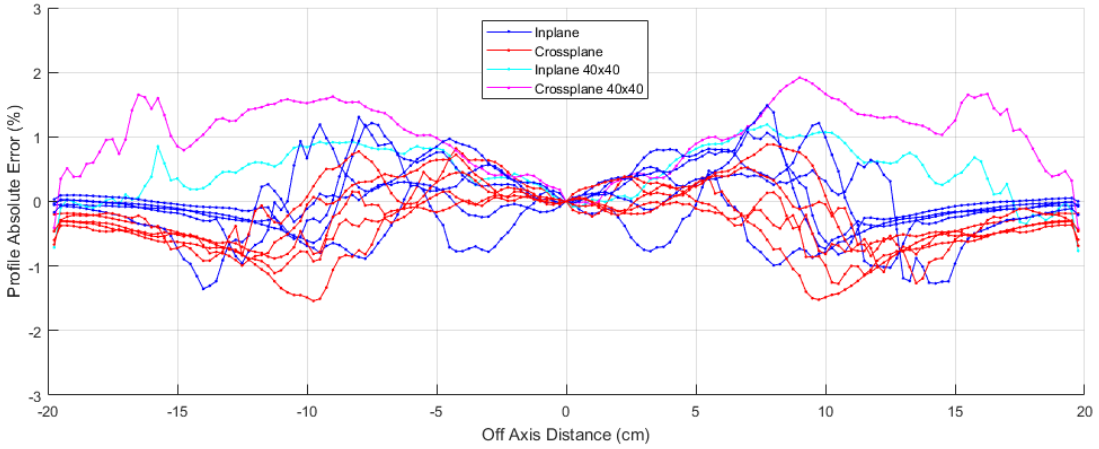

Figure A-18 Agility 80 cm SSD 10 MeV open field D_m profile percentage errors for all applicators

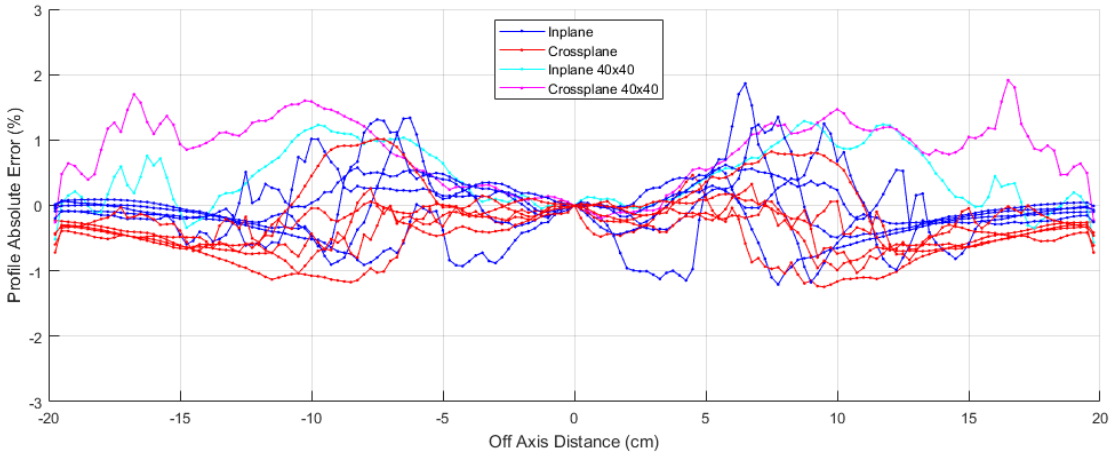

Figure A-19 Agility 80 cm SSD 12 MeV open field D_m profile percentage errors for all applicators

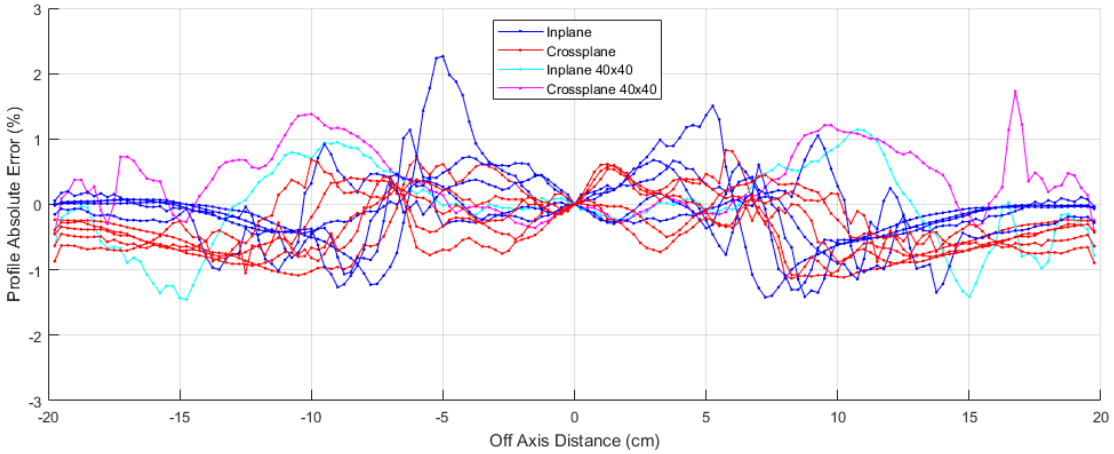

Figure A-20 Agility 80 cm SSD 15 MeV open field D_m profile percentage errors for all applicators

A.3. Output Error over SSDs 80, 90 and 100 cm

A.3.1. Synergy

Table A-1 Synergy 6 MeV open field output accuracy

	Synergy 6 MeV Open Field Simulated Output Accuracy												
	SSD	6x6	10x10	14x14	20x20	25x25	40x40	6x6	10x10	14x14	20x20	25x25	40x40
Measured	100							0.816	1.000	1.039	1.047	1.059	1.056
	90							1.089	1.262	1.306	1.315	1.325	1.321
	80							1.490	1.634	1.691	1.700	1.705	1.698
Simulated	100	6.24E-14	7.53E-14	7.82E-14	7.86E-14	7.94E-14	7.97E-14	0.828	1.000	1.038	1.045	1.054	1.059
	90	8.28E-14	9.47E-14	9.80E-14	9.86E-14	9.93E-14	9.94E-14	1.100	1.258	1.302	1.310	1.319	1.320
	80	1.13E-13	1.22E-13	1.27E-13	1.27E-13	1.27E-13	1.28E-13	1.497	1.624	1.680	1.692	1.692	1.694
Relative Error (%)	100							1.44	0.00	-0.05	-0.25	-0.43	0.29
	90							1.02	-0.32	-0.31	-0.41	-0.43	-0.04
	80							0.51	-0.64	-0.64	-0.44	-0.71	-0.23

Table A-2 Synergy 8 MeV open field output accuracy

	Synergy 8 MeV Open Field Simulated Output Accuracy											
	SSD	6x6	10x10	14x14	20x20	25x25	40x40	6x6	10x10	14x14	20x20	25x25	40x40
Measured	100							0.899	1.000	1.002	1.008	1.019	1.015
	90							1.158	1.257	1.257	1.263	1.273	1.268
	80							1.521	1.617	1.618	1.625	1.635	1.626
Simulated	100	8.37E-14	9.31E-14	9.39E-14	9.44E-14	9.53E-14	9.53E-14	0.899	1.000	1.009	1.014	1.024	1.024
	90	1.08E-13	1.16E-13	1.17E-13	1.18E-13	1.19E-13	1.19E-13	1.156	1.247	1.261	1.268	1.278	1.276
	80	1.41E-13	1.50E-13	1.51E-13	1.52E-13	1.52E-13	1.52E-13	1.518	1.607	1.626	1.632	1.636	1.632
Relative Error (%)	100							0.07	0.00	0.63	0.66	0.49	0.88
	90							-0.26	-0.78	0.31	0.46	0.35	0.62
	80							-0.18	-0.65	0.47	0.41	0.07	0.38

Table A-3 Synergy 10 MeV open field output accuracy

	Synergy 10 MeV Open Field Simulated Output Accuracy											
	SSD	6x6	10x10	14x14	20x20	25x25	40x40	6x6	10x10	14x14	20x20	25x25	40x40
Measured	100							0.960	1.000	1.010	1.015	1.032	1.027
	90							1.212	1.246	1.257	1.263	1.282	1.275
	80							1.564	1.596	1.607	1.611	1.635	1.625
Simulated	100	1.24E-13	1.30E-13	1.31E-13	1.32E-13	1.34E-13	1.34E-13	0.951	1.000	1.009	1.010	1.028	1.026
	90	1.56E-13	1.62E-13	1.63E-13	1.64E-13	1.66E-13	1.66E-13	1.200	1.243	1.253	1.256	1.275	1.273
	80	2.02E-13	2.07E-13	2.08E-13	2.09E-13	2.12E-13	2.11E-13	1.552	1.588	1.598	1.603	1.626	1.618
Relative Error (%)	100							-0.95	0.00	-0.11	-0.54	-0.35	-0.05
	90							-1.02	-0.26	-0.34	-0.57	-0.50	-0.21
	80							-0.77	-0.51	-0.51	-0.49	-0.52	-0.41

Table A-4 Synergy 12 MeV open field output accuracy

	Synergy 12 MeV Open Field Simulated Output Accuracy											
	SSD	6x6	10x10	14x14	20x20	25x25	40x40	6x6	10x10	14x14	20x20	25x25	40x40
Measured	100							0.981	1.000	1.012	1.019	1.032	1.027
	90							1.227	1.243	1.254	1.264	1.281	1.273
	80							1.571	1.585	1.599	1.607	1.628	1.614
Simulated	100	1.31E-13	1.33E-13	1.35E-13	1.36E-13	1.38E-13	1.37E-13	0.984	1.000	1.012	1.023	1.035	1.030
	90	1.64E-13	1.66E-13	1.67E-13	1.69E-13	1.71E-13	1.70E-13	1.231	1.243	1.252	1.266	1.282	1.276
	80	2.10E-13	2.12E-13	2.12E-13	2.15E-13	2.18E-13	2.16E-13	1.574	1.586	1.589	1.613	1.632	1.618
Relative Error (%)	100							0.31	0.00	-0.02	0.43	0.29	0.31
	90							0.31	-0.02	-0.17	0.20	0.06	0.23
	80							0.22	0.07	-0.61	0.35	0.21	0.23

Table A-5 Synergy 15 MeV open field output accuracy

	Synergy 15 MeV Open Field Simulated Output Accuracy												
	SSD	6x6	10x10	14x14	20x20	25x25	40x40	6x6	10x10	14x14	20x20	25x25	40x40
Measured	100							0.989	1.000	1.003	1.009	1.023	1.018
	90							1.229	1.240	1.242	1.250	1.267	1.259
	80							1.564	1.575	1.577	1.587	1.609	1.593
Simulated	100	1.32E-13	1.33E-13	1.34E-13	1.34E-13	1.35E-13	1.34E-13	0.989	1.000	1.002	1.003	1.016	1.009
	90	1.64E-13	1.65E-13	1.65E-13	1.65E-13	1.67E-13	1.66E-13	1.227	1.237	1.237	1.238	1.256	1.245
	80	2.08E-13	2.09E-13	2.09E-13	2.10E-13	2.13E-13	2.10E-13	1.562	1.568	1.569	1.572	1.596	1.577
Relative Error (%)	100							0.02	0.00	-0.02	-0.58	-0.67	-0.90
	90							-0.12	-0.27	-0.41	-0.91	-0.92	-1.14
	80							-0.16	-0.43	-0.48	-0.93	-0.83	-1.05

A.3.2. Agility

Table A-6 Agility 6 MeV open field output accuracy

	Agility 6 MeV Open Field Simulated Output Accuracy												
	SSD	6x6	10x10	14x14	20x20	25x25	40x40	6x6	10x10	14x14	20x20	25x25	40x40
Measured	100							0.882	1.000	1.041	1.059	1.069	1.066
	90							1.148	1.269	1.309	1.329	1.339	1.334
	80							1.539	1.657	1.698	1.717	1.731	1.717
Simulated	100	6.69E-14	7.71E-14	8.00E-14	8.13E-14	8.18E-14	8.13E-14	0.868	1.000	1.038	1.054	1.062	1.054
	90	8.69E-14	9.74E-14	1.01E-13	1.02E-13	1.02E-13	1.01E-13	1.127	1.263	1.304	1.322	1.328	1.314
	80	1.16E-13	1.27E-13	1.30E-13	1.31E-13	1.32E-13	1.30E-13	1.507	1.644	1.688	1.705	1.713	1.687
Relative Error (%)	100							-1.54	0.00	-0.29	-0.41	-0.70	-1.15
	90							-1.77	-0.42	-0.33	-0.50	-0.81	-1.44
	80							-2.09	-0.77	-0.56	-0.69	-1.04	-1.74

Table A-7 Agility 8 MeV open field output accuracy

	Agility 8 MeV Open Field Simulated Output Accuracy												
	SSD	6x6	10x10	14x14	20x20	25x25	40x40	6x6	10x10	14x14	20x20	25x25	40x40
Measured	100							0.919	1.000	1.016	1.030	1.036	1.030
	90							1.175	1.258	1.275	1.291	1.296	1.288
	80							1.546	1.629	1.648	1.667	1.671	1.656
Simulated	100	8.32E-14	9.14E-14	9.31E-14	9.43E-14	9.47E-14	9.39E-14	0.910	1.000	1.018	1.032	1.035	1.027
	90	1.06E-13	1.15E-13	1.17E-13	1.18E-13	1.18E-13	1.17E-13	1.162	1.255	1.275	1.289	1.295	1.279
	80	1.39E-13	1.48E-13	1.50E-13	1.52E-13	1.52E-13	1.50E-13	1.521	1.622	1.641	1.662	1.667	1.637
Relative Error (%)	100							-0.93	0.00	0.25	0.22	-0.03	-0.34
	90							-1.08	-0.22	0.00	-0.20	-0.06	-0.68
	80							-1.59	-0.43	-0.42	-0.28	-0.25	-1.16

Table A-8 Agility 10 MeV open field output accuracy

		Agility 10 MeV Open Field Simulated Output Accuracy											
	SSD	6x6	10x10	14x14	20x20	25x25	40x40	6x6	10x10	14x14	20x20	25x25	40x40
Measured	100							0.940	1.000	1.003	1.017	1.020	1.011
	90							1.186	1.249	1.253	1.267	1.270	1.257
	80							1.536	1.604	1.609	1.627	1.629	1.600
Simulated	100	1.23E-13	1.32E-13	1.33E-13	1.35E-13	1.36E-13	1.34E-13	0.932	1.000	1.007	1.020	1.027	1.013
	90	1.55E-13	1.65E-13	1.66E-13	1.68E-13	1.69E-13	1.66E-13	1.174	1.248	1.256	1.270	1.277	1.257
	80	2.01E-13	2.12E-13	2.13E-13	2.16E-13	2.16E-13	2.12E-13	1.516	1.601	1.611	1.628	1.635	1.600
Relative Error (%)	100							-0.83	0.00	0.37	0.26	0.71	0.15
	90							-1.05	-0.14	0.26	0.18	0.50	-0.01
	80							-1.25	-0.18	0.16	0.06	0.37	-0.03

Table A-9 Agility 12 MeV open field output accuracy

		Agility 12 MeV Open Field Simulated Output Accuracy											
	SSD	6x6	10x10	14x14	20x20	25x25	40x40	6x6	10x10	14x14	20x20	25x25	40x40
Measured	100							0.963	1.000	1.010	1.024	1.028	1.017
	90							1.208	1.248	1.260	1.274	1.278	1.261
	80							1.555	1.600	1.612	1.630	1.631	1.604
Simulated	100	1.27E-13	1.32E-13	1.34E-13	1.37E-13	1.37E-13	1.35E-13	0.959	1.000	1.016	1.034	1.040	1.025
	90	1.58E-13	1.65E-13	1.67E-13	1.69E-13	1.70E-13	1.67E-13	1.199	1.246	1.264	1.283	1.291	1.268
	80	2.04E-13	2.11E-13	2.13E-13	2.17E-13	2.17E-13	2.13E-13	1.543	1.596	1.616	1.641	1.646	1.610
Relative Error (%)	100							-0.42	0.00	0.56	0.96	1.14	0.80
	90							-0.69	-0.17	0.30	0.73	1.03	0.53
	80							-0.80	-0.23	0.25	0.66	0.97	0.35

Table A-10 Agility 15 MeV open field output accuracy

		Agility 15 MeV Open Field Simulated Output Accuracy											
	SSD	6x6	10x10	14x14	20x20	25x25	40x40	6x6	10x10	14x14	20x20	25x25	40x40
Measured	100							0.970	1.000	1.003	1.025	1.028	1.019
	90							1.211	1.245	1.249	1.273	1.277	1.262
	80							1.557	1.597	1.601	1.628	1.628	1.605
Simulated	100	1.26E-13	1.30E-13	1.30E-13	1.33E-13	1.34E-13	1.32E-13	0.971	1.000	1.002	1.029	1.034	1.021
	90	1.56E-13	1.61E-13	1.61E-13	1.65E-13	1.66E-13	1.63E-13	1.206	1.242	1.245	1.275	1.278	1.261
	80	2.00E-13	2.05E-13	2.06E-13	2.11E-13	2.11E-13	2.07E-13	1.545	1.585	1.589	1.627	1.629	1.597
Relative Error (%)	100							0.15	0.00	-0.13	0.43	0.63	0.23
	90							-0.36	-0.21	-0.29	0.16	0.08	-0.07
	80							-0.74	-0.72	-0.72	-0.07	0.08	-0.48

Appendix B - Electron Model RMS Error Indexes

B.1.Combined Energy and Applicator Beam Model Summary Results

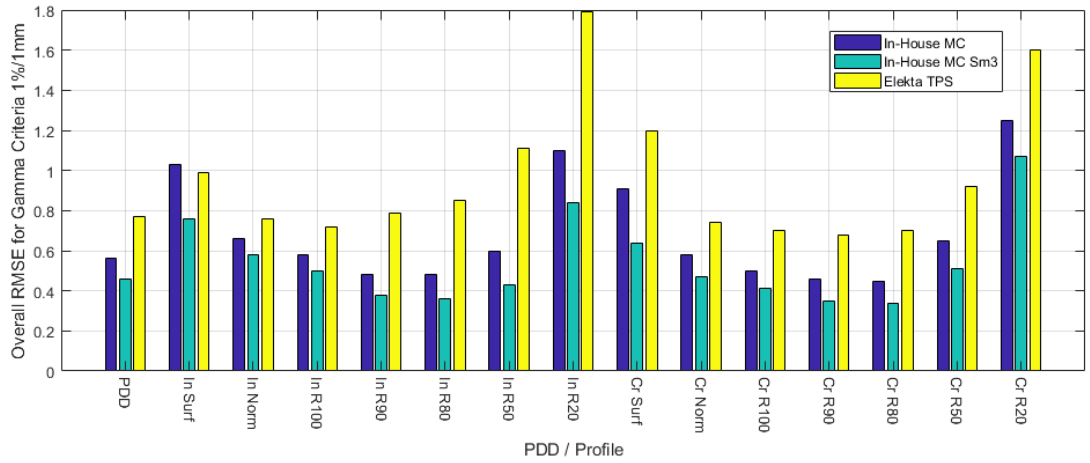

Figure B-1 RMS profile error summary for Synergy models with standard applicator cutouts

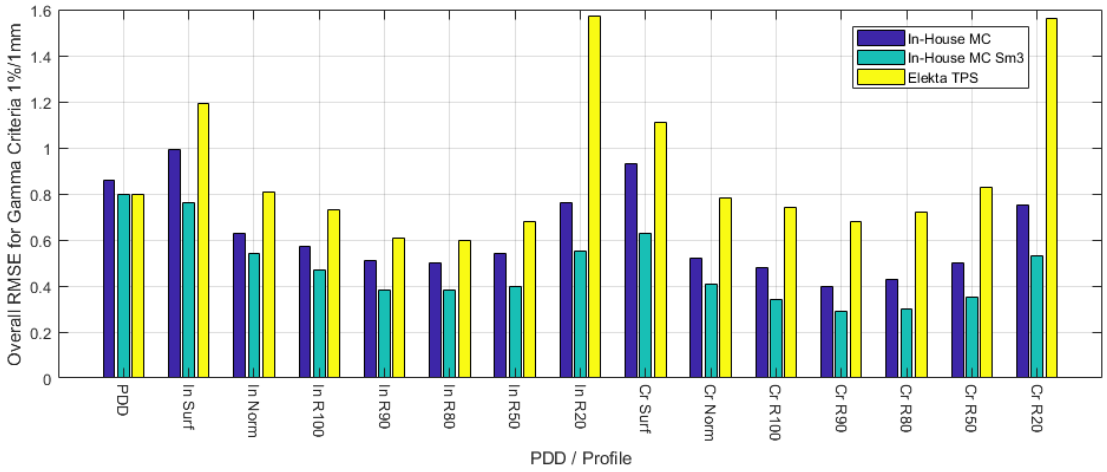

Figure B-2 RMS profile error summary for Agility models with standard applicator cutouts

Table B-1 RMS error index for gamma 1%/1mm – In-House Synergy model

In-House Monte Carlo Synergy Electron Model Standard Applicator Cutout Gamma 1%/1mm Result Summary																		
				Inplane Profiles							Crossplane Profiles							
	Energy (MeV)	Applicator	PDD	Surf	Norm	R100	R90	R80	R50	R20	Surf	Norm	R100	R90	R80	R50	R20
100cm SSD	6	06x06	0.28	0.55	0.43	0.36	0.33	0.31	0.28	0.26	0.37	0.23	0.14	0.08	0.12	0.16	0.29
		10x10	0.38	0.95	0.67	0.58	0.47	0.42	0.38	0.59	0.74	0.42	0.25	0.29	0.23	0.33	0.53
		14x14	0.25	0.78	0.56	0.50	0.31	0.29	0.35	0.63	0.78	0.51	0.36	0.22	0.27	0.44	0.84
		20x20	0.32	1.32	0.99	0.86	0.59	0.69	0.57	0.88	0.86	0.57	0.53	0.41	0.50	0.62	0.94
		25x25	0.33	1.60	1.24	1.14	0.75	0.92	0.80	1.15	0.92	0.69	0.56	0.51	0.55	0.94	1.92
	8	06x06	0.52	0.51	0.32	0.29	0.30	0.30	0.26	0.38	0.53	0.22	0.16	0.22	0.19	0.18	0.23
		10x10	0.62	0.91	0.57	0.50	0.42	0.36	0.42	0.43	0.96	0.51	0.41	0.31	0.34	0.27	0.44
		14x14	0.52	0.79	0.59	0.42	0.35	0.28	0.43	1.13	0.78	0.59	0.40	0.45	0.33	0.43	0.89
		20x20	0.81	1.41	0.84	0.73	0.60	0.52	0.47	1.03	0.88	0.70	0.62	0.49	0.48	0.61	1.03
		25x25	0.74	1.59	1.02	0.91	0.79	0.64	1.12	1.29	1.09	0.70	0.56	0.95	0.54	0.73	1.89
	10	06x06	0.79	0.66	0.28	0.28	0.29	0.31	0.32	0.46	0.57	0.21	0.23	0.20	0.22	0.24	0.21
		10x10	0.67	0.65	0.44	0.44	0.33	0.33	0.31	0.52	0.95	0.30	0.30	0.29	0.31	0.32	0.64
		14x14	0.59	0.78	0.43	0.40	0.33	0.26	0.42	0.82	0.69	0.39	0.33	0.22	0.33	0.50	1.02
		20x20	0.46	1.07	0.71	0.71	0.65	0.55	0.58	0.79	1.18	0.47	0.51	0.58	0.49	0.58	0.90
		25x25	0.51	1.51	0.93	0.88	0.71	0.58	0.89	1.24	1.15	0.65	0.62	0.57	0.54	1.03	1.78
	12	06x06	0.81	0.51	0.23	0.28	0.32	0.32	0.34	0.47	0.49	0.24	0.16	0.22	0.23	0.22	0.30
		10x10	0.59	0.79	0.38	0.38	0.29	0.28	0.32	0.46	0.72	0.40	0.27	0.24	0.27	0.32	0.61
		14x14	0.61	0.88	0.59	0.40	0.26	0.25	0.36	1.12	0.64	0.34	0.38	0.40	0.37	0.43	1.05
		20x20	0.26	1.15	0.81	0.77	0.57	0.61	0.77	0.97	1.10	0.71	0.51	0.50	0.51	0.65	0.89
		25x25	0.57	1.29	0.78	0.69	0.60	0.62	0.77	1.35	1.13	0.91	0.69	0.59	0.61	0.94	1.58
	15	06x06	0.76	0.77	0.39	0.30	0.32	0.34	0.39	0.52	0.68	0.44	0.39	0.18	0.19	0.23	0.36
		10x10	0.69	1.15	0.49	0.50	0.32	0.35	0.33	0.54	0.92	0.32	0.40	0.25	0.21	0.36	0.96
		14x14	0.65	0.70	0.43	0.37	0.41	0.34	0.42	0.65	0.67	0.36	0.40	0.43	0.34	0.46	0.71
		20x20	0.32	1.12	0.78	0.65	0.58	0.59	0.68	1.13	0.95	0.55	0.52	0.59	0.69	0.79	1.45
		25x25	0.92	1.59	1.03	0.87	0.78	0.67	1.01	1.31	1.34	0.81	0.70	0.91	0.71	1.12	1.78
110cm SSD	6	06x06	0.58	0.50	0.43	0.35	0.25	0.23	0.28	0.43	0.53	0.42	0.31	0.23	0.14	0.23	0.97
		10x10	0.63	0.69	0.58	0.49	0.44	0.37	0.24	0.72	0.60	0.40	0.32	0.25	0.21	0.34	1.06
		14x14	0.56	0.87	0.59	0.50	0.38	0.34	0.51	1.12	0.83	0.59	0.62	0.47	0.36	0.55	1.30
		20x20	0.63	1.41	1.04	0.70	0.58	0.59	0.79	0.92	0.98	1.15	0.79	0.46	0.55	0.74	1.14
		25x25	0.68	1.04	0.68	0.52	0.57	0.55	0.92	1.64	1.29	0.79	0.70	0.60	0.64	0.93	1.72
	8	06x06	0.31	0.50	0.37	0.31	0.18	0.18	0.28	0.39	0.50	0.40	0.30	0.15	0.14	0.24	0.83
		10x10	0.38	0.68	0.50	0.45	0.40	0.37	0.36	0.78	0.76	0.38	0.34	0.41	0.38	0.46	0.95
		14x14	0.28	0.89	0.57	0.51	0.38	0.39	0.60	1.45	1.11	0.58	0.46	0.35	0.48	0.66	1.35
		20x20	0.38	1.09	0.90	0.76	0.60	0.67	0.68	1.22	1.15	1.02	0.75	0.69	0.71	0.99	1.51
		25x25	0.40	1.35	0.74	0.78	0.62	1.05	1.03	2.71	1.22	0.76	0.81	0.69	0.68	0.86	2.09
	10	06x06	0.48	0.46	0.40	0.37	0.16	0.12	0.17	0.36	0.62	0.45	0.36	0.25	0.16	0.15	0.56
		10x10	0.47	0.61	0.43	0.35	0.24	0.26	0.33	0.53	0.59	0.38	0.29	0.20	0.20	0.34	0.72
		14x14	0.42	0.79	0.46	0.44	0.33	0.43	0.43	0.97	0.79	0.47	0.41	0.31	0.38	0.51	1.36
		20x20	0.42	1.06	0.73	0.65	0.60	0.47	0.76	1.18	1.07	0.63	0.58	0.50	0.53	0.90	1.55
		25x25	0.45	1.41	0.72	0.63	0.56	0.56	0.90	1.59	1.25	0.77	0.68	0.64	0.64	0.82	1.58
	12	06x06	0.35	0.50	0.40	0.38	0.17	0.12	0.21	0.83	0.57	0.41	0.33	0.16	0.12	0.21	0.68
		10x10	0.30	0.72	0.50	0.43	0.31	0.22	0.54	0.91	0.74	0.37	0.48	0.26	0.26	0.37	0.66
		14x14	0.35	0.88	0.65	0.47	0.39	0.37	0.44	1.40	0.86	0.57	0.51	0.41	0.36	0.55	1.46
		20x20	0.33	1.10	0.80	0.65	0.61	0.57	0.79	1.96	1.04	0.79	0.61	0.55	0.62	1.11	1.85
		25x25	0.65	1.40	0.70	0.64	0.75	0.60	0.84	1.70	1.30	0.73	0.64	0.66	0.71	1.34	1.54
	15	06x06	0.51	0.71	0.44	0.38	0.21	0.18	0.31	1.38	0.73	0.60	0.52	0.35	0.32	0.55	2.03
		10x10	0.34	0.78	0.49	0.36	0.28	0.34	0.42	0.95	0.68	0.41	0.35	0.26	0.38	0.54	1.42
		14x14	0.84	0.89	0.56	0.52	0.38	0.34	0.41	1.01	0.85	0.50	0.52	0.45	0.43	0.58	1.34
		20x20	0.69	1.07	0.71	0.69	0.62	0.67	0.81	1.66	1.10	0.71	0.71	0.71	0.70	1.01	1.92
		25x25	0.88	1.96	0.94	0.75	0.63	0.69	1.05	1.58	1.50	0.80	0.75	0.69	0.78	1.01	1.77
Summary			0.47	1.03	0.66	0.58	0.48	0.48	0.60	1.10	0.91	0.58	0.50	0.46	0.45	0.65	1.25

Table B-2 RMS error index for gamma 1%/1mm – In-House Agility model

In-House Monte Carlo Agility Electron Model Standard Applicator Cutout Gamma 1%/1mm Result Summary																	
				Inplane Profiles							Crossplane Profiles						
	Energy (MeV)	Applicator	PDD	Surf	Norm	R100	R90	R80	R50	R20	Surf	Norm	R100	R90	R80	R50	R20
100cm SSD	6	06x06	0.39	0.75	0.50	0.40	0.35	0.33	0.39	0.41	0.58	0.35	0.27	0.26	0.23	0.25	0.25
		10x10	0.20	0.86	0.68	0.62	0.53	0.49	0.47	0.67	0.74	0.41	0.29	0.25	0.26	0.33	0.59
		14x14	0.14	0.72	0.50	0.47	0.37	0.48	0.36	0.66	0.75	0.50	0.36	0.37	0.38	0.42	0.57
		20x20	0.31	1.23	0.98	0.82	0.63	0.85	0.55	0.84	0.84	0.53	0.42	0.41	0.58	0.64	0.73
	8	06x06	0.69	0.77	0.36	0.32	0.31	0.30	0.44	0.54	0.63	0.28	0.22	0.24	0.23	0.28	0.47
		10x10	0.43	0.93	0.63	0.51	0.44	0.42	0.40	0.65	0.71	0.33	0.35	0.25	0.28	0.38	0.51
		14x14	0.25	0.91	0.53	0.39	0.40	0.39	0.42	0.63	0.90	0.38	0.31	0.40	0.36	0.44	0.61
		20x20	0.41	1.28	0.83	0.80	0.55	0.58	0.65	1.44	1.00	0.53	0.47	0.48	0.45	0.64	1.08
	10	06x06	0.85	0.75	0.24	0.26	0.24	0.30	0.27	0.50	0.83	0.25	0.23	0.18	0.21	0.29	0.29
		10x10	0.73	0.71	0.35	0.36	0.35	0.34	0.33	0.63	1.15	0.30	0.27	0.24	0.33	0.28	0.77
		14x14	0.51	1.49	0.99	0.93	0.79	0.72	0.73	0.95	1.19	0.88	0.78	0.58	0.69	0.88	0.81
		20x20	0.44	1.60	1.20	1.26	0.78	0.85	0.80	0.97	1.28	1.04	1.09	0.54	0.73	0.53	0.84
	12	06x06	0.82	0.84	0.29	0.30	0.31	0.33	0.38	0.61	0.76	0.31	0.20	0.23	0.26	0.26	0.38
		10x10	0.58	0.78	0.57	0.49	0.40	0.38	0.45	0.68	0.79	0.31	0.31	0.35	0.30	0.41	0.47
		14x14	1.02	1.32	0.69	0.41	0.41	0.39	0.50	0.85	0.78	0.40	0.33	0.46	0.28	0.53	0.61
		20x20	0.38	1.29	0.89	0.79	0.55	0.47	0.73	0.71	1.03	0.62	0.53	0.38	0.43	0.66	0.86
	15	06x06	0.83	0.65	0.35	0.30	0.39	0.37	0.45	0.80	0.67	0.30	0.24	0.24	0.24	0.26	0.38
		10x10	0.58	1.06	0.62	0.52	0.45	0.42	0.42	0.70	1.11	0.42	0.45	0.36	0.52	0.54	0.53
		14x14	0.63	0.81	0.43	0.42	0.35	0.32	0.47	0.72	0.92	0.46	0.36	0.33	0.32	0.39	0.57
		20x20	0.54	1.25	0.82	0.74	0.52	0.63	0.71	0.79	1.12	0.60	0.53	0.47	0.51	0.56	1.03
110cm SSD	6	06x06	0.57	0.67	0.53	0.47	0.40	0.37	0.40	0.45	0.65	0.53	0.49	0.44	0.40	0.41	0.39
		10x10	0.68	0.79	0.53	0.49	0.43	0.47	0.49	0.62	0.71	0.47	0.43	0.37	0.36	0.42	0.47
		14x14	0.70	1.03	0.76	0.62	0.62	0.45	0.42	0.67	0.95	0.70	0.54	0.47	0.50	0.45	0.60
		20x20	0.63	1.06	0.73	0.62	0.52	0.52	0.65	0.98	0.95	0.57	0.61	0.43	0.58	0.88	1.83
	8	06x06	0.82	0.61	0.40	0.34	0.30	0.31	0.31	0.53	0.64	0.49	0.43	0.38	0.34	0.38	0.37
		10x10	0.98	0.75	0.41	0.38	0.38	0.56	0.41	0.55	0.70	0.38	0.32	0.34	0.33	0.41	0.43
		14x14	0.97	1.26	0.60	0.57	0.42	0.48	0.45	0.67	1.06	0.48	0.49	0.35	0.45	0.47	0.55
		20x20	0.68	1.30	0.60	0.67	0.53	0.52	0.73	0.83	0.83	0.43	0.50	0.55	0.46	0.62	1.30
	10	06x06	1.19	0.55	0.35	0.31	0.30	0.29	0.33	0.40	0.70	0.43	0.37	0.30	0.29	0.30	0.29
		10x10	1.41	0.77	0.48	0.41	0.38	0.42	0.44	0.52	0.72	0.47	0.34	0.32	0.33	0.34	0.54
		14x14	1.05	1.01	0.81	0.75	0.87	1.05	0.74	0.58	0.91	0.79	0.57	0.43	0.70	0.69	0.80
		20x20	0.81	1.48	0.95	0.73	1.20	0.81	1.07	1.07	1.28	0.84	0.95	0.74	0.93	0.83	0.92
	12	06x06	1.32	0.51	0.32	0.25	0.28	0.29	0.30	0.61	0.58	0.45	0.36	0.29	0.27	0.29	0.37
		10x10	1.34	0.86	0.51	0.37	0.37	0.37	0.37	0.66	0.69	0.37	0.30	0.40	0.32	0.38	0.52
		14x14	1.13	0.85	0.59	0.60	0.45	0.47	0.71	0.72	0.75	0.48	0.35	0.34	0.35	0.47	0.77
		20x20	0.79	1.22	0.79	0.79	0.59	0.44	0.75	0.97	1.29	0.69	0.51	0.52	0.41	0.57	1.16
	15	06x06	1.52	0.48	0.30	0.28	0.34	0.28	0.32	0.61	0.63	0.46	0.40	0.37	0.30	0.25	0.53
		10x10	1.73	0.71	0.44	0.47	0.46	0.41	0.43	0.67	0.80	0.42	0.42	0.35	0.34	0.44	0.54
		14x14	1.31	0.91	0.46	0.37	0.40	0.42	0.45	0.91	1.03	0.47	0.43	0.38	0.48	0.60	1.28
		20x20	0.76	1.19	0.73	0.59	0.59	0.59	0.61	1.24	1.94	0.65	0.87	0.62	0.49	0.68	0.91
Summary			0.74	0.99	0.63	0.57	0.51	0.50	0.54	0.76	0.93	0.52	0.48	0.40	0.43	0.50	0.75

Table B-3 RMS error index for gamma 1%/1mm – Elekta TPS Synergy model

	Elekta Synergy Electron Model Standard Applicator Cutout Gamma 1%/1mm Result Summary																
				Inplane Profiles							Crossplane Profiles						
	Energy (MeV)	Applicator	PDD	Surf	Norm	R100	R90	R80	R50	R20	Surf	Norm	R100	R90	R80	R50	R20
100cm SSD	6	06x06	0.83	0.65	0.44	0.30	0.29	0.36	0.44	1.08	0.88	0.51	0.35	0.29	0.34	0.42	0.90
		10x10	0.73	1.49	1.22	1.02	0.76	0.54	0.41	0.87	1.36	1.06	1.04	0.74	0.43	0.46	0.69
		14x14	0.73	1.39	0.93	0.79	0.57	0.61	0.67	0.89	1.52	1.02	0.80	0.75	0.57	0.59	0.77
		20x20	0.69	1.04	0.76	0.53	0.51	0.56	1.09	1.21	1.50	0.84	0.55	0.43	0.65	0.60	1.83
		25x25	0.73	0.81	0.88	0.78	1.29	1.47	1.40	2.81	1.09	0.61	0.51	0.70	0.89	1.07	3.02
	8	06x06	0.97	0.67	0.28	0.34	0.38	0.44	0.57	1.39	0.86	0.32	0.31	0.34	0.42	0.50	0.95
		10x10	0.42	1.47	0.67	0.82	0.41	0.54	0.52	0.98	1.52	0.71	0.68	0.45	0.51	0.51	1.07
		14x14	0.39	1.62	1.13	0.91	0.65	0.69	0.72	1.10	1.85	1.18	0.97	0.63	0.64	0.62	0.82
		20x20	0.60	1.84	1.07	0.72	0.47	0.79	0.86	1.09	2.05	1.27	0.90	0.51	0.43	0.62	0.79
		25x25	0.63	0.83	0.63	0.69	0.91	0.76	0.85	1.18	1.43	0.85	0.67	1.13	0.65	0.74	1.24
	10	06x06	0.55	0.64	0.35	0.41	0.41	0.42	0.51	1.16	0.85	0.34	0.36	0.37	0.39	0.53	0.85
		10x10	0.65	1.02	0.31	0.27	0.33	0.45	0.53	0.73	1.21	0.65	0.48	0.46	0.44	0.45	0.80
		14x14	0.60	1.11	0.95	0.65	0.54	0.59	0.60	0.87	1.34	0.82	0.75	0.59	0.59	0.57	0.92
		20x20	0.65	0.73	0.51	0.55	0.68	0.56	0.63	1.23	0.98	0.56	0.59	0.63	0.44	0.68	1.24
		25x25	0.44	0.92	1.04	1.02	0.80	0.92	1.37	2.59	1.74	0.70	0.77	0.61	0.60	0.92	2.14
	12	06x06	0.79	0.70	0.39	0.56	0.55	0.55	0.67	1.79	1.03	0.46	0.49	0.46	0.48	0.50	1.34
		10x10	0.81	0.82	0.37	0.50	0.36	0.50	0.48	1.22	0.85	0.36	0.35	0.35	0.51	0.45	1.16
		14x14	0.68	1.15	0.61	0.60	0.55	0.57	0.65	0.94	1.33	0.59	0.52	0.55	0.52	0.53	0.91
		20x20	0.69	1.22	0.69	0.64	0.59	0.69	1.20	1.54	1.29	0.74	0.53	0.47	0.61	1.04	2.06
		25x25	0.81	1.50	1.30	1.20	0.79	0.71	1.02	1.80	2.04	1.16	1.74	0.72	0.66	0.72	1.21
	15	06x06	0.55	0.82	0.48	0.52	0.88	0.93	1.33	3.10	1.17	0.53	0.51	0.68	0.74	1.09	2.25
		10x10	0.64	0.90	0.55	0.44	0.70	0.75	0.91	1.88	1.13	0.52	0.47	0.57	0.59	0.64	1.26
		14x14	0.84	0.92	1.02	1.03	1.18	1.20	1.56	3.08	0.99	0.62	0.75	0.95	0.89	0.90	1.93
		20x20	0.67	0.82	0.77	1.03	1.45	1.74	1.76	3.67	0.85	0.63	0.77	0.95	1.35	1.39	3.08
		25x25	0.80	0.70	0.83	0.88	1.06	1.06	2.02	2.98	1.09	0.67	0.61	0.82	0.91	1.67	2.47
110cm SSD	6	06x06	0.99	0.54	0.41	0.32	0.30	0.30	0.62	1.12	0.60	0.41	0.35	0.38	0.38	0.50	0.71
		10x10	0.68	0.79	0.62	0.46	0.31	0.35	0.68	0.92	0.89	0.54	0.68	0.35	0.41	0.57	1.00
		14x14	0.71	1.02	0.81	0.60	0.69	0.66	0.78	1.11	1.19	1.14	0.67	0.61	0.60	0.70	1.12
		20x20	0.71	0.82	0.50	0.37	0.87	0.82	0.99	1.40	1.04	0.61	0.48	0.62	0.61	1.23	1.85
		25x25	0.78	0.99	1.08	1.32	1.37	1.46	2.37	2.30	1.06	0.88	0.87	1.02	1.08	1.70	1.76
	8	06x06	1.44	0.50	0.26	0.24	0.38	0.44	0.85	1.31	0.53	0.30	0.27	0.39	0.43	0.74	0.98
		10x10	0.62	0.94	0.45	0.48	0.34	0.39	0.74	1.26	1.21	0.66	0.53	0.39	0.43	0.50	0.81
		14x14	0.56	0.99	0.84	0.61	0.70	0.80	0.70	1.08	1.32	0.75	0.69	0.55	0.61	0.68	0.95
		20x20	0.69	1.11	0.58	0.53	0.54	0.51	0.74	1.23	1.11	0.60	0.49	0.57	0.53	0.52	1.15
		25x25	0.60	1.01	0.91	0.96	1.12	1.23	1.34	2.66	1.23	0.90	0.90	0.93	1.04	1.23	2.76
	10	06x06	1.08	0.47	0.25	0.22	0.34	0.42	0.73	1.17	0.54	0.30	0.30	0.37	0.43	0.66	0.92
		10x10	0.79	0.51	0.37	0.37	0.62	0.42	0.56	0.88	0.63	0.41	0.42	0.42	0.42	0.54	0.79
		14x14	0.72	0.88	0.61	0.83	0.65	0.66	0.70	1.13	1.17	0.94	0.87	0.64	0.64	0.73	1.29
		20x20	0.80	0.58	0.55	0.48	0.62	0.73	1.09	1.08	0.95	0.61	0.56	0.53	0.59	1.03	1.53
		25x25	0.47	1.18	1.10	0.99	1.06	1.16	2.32	1.63	1.46	1.08	1.07	0.87	0.99	1.62	1.77
	12	06x06	1.14	0.47	0.30	0.41	0.42	0.53	0.78	1.37	0.56	0.25	0.27	0.43	0.50	0.66	1.22
		10x10	1.09	0.58	0.43	0.41	0.49	0.55	0.56	0.86	0.66	0.53	0.74	0.55	0.74	0.94	0.97
		14x14	0.91	0.79	0.77	0.50	0.82	0.85	0.95	1.16	1.20	0.87	0.50	0.65	0.67	0.77	1.09
		20x20	0.89	1.19	0.89	0.66	0.64	0.68	0.94	1.58	1.26	0.82	0.59	0.56	0.59	1.07	1.57
		25x25	0.90	1.88	1.17	0.89	0.76	0.81	1.04	1.97	2.08	1.29	1.25	0.93	0.97	1.18	2.54
	15	06x06	0.91	0.46	0.44	0.50	0.77	0.83	1.21	2.62	0.73	0.38	0.37	0.60	0.69	0.85	1.80
		10x10	0.72	0.63	0.50	0.54	0.76	0.78	0.96	2.15	0.84	0.42	0.51	0.62	0.60	0.78	1.61
		14x14	0.67	0.95	1.15	1.27	1.57	1.39	1.60	2.98	0.68	0.76	0.82	1.07	1.15	1.31	1.75
		20x20	0.84	0.94	0.92	1.02	1.32	1.57	1.75	2.82	0.98	0.87	0.84	1.50	1.11	1.89	2.69
		25x25	0.94	0.78	0.95	1.04	1.21	1.68	1.97	2.29	1.00	0.70	0.78	0.97	1.18	1.42	2.76
Summary			0.35	0.99	0.76	0.72	0.79	0.85	1.11	1.79	1.2	0.74	0.70	0.68	0.70	0.92	1.60

Table B-4 RMS error index for gamma 1%/1mm – Elekta TPS Agiltiy model

Elekta Agility Electron Model Standard Applicator Cutout Gamma 1%/1mm Result Summary																		
				Inplane Profiles							Crossplane Profiles							
	Energy (MeV)	Applicator	PDD	Surf	Norm	R100	R90	R80	R50	R20	Surf	Norm	R100	R90	R80	R50	R20
100cm SSD	6	06x06	0.98	0.98	0.70	0.38	0.20	0.22	0.27	0.87	1.04	0.66	0.38	0.30	0.27	0.27	0.76
		10x10	1.02	1.66	1.09	0.91	0.64	0.38	0.51	1.08	1.31	0.91	0.65	0.31	0.23	0.28	0.66
		14x14	0.79	1.61	1.13	0.80	0.47	0.60	0.45	0.93	1.28	0.79	0.53	0.53	0.34	0.44	1.43
		20x20	0.80	1.33	0.89	0.85	0.62	0.77	0.93	0.89	1.23	0.84	0.64	0.66	0.93	1.13	1.56
	8	06x06	0.61	1.16	0.38	0.41	0.28	0.23	0.29	0.87	1.09	0.46	0.42	0.38	0.30	0.32	0.67
		10x10	0.52	1.46	0.80	0.54	0.39	0.46	0.37	0.78	1.26	0.60	0.44	0.28	0.29	0.30	0.70
		14x14	0.59	1.87	1.37	1.28	0.74	0.77	1.13	1.08	1.78	1.06	0.88	0.52	0.67	0.51	0.93
		20x20	1.00	1.34	0.93	1.02	0.66	0.55	0.57	2.03	1.47	0.92	0.94	0.56	0.49	0.73	1.96
	10	06x06	0.76	1.08	0.33	0.37	0.31	0.29	0.27	0.79	1.09	0.46	0.44	0.35	0.33	0.33	0.72
		10x10	0.73	1.43	0.68	0.54	0.38	0.28	0.34	1.03	1.34	0.66	0.49	0.33	0.30	0.34	0.65
		14x14	0.63	1.77	1.30	0.99	0.63	0.62	0.45	1.32	1.27	0.93	0.59	0.51	0.58	0.44	0.85
		20x20	0.68	1.92	1.20	1.20	0.73	0.69	0.68	1.50	1.54	0.96	1.15	0.45	0.49	1.21	1.71
	12	06x06	0.87	1.10	0.28	0.33	0.43	0.38	0.40	1.38	1.14	0.43	0.45	0.46	0.39	0.30	1.03
		10x10	0.77	1.28	0.46	0.44	0.38	0.33	0.40	1.38	1.13	0.50	0.45	0.40	0.38	0.48	0.88
		14x14	0.71	1.02	0.89	0.70	0.48	0.44	0.67	1.09	0.74	0.52	0.67	0.71	0.74	0.67	1.15
		20x20	0.71	1.67	1.38	1.13	0.74	0.50	0.51	2.17	1.39	0.75	0.69	0.51	0.53	1.07	2.77
	15	06x06	0.80	1.09	0.41	0.39	0.63	0.63	0.70	1.91	1.22	0.51	0.54	0.55	0.52	0.47	1.41
		10x10	0.62	1.26	0.76	0.51	0.55	0.57	0.58	1.45	1.26	0.71	0.54	0.61	0.74	0.58	1.00
		14x14	0.89	1.19	0.52	0.67	0.80	0.85	0.92	1.66	1.11	1.24	1.16	1.26	1.41	1.39	1.86
		20x20	0.81	1.46	0.94	0.62	0.90	0.76	1.23	2.43	1.15	0.77	1.05	0.99	0.97	1.86	2.90
110cm SSD	6	06x06	1.07	0.76	0.61	0.50	0.30	0.25	0.31	1.05	0.91	0.65	0.49	0.34	0.27	0.31	0.93
		10x10	0.92	0.85	0.60	0.46	0.39	0.48	0.34	1.02	0.86	0.65	0.60	0.45	0.55	0.56	1.06
		14x14	0.81	1.14	0.72	0.81	0.47	0.51	0.60	1.04	1.00	0.65	0.56	0.51	0.59	0.92	1.41
		20x20	0.87	1.15	0.83	0.85	0.49	0.57	0.77	1.58	0.88	0.73	0.66	0.59	1.17	0.91	1.51
	8	06x06	0.57	0.78	0.42	0.30	0.20	0.26	0.45	1.37	0.78	0.55	0.52	0.36	0.62	0.38	1.08
		10x10	0.58	0.86	0.47	0.43	0.31	0.26	0.42	1.07	0.85	0.48	0.40	0.45	0.48	0.43	0.93
		14x14	0.61	1.09	1.06	0.96	0.66	0.75	0.67	1.53	0.88	0.86	0.82	0.54	0.59	0.69	1.34
		20x20	0.98	0.91	0.77	1.07	0.97	0.63	0.75	1.57	0.95	0.78	0.83	0.75	0.64	0.81	1.49
	10	06x06	0.69	0.64	0.40	0.36	0.34	0.29	0.31	0.97	0.84	0.63	0.58	0.44	0.29	0.28	0.74
		10x10	0.61	0.89	0.56	0.71	0.35	0.32	0.48	1.24	0.85	0.54	0.57	0.34	0.48	0.47	1.15
		14x14	0.75	1.07	1.06	0.75	0.81	1.03	0.68	1.17	1.13	1.05	0.74	0.69	0.67	0.70	1.24
		20x20	0.75	1.11	1.05	0.93	0.72	0.70	0.62	1.85	0.92	1.00	1.00	0.69	0.80	0.89	1.98
	12	06x06	0.79	0.60	0.35	0.42	0.46	0.44	0.57	1.73	0.79	0.56	0.58	0.54	0.45	0.60	1.37
		10x10	0.77	0.71	0.48	0.44	0.50	0.52	0.64	1.51	0.81	0.57	0.64	0.57	0.58	0.58	1.13
		14x14	1.09	0.93	0.60	0.68	0.60	0.56	0.74	1.27	0.81	0.81	0.86	0.97	0.80	0.81	1.75
		20x20	0.81	0.91	1.01	0.83	0.89	0.57	0.71	2.09	0.95	0.80	0.82	0.88	0.79	1.08	2.76
	15	06x06	0.74	0.62	0.46	0.63	0.68	0.74	0.91	2.52	0.85	0.73	0.61	0.71	0.66	0.73	2.00
		10x10	0.87	0.79	0.66	0.58	0.77	0.89	0.83	1.88	0.90	0.74	0.73	0.88	1.23	0.95	1.29
		14x14	0.83	1.14	0.85	0.95	0.99	0.95	1.31	2.16	1.43	1.39	1.51	1.46	1.55	1.67	2.64
		20x20	0.97	1.18	0.63	0.73	1.06	1.05	1.32	3.52	1.30	1.14	1.15	1.56	1.36	1.90	3.10
Summary			0.43	1.19	0.81	0.73	0.61	0.60	0.68	1.57	1.11	0.78	0.74	0.68	0.72	0.83	1.56

Table B-5 RMS error index for gamma 1%/1mm – In-House Synergy and Agility model with noise filter of span 3

In-House Monte Carlo Electron Model With Standard Applicator Cutout Gamma 1%/1mm Result Summary with Noise Filter of Span 3																	
			Inplane Profiles							Crossplane Profiles							
		PDD	Surf	Norm	R100	R90	R80	R50	R20	Surf	Norm	R100	R90	R80	R50	R20
Synergy Summary		0.46	0.76	0.58	0.50	0.38	0.36	0.43	0.84	0.64	0.47	0.41	0.35	0.34	0.51	1.07
Agility Summary		0.80	0.76	0.54	0.47	0.38	0.38	0.40	0.55	0.63	0.41	0.34	0.29	0.30	0.35	0.53

B.2. Shaped Fields

Table B-6 RMS error index for shaped cutout fields with gamma 1%/1mm

	Shaped Cutout Fields Gamma 1%/1mm Result Summary										
			PDDs			R100 Inplane Profiles			R100 Crossplane Profiles		
	Energy (MeV)	Applicator	97cm SSD	100cm SSD	105cm SSD	97cm SSD	100cm SSD	105cm SSD	97cm SSD	100cm SSD	105cm SSD
In-house MC Synergy	6	06x06	0.37	0.71	0.71	0.53	0.36	0.23	0.36	0.34	0.39
		10x10	0.42	0.76	0.76	0.53	0.37	0.38	0.37	0.38	0.44
		14x14	0.43	0.72	0.72	0.64	0.42	0.58	0.27	0.25	0.19
	8	06x06	0.66	0.92	0.92	0.46	0.32	0.27	0.40	0.38	0.41
		10x10	0.45	0.64	0.64	0.48	0.31	0.36	0.40	0.41	0.46
		14x14	0.64	0.84	0.84	0.51	0.55	0.46	0.30	0.24	0.25
	10	06x06	0.83	0.98	0.98	0.46	0.40	0.32	0.50	0.53	0.45
		10x10	0.62	0.70	0.70	0.36	0.34	0.27	0.42	0.63	0.40
		14x14	0.51	0.65	0.65	0.59	0.59	0.50	0.29	0.27	0.35
	12	06x06	0.90	1.07	1.07	0.44	0.47	0.32	0.37	0.29	0.31
		10x10	0.38	0.56	0.56	0.32	0.31	0.25	0.52	0.65	0.48
		14x14	0.53	0.67	0.67	0.52	0.72	0.70	0.33	0.35	0.32
	15	06x06	1.12	1.16	1.16	0.52	0.52	0.50	0.41	0.33	0.42
		10x10	0.72	0.79	0.79	0.41	0.37	0.31	0.33	0.34	0.31
		14x14	0.80	0.87	0.87	0.73	0.45	0.51	0.33	0.36	0.26
In-house MC Agility	6	06x06	0.49	0.77	0.77	0.57	0.36	0.22	0.35	0.36	0.30
		10x10	0.43	0.71	0.71	0.58	0.46	0.50	0.40	0.50	0.61
		14x14	0.45	0.79	0.79	0.60	0.45	0.50	0.23	0.24	0.21
	8	06x06	0.77	0.91	0.91	0.52	0.34	0.28	0.39	0.42	0.44
		10x10	0.66	0.80	0.80	0.46	0.34	0.37	0.46	0.46	0.54
		14x14	0.52	0.60	0.60	0.61	0.67	0.78	0.32	0.20	0.37
	10	06x06	0.72	0.83	0.83	0.51	0.36	0.28	0.41	0.39	0.37
		10x10	0.45	0.62	0.62	0.39	0.29	0.27	0.45	0.40	0.44
		14x14	0.28	0.36	0.36	0.40	0.43	0.44	0.34	0.29	0.20
	12	06x06	0.84	0.99	0.99	0.47	0.50	0.39	0.38	0.27	0.23
		10x10	0.57	0.71	0.71	0.37	0.29	0.32	0.40	0.60	0.44
		14x14	0.77	0.88	0.88	0.43	0.41	0.46	0.29	0.34	0.20
	15	06x06	1.01	1.12	1.12	0.61	0.49	0.61	0.37	0.33	0.34
		10x10	0.34	0.42	0.42	0.41	0.41	0.37	0.33	0.34	0.33
		14x14	0.35	0.35	0.35	0.57	0.46	0.44	0.27	0.25	0.30
Elekta TPS Synergy	6	06x06	0.92	0.97	0.97	0.60	0.56	0.54	0.66	0.61	0.69
		10x10	0.73	0.75	0.75	0.17	0.49	0.30	0.23	0.42	0.49
		14x14	0.63	0.63	0.63	0.41	0.38	0.40	0.41	0.37	0.35
	8	06x06	0.69	0.71	0.71	0.68	0.64	0.68	0.67	0.68	0.75
		10x10	0.55	0.69	0.69	0.40	0.43	0.37	0.44	0.64	0.48
		14x14	0.48	0.59	0.59	0.60	0.49	0.42	0.49	0.39	0.42
	10	06x06	0.63	0.64	0.64	0.56	0.77	0.95	0.58	0.78	1.02
		10x10	0.49	0.49	0.49	0.30	0.24	0.31	0.27	0.32	0.46
		14x14	0.59	0.59	0.59	0.43	0.56	0.53	0.46	0.51	0.54
	12	06x06	0.81	0.85	0.85	0.59	0.73	0.66	0.75	0.70	0.81
		10x10	0.92	0.91	0.91	0.23	0.48	0.60	0.37	0.59	0.70
		14x14	1.02	1.03	1.03	0.55	0.66	0.71	0.55	0.58	0.69
	15	06x06	0.36	0.53	0.53	0.66	1.03	0.81	1.12	0.92	1.22
		10x10	0.89	0.98	0.98	0.57	0.63	0.71	0.84	0.91	1.03
		14x14	0.73	0.79	0.79	1.03	1.03	1.19	0.65	0.76	0.93
Elekta TPS Agility	6	06x06	1.12	1.10	1.10	0.48	0.43	0.38	0.48	0.35	0.39
		10x10	1.10	1.08	1.08	0.39	0.46	0.49	0.69	0.71	1.02
		14x14	1.04	1.02	1.02	0.31	0.50	0.45	0.43	0.39	0.38
	8	06x06	0.54	0.55	0.55	0.61	0.56	0.48	0.48	0.48	0.41
		10x10	0.37	0.38	0.38	0.29	0.35	0.35	0.71	0.63	0.84
		14x14	0.16	0.31	0.31	0.56	0.58	0.46	0.34	0.49	0.46
	10	06x06	0.59	0.59	0.59	0.56	0.55	0.52	0.50	0.45	0.53
		10x10	0.70	0.70	0.70	0.39	0.42	0.37	0.62	0.63	0.72
		14x14	0.79	0.79	0.79	0.39	0.46	0.45	0.50	0.49	0.53
	12	06x06	0.61	0.66	0.66	0.55	0.69	0.50	0.63	0.55	0.68
		10x10	0.78	0.82	0.82	0.40	0.49	0.45	0.73	0.89	0.79
		14x14	0.83	0.85	0.85	0.40	0.50	0.65	0.47	0.53	0.58
	15	06x06	0.59	0.67	0.67	0.55	0.89	0.65	0.93	0.65	1.02
		10x10	1.10	1.14	1.14	0.38	0.43	0.53	0.57	0.73	0.81
		14x14	0.91	0.92	0.92	0.53	0.58	0.73	0.53	0.56	0.73

B.3. Oblique Fields

Table B-7 Oblique RMS error index for gamma 1%/1mm

	Electron Model Oblique Fields Gamma 1%/1mm Result Summary															
			Inplane Profiles							Crossplane Profiles						
	Energy (MeV)	PDD	Surf	Norm	R100	R90	R80	R50	R20	Surf	Norm	R100	R90	R80	R50	R20
MC Synergy	6	0.28	1.09	0.88	0.77	0.90	1.15	0.76	0.94	0.87	0.56	0.53	0.53	0.69	0.92	1.28
	8	0.60	1.08	0.96	0.78	0.54	0.55	0.74	1.87	0.90	0.66	0.60	0.56	0.63	0.75	1.17
	10	0.30	1.10	0.73	0.67	0.52	0.51	0.84	1.22	1.00	0.77	0.82	0.55	0.52	0.76	1.54
	12	0.43	1.22	0.72	0.66	0.77	0.57	0.71	1.25	1.01	0.63	0.68	0.59	0.57	0.82	1.28
	15	0.95	1.40	1.08	0.66	0.58	0.64	0.71	1.34	1.05	0.75	0.66	0.74	0.69	1.08	1.80
MC Agility	6	0.47	0.99	0.85	0.61	0.57	0.51	1.67	1.00	1.14	0.89	0.89	0.77	0.74	0.98	1.32
	8	0.32	1.03	0.79	0.63	0.54	0.55	0.78	1.42	1.18	1.48	0.95	0.91	0.97	1.24	1.48
	10	0.25	1.00	0.69	0.81	0.45	0.77	1.24	1.20	1.37	1.15	0.98	1.01	0.92	1.03	1.20
	12	0.48	1.12	0.68	0.52	0.62	0.53	0.83	1.16	1.09	0.93	0.80	0.85	0.74	1.00	1.30
	15	0.74	1.30	0.87	0.60	0.57	0.57	2.86	1.02	1.34	0.94	0.79	0.85	0.79	1.12	1.35
TPS Synergy	6	0.61	1.11	0.78	0.65	0.69	0.62	0.66	1.90	1.39	0.83	0.75	0.55	0.75	0.81	2.98
	8	0.55	1.93	0.86	0.77	0.76	0.58	0.71	1.56	1.83	0.89	0.80	0.58	0.65	0.86	1.52
	10	0.66	1.02	0.51	0.50	0.49	0.57	0.86	2.07	1.23	0.77	0.81	0.78	0.92	1.31	2.42
	12	1.00	1.25	0.57	0.57	0.47	0.45	0.90	2.46	1.46	0.74	0.70	0.76	0.96	1.22	2.37
	15	0.42	0.73	0.94	1.28	1.66	1.64	2.12	3.92	1.65	1.50	1.42	1.46	1.57	2.37	3.70
TPS Agility	6	1.06	1.46	0.92	0.75	0.62	0.48	0.51	1.98	1.40	0.92	0.63	0.75	0.88	1.21	2.33
	8	0.59	1.65	1.32	1.03	0.75	0.64	0.79	1.50	1.68	1.69	0.88	0.75	0.85	1.21	1.79
	10	0.72	2.39	1.20	1.02	0.72	0.80	0.65	1.27	1.88	0.96	0.83	0.68	0.63	1.10	2.17
	12	0.82	1.97	1.31	1.16	0.71	0.56	0.65	2.65	1.60	0.94	0.75	0.73	0.69	1.47	2.53
	15	0.80	1.53	0.64	0.63	0.75	0.97	1.86	3.72	1.53	1.41	1.28	1.25	1.51	2.08	3.45

B.4. Stepped Fields

Table B-8 Stepped surface RMS error index for gamma 2%/2mm

			Electron Model Stepped Fields Gamma 2%/2mm Result Summary								
				Crossplane Profiles							
			Energy (MeV)	Surf	Norm	R100	R90	R80	R50	R20	RMS
Synergy	5 mm step	In-house MC	6	0.65	0.36	0.27	0.61	0.66	1.10	0.46	0.64
			8	0.69	0.40	0.30	0.35	0.19	0.55	0.59	0.47
			10	0.59	0.33	0.28	0.29	0.23	0.37	0.35	0.37
			12	0.81	0.30	0.24	0.33	0.26	0.31	0.51	0.44
			15	0.67	0.29	0.31	0.37	0.42	0.76	0.85	0.57
		Elekta TPS	6	1.17	0.58	0.43	1.86	2.22	2.92	2.00	1.80
			8	0.85	0.52	0.46	1.09	1.61	2.63	2.55	1.62
			10	0.78	0.53	0.43	0.90	1.25	2.00	2.10	1.30
			12	0.56	0.43	0.41	0.54	0.84	1.26	1.89	0.99
			15	0.36	0.39	0.55	0.93	1.18	1.95	2.33	1.31
	10 mm step	In-house MC	6	0.69	0.65	0.40	0.43	0.34	0.25	0.42	0.48
			8	0.58	0.63	0.79	0.62	0.30	0.27	0.41	0.54
			10	0.59	0.48	0.55	0.53	0.48	0.37	0.30	0.48
			12	0.71	0.37	0.35	0.83	0.61	0.47	0.36	0.56
			15	0.59	0.35	0.41	0.35	0.35	0.71	0.53	0.49
		Elekta TPS	6	1.02	0.63	0.44	0.59	0.47	0.28	0.41	0.59
			8	0.88	0.52	0.44	0.44	0.50	0.62	0.53	0.58
			10	0.83	0.59	0.52	0.45	0.41	0.49	0.81	0.61
			12	0.66	0.53	0.65	0.72	0.61	0.75	0.92	0.70
			15	0.44	0.41	0.63	0.73	0.79	0.91	1.29	0.79
	20 mm step	In-house MC	6	0.54	0.59	0.39	0.15	0.14	0.16	0.24	0.36
			8	0.46	0.36	0.45	0.26	0.28	0.20	0.28	0.34
			10	0.39	0.25	0.44	0.23	0.29	0.18	0.32	0.31
			12	0.53	0.31	0.38	0.27	0.34	0.25	0.38	0.36
			15	0.35	0.38	0.66	0.60	0.76	0.37	0.79	0.58
		Elekta TPS	6	0.87	0.62	0.52	0.29	0.33	0.27	0.52	0.53
			8	0.58	1.06	0.96	0.39	0.43	0.36	0.63	0.68
			10	1.08	0.57	0.94	0.45	0.50	0.44	0.84	0.73
			12	0.92	0.52	0.52	0.47	0.53	0.47	1.07	0.68
			15	0.68	0.45	0.71	1.04	0.94	0.73	1.37	0.89
Agility	5 mm step	In-house MC	6	0.60	0.92	0.73	0.27	0.45	0.76	0.75	0.67
			8	0.73	0.52	0.30	1.09	1.60	2.24	1.73	1.34
			10	0.59	0.35	0.40	0.41	0.67	1.44	1.93	1.00
			12	0.51	0.28	0.34	0.48	0.82	1.38	1.87	0.98
			15	0.82	0.36	0.31	0.42	0.56	1.17	2.34	1.08
		Elekta TPS	6	1.72	1.75	1.11	0.82	1.34	2.18	3.13	1.86
			8	1.32	0.99	0.42	2.13	2.98	4.05	3.71	2.58
			10	0.88	0.93	0.57	0.96	1.60	2.40	2.90	1.67
			12	0.91	0.76	0.62	0.84	1.41	2.26	3.15	1.67
			15	1.02	0.88	0.80	0.85	1.29	2.11	3.45	1.74
	10 mm step	In-house MC	6	0.65	1.38	1.54	0.55	0.41	0.34	0.64	0.90
			8	0.54	0.62	0.40	0.60	0.83	0.64	0.52	0.60
			10	0.53	0.48	0.63	0.36	0.31	0.54	0.54	0.49
			12	0.53	0.37	0.46	0.36	0.35	0.43	0.69	0.47
			15	0.79	0.38	0.34	0.48	0.41	0.49	1.18	0.65
		Elekta TPS	6	2.59	3.51	3.54	2.22	1.44	0.21	1.00	2.38
			8	1.16	1.29	1.07	0.46	0.34	0.30	0.73	0.86
			10	0.69	1.09	1.56	1.53	1.43	0.89	0.83	1.19
			12	0.70	0.82	1.12	1.37	1.38	1.02	1.08	1.09
			15	0.96	0.98	0.90	1.02	1.10	1.11	1.79	1.16
	20 mm step	In-house MC	6	0.65	0.29	0.24	0.19	0.22	0.23	0.47	0.36
			8	0.71	1.39	1.47	0.29	0.23	0.26	0.54	0.85
			10	0.52	0.40	0.34	0.42	0.30	0.21	0.40	0.38
			12	0.55	0.44	0.23	0.53	0.40	0.24	0.43	0.42
			15	0.52	0.34	0.30	0.27	0.47	0.33	0.42	0.39
		Elekta TPS	6	3.77	1.74	0.54	0.26	0.20	0.21	0.79	1.62
			8	1.24	0.38	0.54	0.28	0.22	0.25	0.39	0.58
			10	1.14	1.74	1.51	0.60	0.28	0.22	0.85	1.06
			12	0.85	1.18	1.34	0.58	0.32	0.22	1.04	0.89
			15	1.13	1.13	1.07	1.05	0.81	0.41	1.86	1.14

B.5. Inhomogeneities

Table B-9 Half field inhomogeneity RMS error index for gamma 2%/2 mm

			Electron Model Inhomogeneities Half Field Gamma 2%/2mm Result Summary								
				Crossplane Profiles							
			Energy (MeV)	1 mm Below	2 mm Below	4mm below	Dmax	R90	R80	R50	R20	RMS
Synergy	Lung	In-house MC	6	0.69	0.96					2.03	3.07	1.93
			8	0.28	0.25	0.21		0.26	0.65	1.53	3.78	1.57
			10	0.32	0.35	0.35		0.21	0.56	1.41	3.88	1.59
			12	0.31	0.32	0.31	0.23	0.20	0.28	1.02	1.68	0.74
			15	0.29	0.29	0.27	0.24	0.26	0.33	0.40	0.66	0.37
		Elekta TPS	6	1.05	1.16					3.18	12.39	6.44
			8	0.52	0.42	0.45		0.39	0.47	0.86	4.97	1.95
			10	0.57	0.40	0.42		0.38	0.36	1.00	6.11	2.37
			12	0.51	0.34	0.40	0.39	0.30	0.31	0.90	6.32	2.28
			15	0.65	0.52	0.52	0.52	0.41	0.43	0.43	3.24	1.24
	Cortical Bone	In-house MC	6	0.49	0.42					0.54	0.36	0.46
			8	0.68	0.78	0.73		0.61	0.61	0.48	0.54	0.64
			10	0.32	0.41	0.52		0.69	0.84	0.90	0.58	0.64
			12	0.27	0.26	0.30	0.39	0.66	0.75	0.74	0.60	0.53
			15	0.35	0.40	0.39	0.32	0.39	0.41	0.40	0.49	0.40
		Elekta TPS	6	1.90	1.74					1.72	0.55	1.58
			8	1.97	1.52	2.20		2.06	2.14	1.64	0.91	1.83
			10	1.49	0.95	1.37		1.95	2.19	2.20	1.10	1.67
			12	1.24	0.62	0.71	0.85	1.82	2.21	2.37	1.28	1.52
			15	0.99	0.42	0.40	0.46	0.96	1.18	1.72	1.01	0.99
Agility	Lung	In-house MC	6	0.57	0.55					0.50	2.60	1.38
			8	0.44	0.45	0.48		0.60	0.91	2.85	4.19	1.98
			10	0.34	0.40	0.35		0.45	0.38	0.58	2.51	1.03
			12	0.39	0.45	0.35	0.41	0.39	0.46	0.42	1.63	0.69
			15	0.41	0.44	0.39	0.41	0.41	0.56	0.56	0.83	0.52
		Elekta TPS	6	1.37	1.11					2.31	7.96	4.24
			8	0.45	0.46	0.69		0.87	1.53	3.40	4.18	2.17
			10	0.68	0.54	0.46		0.49	0.53	0.62	3.69	1.49
			12	0.61	0.52	0.42	0.44	0.38	0.57	0.42	2.63	1.04
			15	0.66	0.65	0.62	0.62	0.55	0.66	0.67	3.32	1.32
	Cortical Bone	In-house MC	6	1.97	1.67					1.25	0.51	1.46
			8	0.50	0.51	0.49		0.38	0.30	0.39	0.63	0.47
			10	0.62	0.71	0.88		1.34	1.27	0.92	0.43	0.94
			12	0.44	0.39	0.40	0.48	0.97	1.03	0.94	0.41	0.69
			15	0.42	0.39	0.37	0.37	0.87	0.98	0.88	0.46	0.64
		Elekta TPS	6	3.24	3.19					1.87	0.48	2.47
			8	1.93	1.98	2.03		2.02	1.97	1.30	0.95	1.79
			10	1.59	1.32	1.60		2.29	2.42	2.45	1.11	1.90
			12	0.97	0.57	0.75	0.90	1.65	1.94	2.17	1.05	1.37
			15	1.14	0.76	0.78	0.81	1.19	1.43	1.92	0.98	1.19

Appendix C - Shaped Insert Output Errors

Table C-1 Agility measured output factors for various shaped fields

		Agility Measured Output Factors																											
		6 MeV						8 MeV						10 MeV						12 MeV						15 MeV					
SSD (cm)		97	98	99	100	102.5	105	97	98	99	100	102.5	105	97	98	99	100	102.5	105	97	98	99	100	102.5	105	97	98	99	100	102.5	105
6x6	4 C	0.960	0.928	0.894	0.860	0.780	0.713	0.978	0.944	0.914	0.880	0.808	0.747	0.986	0.953	0.923	0.891	0.823	0.766	1.020	0.988	0.955	0.923	0.853	0.798	1.049	1.015	0.982	0.948	0.875	0.820
	5 C	0.971	0.943	0.914	0.883	0.813	0.748	1.000	0.971	0.946	0.914	0.847	0.785	1.009	0.981	0.955	0.925	0.862	0.803	1.038	1.010	0.983	0.955	0.890	0.830	1.057	1.026	0.998	0.970	0.905	0.845
	6 C	0.972	0.941	0.911	0.883	0.818	0.758	1.007	0.976	0.948	0.918	0.857	0.798	1.023	0.993	0.966	0.938	0.878	0.822	1.052	1.021	0.994	0.967	0.905	0.850	1.069	1.035	1.006	0.978	0.916	0.860
10x10	6 C	1.065	1.038	1.009	0.980	0.914	0.856	1.062	1.034	1.004	0.976	0.913	0.857	1.057	1.028	1.002	0.973	0.914	0.861	1.051	1.024	0.999	0.970	0.914	0.862	1.058	1.030	1.003	0.975	0.917	0.865
	7 C	1.067	1.040	1.014	0.988	0.923	0.864	1.066	1.039	1.013	0.987	0.925	0.866	1.062	1.037	1.012	0.986	0.925	0.869	1.060	1.032	1.009	0.983	0.925	0.870	1.062	1.035	1.009	0.984	0.925	0.871
	8 C	1.067	1.041	1.016	0.992	0.932	0.874	1.066	1.042	1.017	0.993	0.934	0.878	1.067	1.041	1.017	0.994	0.937	0.883	1.065	1.040	1.017	0.992	0.937	0.883	1.066	1.041	1.017	0.993	0.935	0.882
	9 C	1.070	1.044	1.020	0.996	0.939	0.883	1.070	1.046	1.022	0.999	0.941	0.889	1.070	1.046	1.023	1.000	0.945	0.892	1.070	1.045	1.023	0.999	0.946	0.892	1.070	1.046	1.022	0.998	0.943	0.891
14x14	10 C	1.098	1.076	1.054	1.031	0.976	0.922	1.069	1.045	1.025	1.003	0.950	0.897	1.049	1.028	1.006	0.985	0.933	0.883	1.062	1.040	1.019	0.998	0.945	0.895	1.054	1.033	1.010	0.989	0.936	0.886
	11 C	1.096	1.075	1.053	1.030	0.978	0.924	1.066	1.045	1.024	1.002	0.951	0.898	1.044	1.025	1.006	0.985	0.934	0.885	1.058	1.039	1.016	0.997	0.946	0.895	1.050	1.030	1.009	0.987	0.936	0.886
	12 C	1.097	1.076	1.054	1.032	0.979	0.929	1.064	1.043	1.022	1.001	0.951	0.902	1.044	1.025	1.005	0.985	0.936	0.889	1.057	1.037	1.016	0.997	0.947	0.900	1.049	1.029	1.008	0.987	0.936	0.890
	13 C	1.094	1.073	1.052	1.030	0.977	0.930	1.061	1.041	1.021	0.999	0.950	0.902	1.042	1.023	1.002	0.983	0.935	0.888	1.053	1.035	1.014	0.995	0.946	0.900	1.044	1.024	1.004	0.984	0.936	0.888
	14 C	1.094	1.075	1.052	1.032	0.981	0.932	1.060	1.042	1.022	1.002	0.952	0.906	1.041	1.023	1.004	0.985	0.939	0.893	1.053	1.035	1.016	0.996	0.950	0.904	1.044	1.027	1.007	0.987	0.939	0.894
20x20	14 C	1.092	1.071	1.051	1.030	0.979	0.929	1.059	1.041	1.021	0.999	0.950	0.902	1.038	1.020	1.001	0.981	0.933	0.886	1.056	1.038	1.018	0.998	0.949	0.902	1.060	1.041	1.021	1.001	0.951	0.903
	14 Sq	1.091	1.071	1.050	1.030	0.979	0.931	1.058	1.039	1.019	0.999	0.951	0.904	1.036	1.018	0.998	0.980	0.933	0.888	1.053	1.035	1.016	0.997	0.950	0.904	1.056	1.037	1.019	0.999	0.951	0.904
	16 Sq	1.090	1.069	1.049	1.028	0.978	0.930	1.056	1.036	1.017	0.997	0.949	0.904	1.035	1.015	0.996	0.978	0.930	0.887	1.052	1.033	1.013	0.994	0.948	0.903	1.052	1.032	1.014	0.996	0.948	0.903
	18 Sq	1.091	1.070	1.049	1.027	0.978	0.931	1.058	1.036	1.017	0.995	0.949	0.903	1.036	1.015	0.995	0.976	0.930	0.887	1.052	1.032	1.012	0.993	0.946	0.903	1.051	1.031	1.011	0.993	0.947	0.902

Table C-2 Agility Elekta TPS output factor Errors for various shaped fields

		Agility Elekta TPS Output Error (%)																											
		6 MeV						8 MeV						10 MeV						12 MeV						15 MeV					
SSD (cm)		97	98	99	100	102.5	105	97	98	99	100	102.5	105	97	98	99	100	102.5	105	97	98	99	100	102.5	105	97	98	99	100	102.5	105
6x6	4 C	-0.9	-0.1	0.5	1.2	2.5	3.6	-2.0	-1.2	-0.6	0.3	1.2	2.5	-0.5	0.1	0.7	1.5	2.6	3.2	-0.1	0.2	1.0	1.8	3.1	3.8	0.6	0.9	1.4	2.6	4.2	5.0
	5 C	-1.3	-0.9	-0.5	0.3	1.1	2.5	-2.0	-1.5	-1.5	-0.9	0.5	1.7	-1.3	-0.8	-0.6	0.4	1.1	2.2	-1.1	-0.4	-0.5	0.1	1.4	2.8	-0.1	0.5	0.9	1.2	2.4	4.3
	6 C	-1.2	-0.5	-0.3	0.4	1.8	2.8	-1.7	-1.4	-1.1	0.0	0.5	1.9	-1.4	-0.8	-0.4	0.3	1.1	2.1	-1.6	-0.9	-0.5	0.1	0.9	2.1	-1.2	-0.5	0.0	0.8	1.2	2.4
10x10	6 C	1.8	2.2	2.3	2.9	3.1	3.4	0.6	1.0	1.3	1.7	2.1	2.7	0.7	0.9	1.2	1.8	1.9	1.7	0.3	0.7	0.8	1.5	1.4	1.6	1.5	1.8	1.9	2.1	2.1	2.6
	7 C	0.8	1.1	1.7	2.1	3.1	3.8	0.4	0.8	1.2	1.2	1.6	2.7	1.1	1.3	1.4	1.7	2.4	3.4	0.7	1.2	1.1	1.5	1.7	2.6	0.7	0.8	0.8	1.1	1.6	2.4
	8 C	0.6	1.0	1.4	1.1	2.1	2.8	0.2	0.6	0.3	0.6	0.9	2.2	-0.5	0.0	0.2	0.5	1.0	1.4	0.2	0.8	0.6	0.9	1.4	2.2	0.1	0.2	0.7	0.9	1.1	2.0
	9 C	0.0	0.6	0.6	0.5	0.7	1.4	-0.5	0.0	0.2	0.3	0.2	1.2	-0.2	0.6	0.5	0.6	0.8	1.2	-0.4	0.2	0.0	0.5	0.7	1.5	0.1	0.4	0.6	1.0	0.9	1.7
14x14	10 C	-0.2	0.0	0.5	0.8	0.1	0.8	0.0	0.5	0.5	0.6	0.6	1.0	-0.4	-0.4	-0.2	-0.2	-0.1	0.4	0.0	0.2	0.2	0.4	0.4	0.9	-0.5	-0.5	-0.5	-0.3	-0.2	0.4
	11 C	0.6	0.7	0.8	0.6	0.2	0.8	0.1	0.1	-0.2	0.1	0.4	0.7	0.4	0.3	0.7	0.6	0.7	0.7	0.5	0.1	0.4	0.6	0.1	1.2	-0.3	-0.3	-0.2	-0.3	-0.1	0.1
	12 C	0.2	0.1	0.0	0.0	1.2	0.2	0.1	-0.1	-0.2	-0.3	-0.5	0.1	0.2	-0.1	-0.1	0.1	-0.5	0.1	-0.1	0.1	0.3	0.3	0.2	0.8	-0.2	-0.1	0.0	-0.1	-0.2	0.2
	13 C	0.0	0.4	0.6	0.8	-0.1	0.1	0.4	0.1	-0.2	0.1	-0.1	0.3	0.3	0.3	0.2	0.4	-0.2	0.6	0.3	-0.1	0.1	-0.3	0.0	0.7	0.1	0.0	0.0	0.3	0.2	0.4
	14 C	-0.3	-0.6	-0.5	-0.7	-0.3	-0.3	0.6	0.3	0.1	0.1	-0.2	-0.1	0.1	-0.2	-0.6	-0.4	-0.5	-0.5	0.2	0.1	0.0	0.0	-0.5	-0.3	0.0	-0.1	0.0	-0.4	-0.6	-0.3
20x20	14 C	0.3	0.3	0.1	0.2	0.2	0.6	-0.4	-0.4	-0.1	0.3	0.0	0.5	0.0	-0.2	-0.2	0.1	-0.1	0.6	-0.3	-0.6	-0.5	-0.1	-0.8	0.0	0.3	0.0	0.0	0.0	-0.3	0.6
	14 Sq	0.6	0.6	0.7	0.6	-0.2	-0.1	-0.8	-0.6	-0.4	-0.1	-0.5	0.1	0.0	-0.3	-0.1	-0.1	0.0	0.7	0.9	0.4	0.5	0.4	0.1	0.6	0.4	0.4	0.4	0.3	0.3	0.9
	16 Sq	-0.1	0.0	-0.4	-0.2	-0.2	-0.2	-0.1	0.2	0.0	-0.1	-0.1	0.3	0.0	0.0	-0.1	-0.5	0.4	0.4	0.2	0.3	0.3	0.1	0.2	0.2	0.8	1.1	0.8	0.4	0.5	0.7
	18 Sq	-0.4	-0.3	-1.0	-0.5	-0.5	-0.4	-0.2	-0.1	-0.1	-0.1	-0.7	-0.5	0.3	0.5	0.3	0.2	0.0	-0.1	0.2	-0.1	0.0	-0.1	0.1	0.1	0.6	0.4	0.3	0.3	-0.2	0.3

Table C-3 Agility In-house BEAMnrc MC output factor Errors for various shaped fields

		Agility In-house MC Output Error (%)																													
		6 MeV						8 MeV						10 MeV						12 MeV						15 MeV					
SSD (cm)		97	98	99	100	102.5	105	97	98	99	100	102.5	105	97	98	99	100	102.5	105	97	98	99	100	102.5	105	97	98	99	100	102.5	105
6x6	4 C	-5.6	-5.5	-5.0	-4.5	-3.2	-2.8	-4.6	-4.0	-4.0	-3.1	-2.0	-1.3	-4.2	-3.9	-3.6	-2.9	-1.9	-1.1	-4.0	-3.8	-3.3	-2.8	-1.5	-1.2	-2.0	-1.9	-1.5	-0.9	0.4	0.8
	5 C	-4.1	-4.1	-4.0	-3.3	-2.4	-1.6	-3.6	-3.5	-3.4	-2.8	-1.9	-1.1	-3.7	-3.5	-3.5	-2.8	-2.1	-1.2	-3.6	-3.5	-3.3	-2.9	-2.2	-1.3	-1.8	-1.6	-1.4	-1.1	-0.7	0.1
	6 C	-3.5	-3.0	-2.6	-2.2	-1.4	-0.7	-2.9	-2.3	-2.0	-1.4	-0.7	0.0	-3.3	-2.8	-2.6	-2.0	-1.3	-0.7	-3.5	-2.9	-2.6	-2.3	-1.6	-1.0	-2.3	-1.6	-1.3	-0.9	-0.3	0.4
10x10	6 C	0.4	0.2	0.4	0.8	1.2	1.4	0.3	0.3	0.7	1.2	1.4	1.5	0.0	0.0	0.2	0.6	0.7	0.9	-0.1	-0.1	0.0	0.5	0.4	1.0	0.3	0.3	0.2	0.6	0.8	1.1
	7 C	0.2	0.3	0.5	0.5	1.1	1.6	0.4	0.5	0.6	0.8	1.3	1.8	0.5	0.4	0.5	0.6	1.2	1.8	0.2	0.4	0.3	0.6	0.7	1.5	0.5	0.6	0.6	0.6	1.2	1.5
	8 C	0.0	0.3	0.3	0.4	0.6	1.3	0.3	0.5	0.5	0.6	1.0	1.4	0.1	0.4	0.4	0.6	0.6	1.2	0.1	0.4	0.2	0.3	0.7	1.0	0.4	0.3	0.4	0.4	0.6	1.2
	9 C	-0.4	-0.2	-0.2	0.1	0.2	0.8	-0.3	-0.1	0.0	0.1	0.4	0.7	-0.1	0.0	-0.1	0.1	0.3	0.7	-0.3	0.0	-0.2	0.0	0.0	0.6	0.1	-0.1	0.1	0.2	0.4	0.7
14x14	10 C	0.7	0.8	0.6	0.5	0.5	0.7	1.2	1.5	1.0	1.2	1.0	1.3	1.4	1.4	1.4	1.4	1.2	1.3	1.4	1.4	1.3	1.1	1.2	1.3	1.1	0.9	1.1	1.0	1.0	1.2
	11 C	0.7	0.6	0.7	0.7	0.5	0.9	1.3	1.2	1.2	1.4	1.2	1.5	1.8	1.5	1.3	1.4	1.4	1.3	1.6	1.4	1.3	1.4	1.2	1.5	1.3	1.1	1.1	1.3	1.0	1.5
	12 C	0.5	0.4	0.5	0.5	0.6	0.3	1.3	1.2	1.2	1.3	1.2	1.2	1.7	1.4	1.4	1.3	1.2	1.2	1.4	1.2	1.3	1.3	1.0	1.1	1.1	1.2	1.0	1.1	1.3	0.8
	13 C	0.8	0.7	0.7	0.5	0.5	0.4	1.5	1.3	1.2	1.4	1.2	1.0	1.6	1.4	1.4	1.6	1.3	1.3	1.5	1.3	1.5	1.4	1.2	1.2	1.3	1.4	1.2	1.3	1.2	1.2
	14 C	0.7	0.3	0.4	0.3	-0.2	-0.2	1.5	1.2	1.1	1.1	0.9	0.7	1.4	1.2	1.2	1.0	0.6	0.7	1.5	1.3	1.0	0.9	0.6	0.7	1.3	0.9	0.9	0.9	0.6	0.7
20x20	14 C	1.8	1.7	1.7	1.6	1.5	1.6	2.3	2.1	2.3	2.4	2.3	2.2	2.4	2.4	2.4	2.5	2.2	2.3	2.2	2.4	2.1	2.2	2.2	2.0	2.0	2.0	2.0	1.9	2.1	2.1
	14 Sq	1.7	1.8	1.5	1.6	1.7	1.8	2.1	2.3	2.3	2.3	2.3	2.3	2.5	2.4	2.2	2.3	2.4	2.4	2.4	2.2	2.2	2.1	2.1	2.2	2.2	2.1	2.0	1.6	2.1	2.1
	16 Sq	1.8	1.7	1.7	1.6	1.6	1.6	2.4	2.4	2.1	2.0	2.3	2.4	2.4	2.5	2.2	2.2	2.5	2.5	2.2	2.0	2.2	2.1	2.2	2.2	2.1	2.2	2.1	1.9	2.0	2.2
	18 Sq	1.6	1.5	1.4	1.5	1.4	1.8	2.2	2.2	2.1	2.3	2.1	2.5	2.2	2.2	2.3	2.4	2.3	2.5	2.1	2.0	2.0	2.0	2.1	2.2	2.1	2.1	2.2	1.8	1.8	1.9

Appendix D - Spectra Distributions

D.1. BEAMnrc determined spectra at exit window

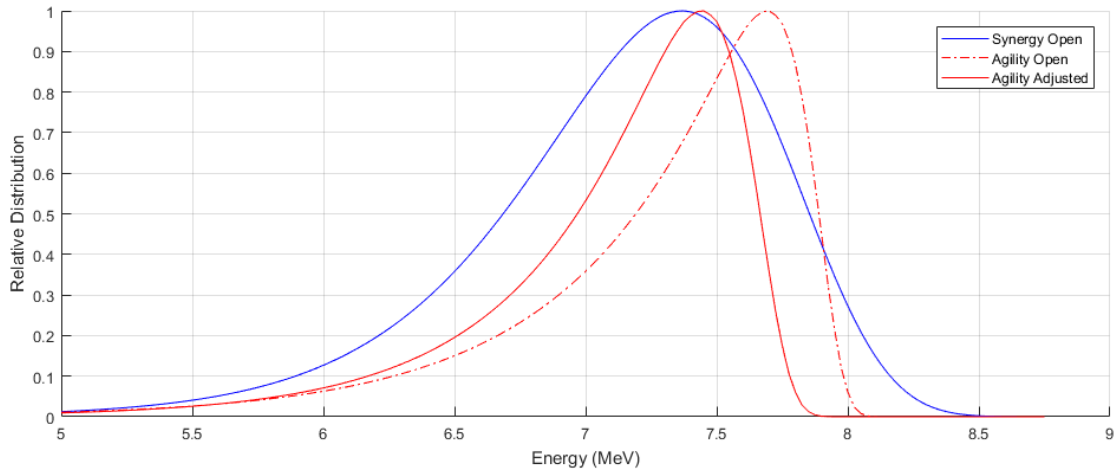

Figure D-1 6 MeV spectra determined by SSS using fields without applicators and if required spectra adjust for fields with applicators

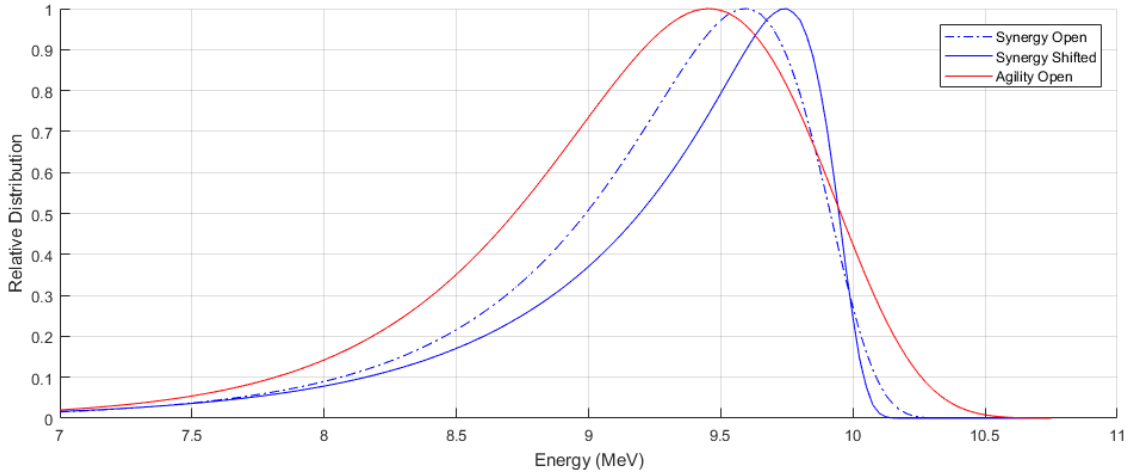

Figure D-2 8 MeV spectra determined by SSS using fields without applicators and if required spectra adjust for fields with applicators

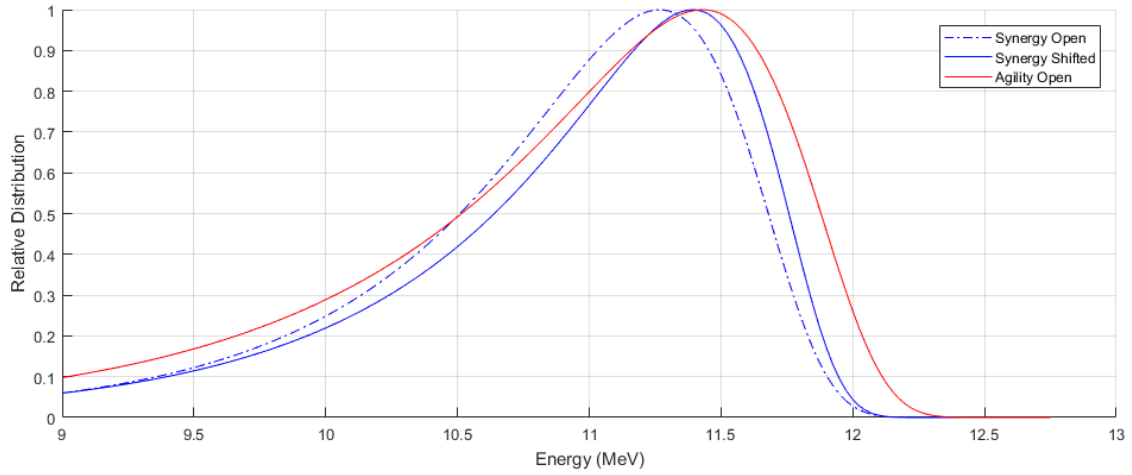

Figure D-3 10 MeV spectra determined by SSS using fields without applicators and if required spectra adjust for fields with applicators

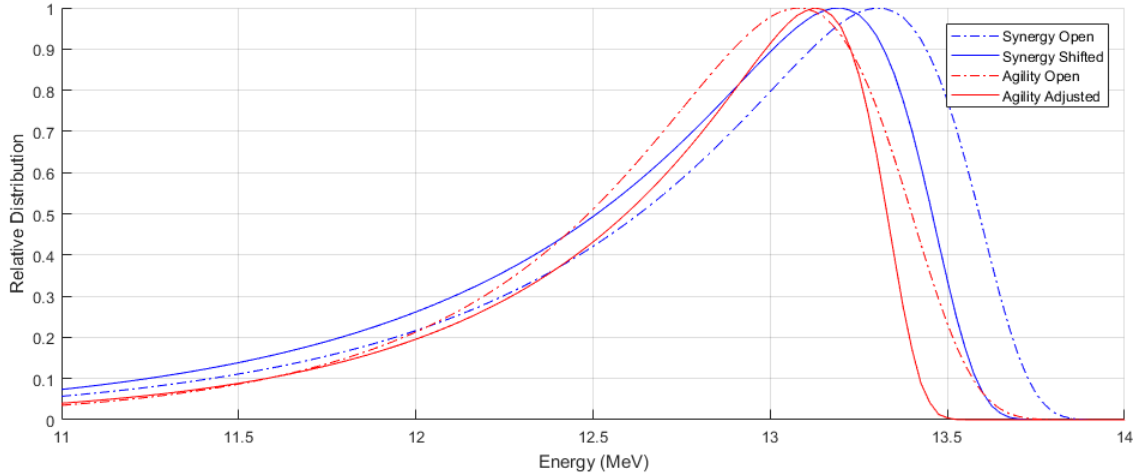

Figure D-4 12 MeV spectra determined by SSS using fields without applicators and if required spectra adjust for fields with applicators

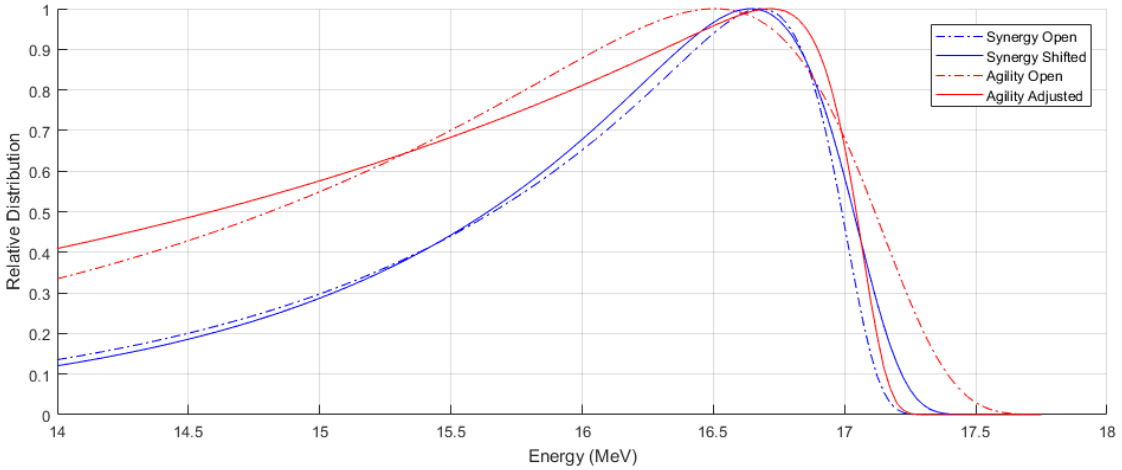

Figure D-5 15 MeV spectra determined by SSS using fields without applicators and if required spectra adjust for fields with applicators

D.2. Comparison between BEAMnrc and Monaco electron energy distribution

D.2.1. Synergy

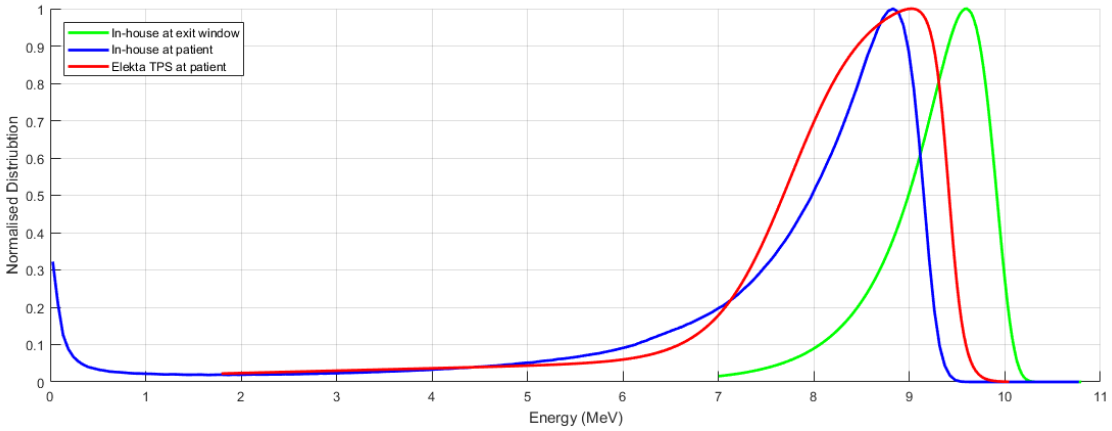

Figure D-6 Synergy 8 MeV spectrum determined by commercial and in-house modelling methods

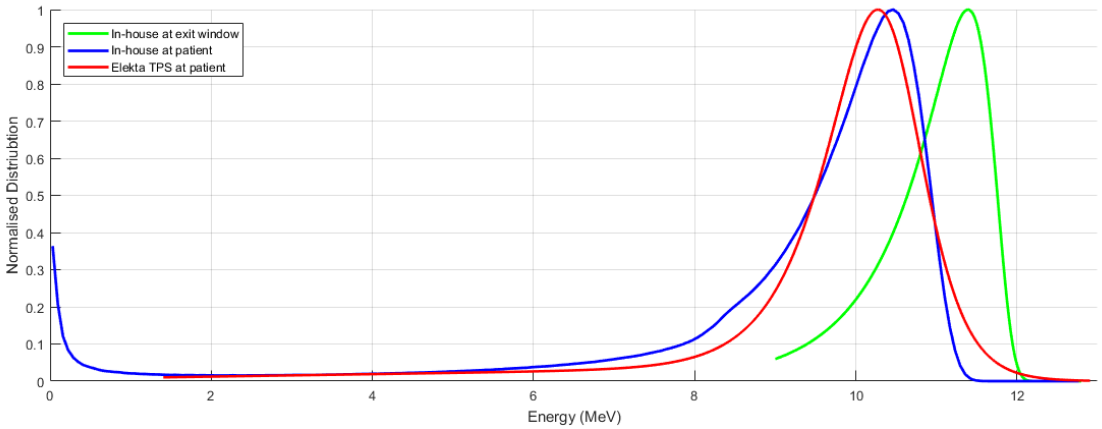

Figure D-7 Synergy 10 MeV spectrum determined by commercial and in-house modelling methods

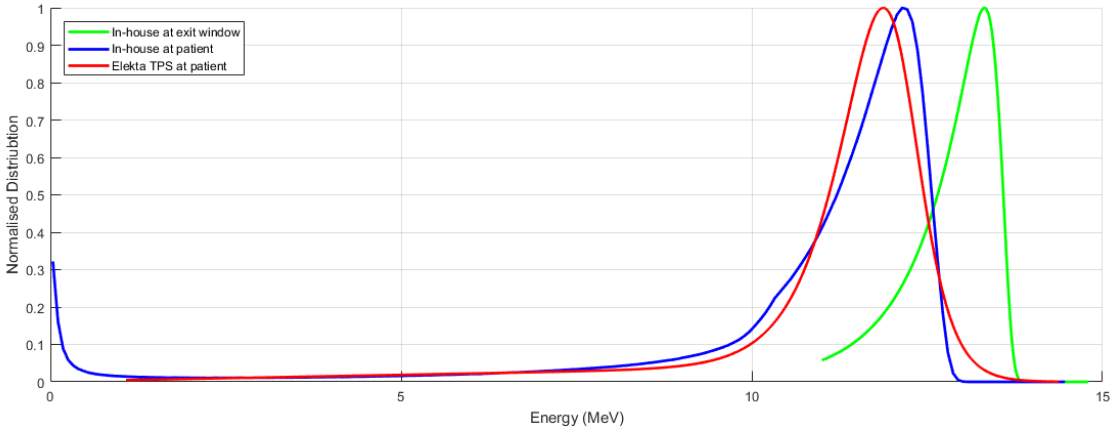

Figure D-8 Synergy 12 MeV spectrum determined by commercial and in-house modelling methods

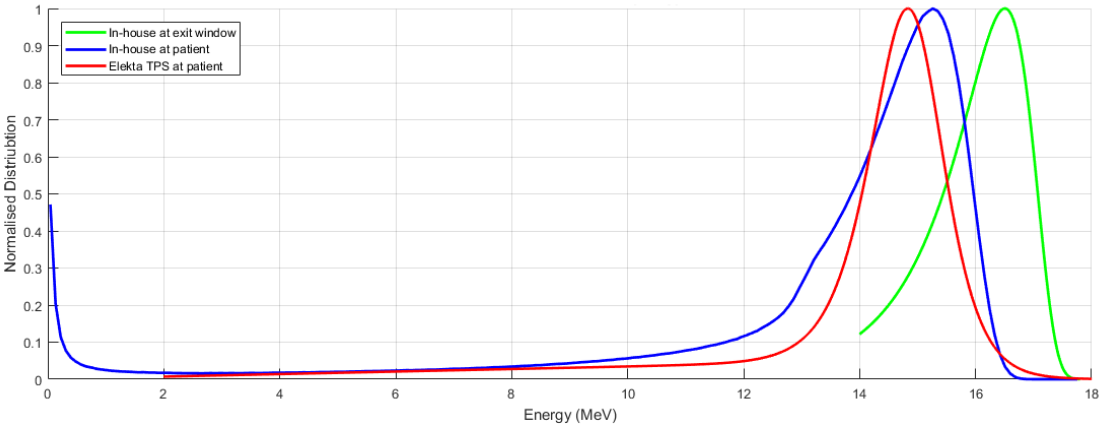

Figure D-9 Synergy 15 MeV spectrum determined by commercial and in-house modelling methods

D.2.2. Agility

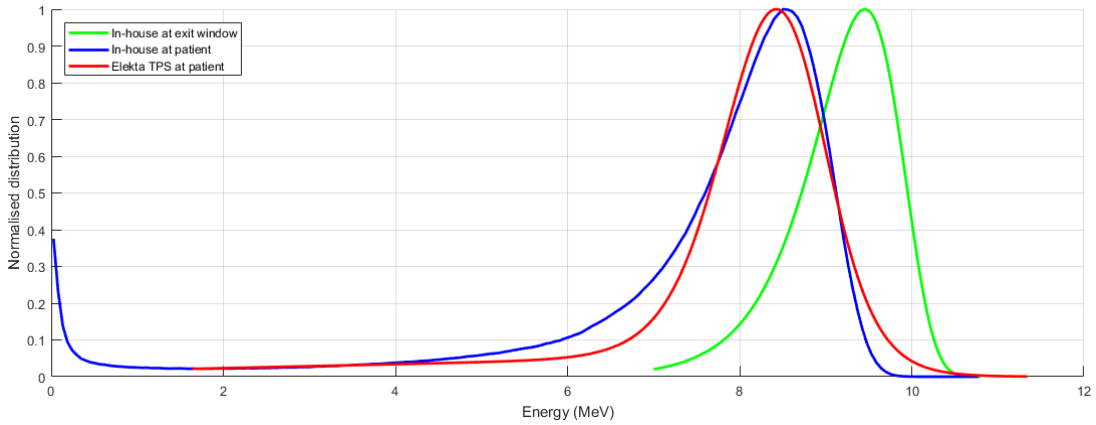

Figure D-10 Agility 8 MeV spectrum determined by commercial and in-house modelling methods

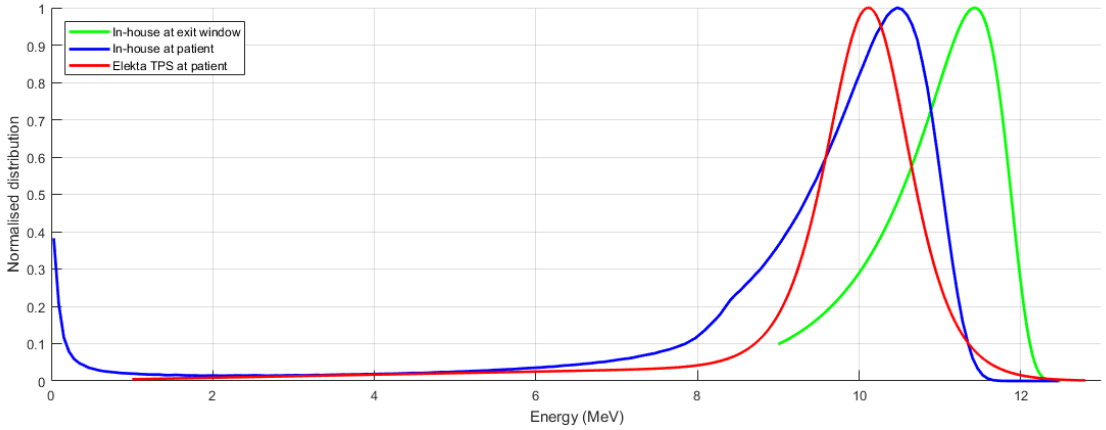

Figure D-11 Agility 10 MeV spectrum determined by commercial and in-house modelling methods

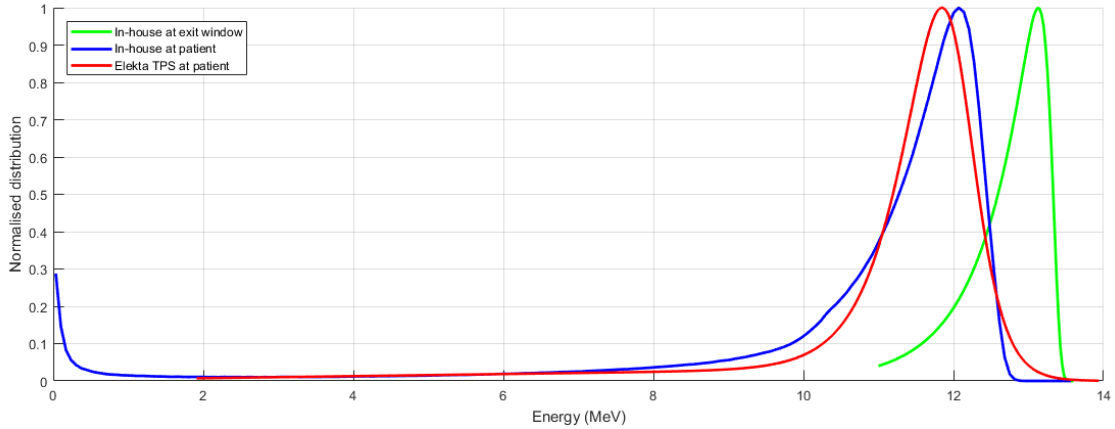

Figure D-12 Agility 12 MeV spectrum determined by commercial and in-house modelling methods

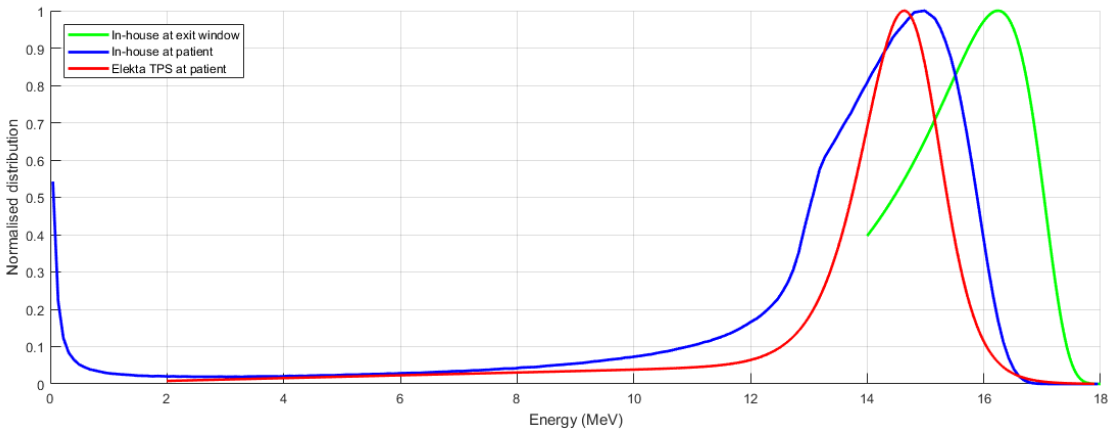

Figure D-13 Agility 15 MeV spectrum determined by commercial and in-house modelling methods

References

American Association of Physicists in Medicine (AAPM). (1978). Practical Aspects of Electron Beam Treatment Planning (Medical Physics Monograph no 2) ed C G Orton and F Bagne (New York: AIP).

Antolak, J. A., Bieda, M. R., & Hogstrom, K. R. (2002). Using Monte Carlo methods to commission electron beams: A feasibility study. Medical Physics, 29(5), 771–786. https://doi.org/10.1118/1.1469626

Bjork, P., Knoos, T., & Nilsson, P. (2002). Influence of initial electron beam characteristics on monte carlo calculated absorbed dose distributions for linear accelerator electron beams. Medical Physics, 47, 4019–4041.

Boyd, R. A., Hogstrom, K. R., & Rosen, I. I. (1998). Effect of using an initial polyenergetic spectrum with the pencil-beam redefinition algorithm for electron-dose calculations in water. Medical Physics, 25(11), 2176–2185. https://doi.org/10.1118/1.598414

Boyd, R. A., Hogstrom, K. R., & Starkschall, G. (2001). Electron pencil-beam redefinition algorithm dose calculations in the presence of heterogeneities. Medical Physics, 28(10), 2096–2104. https://doi.org/10.1118/1.1406521

Brahme, A. (1985). Current algorithms for computed electron beam dose planning. Radiotherapy and Oncology, 3(4), 347–362. https://doi.org/10.1016/S0167-8140(85)80048-7

Cheng, A., Harms Sr, W. B., Gerber, R. L., Wong, J. W., & Purdy, J. A. (1996). Systematic verification of a three-dimensional electron beam dose calculation algorithm. Med Phys, 23(5), 685–693. https://doi.org/10.1118/1.597714

Chetty, I. J., Curran, B., Cygler, J. E., DeMarco, J. J., Ezzell, G., Faddegon, B. A., … Siebers, J. V. (2007). Report of the AAPM Task Group No. 105: Issues associated with clinical implementation of Monte Carlo-based photon and electron external beam treatment planning. Medical Physics, 34(12), 4818–4853. https://doi.org/10.1118/1.2795842

Elekta. (2014). Monaco ® External Beam Dose Calculation Algorithms Technical Reference. IMPAC Medical Systems, Document ID: LRMMON0005.

Eyges, L. (1948). Multiple scattering with energy loss. Phys. Rev., 74, 1534–1535.

Ford, R. L., & Nelson, W. R. (1978). “The EGS Code System: Computer Programs for the Monte Carlo Simulations of Electromagnetic Cascade Showers (Version3)”,

Stanford Linear Accelerator Center. Report SLAC-210.

Hogstrom, K. R., & Almond, P. R. (2006). Review of electron beam therapy physics. Physics in Medicine and Biology, 51(13). https://doi.org/10.1088/0031-9155/51/13/R25

Hogstrom, K. R., Mills, M. D., & Almond, P. R. (1981). Electron beam dose calculations. Phys. Med. Biol., 26(3), 445–459.

Hogstrom, K. R., Mills, M. D., Meyer, J. A., Palta, J. R., Mellenberg, D. E., Meoz, R. T., & Fields, R. S. (1984). Dosimetric evaluation of a pencil-beam algorithm for electrons employing a two-dimensional heterogeneity correction. Int. J. Radiat. Oncol. Biol. Phys., 10, 561–569.

Hu, T., & Wang, N.-Y. (2014). Measurment of the energy spectrum of an electron beam extracted from an accelerator. Chinese Physics B, 23(9), 098702. https://doi.org/10.1088/1674-1056/23/9/098702

International Commission on Radiation Units and Measurements (ICRU). (1984). Radiation Dosimetry: Electron Beams with Energies Between 1 and 50 MeV. ICRU Report 35. https://doi.org/10.1118/1.595780

Jette, D. (1996). Electron dose calculation using multiple-scattering theory: a new theory of multiple scattering. Medical Physics. https://doi.org/10.1118/1.597777

Ju, T., Simpson, T., Deasy, J. O., & Low, D. A. (2008). Geometric interpretation of the γ dose distribution comparison technique: Interpolation-free calculation. Medical Physics, 35(3), 879–887. https://doi.org/10.1118/1.2836952

Kawrakow, I., Fippel, M., & Friedrich, K. (1996). 3D electron dose calculation using a voxel based Monte Carlo algorithm. Med. Phys.

Kawrakow, I., & Rogers, D. W. O. (2011). The EGSnrc code system: Monte Carlo simulation of electron and photon transport. Ionizing Radiation Standards, National Research Council of Canada Technical Report No. PIRS-701, 2001–2015. https://doi.org/10.1118/1.598917

Keall, P. J., & Hoban, P. W. (1996). Super-Monte Carlo: A 3-D electron beam dose calculation algorithm. Medical Physics. https://doi.org/10.1118/1.597842

Kok, J. G. M., & Welleweerd, J. (1999). Finding mechanisms responsible for the spectral distribution of electron beams produced by a linear accelerator. Medical Physics, 26(12), 2589–2596. https://doi.org/10.1118/1.598798

Lillicrap, S. C., Wilson, P., & Boag, J. W. (1975). Dose distributions in high energy

electron beams: Production of broad beam distributions from narrow beam data. Physics in Medicine and Biology, 20(1), 30–38. https://doi.org/10.1088/0031-9155/20/1/002

Low, D. A., & Dempsey, J. F. (2003). Evaluation of the gamma dose distribution comparison method. Medical Physics, 30(9), 2455–2464. https://doi.org/10.1118/1.1598711

Low, D. A., Harms, W. B., Mutic, S., & Purdy, J. A. (1998). A technique for the quantitative evaluation of dose distributions. Medical Physics, 25(5), 656–661. https://doi.org/10.1118/1.598248

Ma, C.-M., Mok, E., Kapur, A., Pawlicki, T., Findley, D., Brain, S., … Boyer, A. L. (1999). Clinical implementation of a Monte Carlo treatment planning system. Medical Physics, 26(10), 2133–2143. https://doi.org/10.1118/1.598729

Mackie, T. R., & Battista, J. J. (1984). A macroscopic Monte Carlo method for electron beam dose calculations: a proposal. Proc. 8th Conf. on Use of Computers in Radiation Therapy, (Toronto:, pp 123–7.

Mah, E., Antolaki, J., Scrimgert, J. W., & Battistas, J. J. (1989). Experimental evaluation of a 2D and 3D electron pencil beam algorithm. Int. J. Radiat. Oncol. Biol. Phys, 10, 561–569.

McShan, D. L., Fraass, B. A., & Ten Haken, R. K. (1994). Dosimetric verification of a 3-D electron pencil beam dose calculation algorithm. Medical Physics, 21(1), 13–23. https://doi.org/10.1118/1.597363

Nelson, W. R., Hideo, H., & Rogers., D. W. 0. (1985). “The EGS4 Code System.” Technical Report SLAC-265, Stanford Linear Accelerator Center, Stanford University.

Neuenschwander, H., & Born, E. J. (1992). A macro Monte Carlo method for electron beam dose calculations. Phys. Med. Bid., 37(1), 107–125.

Neuenschwander, H., Mackie, T. R., & Reckwerdt, P. J. (1995). MMC--- A high-performance Monte Carlo code for electron beam treatment planning. Phys. Med. Biol., 40, 543–574.

Nüsslin, F. (1979). Computerized treatment planning in therapy with fast electrons: a review of procedures for calculation of dose distribution. Medicamundi, 24, 112–118.

Perry, D. J., & Holt, J. G. (1980). A model for calculating the effects of small

inhomogeneities on electron beam dose distributions. Medical Physics, 7(3), 207–215. https://doi.org/10.1118/1.594687

Podgorsak, E. B. (2005). Radiation Oncology Physics: A Handbook for Teachers and Students. IAEA (International Atomic Energy Agency), 33(6). https://doi.org/10.1118/1.2201870

Rogers, D. W. O., Walters, B., & Kawrakow, I. (2011). BEAMnrc Users Manual. NRCC Report PIRS-0509(A)RevL, 509, 1–260.

Rogers D W O, Faddegon B A, Ding G X, C. M. M. J. W. and M. T. R. (1995). Beam: a Monte Carlo code to simulate radiotherapy treatment unit. Medical Physics.

Savitzky, A., & Golay, M. J. E. (1964). Smoothing and Differentiation of Data by Simplified Least Squares Procedures. Analytical Chemistry, 36(8), 1627–1639. https://doi.org/10.1021/ac60214a047

Shiu, A. S., & Hogstrom, K. R. (1991). Pencil-beam redefinition algorithm for electron dose distributions. Medical Physics, 18(1), 7–18. https://doi.org/10.1118/1.596697

Starkschall, G., Shiu, A. S., Bujnowski, S. W., Wang, L. L., Low, D. A., & Hogstrom, K. R. (1991). Effect of dimensionality of heterogeneity corrections on the implementation of a three-dimensional electron pencil-beam algorithm. Physics in Medicine and Biology, 36(2), 207–227. https://doi.org/10.1088/0031-9155/36/2/006

Walters, B., Kawrakow, I., & Rogers, D. W. O. (2016). DOSXYZnrc Users Manual. NRCC Report PIRS-0794, (April), 1–125. https://doi.org/10.1118/1.4773883